komunikácie

COMMUNICATIONS

SCIENTIFIC LETTERS OF THE UNIVERSITY OF ŽILINA

Volume 27

JOURNAL FOR SCIENCES IN TRANSPORT

UNIVERSITY
OF ŽILINA

ISSN 1335-4205

3/2025

UNIVERSITY OF ŽILINA
EDIS-Publishing House
UNIZA

EDIS-Publishing House of the University of Žilina (UZ) is one of the University of Žilina's consituents. The beginning of its existence dates back to 1990. In the course of its work, the publishing house has published more than 5 000 titles of book publications, especially university textbooks, scientific monographs, scripts, prose, but also enriched the book market with titles of regional, children's and popular literature.
Students and professional public have the opportunity to purchase published titles in the „Selling Study Literature" directly on the premises of the University of Žilina, in the EDIS shop or upon order on a „cash on delivery" basis. All published titles are available at: www.edis.uniza.sk.

EDIS-Publishing House of the University of Žilina offers book titles in English

Lenka Černá, Jozef Daniš
APPLICATION OF COST ALCULATIONS IN THE TARIFF POLICY FORMATION IN RAILWAY TRANSPORT
ISBN 978-80-554-1391-4 Price 7.61 €

Eva Nedeliaková, Jana Sekulová
EVALUATION OF QUALITY IN RAILWAY TRANSPORT
ISBN 978-554-1272-6 Price 8.00 €

Martin Bugaj
AEROMECHANICS 1
ISBN 978-80-554-1675-5 Price 14.50 €

Anna Tomová
ECONOMICS OF AIR NAVIGATION SERVICES
ISBN 978-80-554-0905-4 Price 14.30 €

Marica Mazurek
MODELS OF BRANDING AND THEIR APPLICATION
ISBN 978-80-554-1705-9 Price 9.00 €

Jozef Melcer
DYNAMICS OF STRUCTURES
ISBN 978-80-554-1698-4 Price 19.00 €

Jozef Gašparík et al.
RAILWAY TRAFFIC OPERATION
ISBN 978-80-554-1281-8 Price 15.80 €

Tetiana Hovorushchenko et.al.
CD - INTELLIGENT INFORMATION-ANALYTICAL TECHNOLOGIES...
ISBN 978-80-554-1729-5 Price 3.50 €

Karol Matiaško, Michal Kvet, Marek Kvet
CD - PRACTICES FOR DATABASE SYSTEMS
ISBN 978-80-554-1397-6 Price 2.20 €

Michal Kvet, Karol Matiaško, Štefan Toth
USB - PRACTICAL SQL FOR ORACLE CLOUD
ISBN 978-80-554-1880-3 Price: 11,30 €

Veronika Valašková, Daniela Kucharová
USB - STATICS OF STRUCTURES 3
ISBN 978-80-554-1826-1 Price: 8,90 €

Michal Kvet, Karol Matiaško, Marek Kvet
USB - BECOME EXPERT IN MYSQL PRACTICES FOR DATABASE SYSTEMS IN MYSQL
ISBN 978-80-554-1786-8 Price 13.50 €

Michal Kvet, Alenka Baggia, Monika Borkovcová, Diana Mudrinić, Frane Urem
E-book - Environmental Data Analysis
ISBN 978-80-554-2145-2 Price 0,00 €

Michal Kvet
E-book – Become master in SQL
ISBN 978-80-554-2132-2 Price 0,00 €

EDIS-Publishing House UNIZA
Univerzitná 8215/1,
010 26 Žilina,
Slovakia

e-mail: edis_objednavky@uniza.sk, edis@uniza.sk
www.edis.uniza.sk

kOMUNIKÁCIE
COMMUNICATIONS

VEDECKÉ LISTY ŽILINSKEJ UNIVERZITY
SCIENTIFIC LETTERS OF THE UNIVERSITY OF ZILINA
journal for sciences in transport

A - OPERATION AND ECONOMICS IN TRANSPORT

B - MECHANICAL ENGINEERING IN TRANSPORT

D - CIVIL ENGINEERING IN TRANSPORT

E - MANAGEMENT SCIENCE AND INFORMATICS IN TRANSPORT

F - SAFETY AND SECURITY ENGINEERING IN TRANSPORT

Dear colleagues,

Journal for sciences in transport Communications - Scientific Letters of the University of Žilina are a well-established open-access scientific transport journal aimed primarily at the topics connected with the field of transport. The main transport-related areas covered include Civil engineering, Electrical engineering, Management and informatics, Mechanical engineering, Operation and economics, Safety and security, Travel and tourism studies. Research in the field of education also falls under these categories. The full list of main topics and subtopics is available at: *https://komunikacie.uniza.sk/artkey/inf-990000-0500_Topical-areas.php*

Journal for sciences in transport Communications - Scientific Letters of the University of Žilina is currently indexed, abstracted and accepted by CEEOL, CLOCKSS, COPE (Committee on Publication Ethics), Crossref (DOI), digitálne pramene, DOAJ, EBSCO Host, Electronic Journals Library (EZB), ERIH Plus, Google Scholar, Index Copernicus International Journals Master list, iThenticate, JournalGuide, Jouroscope, Norwegian Register for Scientific Journals Series and Publishers, Portico, ROAD, ScienceGate, SCImago Journal & Country Rank, SciRev, SCOPUS, Web of Science database, WorldCat (OCLC).

Journal for sciences in transport Communications - Scientific Letters of the University of Žilina is preserved in CLOCKSS and Portico to guarantee long-term digital preservation and is archived in the national deposit digitalne pramene.

Authors can share their experiences with publishing in our journal on SciRev.

Journal for sciences in transport Communications - Scientific Letters of the University of Žilina has been selected for inclusion in the Web of Science™. Articles published after 2022, beginning with 24(1), will be included in the product Emerging Sources Citation Index (ESCI).

I would like to invite authors to submit their papers for consideration. We have an **open access policy under Creative Commons (CC BY) license** and Article Processing Charge (APC) is **400 Euro** (price excluding VAT). The price of one additional page of the submitted article beyond the prescribed scope (15 pages) is **50 Euro** (price excluding VAT). Print edition fee is **100 Euro** per one piece (price excluding VAT) including shipping costs. Our journal operates a standard single-anonymous peer-review process, the successful completion of which is a prerequisite for publication of articles.

Our journal is issued four times a year (in January, in April, in July and in October).

I would also like to offer you the opportunity of using already published articles from past issues as source of information for your research and publication activities. All papers are available at our webpage: http://komunikacie.uniza.sk, where you can browse through the individual volumes. Our journal offers access to its contents in the open access system on the principles of the license Creative Commons (CC BY 4.0).

For any questions regarding the Journal for sciences in transport Communications - Scientific Letters of the University of Žilina please contact us at: *komunikacie@uniza.sk*.

We look forward to future cooperation.

Sincerely

Branislav Hadzima
editor-in-chief

ECONOMIC DETERMINANTS OF GASOLINE PRICES: A COINTEGRATION ANALYSIS FOR CZECHIA

Jiří Alina[1,*], Jiří Nožička[2]

[1]Department of Applied Economics and Economy, Faculty of Economics, University of South Bohemia in Ceske Budejovice, Ceske Budejovice, Czech Republic
[2]Department of Transport Management, Marketing and Logistics, Faculty of Transport Engineering, University of Pardubice, Pardubice, Czech Republic

*E-mail of corresponding author: jalina@ef.jcu.cz

Jiří Alina 0000-0002-3652-3597, Jiří Nožička 0000-0001-5427-1066

Resume
The long-term relationships between the N95 ("Natural 95") gasoline prices and economic factors, such as Brent crude oil prices, diesel fuel prices, and the CZK/USD exchange rate from 2014 to 2024, was investigated within this research. The Engle-Granger cointegration test was used to identify any stable long-term connections between these variables. Despite the comprehensive tests, facilitated by the Matlab software, no evidence of cointegration was consistently found, indicating that these economic factors do not significantly influence N95 gasoline prices over the long term. The findings suggest that, while the short-term fluctuations in these economic indicators may temporarily impact gasoline prices, they are not reliable predictors of the long-term trends.

Article info
Received 7 January 2025
Accepted 28 May 2025
Online 16 June 2025

Keywords:
Engle-Granger test
cointegration
prices
oil
gasoline

Available online: https://doi.org/10.26552/com.C.2025.043

ISSN 1335-4205 (print version)
ISSN 2585-7878 (online version)

1 Introduction

Fuel prices have a significant impact on the development of both the global economy and national economies. Fuels price affects the level of logistics costs and thus enters all the market prices. In this way, it significantly affects the inflation rate and the development of GDP. The ability to estimate the development of fuel prices increases the competitiveness of both the state and the economy.

In economies with a market mechanism, fuel prices are to a certain extent dependent on the level of competition between gas station networks and also on the level of fuel taxation in individual economies. However, other factors, such as the geopolitical situation in the world, the OPEC cartel, and others, can also play a significant role.

The author's teams in China have been searching for factors affecting fuel prices for a long time. Research on this topic in the environment of European economies is not as widespread. With this article, the authors want to increase the level of knowledge in this issue for the market in the Czech Republic. Therefore, it was chosen to assess the relationship between the Natural 95 prices and diesel fuel in the Czech Republic from 2014 to 2024 against selected indicators, including the time shift.

1.1 Literature review

Investigating the relationship between the price of crude oil and fuel in Brazil, Gerrio et al. 2024 analysed the development of WTI oil by using statistical tools, such as nonlinear models of the self-exciting threshold autoregressive (SETAR) and logistic smooth transition autoregressive (LSTAR) [1].

Arun 2017 dealt with the sensitivity of fuel prices and their changes depending on oil prices. He tracked the development of fuel prices in India depending on the oil prices [2].

Ozdurak and Veysel 2020 investigated the relations between financial derivatives with crude oil prices. They were looking for intraday volatility interactions between crude oil futures and energy exchange traded funds. They did not identify the relationship where the spot market and the futures market would be affected. They

believe that causality is more likely to be bidirectional from the futures market to the spot markets for crude oil [3].

Choi et al. 2015 used the Granger causality to test the effect of crude oil spot prices on the crack spread futures market. They identified three periods (precrisis, crisis, and postcrisis periods). They found the unidirectional relationship between the precrisis and crisis periods from the crude oil spot market to crack spread futures. An interesting thing is that they found reverse relationships during the post-crisis period [4].

Arouri et al. 2011 also dealt with the difference between the price of oil and the price of fuel. They identified differences between price developments. They then explained these differences with current risks for the oil industry, as this will subsequently affect International portfolio management, which strongly reacts to developments on the level of return and volatility spillovers between world oil prices and GCC stock markets [5].

Borenstein and Kellogg 2014 investigated whether the fuel prices in the American Midwest change with the development of oil prices. They concluded that during the period under review, the decrease in crude oil prices in the Midwest market did not lead to a decrease in fuel prices. One of the reasons, they cited, is that the fuel is also imported into the Midwest from the Gulf of Mexico region, where crude oil prices were higher during the period under review [6].

An analysis of the types of demand and supply shocks that affect the oil prices was carried out by Li and Zhao 2011. Their structural vector autoregression model is based on the generalised supply and demand analysis of crude oil price fluctuation and performance the structural decomposition of price shocks with impulse response analysis of those factors. They found these kinds of structural shocks. First, the supply side shocks (the exogenous geopolitical shocks and other oil supply shocks) are the first group. The second group are the demand side shocks (the aggregate demand shock and the other oil market demand shock). This second group has a very strong effect on prices of oil. The next shocks are from the impact of the liquidity of the US dollar [7].

Choi et al. 2021 investigated the long-term and short-term dependencies between the price of crude oil and the price of fuels in the cities of Shenzhen, Hong Kong and Macao. They used an asymmetric error correction model (AECM). They found a long-term relationship between the fuel and crude oil prices in all three cities. For Hong Kong and Macao, they also found that fuel prices are rising faster than they are falling. For this reason, they hypothesised that the fuel market in these cities does not have a very strong competitive environment. For the city of Macao, the difference between the increase rate and the decrease of prices was not demonstrated [8].

The same method was used by Yufeng et al. 2017, who analysed monthly crude oil and fuel prices in China, in the observed period between 2006 and 2013. They found a strong dependence and confirmed that fuel prices rise faster when oil prices rise than they fall when oil prices fall. They also found a stronger effect on diesel prices than on gasoline prices. They also demonstrated that the Chinese government's interventions in oil prices during their longer-term growth led to significant market asymmetry [9].

Szomolanyi et al. 2022 based on the assumption from the results of many researches, i.e., that fuel prices rise faster than they subsequently fall. In their work, they analyse weekly US fuel prices and their response to oil prices. For their research, they used an empirical approach based on the linear exponential adjustment costs formulation. They found that US retail gasoline and diesel prices react asymmetrically to changes in WTI crude oil spot prices. However, they could not estimate statistically significant coefficients of specification with the input price c representing the WTI crude oil price time series and with the output price representing the time series of the gasoline and diesel price at the time [10].

Adrangi et al. 2001 used the VAR methodology and bivariate GARCH model in finding the relationship between the prices of crude oil (Alaska North Slope crude oil) and diesel prices in California. They confirmed a strong relationship between these prices [11].

Manera and Grasso 2005, carried out an econometric study of the sensitivity of gasoline price changes to oil price changes. They used a multi-model investigation in which they followed the development of monthly prices in France, Germany, Italy, Spain, and the UK between 1985 - 2003. They also worked with different time lags of reactions in the models. Their results demonstrated a long-term asymmetry of gasoline prices with oil prices for all the examined countries, in the given period [12].

Cheng 2024 examined the lag in price increases for selected energy market commodities. He created an updated time-delay function. He claimed that most of the impact of change occurs in the first 6 months. According to his results in the first 3 months, there is 50% of the effect of oil price change. Therefore, in this initial phase there are the most significant price changes [13].

2 Methods

2.1 Research questions

The authors asked four main research questions, which are:

Research Question 1 (RQ1). Is the price of gasoline "Natural 95" (N95) affected by the price of Brent crude oil, the price of diesel fuel and the CZK/USD exchange rate?

Research question 2 (RQ2). Is the price of N95 affected by the price of Brent crude oil and the CZK/USD exchange rate?

Research question 3 (RQ3). Is the price of N95 affected by the price of Brent crude oil and the price of diesel?

Research question 4 (RQ4). Is the price of N95 affected by the price of Brent crude oil?

The authors' interest in RQ 4 was the influence of the time shift and its results.

2.2 Data and tests

Data used for analysis were mainly extracted from the website kurzy.cz. It was necessary to recalculate them for months of the year. Collecting data over a 10-year period from 2014 to 2024 proved to be a complex and time-consuming task. The primary challenge was ensuring the consistency and reliability of data throughout such an extended timeframe, as data reporting standards and availability can vary significantly over the years. Additionally, the economic landscape during this period included numerous market events and fluctuations, such as oil price shocks and changes in currency exchange rates, which added layers of complexity to the data collection process. Those factors required meticulous attention to detail and rigorous validation to ensure that the data accurately reflected the economic conditions relevant to N95 gasoline prices. Furthermore, the integration of diverse datasets, including those for Brent crude oil prices, diesel fuel prices, and exchange rates, required a comprehensive approach to manage inherent volatility and potential discrepancies in the data sources. In general, the process was not only labour-intensive, but required significant expertise in data analysis tools like Matlab, as well, to handle and analyse large volumes of data effectively.

The kurzy.cz database is not an international database like Eurostat or OECD, it is a widely recognised Czech financial portal that aggregates data directly from authoritative institutions such as the Czech National Bank (CNB) and the major commercial banks. This ensures the accuracy and reliability of the information provided. The comprehensive historical coverage of the platform was essential for the ten-year analysis (2014-2024), and its open data policy allows transparent and reproducible research. To ensure the data reliability and consistency, authors cross-validated a sample of kurzy.cz data points with official CNB records and, where possible, with Eurostat. Authors also conducted completeness checks to identify missing or inconsistent records. Any gaps in the data were addressed using standard imputation methods (such as linear interpolation for time-series data), following best practices in economic research. The data handling procedures included programmatic extraction from kurzy.cz's API, systematic data cleaning, outlier detection, and thorough documentation of all preprocessing steps. Those procedures, along with the availability of the scripts and documentation as supplementary materials, ensure transparency and reproducibility. In summary, kurzy.cz provides reliable, granular and long-term economic data for the Czech context. Rigorous data validation and preprocessing steps address concerns about data credibility and ensure the robustness of the analysis. Authors are happy to provide additional details or documentation upon request.

To investigate the four research questions, the Engle-Granger test was used. The Engle-Granger test is a method used to test for cointegration between two or more time series. It is a two-step procedure that involves two steps: the first of which is to estimate the cointegrating regression, and the second is to test the residuals for stationarity.

The Engle-Granger test, which was first proposed by Robert F. Engle and Clive W.J. Granger in 1987, is a statistical method that can be employed to test for cointegration between two or more time series. The term "cointegration" is used to describe a situation in which a linear combination of nonstationary series yields a stationary series. This indicates a stable long-term relationship between variables [14]. One possible approach to the two-step Engle-Granger procedure is to first estimate the long-term relationship using ordinary least squares (OLS) and then apply the augmented Dickey-Fuller (ADF) test to the residuals to determine their stationarity [15-16].

One of the primary applications of the Engle-Granger test is in the field of econometrics and financial studies, particularly for modelling the relationships between economic variables over time. For example, researchers often use the test to examine long-term relationships between the stock prices and economic indicators, which can inform investment decision making [17]. Despite its limitations, including its applicability mainly to systems of two variables [18], this test is popular among economists due to its simplicity and efficiency.

The Engle-Granger test has been the subject of both praise and criticism in numerous studies. While some researchers have found the test to be effective in identifying cointegration, others have identified potential issues related to the dependence of the test on estimated residuals [19].

The Engle-Granger test is particularly suitable for systems involving two variables due to its simplicity and efficiency, making it a popular choice among economists. This method is effective in identifying cointegration, indicating a long-term equilibrium relationship between time-series data. The straightforward application of the test involves estimating residuals from a regression model and checking for their stationarity, thus determining if the variables move together over time. Despite some criticisms regarding its dependence on estimated residuals, the Engle-Granger test remains a valuable tool for initial cointegration analysis, especially when dealing with smaller datasets or when computational resources are limited. Its implementation in software like Matlab further enhances its accessibility and ease

of use, allowing researchers to quickly assess potential long-term relationships between economic variables.

The Engle-Granger two-step method is a classic approach to testing cointegration between non-stationary time series. It first estimates a long-term equilibrium relationship using ordinary least squares and then checks whether the residuals are stationary. Its main strengths are simplicity and ease of implementation. However, it has notable limitations: it can only detect a single co-integrating relationship and is sensitive to errors in the first regression step, which can bias results. Furthermore, the critical values of the method depend on the number of variables, which complicates inference in larger systems [20]. The Johansen test addresses many of these issues by using a vector autoregressive (VAR) framework to test multiple co-integrating vectors simultaneously. This makes it more suitable for multivariate systems and is generally more powerful when the model is correctly specified. However, the Johansen method is computationally more complex and sensitive to model misspecification, such as incorrect lag length or the presence of structural breaks. In some cases, it may detect spurious cointegration if the underlying assumptions are violated [21]. Other alternatives include the Phillips-Ouliaris test, which improves upon Engle-Granger by better accounting for uncertainty in residual estimation, and Bayesian methods that allow for more flexible modelling, especially in the presence of structural breaks or uncertain cointegration ranks [18]. In practice, researchers often use Engle-Granger and Johansen tests to cross-check results, as they can sometimes yield different conclusions. While Johansen is preferred for systems with several variables and potential co-integrating relationships, Engle-Granger remains valuable for its simplicity and robustness, especially in bivariate settings or when model assumptions are in doubt. Ultimately, careful model specification and diagnostic checking are crucial regardless of the chosen method [20].

3 Results

The authors obtained the main results by using Matlab software. Figure 1 shows the time series of all four variables (their prices), such as Brent crude oil, diesel, CZK/USD exchange rate and gasoline 'natural 95'. The horizontal axis shows the months and the vertical axis shows the values of the variables in CZK. This chart was generated in Matlab.

The first three research questions led to the creation of hypothesis, which is given as follows:

Null hypothesis: There is no cointegration between the time series.

After running all tests, authors got results as can be seen in Tables 1, 2 and 3.

The research question No 4 was answered using the Engle Grenger test in Matlab software. Table 4 shows the results of the Engle-Granger test used for analysis.

The authors included lagged (time shift) values (1-3 months) in their analysis for RQ1-RQ3 to better assess whether cointegration is truly absent or if it

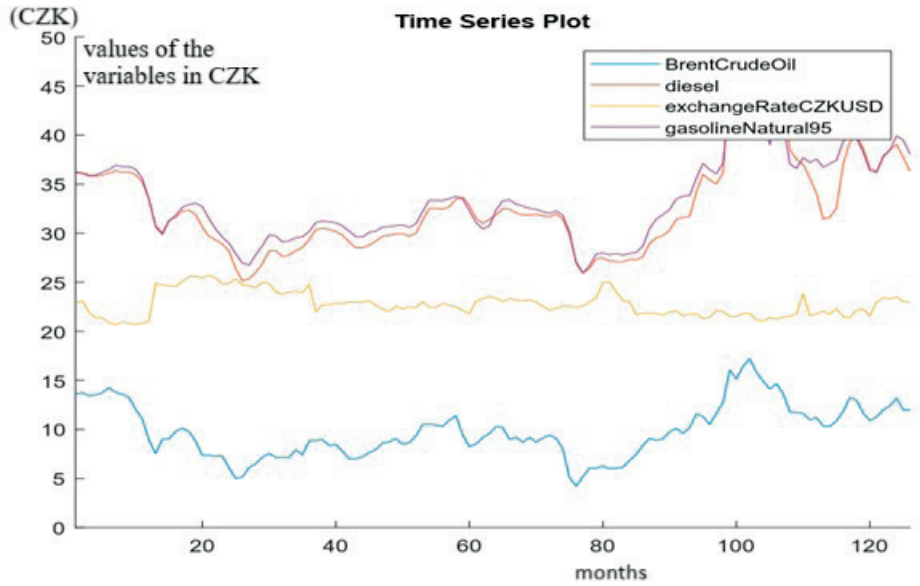

Figure 1 *The time series plot*

Table 1 *Results of the Engle-Granger test, RQ1*

Null Rejected	P-Value	Test Statistic	Critical Value
false	0.23086	-3.4493	-3.8799

Table 2 *The results of the Engle-Granger test, RQ2*

Null Rejected	P-Value	Test Statistic	Critical Value
false	0.27212	-4.3551	-3.5034

Table 3 *The results of the Engle-Granger test, RQ3*

Null Rejected	P-value	Test Statistic	Critical Value
false	0.10818	-3.4676	-3.5034

Table 4 *The results of the Engle-Granger test, RQ4*

Shift in months	P - value	Null Rejected
0	0.0039119	True
1	0.001	True
2	0.001	True
3	0.0053748	True
4	0.060452	False
5	0.15605	False
6	0.22785	False
7	0.36603	False
8	0.49718	False
9	0.50359	False

Table 5 *The results of the Engle-Granger test for RQ1, RQ2, RQ3 with time lag (-1,-2,-3)*

RQ 1			
Null Rejected	P-Value	Test Statistic	Critical Value
false (t -1)	0.0641	-5.5741	-4.1905
false (t -2)	0.0884	-4.869	-4.1913
false (t -3)	0.0721	-4.0333	-4.1920
RQ 2			
Null Rejected	P-Value	Test Statistic	Critical Value
false (t -1)	0.0915	-5.0714	-3.8125
false (t -2)	0.0534	-4.8450	-3.8131
true (t -3)	0.0488	-4.1091	-3.8137
RQ 3			
Null Rejected	P-Value	Test Statistic	Critical Value
false (t -1)	0.0715	-5.5359	-3.8125
false (t -2)	0.0832	-4.8725	-3.8131
false (t -3)	0.1322	-4.1156	-3.8137

only manifests with a time delay. For all three Research questions (RQ - 1 -3), the authors used the Engle-Granger cointegration test with shifts of 1, 2 and 3 months. The results are shown in Table 5. Only one time lag, for RQ 2, time lag -3 months has results as the slide cointegration, and all other results confirmed no cointegration.

4 Results description

The Engle-Granger cointegration tests conducted in the attached file provide insight into the relationships between the price of N95 gasoline and various economic factors, specifically Brent crude oil prices, diesel fuel prices, and the CZK/USD exchange rate. The following are the most significant implications of the test results for each research question.

4.1 Results of research question 1

Objective: To assess whether the price of N95 gasoline is influenced by the price of Brent crude oil, diesel fuel, and the CZK/USD exchange rate.

Implications: The test results did not find evidence of cointegration, as the null hypothesis was not rejected (p-value = 0.23086).

Significance: This implies that, collectively, these three factors do not exhibit a stable long-term relationship with the prices of N95 gasoline.

Consequences: Policymakers and market analysts may consider that changes in these factors, when combined, do not predict long-term trends in N95 gasoline prices. This suggests that other variables or combinations may be more relevant to understand and forecast gasoline price movements.

4.2 Results of research question 2

Objective: Determine if the price of N95 gasoline is affected by the price of Brent crude oil and the CZK/USD exchange rate.

Implications: The test results did not show evidence of cointegration, and the null hypothesis was not rejected (p-value = 0.27212).

Significance: This finding indicates that there is no significant long-term relationship between N95 gasoline prices and the combination of Brent crude oil prices and the CZK/USD exchange rate.

Consequences: This relationship cannot be crucial for stakeholders, such as energy traders and policymakers, who need to consider these factors in their strategic planning and forecasting. It suggests that fluctuations in Brent crude oil prices and exchange rates are unlikely to have a lasting impact on N95 gasoline prices, making them key indicators for market analysis.

4.3 Results of research question 3

Objective: To evaluate whether the price of N95 gasoline is influenced by the price of Brent crude oil and the price of diesel.

Implications: The test results did not find evidence of cointegration, as the null hypothesis was not rejected (p-value = 0.10818).

Significance: This suggests that the combination of Brent crude oil prices and diesel prices does not exhibit a stable long-term relationship with the prices of N95 gasoline.

Consequences: This outcome indicates that these two factors, when considered together, may not be reliable predictors of long-term trends in N95 gasoline prices. Stakeholders might need to explore other variables or combinations to better understand and anticipate changes in gasoline prices.

4.4 Results of research question 4

Objective: Determine if the price of N95 gasoline is affected by the price of Brent crude oil with some time shift.

Implications: The test results divide the time shifts into two groups. The first group is for time shifts 0,1,2 and 3 months. The second group is for time shifts of 4 months and more. For time shifts in the first group, there is evidence of cointegration, with the null hypothesis being rejected (p-value = 0.0039119, 0.001, 0.001 and 0.0053748). For the time shifts in the second group, there is no evidence of cointegration, and the null hypothesis can not be rejected (p-value = 0.060452, 0.15605, 0.22785, 0.36603, 0.49718, 0.50359).

Significance: This finding indicates that the N95 gasoline prices absorb the change in the price of Brent crude oil gradually and this change is statistically demonstrable in the first 3 months.

Consequences: These results mean that changes in crude oil prices do not have a one-off effect on fuel prices, but are gradual. The change will be felt by auto users in the first few months. From the industry perspective, this is a relatively short period, and therefore it can be expected that the change will affect mainly the first stages of production, which will gradually absorb the price change into their prices. It suggests that fluctuations in Brent crude oil prices have almost no effect in long-term relationship with N95 gasoline prices.

4.5 Detailed breakdown of results

The research analysed three specific research questions:

1. Impact of Brent crude oil, diesel fuel, and the CZK/USD exchange rate on N95 price: The Engle-Granger test revealed no evidence of cointegration, indicating that the price of N95 gasoline does not exhibit a long-term dependency on the combined influence of Brent crude oil, diesel fuel, and the CZK/USD exchange rate. This implies that, although the short-term fluctuations in these economic variables may cause temporary price changes in N95 gasoline, there is no persistent and stable relationship between them.
2. Influence of Brent crude oil and the CZK/USD exchange rate on the N95 price: The analysis again did not produce cointegration, indicating that the price of N95 gasoline is not significantly influenced by the simultaneous variations in Brent crude oil and the CZK/USD exchange rate. This suggests that the relationship between these factors and the price of N95 gasoline is largely independent and short-lived.
3. Relationship between the Brent crude oil and diesel fuel prices and N95 price: The third research question, investigating the joint influence of Brent crude oil and diesel fuel prices on the price of N95 gasoline, also did not result in cointegration. This finding confirms that the price of N95 gasoline is not significantly influenced by long-term changes in the prices of these energy commodities.
4. Relationship between the Brent crude oil and the price of N95 with time changes: The fourth research question, investigating the influence of Brent crude oil on the price of N95 with monthly shifts, divides the results into two groups. For a short-term period (3 months and less) there was cointegration and for a longer-term period (4 months and more) there was no cointegration. This finding confirms that the price of N95 gradually reacts on crude oil changes in the first quatter. These results confirm the conclusions of Cheng [13], although a different approach was used for the test.

4.6 Consequences of the findings

The absence of cointegration between the price of N95 gasoline and the examined economic factors has several key consequences:

- Limited Influence of Economic Factors on N95 Prices: The findings suggest that the price of N95 gasoline is largely determined by other factors, such as supply and demand dynamics, manufacturing costs, and government regulations, rather than the fluctuations in Brent crude oil, diesel fuel, and the CZK/USD exchange rate. This implies that the price of N95 gasoline is relatively insulated from the volatility of these economic indicators.
- Independent Price Dynamics: The results suggest that the price of N95 gasoline follows its own independent trajectory, largely uninfluenced by the long-term movements of Brent crude oil, diesel fuel, and the CZK/USD exchange rate. This implies that market forces specific to the demand and supply of N95 gasoline play a more significant role in shaping its price.
- Uncertainty in Predicting N95 Prices: The lack of cointegration between the price of N95 gasoline and the economic factors examined makes it challenging to predict future price movements using these indicators. The price of N95 gasoline is likely influenced by a complex interplay of factors, making accurate forecasting difficult.
- Gradual Impact of Changes: Time shifts have shown that changes in N95 prices are short-term, so there is only a small chance that policymakers will be able to respond effectively. On the other hand, the impacts are unlikely to be long-term, so there is less risk of market jitters.

4.7 Future prediction and recommendations

Although the study provides information on the lack of cointegration between the price of N95 gasoline and the economic indicators examined, it does not negate the importance of these factors. It is essential to acknowledge that:

- Short-Term Fluctuations are Still Relevant: Although the study indicates a lack of long-term dependency, short-term price fluctuations in Brent crude oil, diesel fuel, and the CZK/USD exchange rate can still affect the short-term price of N95 gasoline. These factors might influence the transportation costs, raw material prices, and overall manufacturing costs, which can temporarily affect the price of N95 gasoline.
- Other Factors Can Influence Prices: The price of N95 gasoline is likely to be determined by a wide range of factors beyond those examined in this study. Factors, such as global demand, pandemic situations, government policies, and manufacturing capacity, play a crucial role in the shape of the price.
- More research is needed: The study provides valuable information, but it is just a starting point. Future research should investigate the influence of other potential factors on the price of N95 gasoline, including the role of government subsidies, supply chain disruptions, and consumer behaviour.

5 Conclusion

The findings of the research report highlight the complexity of the factors that influence the price of N95 gasoline. Although the absence of cointegration with Brent crude oil, diesel fuel and the CZK/USD exchange rate suggests a limited direct impact, it is important to remember that other economic factors and market dynamics can still influence prices. Further research is crucial to understand the intricate interplay of factors that ultimately shape the price of this essential item.

Acknowledgements

The authors received no financial support for the research, authorship and/or publication of this article.

Conflicts of interest

The authors declare that they have no known competing financial interests or personal relationships that could have appeared to influence the work reported in this paper.

References:

[1] BARBOSA, G., SOUSA, D., DA NOBREGA BESARRIA, C., LIMA, R., PITTA DE JESUS, D. Asymmetry in the prices of crude oil and diesel and gasoline prices in Brazil. *Journal of Economic Studies* [online]. 2024, **51**(1), p. 71-95 ISSN 0144-3585. Available from: https://doi.org/10.1108/JES-08-2022-0437

[2] ARUN, M. G., Dynamic fuel pricing in Jamshedpur, Chandigarh, Vizag, Puducherry, Udaipur from May. India Today [online]. 2017. Available from: https://www.indiatoday.in/magazine/up-front/story/20170501-fuel-price-change-daily-global-crude-oil-price-986240-2017-04-22

[3] OZDURAK, C., ULUSOY, V. Price discovery in crude oil markets: intraday volatility interactions between crude oil futures and energy exchange traded funds. *International Journal of Energy Economics and Policy* [online].

2020, **10**(3), p. 402-413. ISSN 2146-4553. Available from: https://www.econjournals.com/index.php/ijeep/article/view/9014

[4] CHOI, H., LEATHAM, D.J., SUKCHAROEN, K. Oil price forecasting using crack spread futures and oil exchange traded funds. *Contemporary Economics* [online]. 2015, **9**(1), p. 29-44. ISSN 2084-0845, eISSN 2300-8814. Available from: https://doi.org/10.5709/ce.1897-9254.158

[5] AROURI, M. E. H., LAHIANI, A., NGUYEN, D. K. Return and volatility transmission between world oil prices and stock markets of the GCC countries. *Economic Modelling* [online]. 2011, **28**(4), p. 1815-1825. ISSN 0264-9993, eISSN 1873-6122. Available from: https://doi.org/10.1016/j.econmod.2011.03.012

[6] BORENSTEIN, S., KELLOGG, R. The incidence of an oil glut: who benefits from cheap crude oil in the Midwest? *The Energy Journal* [online]. 2014, **35**(1), p. 15-34. ISSN 0195-6574, eISSN 1944-9089. Available from: https://doi.org/10.5547/01956574.35.1.2

[7] LI, Z., ZHAO, H. Not all demand oil shocks are alike: disentangling demand oil shocks in the crude oil market. *Journal of Chinese Economic and Foreign Trade Studies* [online]. 2011, **4**(1), p. 28-44. ISSN 1754-4408. Available from: https://doi.org/10.1108/17544401111106798

[8] CHOI, K., MING-HUA, L., ZHANG, Y. The relationship between refined retail oil prices and crude oil prices: a tale of three cities in the Greater Bay Area of China. *The Chinese Economy* [online]. 2021, **54**(3), p. 157-175. ISSN 1097-1475, eISSN. Available from: https://doi.org/10.1080/10971475.2020.1848471

[9] YUFENG, CH., HUANG, G., MA, L. Rockets and feathers: the asymmetric effect between China's refined oil prices and international crude oil prices. *Sustainability* [online]. 2017, **9**(3), 381. eISSN 2071-1050. Available from: https://doi.org/10.3390/su9030381

[10] SZOMOLANYI, K., LUKACIK, M., LUKACIKOVA, A. Estimation of asymmetric responses of U.S. retail fuel prices to changes in input prices based on a linear exponential adjustment cost approach. *CEJOR. Central European Journal of Operations Research* [online]. 2022, **30**(2), p. 757-779. ISSN 1435-246X, eISSN 1613-9178. Available from: https://doi.org/10.1007/s10100-021-00783-0

[11] ADRANGI, B., CHATRATH, A., RAFFIEE, K., RIPPLE, R. D., Alaska north slope crude oil price and the behavior of diesel prices in California. *Energy Economics* [online]. 2001, **23**(1), p. 29-42. ISSN 0140-9883, eISSN 1873-6181. Available from: https://doi.org/10.1016/S0140-9883(00)00068-2

[12] MANERA, M., GRASSO, M. Asymmetric error correction models for the oil-gasoline price relationship [online]. Working paper No. 75.2005. Milan: Eni Enrico Mattei Foundation (FEEM), 2005. Available from: http://dx.doi.org/10.2139/ssrn.731524

[13] CHENG, Y. Forecasting the delayed impact of energy price fluctuations on China's general prices based on a temporal input-output approach. *Energy Strategy Reviews* [online]. 2024, **52**, 101340. ISSN 2211-4688. Available from: https://doi.org/10.1016/j.esr.2024.101340

[14] ENGLE, R. F., GRANGER, C. W. J. Co-integration and error correction: representation, estimation, and testing. *Econometrica* [online]. 1987, **55**(2), p. 251-276. ISSN 0012-9682, eISSN. 1468-0262. Available from: https://doi.org/10.2307/1913236

[15] LEE, H., LEE, J. More powerful Engle-Granger cointegration tests. *Journal of Statistical Computation and Simulation* [online]. 2015, **85**(15), p. 3154-3171. ISSN 0094-9655, eISSN 1563-5163. Available from: https://doi.org/10.1080/00949655.2014.957206

[16] NORIEGA, A. E., VENTOSA-SANTAULARIA, D. The effect of structural breaks on the Engle-Granger test for cointegration. *Economical Studies of the College of Mexico / Estudios Economicos de El Colegio de Mexico* [online]. 2012, **27**(1), p. 99-132. ISSN 0188-6916, eISSN 0186-7202. Available from: https://doi.org/10.24201/ee.v27i1.94

[17] CAMBA JR, A., CAMBA, A. An Engle-Granger and Johansen cointegration approach in testing the validity of Fisher Hypothesis in the Philippines. *Journal of Asian Finance Economics and Business* [online]. 2021, **8**(12), p. 31-38. ISSN 2288-4637, eISSN 2288-4645. Available from: https://doi.org/10.13106/jafeb.2021.vol8.no12.0031

[18] HJALMARSSON, E., OSTERHOLM, P. Testing for cointegration using the Johansen methodology when variables are near-integrated: size distortions and partial remedies. *Empirical Economics* [online]. 2010, **39**, p. 51-76. ISSN 0377-7332, eISSN 1435-8921. Available from: https://doi.org/10.1007/s00181-009-0294-6

[19] HARRIS, R. *Using cointegration analysis in econometric modelling*. London: Harvester Wheatsheaf, Prentice Hall, 1995. ISBN 9780133558920.

[20] BILGILI, F. Stationarity and cointegration tests: comparison of Engle-Granger and Johansen methodologies. *Erciyes University Journal of Faculty of Economics and Administrative Sciences* [online]. 1998, **13**, p. 131-141. ISSN 1301-3688, eISSN 2630-6409. Available from: https://mpra.ub.uni-muenchen.de/75967/

[21] GONZALO, J., LEE, T. H., Pitfalls in testing for long run relationship. *Journal of Econometrics* [online]. 1998, **86**(1), p. 129-154. ISSN 0304-4076, eISSN 1872-6895. Available from: https://doi.org/10.1016/S0304-4076(97)00111-5

DETERMINATION OF OPTIMAL PARAMETERS FOR ULTRASONIC CLEANING OF VEHICLE RADIATORS

Aliya Kukesheva, Adil Kadyrov, Baurzhan Moldabaev, Kirill Sinelnikov, Akbope Karsakova, Elvira Kyzylbayeva*

Abylkas Saginov Karaganda Technical University NPJSC, Karaganda, Kazakhstan

*E-mail of corresponding author: elvirakiz@mail.ru

Aliya Kukesheva 0000-0002-3063-5870,
Baurzhan Moldabaev 0000-0002-2102-1834,
Akbope Karsakova 0009-0005-0305-6741,
Adil Kadyrov 0000-0001-7071-2300,
Kirill Sinelnikov 0000-0001-5073-5716,
Elvira Kyzylbayeva 0000-0002-0991-105X

Resume

The research presented in this article was concerned with the efficiency of ultrasonic cleaning of vehicle radiators based on the cavitation phenomenon. A technique has been developed that takes into account the effect of the ultrasonic vibration amplitude and the time of exposure on the process of removing contaminants. The results of experimental studies are presented that confirm that increasing the exposure time contributes to increasing the washed scale mass and decreasing the time of liquid outflow. The developed regression model describes well the changes in the mass of washed scale, which is confirmed by a high coefficient of determination and correlation. The obtained results allow for optimizing the parameters of the ultrasonic cleaning process, increasing its efficiency and reducing the risk of damage to the structural elements of the radiator.

Article info

Received 4 February 2025
Accepted 9 March 2025
Online 16 April 2025

Keywords:

vehicle radiators
ultrasonic cleaning
cavitation
vibration amplitude
exposure time
scale mass
regression analysis

Available online: https://doi.org/10.26552/com.C.2025.031

ISSN 1335-4205 (print version)
ISSN 2585-7878 (online version)

1 Introduction

Present day vehicle engine cooling systems play the key role in maintaining the efficient and safe operation of a vehicle. Being the main element of such systems, radiators are subject to significant operational loads, which leads to the accumulation of various types of contaminants on the inner surfaces of the tubes. Scale, rust, oil and organic deposits prevent the normal heat exchange and can significantly reduce the efficiency of cooling. This in turn leads to engine overheating, increased fuel consumption and decreasing the service life of the cooling system. Therefore, the problem of cleaning radiators and maintaining them in optimal condition is relevant to ensure reliable operation of vehicles.

Traditional methods of cleaning radiators, such as mechanical and chemical cleaning, have a number of disadvantages. Mechanical cleaning damages the inner surfaces of the tubes, especially in narrow and hard-to-reach places. Chemical reagents in turn cause metal corrosion. For example, studies carried out by Said et al. prove that standard chemical methods compromise the design of the radiator and reduce their overall performance [1]. Studies carried out by Habeeb et al. also confirm that chemical compounds have a negative impact on aluminum radiators and lead to increased corrosion [2].

In addition, some reagents are difficult to completely remove from the system after the cleaning, which affects the durability of radiator materials. The use of aggressive chemicals requires careful handling and special disposal procedures, which increases the cleaning costs and creates potential risks for the environment. In this regard, the use of ultrasonic cavitation for cleaning radiator tubes is an optimal method.

Ultrasonic exposure is an effective cleaning method due to the phenomenon of cavitation. Bubbles that arise in the liquid under ultrasonic exposure collapse and generate hydrodynamic forces, reaching temperatures of up to 10,000 °C. This allows for the effective removal of scale and dirt from radiator tubes. A study carried out by Yamashita et al. shows that cavitation effects provide a multiple increase in the cleaning coefficient [3].

In previous studies [4-5], the theoretical and experimental foundations of the use of ultrasound

for cleaning vehicle radiators were established, which confirmed its effectiveness due to cavitation processes. However, in those studies the effect of the key parameters of ultrasonic action on the cleaning efficiency indicators was not considered, in particular characteristics of the ultrasound effect on the mass of scale washed out. In this regard, the hypothesis of the study was the probability of increasing the mass of scale washed out of the radiator tubes due to changing the amplitude indicators and increasing the accumulated time of exposure to ultrasonic vibrations.

The goal of the study was to establish dependences that describe changing the mass of washed scale from the amplitude and accumulated time of exposure to ultrasonic vibrations.

To achieve the goal of the study, the following tasks were solved:

- analyzing the existing studies and establishing the degree of the parameters effect on the cavitation and cleaning processes;
- using the similarity theory and dimensional analysis, additional similarity criteria were obtained that allowed evaluating the cleaning efficiency;
- the design of the developed experimental bench for cleaning radiator tubes was improved;
- experimental studies were carried out on the stand;
- the obtained results were analyzed;
- a regression equation was obtained that described changing the mass of washed scale depending on the exposure time and the amplitude of ultrasonic vibrations;
- the optimal amplitude values were determined according to the obtained similarity criterion.

The scientific novelty lies in obtaining dependencies that allow studying the pattern and the efficiency of the ultrasonic cavitation process.

The practical significance of the study consists of the following:

- further development of an effective method of ultrasonic cleaning of radiators, ensuring the removal of dirt and scale without risk of damaging structural elements;
- reducing maintenance costs and extending the service life of radiators;
- the possibility of industrial application of the proposed technology for servicing vehicle radiators;
- improving the environmental safety of the technology of cleaning radiator tubes by eliminating aggressive chemicals.

2 Materials and methods

The results of studies by a number of well-known scientists in the field of ultrasonic cavitation cover the period of 1934-2020 (Figure 1) and contribute to more detailed understanding of the cavitation mechanism and establishment of the factors affecting the efficiency of cleaning (Table 1).

The analysis of the results of studies by scientists in this area made it possible to establish the key parameters that affect the cavitation process (Table 2).

Among the parameters considered, and according to the technical characteristics of the ultrasonic equipment operating at one frequency and power, as well as the conditions of the experimental studies, the most adjustable and fixed parameters that directly affect the cleaning result are the duration of ultrasound exposure and the amplitude of ultrasonic vibrations.

Despite the significant studies conducted in the previous works [4-5, 21-24] on ultrasonic cleaning of radiator tubes, the experimental technique had certain limitations that did not allow for complete determination of the optimal parameters of the cleaning process. In particular, insufficient attention was paid to the effect of such parameters as the cumulative effect of

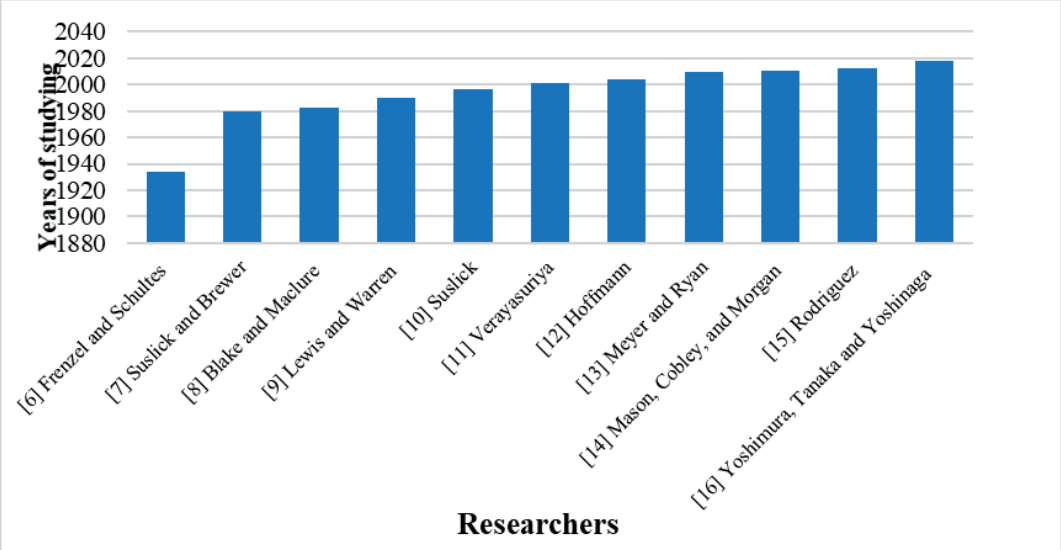

Figure 1 *The timeline of research in the field of ultrasonic cavitation*

Table 1 *Results of the scientists' studies the area of ultrasonic cavitation*

Researchers	Research area	Main results
Frenzel and Schultes	Low pressure high intensity ultrasound cavitation	It has been established that ultrasonic cavitation creates local zones with high temperatures and pressures, which improves cleaning due to microexplosions and mechanical action [6].
Suslick and Brewer	Chemical effects of cavitation	It has been found that the collapse of bubbles forms radicals (hydroxide and hydrogen), which destroy organic contaminants. The study is important for environmental cleaning technologies [7].
Blake and Maclure	Effect of pressure and fluid composition	The optimum pressure for cavitation is 1.5-2 bar. Carbon dioxide and oxygen enhance bubble stability and improve cleaning efficiency [8].
Lewis and Warren	Viscosity and chamber geometry	Using low-viscosity liquids and an optimized chamber improves cavitation and bubble collapse [9].
Suslick	Effect of ultrasound frequency	It has been shown that low frequencies (20-40 kHz) contribute to the formation of large bubbles, which increase the intensity of cleaning due to powerful collapse [10].
Verayasuriya	Effect of temperature on cavitation	It has been established that at the temperature of 30-60 °C, cleaning efficiency increases due to a decrease in the viscosity and density of the liquid. Adding gases also enhances the effect [11].
Hoffmann	Chemical additives to enhance cavitation	Adding hydrogen peroxide increases the formation of hydroxide radicals, which improves the destruction of organic contaminants [12].
Meyerand Ryan	Duration of ultrasonic action	Short sessions (about 10 minutes) are quite effective for cleaning, while longer sessions increase the risk of damaging materials [13].
Mason, Cobley, Graves and Morgan	Mechanical impact of cavitation on metal	Under certain conditions, cavitation can cause erosion of metal surfaces, which is important to consider when developing cavitation systems [14].
Rodriguez	Cavitation for water disinfection	A study showed that ultrasonic cavitation can effectively destroy bacteria and viruses in water without the use of chemicals, which opens up new possibilities for water purification [15].
Yoshimura, Tanaka and Yoshinaga	Effect of ultrasound power	Increasing the ultrasound power to 500 W improves the cleaning of metal parts from rust and oils without aggressive chemicals [16].

Table 2 *Key parameters that affect the process of cleaning the radiator tubes with ultrasound*

Parameter	Description
Ultrasound frequency	Low frequencies for removing dense dirt (scale, rust); high frequencies for delicate cleaning.
Amplitude of ultrasonic vibrations	High amplitude for dense dirt, but exceeding the value can damage the radiator tubes [17].
Power	High power increases the intensity of bubble collapse, which enhances cleaning; low power is suitable for delicate cleaning [18].
Duration of exposure	Long exposure allows removing stubborn dirt; short exposure is suitable for delicate cleaning, reducing the risk of tube wear.
Homogeneity of wave distribution	Uniform distribution of waves ensures effective cleaning of the entire surface, including hard-to-reach areas [19].
Temperature of ultrasonic transducer	Optimum temperature stabilizes the ultrasonic effect and increases the efficiency of cavitation, extending the service life of the equipment [20].

the time of ultrasound exposure and the amplitude of ultrasonic vibrations on the cleaning efficiency, which limited the understanding of their role in increasing the effectiveness of the cleaning process and preventing damage to the cleaned surface.

The time of ultrasound exposure is critically important, since increasing its duration contributes to a longer effect of cavitation bubbles on contaminants, which improves the removal of stubborn deposits. The amplitude of ultrasonic vibrations, in turn, determines the level of energy transferred to the bubbles and directly affects the intensity of their collapse, the release of energy in the form of microjets and shock waves, which increases their destructive effect on deposits. These parameters have the key impact on the main indicator of cleaning efficiency: the mass of removed contaminants. Optimization of these parameters can significantly increase the efficiency of the process, while

minimizing the risk of damage to the cleaned surface. The absence of a detailed study of these factors limits the ability to fine-tune ultrasonic cleaning for different types of contaminants in radiator tubes.

In the previous studies, using the similarity theory and dimensional analysis methods, the criteria were determined by which the efficiency of tube cleaning by ultrasonic cavitation was assessed. However, the criteria obtained did not take into account the parameters of the mass of scale removed and the amplitude of ultrasonic waves. Therefore, the additional calculations of the similarity criteria were performed, taking into account the parameters of time, ultrasound amplitude and the mass of scale removed. According to the method of determining the similarity criteria, an equation was drawn up for the mass of scale removed dependence on the remaining parameters:

$$m = f(r,\rho,g,A,m,t)\,. \tag{1}$$

From here follows the equation:

$$\varphi(r,\rho,g,A,m,t) = 0\,. \tag{2}$$

Then all the variables were transformed according to their dimensions in relation to three basic units of measurement: length L, mass M and time T (Table 3).

A detailed methodology of calculating the criteria is presented in the previous studies [5]. Based on this methodology, the calculation of similarity criteria was performed. The calculation results are shown in Table 4.

Then, the obtained criteria were transformed among themselves by means of a mutual relationship, as a result of which a single criterion was obtained.

$$k = \frac{m \cdot t}{r^{3/2}\sqrt{g}\,\rho A} \tag{3}$$

The physical meaning and significance of the obtained criterion is as follows. The obtained criterion reflects the balance between the time, geometric and energy characteristics of the ultrasonic cleaning process, indicating the efficiency of interaction of the system parameters. If the value of k > 1, that indicates that more time is required to remove contaminants, or the mass of contaminants is large relative to the geometry and energy characteristics of the system. This means that the system is not efficient enough, and optimization of such parameters as the ultrasound amplitude or the exposure time, is required. If k < 1, this indicates predominance of the effect of energy parameters, indicating high cleaning efficiency with relatively low time costs.

If k = 1, this indicates the balance of the system between the time, geometric and energy characteristics of the ultrasonic cleaning process. This means that the system operates with the optimal efficiency, where time and energy costs are in balance, and each of the parameters makes an equal contribution to the cleaning process. However, to confirm the optimality of the parameters by this criterion, experimental studies are required.

Thus, the application of the similarity theory method was justified for such complex processes as cavitation, since a complete mathematical analysis of the behavior

Table 3 *Dimension formulas for the main values of variables*

No.	Variable	Designation	Unit	Dimension formula
1	Tube radius	r	m	L
2	Tube length	l	m	L
3	Liquid density	ρ	kg/m^3	ML^{-3}
4	Gravity acceleration	g	m/s^2	LT^{-2}
5	Ultrasound exposure time	t	s	T
6	Ultrasound amplitude	A	m	L
7	Mass of scale washed out	m	kg	M

Table 4 *Results of calculating the criteria*

Parameter	Amplitude	Time	Mass
Methodology of calculating	$\pi_1 = r^{x1}\rho^{y1}g^{z1}A^{-1}$ $\pi_1 = L^{x1}\left(\frac{M}{L^3}\right)^{y1}\left(\frac{L}{T^2}\right)^{z1}(L)^{-1}$, $\pi_1 = L^{x1-3y1+z1-1}M^{y1}T^{-2z1}$, $\begin{cases} x_1 - 3y_1 + z_1 - 1 = 0 \\ y_1 = 0 \\ -2z_1 = 0 \end{cases}$, $x_1 = 1, y_1 = 0, z_1 = 0.$	$\pi_2 = r^{x2}\rho^{y2}g^{z2}t^{-1}$ $\pi_2 = L^{x2}\left(\frac{M}{L^3}\right)^{y2}\left(\frac{L}{T^2}\right)^{z2}(T)^{-1}$, $\pi_2 = L^{x2-3y2+z2-1}M^{y2}T^{-2z2-1}$, $\begin{cases} x_2 - 3y_2 + z_2 = 0 \\ y_2 = 0 \\ -2z_2 - 1 = 0 \end{cases}$, $x_2 = -1/2, y_2 = 0, z_2 = 1/2.$	$\pi_3 = r^{x3}\rho^{y3}g^{z3}m^{-1}$ $\pi_3 = L^{x3}\left(\frac{M}{L^3}\right)^{y3}\left(\frac{L}{T^2}\right)^{z3}(m)^{-1}$, $\pi_3 = L^{x3-3y3+z3}M^{y3-1}T^{-2z3}$, $\begin{cases} x_3 - 3y_3 + z_3 = 0 \\ y_3 = 0 \\ -2z_3 = 0 \end{cases}$, $x_3 = 3, y_3 = 1, z_3 = 0.$
Criterion obtained	$\pi_1 = \frac{r}{A}$	$\pi_2 = \sqrt{\frac{r}{g}}t$	$\pi_3 = \frac{r^3\rho}{m}$

Figure 2 *Experimental bench for cleaning radiator tubes*

a) ultrasonic emitter

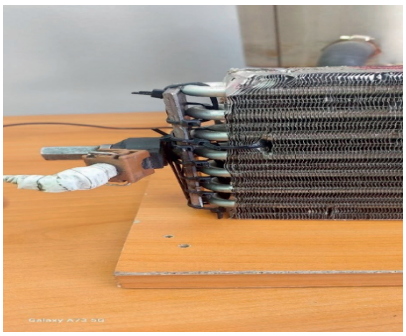

b) knock sensor

Figure 3 *Ultrasonic emitter and knock sensor placed on the radiator*

of cavitation bubbles is difficult due to the many factors affecting the process. Thanks to the criterion obtained, not only the cleaning process is described but the conditions for effective removal of contaminants, as well. The proposed criterion for the effectiveness of ultrasonic radiator cleaning can be applied to all the other types of radiators, such as, radiators of aviation and marine engines, heating and air conditioning systems, as well as the heat exchangers used in nuclear energy. All those systems are subject to contamination during operation, and the use of ultrasonic cavitation for their cleaning can significantly improve efficiency and extend service life without the risk of damaging the structural elements. At the same time, it is necessary to consider the specifics of each type of radiator, including parameters such as tube material, operating environment, and the level of contamination.

Then, experimental studies were carried out to determine the mass of washed scale depending on changing the time and amplitude parameters. The study was conducted on a more advanced experimental bench (Figure 2).

The main element of the bench was a heater radiator with operational deposits. To create an ultrasonic effect, a transmitter with the operating frequency of 40 kHz and power of 50 W was mounted and fixed on one of the ends of the radiator (Figure 3, a). On the opposite side of the radiator, a detonation sensor was placed to record the amplitude of ultrasonic vibrations (Figure 3, b).

An oscilloscope was used to monitor and to record the amplitude characteristics of the oscillations, and a circulation system supplied liquid through the radiator. The liquid temperature was maintained at 50 °C.

At the first stage, the radiator was filled with a liquid, and the initial parameters were recorded, including the mass and density of the liquid, as well as the time it took to flow through the radiator. Then, the ultrasonic emitter was turned on, and the initial value of the ultrasonic wave amplitude was recorded.

At the second stage of the experiment, the ultrasonic emitter was turned on, the effect of which was carried out over a specified time interval of 600 seconds. At the end of this time interval, the key parameters were measured: the time of liquid flow through the radiator, the mass of the liquid, the density of the liquid, the mass of the washed-out scale (calculated as the difference in the mass of the sediment before and after the effect). The procedure for ultrasound exposure and measurements was repeated three times with accumulation of the cleaning effect.

3 Results

The results of experiments are presented in Table 5.

The obtained experimental results indicate a gradual increase in the efficiency of radiator cleaning with each cycle of ultrasound exposure.

This approach allowed objective evaluating of the efficiency of ultrasound exposure, linking its parameters with the quality characteristics of the purified liquid and

Table 5 *Results of experimental studies*

Ultrasound action	Added time of exposure to ultrasound, s	Amplitude, m	Outflow time, s	Liquid mass, g	Liquid density, g/m^3	Mass of scale washed out, g
Before the ultrasound action	-	2.01	12.54	44.55	0.990000	0.00
With ultrasound action, f = 40 kHz	600	2.1	12.09	44.56	0.990222	0.01
	1200	2.26	11.39	44.6	0.991111	0.05
	1800	2.29	11.03	44.79	0.995333	0.24

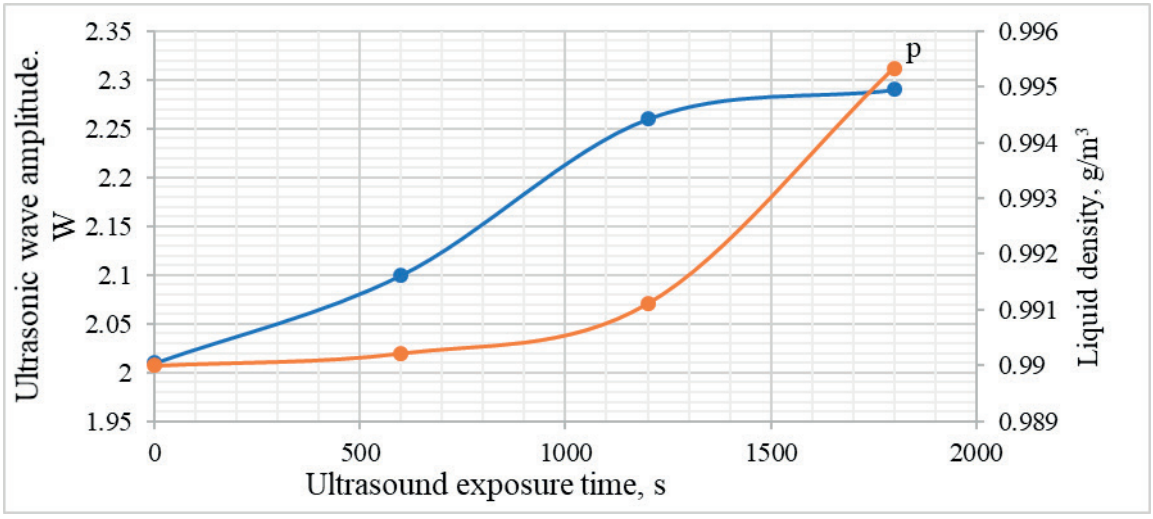

Figure 4 *Changing the ultrasound amplitude and liquid density with increasing the ultrasound exposure time*

the mass of contaminants removed from the radiator tubes.

Based on the obtained results of experimental studies, graphs of the parameters of ultrasound amplitude and liquid density dependence on the time of ultrasound exposure were constructed.

The graph in Figure 4 shows the amplitude increasing with increasing the cumulative effect of the ultrasound exposure time. This is due to increasing the efficiency of energy transfer from the emitter to the medium. Ultrasonic waves are reflected from the tube walls and create multiple reflections. As a result, the waves add up, which leads to increasing the amplitude of pressure and vibration in the liquid.

Increasing the amplitude when ultrasound affects the liquid in radiator tubes is caused not only by a combination of resonance, interference and cavitation effects but by the geometry of the tubes and changes in the properties of the liquid under the effect of ultrasonic waves, as well. Narrow and long radiator tubes act as waveguides focusing ultrasonic energy. This focusing leads to the concentration of energy and increasing the amplitude of sound pressure in a limited space.

Ultrasound creates acoustic flows in the liquid (the liquid movement under the effect of sound waves). These flows increase turbulence and the movement of bubbles, which leads to additional increasing the oscillations amplitude.

The graph also shows increasing of the liquid density with increasing the time of ultrasound exposure. This indicates that with each cycle of ultrasound exposure, the number of particles remaining in the liquid increases. This accumulation explains the gradual increasing of the density. When the density of a liquid increases, it means that the mass of liquid per unit volume also increases. The mass of the liquid has increased due to the inclusion of solid particles that were previously part of the contaminants. This indicates that ultrasound is successfully breaking down and dispersing contaminants.

According to the graph in Figure 5 the reduction in the time it takes for the liquid to flow through the radiator and the increase in the mass of scale washed out are interconnected and indicate the effectiveness of ultrasonic cleaning. When exposed to ultrasound, scale and deposits that previously partially blocked the passage of liquid through the radiator tubes are destroyed. Ultrasonic vibrations create cavitation bubbles that affect the contaminants, breaking them off and destroying them. With each cleaning cycle, these contaminants are gradually removed, which leads to increasing the diameter of the tubes and decreasing their hydraulic resistance. As a result, the flow of liquid

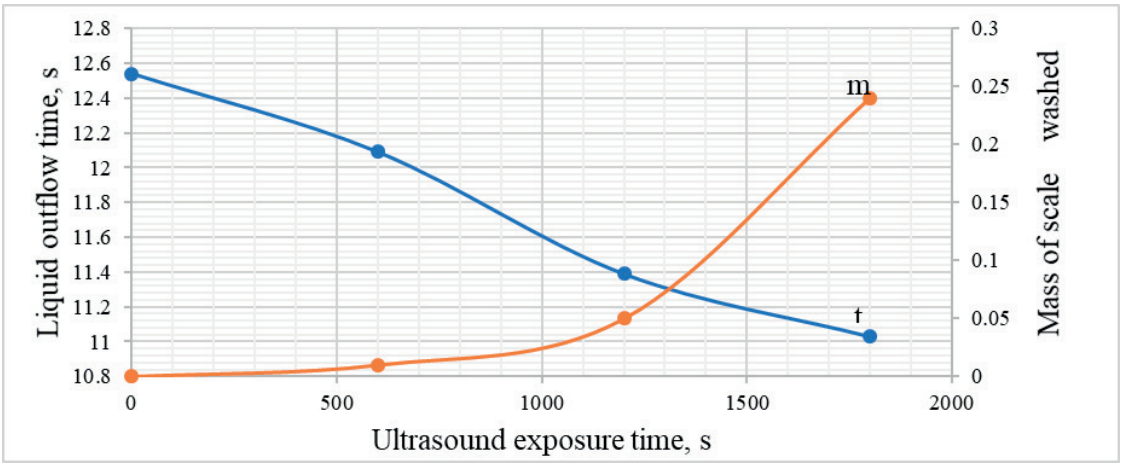

Figure 5 *Changing the liquid outflow time and the mass of scale washed out with increasing the ultrasound exposure time*

through the radiator becomes freer, which reduces its flow time.

At the same time, the mass of scale washed out increases, since each new cycle of ultrasonic action removes both the surface and deep layers of deposits. Ultrasound destroys the structure of contaminants, converting them into a finely dispersed state, which is then washed out of the system. This process has a cumulative effect: the longer the exposure, the more contaminants are removed. As a result, the mass of scale washed out increases linearly, reflecting the progressive cleaning of the radiator.

Thus, the reduction in the liquid outflow time and the increase in the mass of washed-out scale complements each other, demonstrating the effectiveness of ultrasonic cleaning. These changes demonstrate that ultrasound not only improves permeability of liquid through the radiator but also actively removes contaminants, improving the overall performance of the system.

Based on the results of experimental studies, a multivariate regression equation was compiled that described the change in the mass of washed-out scale from the time of ultrasound exposure and the amplitude of ultrasonic waves.

$$m = 8.88 \cdot 10^{-6} A^2 - 51.3 \cdot 10^{-6} At - \\ - 1.98 \cdot 10^{-6} A + 1.78 \cdot 10^{-7} t^2 + \\ + 986 \cdot 10^{-6} t + 3.99 \cdot 10^{-5} \quad (4)$$

The use of this type of regression is due to the fact that the dependent variable (m) is determined by several independent experimental variables A and t. Unlike the one-dimensional regression that considers the effect of only one of the factors, multivariate regression more accurately reflects complex relationships between variables, which is especially important for analyzing processes where the result depends on the interaction of several parameters.

The obtained value of the determination coefficient ($R^2 = 0.98$) according to the regression equation shows that the multivariate regression model describes well the dependence of the mass of washed scale on the exposure time and the amplitude of ultrasonic waves. This means that the model is reliable for describing the cleaning process within these limits.

The obtained value of the correlation coefficient (r = 0.97) also indicates a strong linear relationship between the predicted model and the actual experimental values. This confirms that the model accurately describes changes in the scale mass with changes in time and amplitude. The approximation error shows that on average the regression model predictions deviate from the experimental data by 1.84%. This error rate is due to the small number of experimental runs, which limits the accuracy of the model. Therefore, to reduce the approximation error, it is necessary to increase the number of experimental runs.

Based on the obtained regression equation, the mass of washed scale was calculated (Table 6).

Then, a comparison was made between the experimental values and the calculated values from the regression equation for the mass of removed scale, taking into account the cumulative ultrasonic exposure time (Figure 6).

The graph in Figure 6 shows how accurately the regression model describes the process of ultrasonic radiator cleaning and how the experimental data compares to theoretical calculations.

Comparison to the regression equation shows that the calculated model matches the experimental data, with a small deviation. The deviation can be caused by the fact that experimental conditions, such as the heterogeneity of contaminants, or the dynamics of their removal, are not fully taken into account in the model.

The three-dimensional graph in Figure 7 also highlights the importance of the duration of ultrasound exposure: longer exposure allows removing not only the surface but the deeply embedded contaminants, as well. The increase in the mass of washed-out scale confirms that ultrasound successfully copes with the destruction

Table 6 *The calculated mass of washed out scale based on the regression equation*

Time (s)	Amplitude (m)	Mass based on the experimental results (g)	Mass based on the regression equation (g)
0	2.01	0.00	0.0320
600	2.10	0.01	0.0092
1200	2.26	0.05	0.0480
1800	2.29	0.24	0.2360

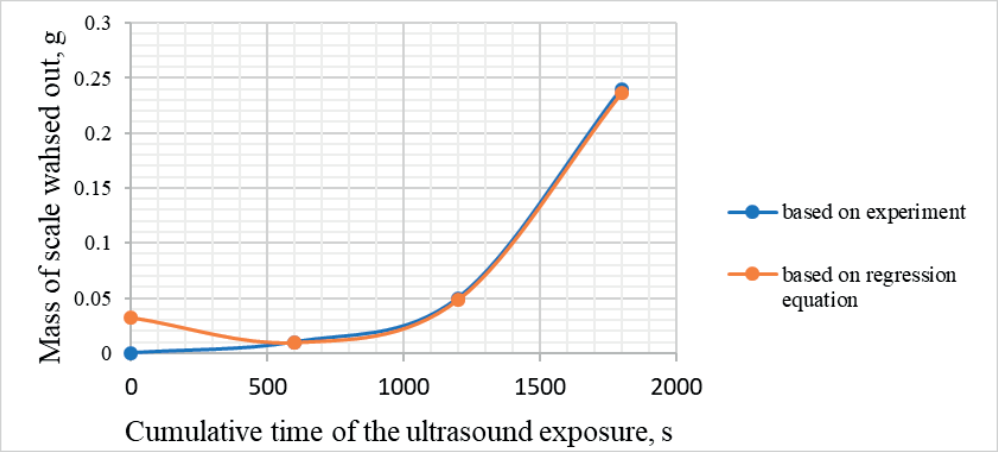

Figure 6 *Regression model for the process of radiator ultrasonic cleaning*

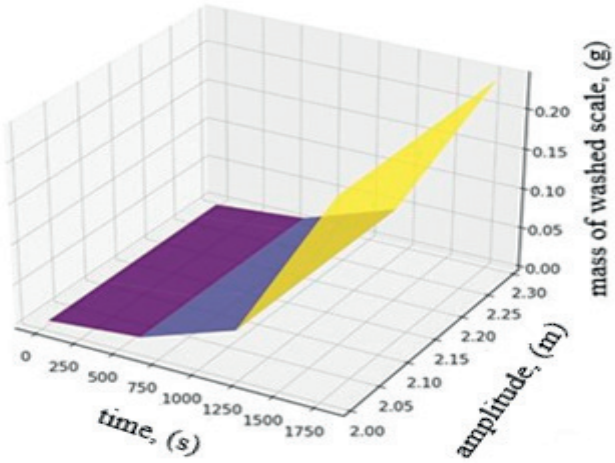

Figure 7 *The change in the mass of removed scale as a function of time and amplitude*

of various layers of deposits, and this is a key factor in increasing the efficiency of cleaning.

The lilac area in the graph is located between the purple and yellow zones and represents intermediate values of the mass of removed scale. This zone shows that the cleaning process is already actively underway, and the mass of removed contaminants is increasing, although it has not yet reached maximum values. The lilac area corresponds to moderate values of ultrasound exposure time and average amplitude of ultrasonic vibrations. It demonstrates the transitional stage of cleaning, when ultrasonic cavitation is already effectively affecting contaminants, but the time and energy of exposure are not yet sufficient to completely remove stubborn deposits. In this zone, deposits are partially destroyed, but the rate of their removal is lower than in the yellow zone, where the process reaches maximum intensity. Thus, the purple area shows how cleaning gradually gains efficiency as the time and amplitude of ultrasound increases, moving towards the yellow zone, where the greatest results are achieved.

On the whole, the graph demonstrates that the proposed regression model can be used to predict cleaning results, but its accuracy depends on the specifics

of the contaminants and the experimental conditions.

Then a mathematical analysis of the regression equation was carried out, which made it possible to determine how changes in the amplitude (A) and the time (t) affect the mass of washed scale (m). Partial derivatives of the equation were determined, which made it possible to establish the rate of change in mass m with changes in A and t:

Partial derivatives of the regression equation are as follows:
by the amplitude:

$$\frac{dm}{dA} = -1.776 \cdot 10^{-5}A - \\ -0.000513t - 1.98 \cdot 10^{-6}, \quad (5)$$

by the time:

$$\frac{dm}{dt} = -0.000513A + 356 \cdot 10^{-7}t + 0.000986\,, \quad (6)$$

show that the amplitude reduces the mass of scale removed, especially at high values, and increasing the time always contributes to its growth.

Then, the critical points of the equations were determined, provided that $\frac{dm}{dA} = 0$ and $\frac{dm}{dt} = 0$. The solution of the two systems of equations is as follows:

$$\begin{cases} -1.776 \cdot 10^{-5}A - 0.000513t - 1.98 \cdot 10^{-6} = 0, \\ -0.000513A + 3.56 \cdot 10^{-7}t + 0.000986 = 0, \end{cases} \quad (7)$$

and it allowed obtaining the critical values of the parameters A = 1.92, t = –0.07, at which the change in the mass of washed-out scale m in terms of the amplitude (A) and the time (t) stops. However, the time cannot be negative in the physical sense, so there is no extremum of the function, and in the region t > 0 the function m = f(A,t) monotonically increases with the time t. This is also confirmed by the second derivative of the equations, which describes the nature of the critical point:
by the amplitude:

$$\frac{d^2m}{dA^2} = -1.776 \cdot 10^{-5}, \quad (8)$$

by the time:

$$\frac{d^2m}{dt^2} = 3.56 \cdot 10^{-7}, \quad (9)$$

by the amplitude and the time:

$$\frac{d^2m}{dAdt} = -0.000513A\,. \quad (10)$$

According to the calculated Hessian determinant H = $-2.63 \cdot 10^{-7}$, it is negative (H < 0), which indicates a saddle point. This means that the function behaves in different directions. With increasing the time (t), the mass of washed-out scale (m) increases, and with increasing the amplitude (A), the mass (m) decreases. This means that an increase in time (t) always contributes to an increase in the mass of washed-out scale, and the amplitude value A should not go beyond the boundary values of its negative impact.

Therefore, to optimize the cleaning process, the amplitude A and the time t should be selected so as to take into account their combined effect, namely, to increase t so that the mass grows and to control A to avoid its excessive decrease.

Then, according to the established criterion k, which describes how efficiently the cleaning system uses its energy resources, the optimal amplitude values are determined, which must be adjusted for different degrees of contamination by the mass of washed out scale.

$$k = \frac{m \cdot t}{r^{3/2}\sqrt{g}\,\rho A} \rightarrow A = \frac{m \cdot t}{r^{3/2}\sqrt{g}\,\rho k} \quad (11)$$

where k = 1, since its value indicates the balance of the cleaning system between the time, geometric and energy characteristics of the ultrasonic cavitation process. This confirms that the time and energy costs are balanced, and each parameter makes an equal contribution to the cleaning efficiency.

Table 7 *Results of calculating the amplitude optimal values*

No.	Scale mass, kg	Time, s	Radiator tube radius, m	Cooling liquid density, kg/m^3	Optimal amplitude, 10^{-3} m
1	0.005	600	0.005	1070	2.56
2	0.01				5.12
3	0.015				7.68
4	0.02				10.24
5	0.025				12.79
6	0.03				15.35
7	0.035				17.91
8	0.04				20.47
9	0.045				23.03
10	0.05				25.59

During the standard ultrasonic cleaning, the mass of the removed scale varies from 5 to 50 grams, which is determined by the degree of contamination of the tubes. Modern aluminum radiators are characterized by a standard tube radius in the range from 2 to 5 mm. The ultrasound exposure time in the experiments was 600 seconds. The average density of the coolant used in radiators with antifreeze is about 1070 kg/m^3. The results of calculating the optimal amplitude values are presented in Table 7.

The obtained amplitude values allow for carrying out further studies and obtaining more accurate results on the degree of radiator tubes cleaning by ultrasonic cavitation.

4 Conclusion

Based on the studies carried out, the high efficiency of ultrasonic cleaning of vehicle radiators due to the cavitation phenomenon has been proven. The results of experimental studies have shown that increasing the ultrasound exposure time leads to a significant increase in the mass of washed-out scale, improved liquid characteristics and reducing the flow time.

The developed regression model confirmed a strong relationship between the process parameters, such as the amplitude and the exposure time, with the cleaning efficiency indicators. The resulting regression model makes it possible to establish the quantitative dependences between the process parameters, which provides predicting the cleaning results under various conditions. It has been established that the exposure time has a positive effect on the cleaning results, while increasing the amplitude requires precise optimization to prevent a negative effect. The identified saddle point in the parameter system emphasizes the need to balance the amplitude and the exposure time to achieve the maximum cleaning efficiency. According to the obtained criterion, the optimal values of the ultrasonic vibration amplitude were determined depending on the values of the washed-out scale mass. The optimum amplitude values were determined at $k = 1$, demonstrating the optimum balance of the system between the time, geometric and energy characteristics of the ultrasonic cleaning process. The obtained results confirm that the use of ultrasound can significantly improve the operational characteristics of radiators, reducing their maintenance costs and increasing their service life. The practical significance of the results lies in the development of an ultrasonic cleaning technique that ensures the removal of contaminants without the risk of damaging the radiator structural elements, as well as in the possibility of its industrial application.

Future research in this field may focus on studying the effect of ultrasonic frequency on cleaning efficiency. Investigating different frequency ranges will help determine the optimal parameters for removing specific contaminants while minimizing potential destructive effects on radiator materials. Optimizing cavitation parameters is another important area, as the power of ultrasonic exposure and the characteristics of cavitation bubbles directly influence the cleaning quality. Computer modelling of these processes will help predict the conditions under which cavitation is most effective.

Additionally, it is important to consider the influence of radiator geometry on the propagation of ultrasonic waves. Research can focus on analyzing the shape of tubes and their ability to transmit ultrasonic vibrations, allowing the method to be adapted to radiators of various configurations. Another key aspect is the durability of radiators after the regular ultrasonic exposure. Studies should assess the long-term effects of ultrasonic vibrations on radiator materials and determine the economic efficiency of this method compared to traditional mechanical and chemical cleaning techniques. These future research directions would not only enhance the effectiveness of ultrasonic cleaning but would expand its applications, as well, making the radiator cleaning process safer, more cost-effective, and more versatile.

Acknowledgements

The authors received no financial support for the research, authorship and/or publication of this article.

Conflicts of interest

The authors declare that they have no known competing financial interests or personal relationships that could have appeared to influence the work reported in this paper.

References

[1] SAID, Z., ASSAD, M. E. H., HACHICHA, A. A., BELLOS, E., ABDELKAREEM, M. A., ALAZAIZEH, D. Z., YOUSEF, B. A. Enhancing the performance of automotive radiators using nanofluids. *Renewable and Sustainable Energy Reviews* [online]. 2019, **112**(14), p. 183-194 accessed [2019-05-23]. ISSN 1364-0321. Available from: https://doi.org/10.1016/j.rser.2019.05.052

[2] HABEEB, H., MOHAN, A., NORANI, N., AZMAN, M., ABDULLAH, M. H. H. Analysis of engine radiator performance at different coolant concentrations and radiator materials. *International Journal of Recent*

Technology and Engineering [online]. 2020, **8**(6), p. 2277-3878 accessed [2020-03-01]. ISSN 2277-3878. Available from: https://doi.org/10.35940/ijrte.F7866.038620

[3] YAMASHITA, T., YAMAUCHI, R., ANDO, K. Progress in ultrasonic cleaning research. *Japanese Journal of Multiphase Flow* [online]. 2018, **32**(2), p. 210-217 accessed [2018-05-10]. ISSN 0914-2843. Available from: https://doi.org/10.1016/j.rser.2019.05.052

[4] KADYROV, A., SINELNIKOV, K., SAKHAPOV, R., GANYUKOV, A., KURMASHEVA, B., SUYUNBAEV, S. Studying the process of transport equipment cooling system ultrasonic cleaning. *Communications - Scientific Letters of the University of Zilina* [online]. 2022, **24**(4), p. 288-300 [accessed 2022-07-28]. ISSN 1335-4205. Available from: https://doi.org/10.26552/com.C.2022.4.B288-B300

[5] MOLDABAEV, B., SINELNIKOV, K., KUKESHEVA, A. Justification of the method of vehicle engine radiator ultrasonic cleaning. *Communications - Scientific Letters of the University of Zilina*. 2025, **27**(1), p. 75-84 [accessed 2024-11-26]. ISSN 1335-4205. Available from: https://doi.org/10.26552/com.C.2025.015

[6] FRENZEL, H., SCHULTES, H. Luminescence in water exposed to ultrasound/Luminescenz im ultraschallbeschickten Wasser (in German). *Zeitschrift für Physikalische Chemie / International Journal of Research in Physical Chemistry and Chemical Physics* [online]. 1934, **27**(1), p. 421-424 [accessed 1934-10-26]. ISSN 2196-7156. Available from: https://doi.org/10.1515/zpch-1934-0137

[7] SUSLICK, K., BREWER, K. Studying chemical effects of cavitation, formation of hydroxyl and hydrogen radicals initiated by ultrasound, and application in the purification of liquid media. *Sonochemistry and Cavitation. Ultrasonics*. 1980, **19**(2), p. 59-62. ISSN 0041-624X.

[8] BLAKE, J. C., MACLURE, A. C. Pressure and liquid composition effect on cavitation dynamics. *Physics of Fluids*. 1983, **26**(2), p. 122-128. ISSN 1089-7666.

[9] LEWIS, D. M., WARREN, R. A. Viscosity and chamber geometry effects on cavitation. *Ultrasonic Sonochemistry*. 1990, **4**(4), p. 229-234. ISSN 1873-2828.

[10] SUSLICK, K. S. Sonoluminescence and sonochemistry. In: 1997 IEEE Ultrasonics Symposium Proceedings. An International Symposium (Cat. No. 97CH36118): proceedings [online] [accessed 1997-08-05]. IEEE. 1997. ISSN 1051-0117, p. 523-532. Available from: https://doi.org/10.1109/ULTSYM.1997.663076

[11] VERAYASURIYA, V. K. Temperature effects on cavitation and ultrasonic cleaning efficiency. *Journal of Applied Physics*. 2001, **90**(7), p. 3575-3581. ISSN 1089-7550.

[12] HOFFMANN, F. S. Studying chemical additives impact on cavitation efficiency. *Chemical Engineering Journal*. 2004, **98**(3), p. 193-200. ISSN 1385-8947.

[13] MEYER, S. L., RYAN, M. P. Duration and ultrasonic impact on cavitation effectiveness. *Ultrasonics*. 2010, **50**(6), p. 514-520. ISSN 1874-9968.

[14] MASON, T. J., COBLEY, A. J., GRAVES, J. E., MORGAN, D. New evidence for the inverse dependence of mechanical and chemical effects on the frequency of ultrasound. *Ultrasonics Sonochemistry* [online]. 2011, **18**(1), p. 226-230 [accessed 2011-01-05]. ISSN 1350-4177. Available from: https://doi.org/10.1016/j.ultsonch.2010.05.008

[15] RODRIGUEZ, M. D. C. M. Ballast water and sterilization of the sea water. In: *Municipal and industrial waste disposal*. YU, X.-Y. (Ed.). London: IntechOpen, 2012. ISBN 978-953-51-0501-5.

[16] YOSHIMURA, T., TANAKA, K., YOSHINAGA, N. Nano-level material processing by multifunction cavitation. *Nanoscience and Nanotechnology - Asia* [online]. 2018, **8**(1), p. 41-54 [accessed 2016-08-30]. ISSN 2210-6812. Available from: 10.2174/2210681206666160922164202

[17] BARNETT, S. Nonthermal issues: cavitation - its nature, detection and measurement. *Ultrasound in Medicine and Biology* [online]. 1998, **24**(1), p. S11-S21. ISSN 0301-5629. Available from: https://doi.org/10.1016/S0301-5629(98)00074-X

[18] ZHANG, H., FAN, C., WANG, L., LU, W., LI, D. The generation methods and applications of cavitating jet by using bubble collapse energy. *Energies* [online]. 2024, **17**(23), 5902 [accessed 2024-11-20]. ISSN 1996-1073. Available from: https://doi.org/10.3390/en17235902

[19] LAUTERBORN, W., KURZ, T. Physics of bubble oscillations. *Reports on Progress in Physics* [online]. 2010, **73**(10), 106501 [accessed 2011-07-05]. ISSN 1361-6633. Available from: https://doi.org/10.1088/0034-4885/73/10/106501

[20] FLANNIGAN, D. J., SUSLICK, K. S. Studying plasma formation and temperature during single-bubble cavitation. *Nature* [online]. 2005, **434**(7029), p. 52-55 [accessed 2005-03-03]. ISSN 1476-4687. Available from: https://doi.org/10.1155/2021/1009231

[21] SINELNIKOV, K. A. Developing and studying methods of maintenance and operation of a car using ultrasound. Dissertation for the degree of Doctor of Philosophy (PhD). Karaganda, 2023.

[22] KADYROV, A., BEMBENEK, M., SARSEMBEKOV, B., KUKESHEVA A., NURKUSHEVA, S. The influence of the frequency of ultrasound on the exhaust gas purification process in a diesel car muffler. *Applied Science* [online]. 2024, **14**(12), p. 1-19 [accessed 2024-06-24]. ISSN 2076-3417. Available from: https://doi.org/10.3390/app14125027

[23] KADYROV, A. S., SARSEMBEKOV, B. K., GANYUKOV, A. A., ZHUNUSBEKOVA, Z. Z., ALIKARIMOV, K. N. Experimental research of the coagulation process of exhaust gases under the influence of ultrasound. *Communications - Scientific Letters of the University of Zilina* [online]. 2022, **23**(4), p. 288-298 [accessed 2021-03-08]. ISSN 1335-4205. Available from: https://doi.org/10.26552/com.C.2021.4.B288-B298

[24] IBATOV, M., KADYROV, A., PAK, I., KADYROVA, I., ASKAROV, B. The results of experimental studies of the capacitive equipment of ultrasonic cleaning of exhaust gases of vehicles. *Ugol / Coal* [online]. 2020, **2**(1), p. 73-78 [accessed 2020-02-08]. ISSN 0041-5790 Available from: http://dx.doi.org/10.18796/0041-5790-2020-2-73-78

THE OPERATING PROCEDURE OF THE DEVICE ENHANCING THE WHEEL-RAIL ADHESION

Yuriy Y. Osenin[1], Nataliia Chernetska-Biletska[2], Sergii Kliuiev[2,*]

[1]Private Company Scientific Production Company "Poisk", Kyiv, Ukraine
[2]Department of Logistics and Transport Safety, Volodymyr Dahl East Ukrainian National University, Kyiv, Ukraine

*E-mail of corresponding author: kliuiev@snu.edu.ua

Yuriy Y. Osenin 0009-0002-4992-6018, Nataliia Chernetska-Biletska 0000-0002-7782-4003, Sergii Kliuiev 0000-0003-3698-9917

Resume

The results of the analysis of sand application efficiency for improving wheel-rail adhesion are presented. An algorithm for the sandbox operation is substantiated, based on supplying sand under the wheels when their slip reaches a critical level, delivering sand in proportion to the vehicle speed, and automatically purging the sand supply pipes. The principle of sandbox operation is based on the mechanical interaction between the moving elements and sand. It has been established that the maximum adhesion coefficient is achieved when the sand is evenly distributed in a single layer within the wheel-rail contact area. The important role of the contact area in the wheel-rail adhesion is emphasized. A sandbox implementing the developed sand supply algorithm is proposed. The introduction of this sandbox on Ukrainian-manufactured trams is described.

Article info

Received 11 December 2024
Accepted 10 March 2025
Online 8 April 2025

Keywords:

sand supply
adhesion coefficient
sand saving
wheel-rail contact area

Available online: https://doi.org/10.26552/com.C.2025.032

ISSN 1335-4205 (print version)
ISSN 2585-7878 (online version)

1 Introduction

The main idea of creating the rail transport is to reduce the rolling resistance of wheels on the base. This is primarily achieved by increasing stiffness of wheels and the base, as well as giving them rational geometric shapes. As a base, it was proposed to use rails laid on sleepers that would simultaneously serve as guiding elements for the train.

The first studies with a steam locomotive built in 1809 by engineer R. Trevithick revealed the imperfection of this idea. It was noticed that the application of traction force to the wheel was accompanied by an increase in the skidding of wheels on rails, which complicated movement or made it impossible in some cases. This phenomenon was called slipping later [1-2].

A well-known method of combating skidding by placing quartz sand between bodies in relative motion allowed increasing the traction force and preventing slipping [3-5]. Sand expectedly enhanced the wheel-rail adhesion in all weather conditions and, moreover, was an available material. The effectiveness of using sand to enhance the wheel-rail adhesion provided this method with absolute priority and spread in rail and urban rail transport. This is explained by the relative cheapness of sand and its unique property to instantly and effectively enhance the wheel-rail adhesion [6-8]. For example, the braking distance of a train when using sand is approximately 30% smaller than without sand in the same conditions [3, 9].

Sand is still the main means of short-term levelling of wheel skidding on the rail. Increased volumes of sand purchases for enhancing the wheel-rail adhesion, as well as large expenses for cleaning sand from the rail bed and city streets, have determined the need to use sand even more effectively and economically while achieving the maximum possible wheel-rail adhesion coefficient with minimal amounts of sand [9-10].

2 Presentation of basic materials

The imprinting film method was used to assess the contact area of the vehicle wheels with different wear indicators. The fractional composition of sand was carried out taking into account a sieve analysis. The

algorithm of supplying sand to the wheel-rail contact area was created and justified by comparative analysis using experimental and theoretical results.

Sanding systems in the technical literature are evaluated by two indicators, namely, efficiency (η) and sand supply performance [11]. Efficiency is an important characteristic of a sandbox. It can be used to assess the completeness of sand supply to the wheel-rail contact area, but efficiency cannot be considered an exhaustive characteristic, since it does not define the most important purpose of the sandbox, which is to enhance the wheel-rail adhesion.

Since the sand supply to the wheel-rail contact area without losses is not identical to the concept of increasing the wheel-rail adhesion coefficient, the efficiency of the sanding system can be considered only as a characteristic of sand losses while supplied to the contact area. The efficiency of the sanding system is defined as the ratio of the amount of sand that has come into the wheel-rail contact area to the total mass of sand supplied under the locomotive wheel [11]:

$$\eta = \frac{m_1}{m_2}, \tag{1}$$

where:
η - the efficiency of the sanding system;
m_1 - the amount of sand that has come into contact, kg;
m_2 - the total amount of sand supplied to the contact, kg.

Analysis of Equation (1) shows that efficiency is in no way related to the amount of sand required to achieve the maximum wheel-rail adhesion coefficient. This suggests that efficiency is an incomplete characteristics of the system and does not answer the question of whether this system is efficient and what part of sand is excessively supplied to the contact area.

Some specifications provide the efficiency of the sandbox, but it is not indicated under which conditions these values are valid. The conditions for obtaining efficiency are very important since it is obvious that with fixed constant values of the sand supply performance at different movement speeds, the values of the efficiency of the sandbox will be different.

To answer this question, information is needed about the amount of sand leading to the maximum adhesion coefficient. Studies show that this amount of sand is a variable value and depends on many factors, namely [11]:

- the wheel-rail contact area size;
- conditions of wheels and rails (level of wear);
- physicochemical and physicomechanical properties of the contacting surfaces;
- natural losses of sand on the way to the wheel-rail contact area;
- relative skidding of wheels;
- level of load on the wheel-rail contact area by normal and tangential forces;
- ambient temperature and temperature in the wheel-rail contact area.

Each of these factors of the wheel-rail interaction has a strictly defined amount of sand at which the maximum possible adhesion coefficient is achieved. Experimental determination of the sandbox efficiency involves conducting a series of measurements at different vehicle speeds and in different weather conditions. This requires equipment that allows for collecting sand that did not come into the wheel-rail contact area. Although the experimental equipment needed is simple, conducting experiments is quite problematic.

In addition to efficiency, an informative characteristic of the sandbox is its performance, which is expressed as the ratio of the amount of sand supplied by the sandbox per unit of time [1]:

$$P = \frac{M_k}{t} \tag{2}$$

where:
P - sandbox performance, kg/s;
M_k - the amount of sand supplied to the wheel-rail contact area, kg;
t - time, s.

However, just like efficiency, the sand supply performance does not define the purpose of the sanding system, which contributes to achieving the maximum adhesion coefficient and does not give recommendations for the rational use of sand to enhance the wheel-rail adhesion. This problem has a technical, economic, environmental, and social nature and affects such characteristics of sand use as the adhesion coefficient, the costs of purchasing and preparing sand, as well as human health, since after putting the sanding systems into operation small particles of sand remain in the atmosphere for a long time and lead to serious diseases while getting into the human lungs.

Despite the apparent chaos, the mechanical and physicochemical processes occurring during the interaction of sand with the wheel-rail contact area are interconnected, mutually dependent and are subject to the basic laws of the molecular-mechanical theory of friction [12].

When the sand particles are supplied to the contact area, their multiple crushing is observed, which begins in the micro-gap between the wheel and the rail and continues in the contact area itself. Small particles that do not come into the wheel-rail contact, and those that were in contact, play an unfavourable role. They can remain in the atmosphere for a long time and cause diseases when inhaled into human lungs [13].

It has been experimentally established that before the sand crushing, almost 80% of sand particles have a size of 0.1 to 0.3 mm. After the sand crushing, its main part (70%) has a particle diameter of 0.05 mm and less [14-15].

The size of sand particles was determined by sieving it through cells of different diameters. Sand crushing was caused by a single pair of locomotive wheels running into it, the axle load of which was 115 kN (this

experiment was performed with sand used to enhance the wheel-rail adhesion on Donetsk Railway of Ukraine) [16].

The maximum adhesion coefficient is achieved under conditions when a sand particle penetrates into the wheel-rail surfaces simultaneously, i.e., the sand is distributed in the contact in one layer [5-6]. The strength of the metal-particle-metal bond determines the wheel-rail friction coefficient and force. The penetration of a sand particle occurs to a depth that depends on the Brinell hardness of the material, the particle radius and shape. We assume that the sand particles are spherical for simplification, although in reality, their shapes may vary.

The criterion that evaluates the particle crushing is the following dependence [17]:

$$(h/r) = 1/2\,(\sigma/HB), \tag{3}$$

where: h - the depth of penetration, m;
r - the particle radius, m;
σ - the particle crushing stress, Pa;
HB - Brinell hardness of the material, Pa.

As a result of the sand crushing, the total surface area increases by many times. The new sand surface formed has high molecular activity due to a large number of uncompensated molecular bonds. This process has a beneficial effect on the implementation of the molecular component of the adhesion coefficient [18].

When coming into contact, sand can be distributed both in one layer and several layers. It has been experimentally proven that the first option is effective in terms of the adhesion coefficient for dry wheel-rail surfaces. In the second option, the adhesion coefficient tends to decrease with an increase in the amount of sand.

In the first option, each particle of sand has favourable conditions for simultaneous penetration into the wheel-rail surfaces and fixing in them. Thus, the best conditions are created to achieve the maximum possible values of the mechanical component [10]. For a single sand particle, the mechanical component of the adhesion coefficient is equal to the ratio of the particle application value to its radius [18]:

$$f_{mech} = \frac{h}{r}, \tag{4}$$

where:
f_{mech} - the mechanical component of the adhesion coefficient;
h - the amount of micro-roughness penetrated into the surface, m;
r - the radius of curvature of the micro-roughness apex, m.

As follows from Equation (4), the mechanical component of the adhesion coefficient will be the higher, the smaller is the sand particle formed after crushing. The mechanical component as a whole, for the wheel-rail adhesion coefficient, is respectively equal to the sum of the effects of all individual particles.

In this case, the magnitude of forces transmitted from the wheel to the rail depends on the following factors:

- the strength of sand particles;
- the depth of penetration of sand particles into the wheel-rail surfaces;
- the strength of the mechanical bond between sand particles and the material of the wheel and the rail;
- the strength of the molecular bond between the sand particles and the material of the wheel and the rail.

In addition, no less favourable conditions are created for implementing the molecular component. Each sand particle has the largest contact area with the wheel-rail surfaces. In the considered option of sand distribution in the contact area, both the mechanical and molecular components can reach their maximum possible values.

In the second option, there is no possibility of simultaneous penetration of each sand particle into the wheel-rail surfaces. In this regard, the efficiency of force transmission due to the mechanical component will be correspondingly lower.

In addition, despite the fact that the contact area of sand particles and the wheel-rail surfaces will be quite large, there is no reason to assume that the molecular component of the adhesion coefficient will also be quite large since the transmission of traction forces will be localized in sand thickness, the shear strength of which is low [9].

Additionally, the more sand particles are in the contact area, the less intensively they will be crushed and, therefore, lower values of the molecular component of the adhesion coefficient will be achieved.

Compared to the first option, this option is inferior in terms of the level of both mechanical and molecular interaction. Therefore, the first option of the distribution of sand particles in the contact is better from the point of view of achieving maximum values of the wheel-rail adhesion coefficient.

The wheel-rail adhesion takes place on small contact areas. The size of these contact areas is only a few square centimetres (for new wheels 1 - 2 cm^2) [19]. Nevertheless, with the help of such small areas, traction forces of several tens of tons can be transmitted from the wheel to the rail.

The contact area plays an important role in the wheel-rail interaction, both with and without sand. The larger the contact area is, the more sand particles can be placed there, so the more sand will affect the wheel-rail adhesion.

The wheel-rail adhesion coefficient with quartz sand in the contact area is shown by the equation [20]:

$$f_{ad} = f_{mol} + 1.4\left(\frac{p_w}{2r^2 HBn}\right), \tag{5}$$

where:
f_{ad} - the adhesion coefficient;

f_{mol} - the molecular component of the adhesion coefficient;
r - the radius of a quartz sand particle, m;
HB - Brinell hardness of the wheel surface, Pa;
n - the number of quartz sand particles;
P_w - the normal wheel load, N.

This equation is approximate, as it is derived from the assumption that sand particles are distributed in a single layer. The equation takes into account the contact area through the parameter of the amount of sand in the contact (the molecular component of the adhesion coefficient is determined experimentally).

The parameter n in Equation (5) attracts attention, as it means the number of quartz sand particles in the contact. Since the contact area of worn wheels is larger, the number of sand particles will be bigger, and therefore the wheel-rail adhesion will be larger.

The wheel-rail contact area mainly depends on the load level, the diameter of the wheel, and the degree of wear of the wheel-rail working surfaces. Since the contact area has its limits, the number of particles placed in the contact is also limited. Other things being equal, the contact area differs depending on the wear of wheels and rails.

Figure 1 shows the average statistical imprints of the spots of the wheel-rail contact. The imprints were obtained by the imprinting film method. The diameter of the wheels studied was within 1000 - 1050 mm [20].

As follows from Figure 1, the contact area of worn wheels is several times bigger than of the unworn ones. Therefore, the number of sand particles placed in the contact area of worn wheels will also be several times bigger, and the adhesion is correspondingly larger.

3 Findings and discussion

The developed sand dispensing system has been implemented on T3L441 trams manufactured by Electrontrans (Lviv, Ukraine). The system's performance characteristics are presented in Figure 2. For comparison, the performance characteristics of a system, based on a pneumatic dosing method, are also shown. As follows from the presented characteristics, the developed system demonstrates higher efficiency in economic parameters [10-11].

The shaded area indicates the sand savings achieved through the use of the mechanical dosing method.

With increasing speed, the drawback of the stepwise sand dispensing performance, shown in Figure 2, became apparent. For example, with stepwise sandbox performance when beginning motion and at a speed of 100 km/h, the amount of sand that comes into the wheel-rail contact area differs several times. This is due to the fact that in the first and second cases, the train passes a different path per unit of time, therefore, with the same sandbox performance, the density of sand distribution along the rail will be different.

It can be assumed that the wheel-rail adhesion

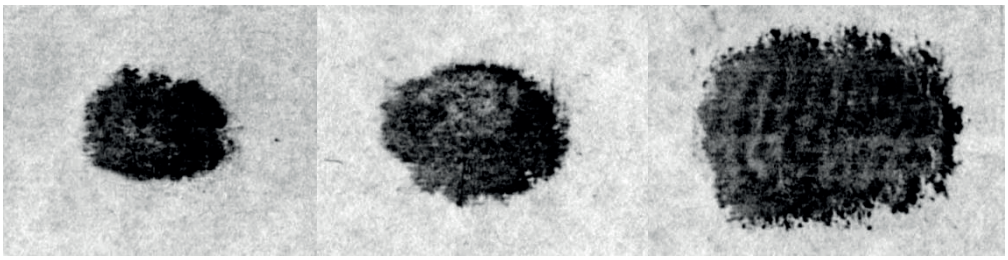

Figure 1 *Imprints of contact spots of a new and worn wheel with the rail: 1 - a new wheel; 2 - rolled 2.0 mm; 3 - rolled 5.0 mm*

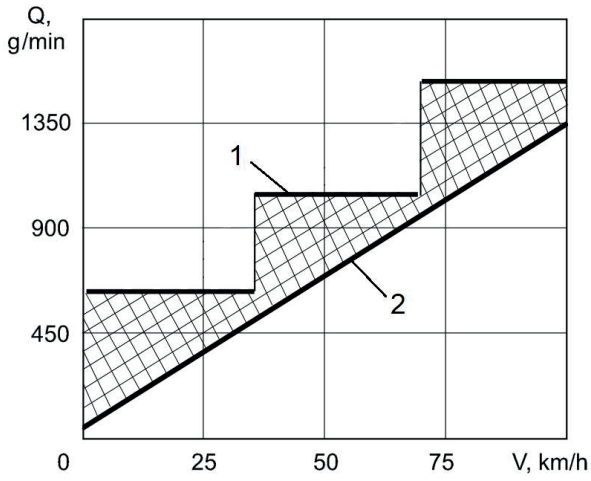

Figure 2 *Dependence of the sand supply productivity on tram speed, 1 - pneumatic sand dosing method, 2 - mechanical sand dosing method*

Table 1 *Percentage of sand supply to the wheel-rail contact area depending on the fractional composition of sand*

Fractional composition	%
Fraction >1.6 mm	100
Fraction 1.6 to 1.0 mm	90
Fraction 1.0 to 0.63 mm	70
Fraction 0.63 < mm	25

coefficient would change in accordance with the density of sand distribution. That is, stepwise sand supply performance by a sandbox does not provide stable values of the wheel-rail adhesion coefficient.

In this regard, a sandbox is created that allows sand to be supplied depending on the vehicle speed [6, 11, 16]. There are three methods that can be used. The first method is characterized by a stepwise dependence of the change in the sand supply performance on the movement speed, and the second is a linear dependence (Figure 2), and the third method is constant sand dispensing performance. The third method is apparently less effective. Its main advantage is in the relative simplicity of implementation.

The advantages of the second method, characterized by the linear sand supply performance, are obvious both in comparison to the constant sandbox performance and in comparison to the stepwise sand supply performance. The linear characteristics allows for providing the same density of sand distribution on the rail head at any speed, which ensures stability of the wheel-rail adhesion coefficient. However, its implementation requires creating new sandbox designs.

Attempts to create such sandboxes based on the already well-tested method of capturing and supplying sand with compressed air, which was implemented in almost all designs of existing sandboxes, were unsuccessful. The maximum that was possible to do on that basis was to provide a stepwise change in the sand supply performance (Figure 2). The stepwise change in the sand supply performance was ensured by controlling the compressed air parameters.

Creating sandboxes capable of changing the sand supply performance depending on the vehicle speed became possible based on the mechanical principle of sand dosing, which involves the mechanical impact on sand.

Experiments on the effectiveness of sand use were performed on a full-scale stand developed at the Department of Locomotive Engineering of Volodymyr Dahl East Ukrainian National University under the mentorship of Professor O. L. Holubenko. The stand reproduced the interaction of a wheel with a diameter of 1050 mm and a section of the P65 rail 12 meters long in the dynamic mode [2].

When the train starts moving and at a speed of 100 km/h, the amount of sand reaching the wheel-rail contact varies significantly (by several times) depending on the dispensing mode. This is explained by the fact that the train passes different distances per unit of time, which affects the sand distribution density.

With the stepwise sand dispensing performance, uneven sand distribution is observed, leading to a change in the adhesion coefficient. According to the data in Figure 2, the sand dispensing performance characteristics of the mechanical method differs significantly from the pneumatic method in terms of sand savings.

To save sand when supplying it under wheels, it is possible to achieve a high percentage of sand supply to the wheel-rail contact area by screening out small sand particles during its preparation. Screening out sand particles with a diameter of less than 0.63 mm will ensure a loss of sand particles of only about 15% [18]. When screening out sand particles smaller than 1.6 mm, 100% sand supply to the wheel-rail contact is ensured, Table 1.

The wheel-rail adhesion coefficient in real operating conditions varies over a wide range. The minimum and maximum values of the adhesion coefficient differ by 6-7 times. When the weather conditions deteriorate, the adhesion coefficient can reach record low values, at which the rolling stock movement becomes impossible at all [15].

As studies have shown, such significant changes in the adhesion coefficient are largely due to the physicochemical state of the wheel-rail surfaces, which is formed under the influence of many factors. The most important of them are the weather and climatic conditions of the rolling stock operation, which are mainly due to the influence of temperature, humidity, and the accidental presence of various components on the rails [15].

Currently, the operation of trains is carried out without strict consideration of the influence of weather and climatic factors. This explains the fact that currently existing recommendations on the sand supply performance differ quantitatively several times.

The lack of influence of weather and climatic conditions leads to overconsumption of sand, a decrease in its frictional capabilities, an increase in wear of the wheel-rail working surfaces, as well as a loss of technical and economic efficiency of the locomotive as a traction vehicle.

The developed algorithm was implemented in the tram sandbox, which was introduced on T3L441 trams manufactured by LLC SP “Electrontrans” (Lviv, Ukraine). The sandbox was developed by the research

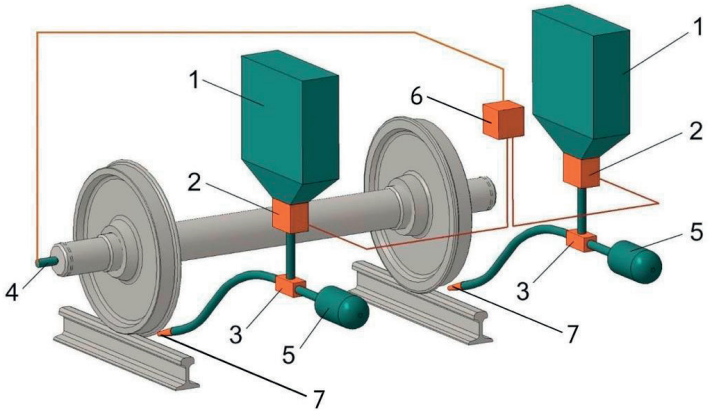

Figure 3 *Block diagram of placing sandboxes on the running gear of the tram: 1 - sand hopper; 2 - dispenser; 3 - nozzle; 4 - relative wheel slip sensor; 5 - small-sized compressor; 6 - control unit; 7 - tip*

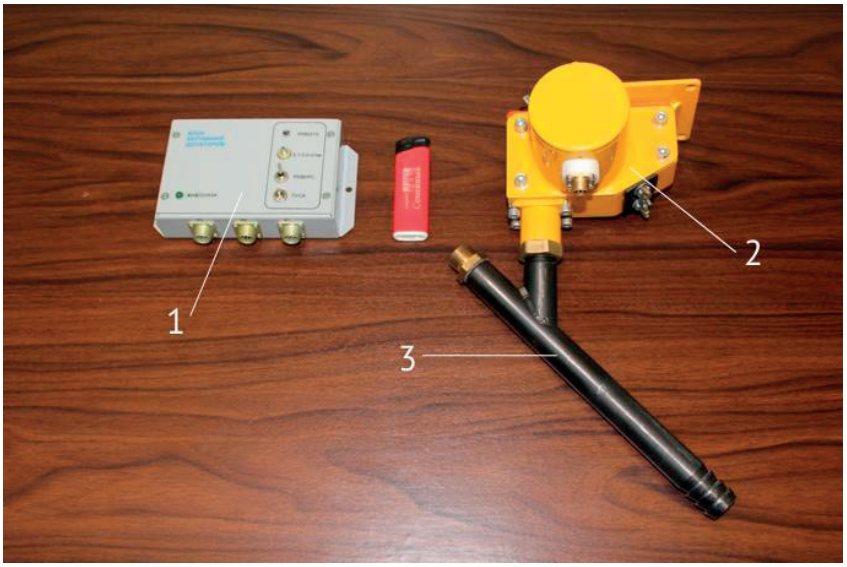

Figure 4 *Sandbox design: 1 - control unit; 2 - sand supply dispenser; 3 - nozzle*

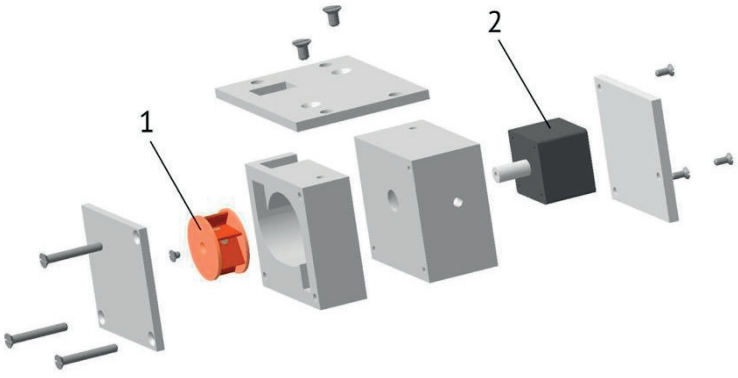

Figure 5 *Sand supply dispenser: 1 - impeller; 2 - stepper motor*

and production association "Poshuk" (Severodonetsk, Ukraine) [9]. The block diagram of placing sandboxes on the running gear of the tram and their design are presented in Figures 3 and 4, respectively.

Figure 4 does not show the elements used by the sandbox but developed and supplied by other developers and manufacturers (compressor, relative wheel slip sensor).

The sandbox is designed based on the mechanical principle of sand dosing and provides the sand supply to the contact proportional to the locomotive speed, which is provided by the impeller 1 (Figure 5). The installation of the sandbox on the tram is shown in Figure 6.

The sandbox operation algorithm involves blowing out the sand supply hoses after each sand supply cycle, as well as blowing out the sand supply hoses without

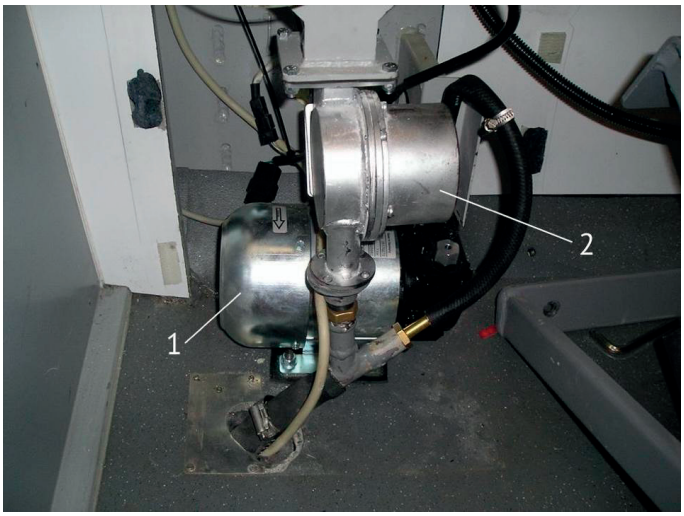

Figure 6 *Installation of the sandbox on the tram: 1 - compressor; 2 - sand supply dispenser*

sand supply, which is carried out with a given duration and frequency depending on the season (winter/summer).

Due to the use of the developed sand dispensing algorithm, the sandbox achieves the following characteristics (compared to analogues):

- high efficiency in terms of the wheel-rail adhesion coefficient;
- sand savings due to sand dispensing under the wheels, depending on the tram's speed;
- high operational performance due to the reliability of the dispenser and the purging of the sand dispensing pipes.

The author's supervision, conducted over 18 months, confirmed the high reliability of the sandbox.

4 Conclusions

1. The optimal procedure of supplying the sand to the locomotive wheels in accordance with the criteria of the adhesion coefficient and sand saving should have the following functions:
   - supplying sand to wheels when reaching the critical level of the wheel skidding relative to rails;
   - pulsed supply of sand carried out proportional to the movement speed;
   - automatic blowing out of sand supply hoses after each sand-supply cycle;
   - automatic periodic blowing out of sand supply hoses without sand supply in summer and winter.
2. Sand supply by modern sanding systems should be based on the predominant principle of the mechanical impact on sand during its dosing. The developed sand dispenser corresponds to this principle.
3. A high percentage of sand supply to the wheel-rail contact area can be achieved by screening out small sand particles during its preparation. Screening out sand particles with a diameter of less than 0.63 mm will ensure an approximately 15% loss of sand particles. When screening out sand particles smaller than 1.6 mm, 100% sand supply to the wheel-rail contact area is ensured.
4. The maximum adhesion coefficient is achieved in conditions when the sand is distributed in the wheel-rail contact area in a single layer and a sand particle simultaneously gets into the wheel-rail surfaces. The strength of the metal-particle-metal bond determines the wheel-rail adhesion coefficient and force.
5. The contact area plays an important role in the wheel-rail interaction, both with and without sand. The larger the contact area is, the more sand particles can be placed there and, thus, the more sand will affect the wheel-rail adhesion. All other things being equal, the adhesion of worn wheels (with sand particles) is greater as compared to the new wheels.
6. A locomotive sandbox is proposed, which is designed on the mechanical principle of sand dosing. The sandbox provides dosed sand supply to the contact area proportional to the locomotive speed and has the functions of blowing out the sand supply hoses after each sand-supply cycle, as well as blowing out the sand supply hoses without sand supply, which is carried out with a given duration and frequency depending on the season (winter/summer).

Acknowledgements

The authors received no financial support for the research, authorship and/or publication of this article.

Conflicts of interest

The authors declare that they have no known competing financial interests or personal relationships that could have appeared to influence the work reported in this paper.

References

[1] BLANCO-LORENZO, J., VOLLEBREGT, E. A. H., SANTAMARIA, J., VADILLO, E. G. Approximating the influence coefficients of non-planar elastic solids for conformal contact analysis. *Tribology International* [online]. 2021, **154**, 106671 [accessed 2024-12-10]. ISSN 0301-679X. Available from: https://doi.org/10.1016/j.triboint.2020.106671

[2] BUCKLEY-JOHNSTONE, L. E., TRUMMER, G., VOLTR, P., SIX, K., LEWIS, R. Full-scale testing of low adhesion effects with small amounts of water in the wheel/rail interface. *Tribology International* [online]. 2020, **141**, 105907 [accessed 2024-12-10]. ISSN 0301-679X. Available from: https://doi.org/10.1016/j.triboint.2019.105907

[3] CHEN, H. Review of various influencing factors and improvement measures on wheel-rail adhesion. *Wear* [online]. 2024, **550-551**, 205283 [accessed 2024-12-10]. ISSN 0043-1648. Available from: https://doi.org/10.1016/j.wear.2024.205283

[4] LI, Q., ZHANG, S.-Y., WU, B.-N., LIN, Q., DING, H.-H., GALAS, R., KVARDA, D., OMASTA, M., WANG, W.-J., WEN, Z.-F. Analysis on the effect of starved elastohydrodynamic lubrication on the adhesion behavior and fatigue index of wheel-rail contact. *Wear* [online]. 2022, **510-511**, 204506 [accessed 2024-12-10]. ISSN 0043-1648. Available from: https://doi.org/10.1016/j.wear.2022.204506

[5] LI, Q., WU, B.-N., DING, H.-H., GALAS, R., KVARDA, D., LIU, Q.-Y., ZHOU, Z.-R., OMASTA, M., WANG, W.-J. Numerical prediction on the effect of friction modifiers on adhesion behaviours in the wheel-rail starved EHL contact. *Tribology International* [online]. 2022, **170**, 107519 [accessed 2024-12-10]. ISSN 0301-679X. Available from: https://doi.org/10.1016/j.triboint.2022.107519

[6] KLIUIEV, S., MEDVEDIEV, I., KHALIPOVA, N. Study of railway traffic safety based on the railway track condition monitoring system. *IOP Conference Series: Materials Science and Engineering* [online]. 2020, **985**, 012012 [accessed 2024-12-10]. ISSN 1757-899X. Available from: https://doi.org/10.1088/1757-899X/985/1/012012

[7] MAZZU, A., BATTINI, D. A Model for the assessment of wheel-rail contact in the presence of solid contaminants. *Tribology Transactions* [online]. 2019, **62**(2), p. 230-238 [accessed 2024-12-10]. ISSN 1547-397X. Available from: https://doi.org/10.1080/10402004.2018.1535104

[8] SHEN, M.-X., LI, J.-Q., LI, L., LI, S.-X., MA, CH.-Y. Adhesion and damage behaviour of wheel-rail rolling-sliding contact suffering intermittent airflow with different humidities and ambient temperatures. *Tribology Letters* [online]. 2024, **72**(1), 18 [accessed 2024-12-10]. ISSN 1573-2711. Available from: https://doi.org/10.1007/s11249-023-01817-1

[9] SKIPPER, W. A., CHALISEY, A., LEWIS, R. A review of railway sanding system research: wheel/rail isolation, damage, and particle application. *Proceedings of the Institution of Mechanical Engineers, Part F: Journal of Rail and Rapid Transit* [online]. 2019, **234**(6), p. 567-583 [accessed 2024-12-10]. ISSN 2041-3017. Available from: https://doi.org/10.1177/0954409719851634

[10] VOLLEBREGT, E., SIX, K., POLACH, O. Challenges and progress in the understanding and modelling of the wheel-rail creep forces. *Vehicle System Dynamics* [online]. 2021, **59**(7), p. 1026-1068 [accessed 2024-12-10]. ISSN 1744-5159. Available from: https://doi.org/10.1080/00423114.2021.1912367

[11] WANG, W. J., ZHANG, H. F., WANG, H. Y., LIU, Q. Y., ZHU, M. H. Study on the adhesion behavior of wheel/rail under oil, water and sanding conditions. *Wear* [online]. 2011, **271**(9-10), p. 2693-2698 [accessed 2024-12-10]. ISSN 0043-1648. Available from: https://doi.org/10.1016/j.wear.2010.12.019

[12] WANG, X., HUA, H., PENG, K., WU, B., TANG, Z. Study on the wheel/rail adhesion characteristic under water and soil conditions by using mixed lubrication model. *Wear* [online]. 2024, **544-545**, 205279 [accessed 2024-12-10]. ISSN 0043-1648. Available from: https://doi.org/10.1016/j.wear.2024.205279

[13] WANG, Z., WU, B., HUANG, J. A simplified non-hertzian wheel-rail adhesion model under interfacial contaminations considering surface roughness. *Lubrication Science* [online]. 2025, **37**(1), p. 105-116 [accessed 2024-12-10]. ISSN 1557-6833. Available from: https://doi.org/10.1002/ls.1726

[14] WU, B., YANG, Y., XIAO, G. A transient three-dimensional wheel-rail adhesion model under wet condition considering starvation and surface roughness. *Wear* [online]. 2024, **540-541**, 205263 [accessed 2024-12-10]. ISSN 0043-1648. Available from: https://doi.org/10.1016/j.wear.2024.205263

[15] WU, B., XIAO, G., AN, B., WU, T., SHEN, Q. Numerical study of wheel/rail dynamic interactions for high-speed rail vehicles under low adhesion conditions during traction. *Engineering Failure Analysis* [online]. 2022, **137**, 106266 [accessed 2024-12-10]. ISSN 1350-6307. Available from: https://doi.org/10.1016/j.engfailanal.2022.106266

[16] KLIUIEV, S., MEDVEDIEV, I., SOROKA, S., DUBIK, V. Development of the intelligent rail vehicle control system. In: 2020 IEEE 15th International Conference on Computer Sciences and Information Technologies CSIT: proceedings [online] [accessed 2024-12-10]. IEEE. Vol. 1. 2020. ISSN 2766-3639, p. 369-372. Available from: https://doi.org/10.1109/CSIT49958.2020.9321866

[17] YANG, Y., WU, B., XIAO, G., SHEN, Q. Numerical investigation on wheel-rail adhesion under water-lubricated condition during braking. *Industrial Lubrication and Tribology* [online]. 2023, **75**(5), p. 568-577 [accessed 2024-12-10]. ISSN 0036-8792. Available from: https://doi.org/10.1108/ilt-02-2023-0040

[18] ZANI, N., MAZZU, A., SOLAZZI, L., PETROGALLI, C. Examining wear mechanisms in railway wheel steels: experimental insights and predictive mapping. *Lubricants* [online]. 2024, **12**(3), 93 [accessed 2024-12-10]. ISSN 2075-4442. Available from: https://doi.org/10.3390/lubricants12030093

[19] ZHANG, M., YAN, Z. Effects of near-surface composites on frictional rolling contact solved by a semi-analytical model. *Journal of Tribology* [online]. 2021, **144**(2), 021502 [accessed 2024-12-10]. ISSN 1528-8897. Available from: https://doi.org/10.1115/1.4052330

[20] ZHOU, J., TIAN, CH., MA, T., ZHAI, G. Mechanism of wheel-rail adhesion recovery during large sliding processes under water lubrication condition. *Tribology Transactions* [online]. 2024, **67**(6), p. 1232-1251 [accessed 2024-12-10]. ISSN 1547-397X. Available from: https://doi.org/10.1080/10402004.2024.2415476

INDICATORS OF THE DYNAMIC INTERACTION OF THE TRACK AND FREIGHT WAGONS WITH INCREASED AXIAL LOAD

Natalya Tokmurzina-Kobernyak[1], Arailym Tursynbayeva[1,*], Laila Sagatova[1], Marat Shurenov[2], Assel Kurbenova[1]

[1]Satbayev University, Almaty, Kazakhstan
[2]Kazakh National Agrarian Research University, Almaty, Kazakhstan

*E-mail of corresponding author: nurtassovna.iqo@mail.ru

Natalya Tokmurzina-Kobernyak 0000-0001-5589-5663, Arailym Tursynbayeva 0000-0003-0249-4991, Marat Shurenov 0009-0002-0503-8342

Resume

The article is devoted to the study of dynamic interaction of rail track and freight wagons under increased axial load. In conditions of increasing the freight traffic volumes and axial loads, the importance of accurate understanding of the mechanisms affecting the wear of rail track elements becomes especially important. In this paper the authors have carried out experimental research and comparative analysis of freight wagon trolleys of different models. As a result of dynamic tests of the freight wagon trolleys, the necessary parameters of dynamic qualities of different models of wagons and their optimal values of axial loads of freight wagons are obtained. The necessity of improving the current design of wagon trolleys and reinforcing the design of railway track with the use of R65 type rails and reinforced concrete sleepers is substantiated. According to the data of trolley design comparison of different models, the bending moment and maximum load indices are established.

Article info

Received 16 November 2024
Accepted 10 March 2025
Online 8 April 2025

Keywords:

dynamic indicators
railway rolling stock
trolleys
load on rails
dynamic tests

Available online: https://doi.org/10.26552/com.C.2025.033

ISSN 1335-4205 (print version)
ISSN 2585-7878 (online version)

1 Introduction

Modern railway transport plays a key role in the economies of most countries, transporting large volumes of goods over long distances. In recent decades, due to increasing freight traffic volumes and the growing need for more efficient and powerful vehicles, there has been a tendency to increase axle loads on the railway track [1]. Under conditions of increased axial load, freight wagons are subjected to significant dynamic effects, which directly affect the track performance and wear.

One of the most important aspects that require attention is the study of the dynamic interaction between the track and wagon wheels, which has an impact on traffic stability, transport safety and infrastructure durability. This interaction becomes especially relevant in the context of increasing axial loads, which requires a more thorough study of its influence on the mechanical properties of rails, joints, ballast base and other track elements [1-2].

The importance of studying dynamic indicators of interaction between the rail track and wagons under conditions of increased axial load is due to the need to develop new standards for railway design and operation, as well as to create effective methods of monitoring and diagnostics of track infrastructure condition. This research is aimed at optimizing the operational characteristics of railway transport, improving its reliability and safety, as well as reducing economic losses associated with infrastructure wear and tear [2].

Analysis of literature sources shows that the issue of dynamic interaction between the rail track and freight wagons under increased axle load is actively investigated in various aspects: from mechanics and modelling to diagnostics and forecasting.

The dynamic interaction between the car and the track is determined by many factors, including bogie design, track condition, speed and axle load. Studies show that as the axle load increases, the amplitudes of vibration increase, as well as the forces transmitted to the rail-tie grid. This leads to increased stresses in rails and sleepers, which accelerates their fatigue failure processes.

Increased axial loads lead to increased vibrations in the rolling stock, which affects the comfort and safety of

transportations. According to studies [3-4], increasing the axle load from 23.5 tons to 27 tons increases the level of vibrations in the low frequency range (1-5 Hz), which negatively affects the condition of the running parts of wagons and track elements.

Various technical solutions are proposed to minimize the negative effects [3]:

- Improving the design of freight wagon bogies;
- Use of rails of higher strength and modern elastic fasteners;
- Application of improved methods of diagnostics and monitoring of the track and wagon condition.

Mathematical modelling methods are widely used to study dynamic interaction processes. Authors of a number of works [4-5] use multi-car and rail track models to analyze the impact of various factors, such as rail defects, wheelset profile and car suspension parameters.

Numerical modelling methods, based on the finite element method, and dynamic analysis of contact interactions have also been used recently. This makes it possible to evaluate the stress distribution in rails, sleepers and ballast layer under different traffic modes.

However, despite the considerable amount of research, there is a need to further develop diagnostic, modelling and prediction methods, especially in the context of more intensive railway operation and increased axle loads. The topic requires further research considering new technologies and materials to improve the safety, durability and efficiency of railway infrastructure [3].

The purpose of this paper was to analyze the performance of the dynamic interaction between rail track and freight wagons under increased axial load, to identify the key factors affecting its behavior, and to develop recommendations to improve the efficiency and safety of rail transport [1-6].

Thus, the topic of research of dynamic interaction of rail track and freight cars under increased axial load is relevant both from the point of view of engineering solutions and from the point of view of ensuring safety and economic efficiency of railway transport in the conditions of modern traffic growth and the requirement to increase freight capacity [1, 6].

The novelty of the research lies in the complex approach to the study of the dynamic interaction of the rail track and freight cars under increased axial load, which allows a more accurate assessment of the impact of such loads on the operational characteristics of railway infrastructure and vehicles.

Thus, the novelty of this study lies in the integration of modern methods of analysis, diagnostics and forecasting to create more sustainable and safer railway operating conditions under increased axial loads. These results can significantly influence practical applications in the field of railway transport, improving its safety, economic efficiency and infrastructure durability [6].

In modern conditions of cargo transportation using the rail transport, there is a tendency to increase the axial load on wagons. This necessitates an in-depth analysis of the dynamic interaction between rolling stock and the railway track. This article examines the key indicators that determine the effectiveness and safety of such interaction [1].

1.1 Dynamic loads

Dynamic loads arising from the movement of freight wagons can significantly exceed the static loads. The main indicators are:

- Axial load: The maximum pressure on the axle of the car, affecting the deformation of the track.
- Dynamic coefficients: The ratio of dynamic loads to static loads, which depends on the speed of movement and the condition of the rails.

1.2 Condition of rails and tracks

With an increase in the axial load, the following changes were observed [2-3]:

- Wear of the trackbed: An increase in the intensity of wear, requiring more frequent maintenance.
- Path deformation: Increased risk of deformations, which can lead to emergencies.

1.3 Impact on rolling stock

Dynamic interaction has an impact on freight wagons, as well:

- Depreciation: Effective depreciation systems can reduce the negative impact on the rails.
- Directional stability: Increased axial load can worsen the stability of wagons on curved sections of the track.

1.4 Assessment methods

Various methods are used to analyze dynamic interaction:

- Computer modelling: Models allow to predict the behavior of a rail track under the influence of various loads.
- Field testing: Real-world data collection helps refine models and assess actual performance.

The dynamic interaction of the track and freight wagons with increased axial load requires an integrated approach to research and evaluation. The sustainable development of railway transport depends on the introduction of modern technologies and control methods, which will ensure the safety and efficiency of freight transportation [5-6].

2 Materials and methods

The main models are: models 18-100, 18-9810 (Barber) with an axial load of 23.5 t/axle, models 18-194-1 (Uralvagonzavod), 18-9996 (ZK1) with an axial load of 25 t/axle.

To compare the indicators of dynamic interaction of the track and wagons, the following indicators were calculated [4]:

- the coefficient of vertical dynamics;
- dynamic maximum load from the wheel to the rail;
- bending moment in rails;
- maximum deflection of the rail.

The calculation was carried out for track structures: rail R65, wooden sleepers, laying plot 2000 pcs./km, ballast - crushed stone.

The main technical parameters of the trolleys of the wagons used in the calculation are shown in Table 1.

The safety of the carriage and the smoothness of its movement along the irregularities of the track are estimated by the coefficients of vertical dynamics, which for freight wagons should not exceed k_d = 0.65.

The k_d value is determined by the formula [7]:

$$k_d = 0.1 + 0.2\,V/f_{st}\,, \tag{1}$$

where V - is the speed of movement, km/h;
f_{st} - static deflection of the spring suspension, mm;

Figure 1 shows the values of the coefficient of vertical dynamics of wagons presented in Table 1.

As can be seen from Figure 1, all the wagons meet the requirements in terms of the permissible coefficient of vertical dynamics, however, trolleys of models 18-194-1 and 18-9996 (with an axial load of 25 tons) have this indicator smaller than wagons with an axial load of 23.5 tons. This phenomenon is explained by the improved characteristics of spring suspension [8].

The vertical dynamic load P_{avg} occurs when the car moves along the rail track due to the acceleration of the mass of the car and cargo during vibrations on the

Table 1 *Calculated parameters of trolleys*

No.	Indicator	Cart Model			
		18-100	18-9810	18-194-1	18-9996
1	The number of axles in the cart	2	2	2	2
2	Axial load, t/axle	23.5	23.5	25	25
3	Static deflection of the spring suspension	47	48	76	55
4	Structural speed, km/h	100	120	120	120
5	Weight of the trolley, t	4.76	4.8	4.9	5.3
6	The weight of the unsprang parts attributed to the wheel, kN	995	995	995	1005
7	Trolley base, mm	1850			

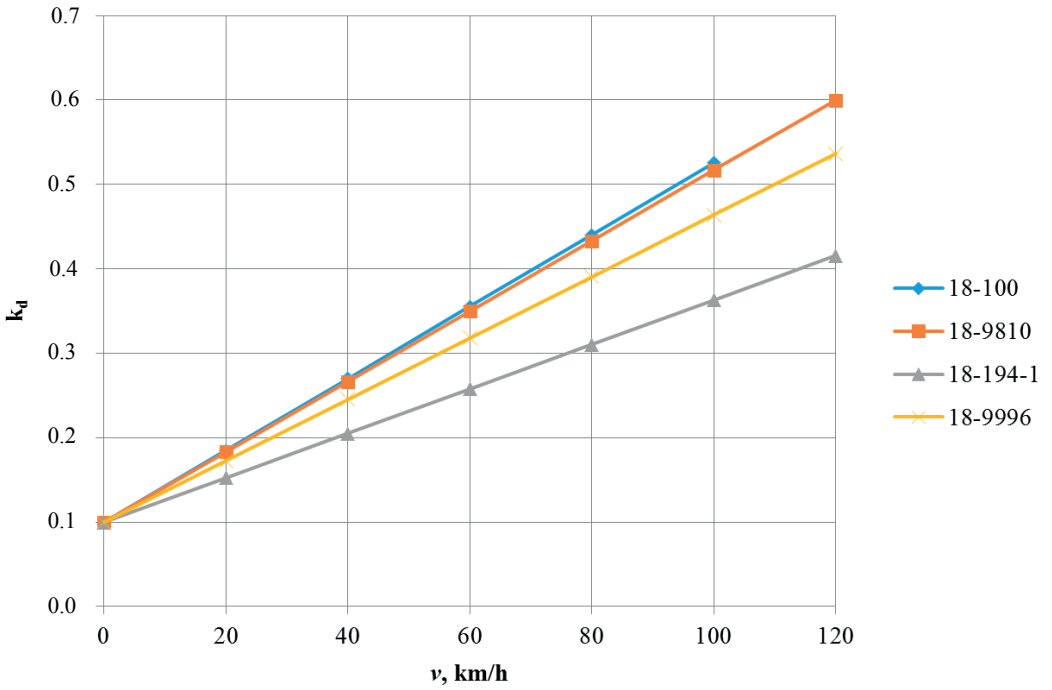

Figure 1 *Coefficient of vertical dynamics of freight wagons*

springs and the passage of track irregularities [9]. It is determined by multiplying the static load by the vertical dynamic coefficient.

The dynamic maximum load from the wheel to the rail is determined by the formula [5]:

$$P_{dyn}^{\max} = P_{avg} + \lambda S, \text{ (kg)} \quad (2)$$

where P_{avg} - the average value of the vertical load of the wheel on the rail, kg;
S - the average square deviation of the dynamic vertical load of the wheel on the rail, kg;

λ = 2.5 - a normalizing multiplier that determines the probability of an event, i.e., the occurrence of a maximum dynamic vertical load.

The average value of the vertical load of the wheel on the rail is determined by the formula [10]:

$$P_{avg} = P_{st} + P_{\dot{p}}^{avg}, \text{ (kg)} \quad (3)$$

where P_{st} is the static load of the wheel on the rail, kg;
$P_{\dot{p}}^{avg}$ - the average value of the dynamic load of the wheel on the rail from vertical vibrations of the superstructure of the crew, kg [10]:

$$P_{\dot{p}}^{avg} = 0.75 \cdot P_{\dot{p}}^{\max}, \text{ (kg)} \quad (4)$$

where $P_{\dot{p}}^{\max}$ - - the dynamic maximum load of the wheel on the rail from vertical vibrations of the superstructure, kg.

The dynamic maximum load of the wheel on the rail from vertical vibrations of the superstructure $P_{\dot{p}}^{\max}$ is determined by the formula:

$$P_{\dot{p}}^{\max} = k_d(P_{st} - q) \text{ (kg)} \quad (5)$$

where q - the weight of the unsprang parts attributed to the wheel, kg;
k_d - the coefficient of vertical dynamics.

The calculation of the maximum dynamic load (Equation (5)) was performed using the Excel application and is shown in Figure 2.

As can be seen from Figure 2, the amount of dynamic load is affected by the speed of movement. With an increase in the speed from 20 to 100 km, the load of the wheel on the rail increases almost 1.5-2 times. In addition, an increase in the weight of the unsprang parts of the car leads to an increase in the dynamic load.

When calculating a rail as a beam on a solid elastic base, the system of concentrated wheel loads (Figure 3) is replaced by equivalent single loads, respectively, when determining bending moments and stresses in rails using a function μ and when determining loads and deflections using a function η [11]. Since, due to the random nature, the probable maximum dynamic load of the design wheel does not coincide with the probable maximum loads of neighboring wheels, the maximum probable load of the design wheel and the average value of the loads of neighboring wheels are taken into account when determining the equivalent loads.

The maximum equivalent load for calculating stresses in rails from bending and torsion is determined by, [11]:

$$P_{eq}^{I} = P_{dyn}^{\max} + \sum \mu_i P_{cpi}, \text{ (kg)} \quad (6)$$

where μ_i - the ordinates of the line of influence of the bending moments of the rail in the sections of the track

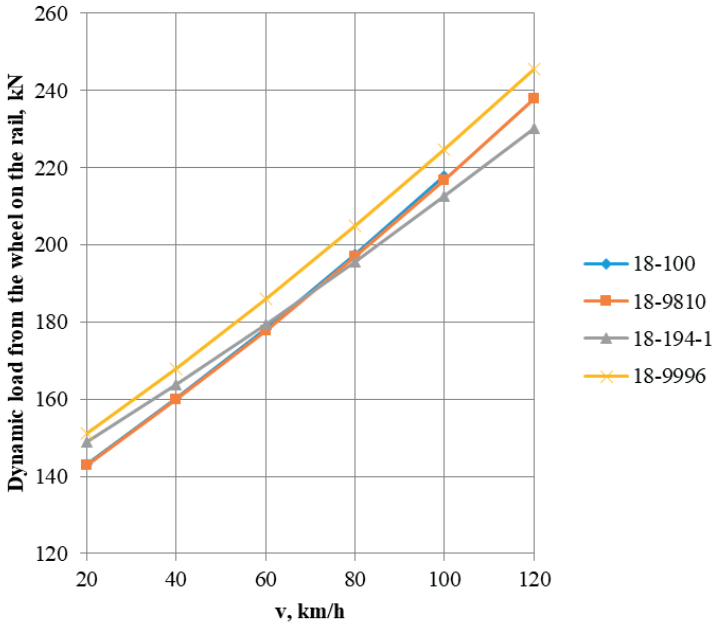

Figure 2 *Dynamic maximum load from the wagon wheel on the rail*

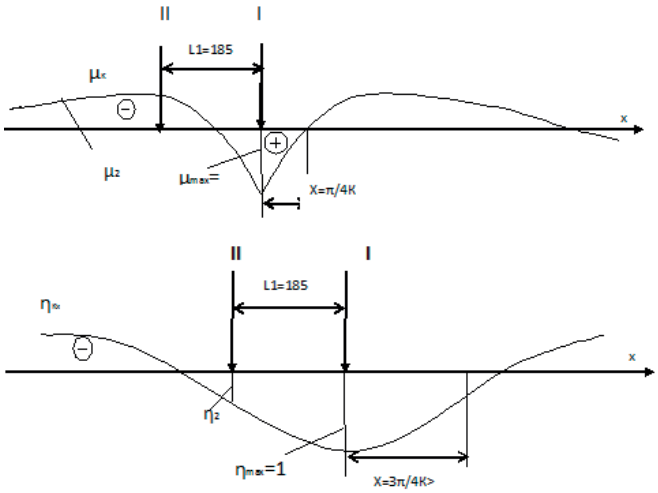

Figure 3 *Lines of influence of deflections η (x) and moments μ (x) from the action of the wheel load*

located under wheel loads from the axles of the carriage adjacent to the design axis (Figure 4).

The magnitude of the ordinate can be determined by the formula:

$$\mu_i = e^{-kli}(\cos kl_i - \sin kl_i), \quad (7)$$

where k = 0.001 - the coefficient of relative stiffness of the rail base and rail, mm^{-1};
l_i =1850 mm - the distance between the center of the axis of the calculation wheel and the wheel of the i-axis adjacent to the calculation;
e - the basis of natural logarithms (e = 2.72828 ...).

The maximum equivalent load for calculating stresses and forces in the elements of the sub-rail base is determined by the formula [10]:

$$P_{eq}^{II} = P_{dyn}^{\max} + \sum \eta_i P_{cpi}, \text{ (kg)} \quad (8)$$

where η_i - ordinates of the line of influence of rail deflections in track sections located under the wheel loads from the carriage axles adjacent to the design axis (Figure 3):

$$\eta_i = e^{-kli}(\cos kl_i + \sin kl_i). \quad (9)$$

The bending moment in the rails from the impact of an equivalent load is [12]:

$$M = P_{eq}^{1}(\mu_i)/4k, \quad (10)$$

where P_{eq}^{1} - the maximum equivalent load for calculating stresses in rails from bending and torsion, kg.

Maximum load on the sleeper:

$$Q = P_{eq}^{II} \cdot kl_s/2, \quad (11)$$

where l_s = 550 - the distance between the sleeper axes, mm;
P_{eq}^{II} - the maximum equivalent load for calculating stresses and forces in the elements of the sub-rail base, kg.

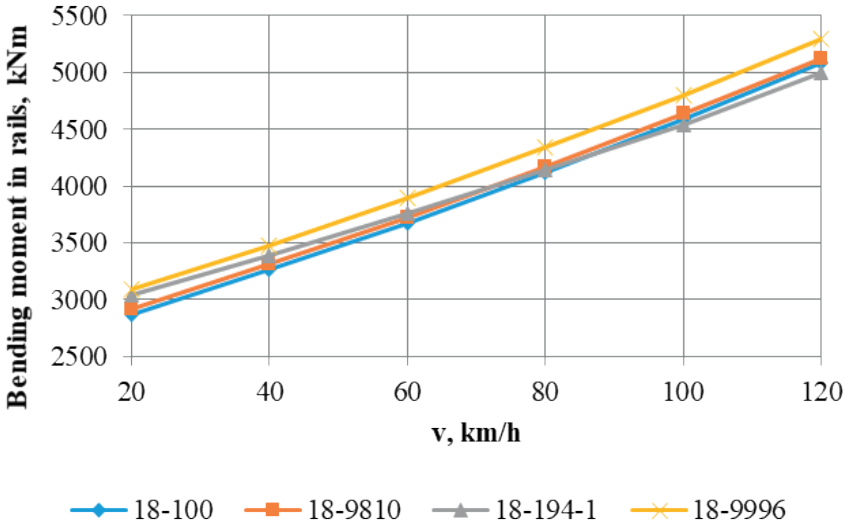

Figure 4 *Bending moment in the rails under the action of the wagon wheel*

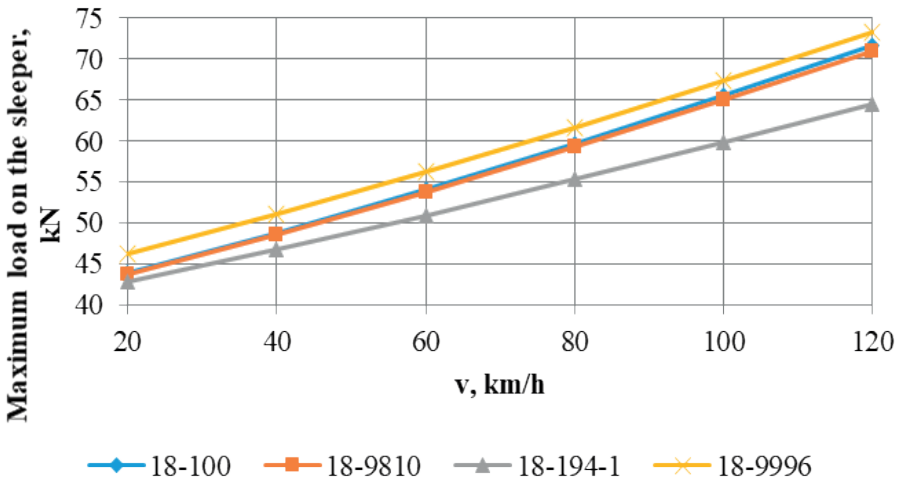

Figure 5 *Maximum load on the sleeper under the action of the wagon wheel*

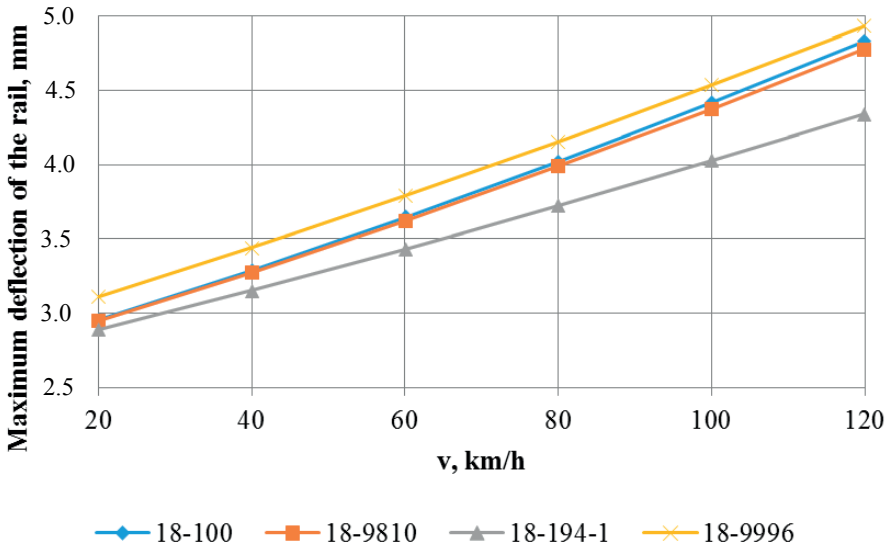

Figure 6 *Maximum deflection of the rail under the action of the wagon wheel*

Maximum deflection of the rail:

$$y = P_{eq}^{II} \cdot k/2U\,, \text{ (mm)} \qquad (12)$$

where U = 2.7 - modulus of elasticity of the rail base, kg/mm^2

Figures 4-6 show the results of calculating the bending moment in the rail, the load on the sleeper and the deflection of the rail from wagons with different axial loads, respectively [13-14].

The analysis of Figures 4-6 showed that the trolleys of the model 18-194-1 have the most favorable effect on the track over the entire speed range, the trolleys of the model 18-9996 have the worst indicators of interaction between the track and rolling stock. The worst indicators of interaction between the track and the trolley of the model 18-9996 are explained by the fact that the trolley has a 7.5% higher mass compared to other trolleys, as well as a greater unsprang weight [15].

3 Results and discussion

The gondola cars 12-196-01 on trolleys 18-194-1 have passed a full cycle of acceptance tests, and the main components and parts of the trolley have been bench tested in terms of strength and service life. The running, dynamic strength and impact tests carried out on the track, some of the results of which are presented in Figures 7-9 [16-17], indicate that the dynamic performance of the gondola car on trolleys 18-194-1 meets the requirements of the Norms for calculating and designing railway wagons of the Republic of Kazakhstan gauge of 1520 mm and generally do not exceed the performance of the standard wagon on trolleys 18-100, including the impact on the path and switches.

From the presented dependencies can also be seen that, due to the optimally selected parameters of the spring set of trolleys 18-194-1 for them in the speed range of 60-120 km/h, the coefficients of vertical additives for

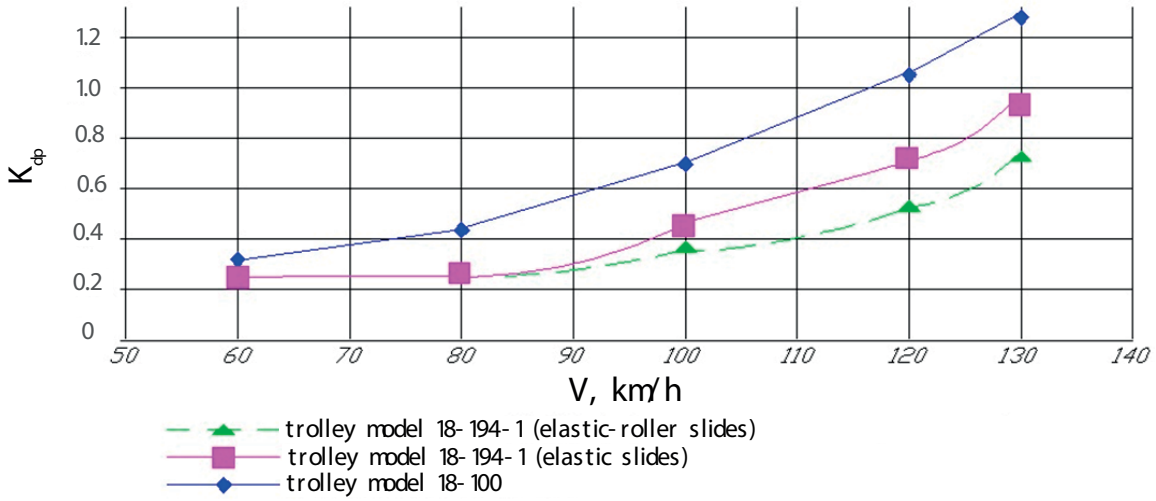

Figure 7 *Coefficients of vertical dynamic additives for sprung masses when moving open wagons (K_{dp}) (straight line)*

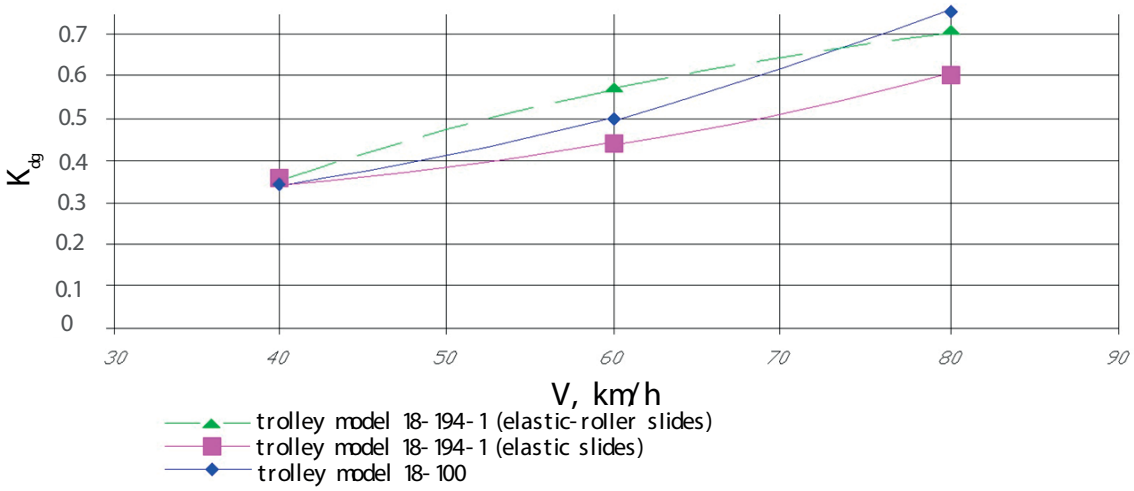

Figure 8 *Coefficients of vertical dynamic additives for unsprang masses when moving gondola cars in loaded condition (K_{dg}) (curve R=350 m)*

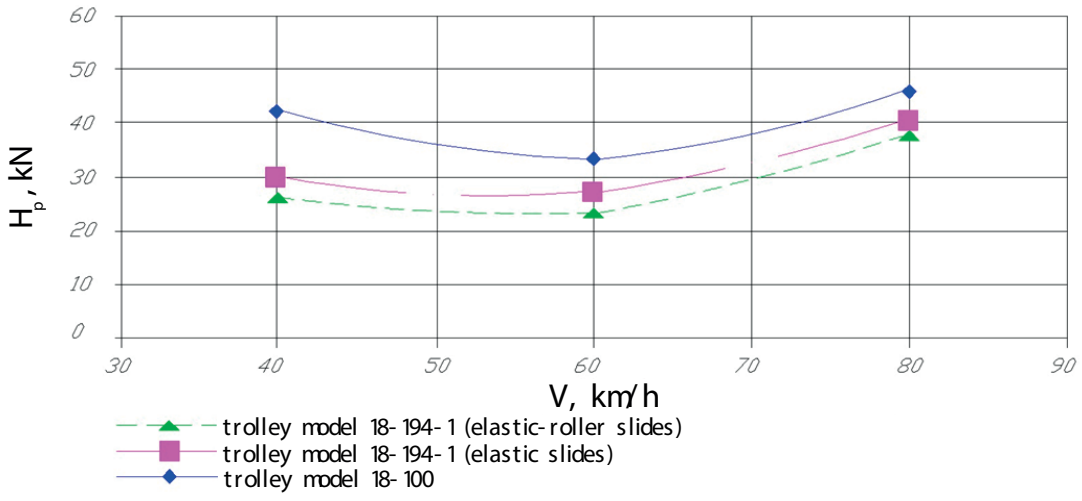

Figure 9 *Frame forces (H_p) when moving gondolas in loaded condition (curve R =350 m)*

sprung masses were significantly lower compared to the trolley 18-100 [18-19].

Running tests of trolleys on the Experimental ring of Scientific Research Institute of Railway Transport showed that the inter-repair mileage of their main components and parts reaches 750 thousand km. Thus, the trolley has the improved driving characteristics and an increased resource of main components, parts and friction pairs, which reduces the cost of maintaining wagons, increases train safety, increases the speed of cargo delivery [20-21].

Certification tests of these wagons were conducted in November 2011 on the Kazakh Railways by the Branch Scientific Research Laboratory of Dynamics and Strength of Rolling Stock of the Dnipropetrovsk National University of Railway Transport named after Academician V. Lazaryan, which has the status of a rolling stock testing laboratory. General technical conditions. The wheels of the prototype had a non-worn profile (Figure 10) [22].

A certificate of compliance with the Railway transport certification system was obtained for the trolley 18-194-1. The first 420 universal gondola cars 12-196-01 with increased load capacity on trolleys 18-194-1 are already in operation on the railway network. The freight wagons, which use the 18-194-1 trolley in their design, have increased technical and commercial parameters due to increased load capacity and reliability of the chassis and will be in demand on the rolling stock market.

The creation of promising cargo trolleys with increased axial load is the most urgent and knowledge-intensive task in the complex of works on development of the new generation wagons. Increasing the axial loads

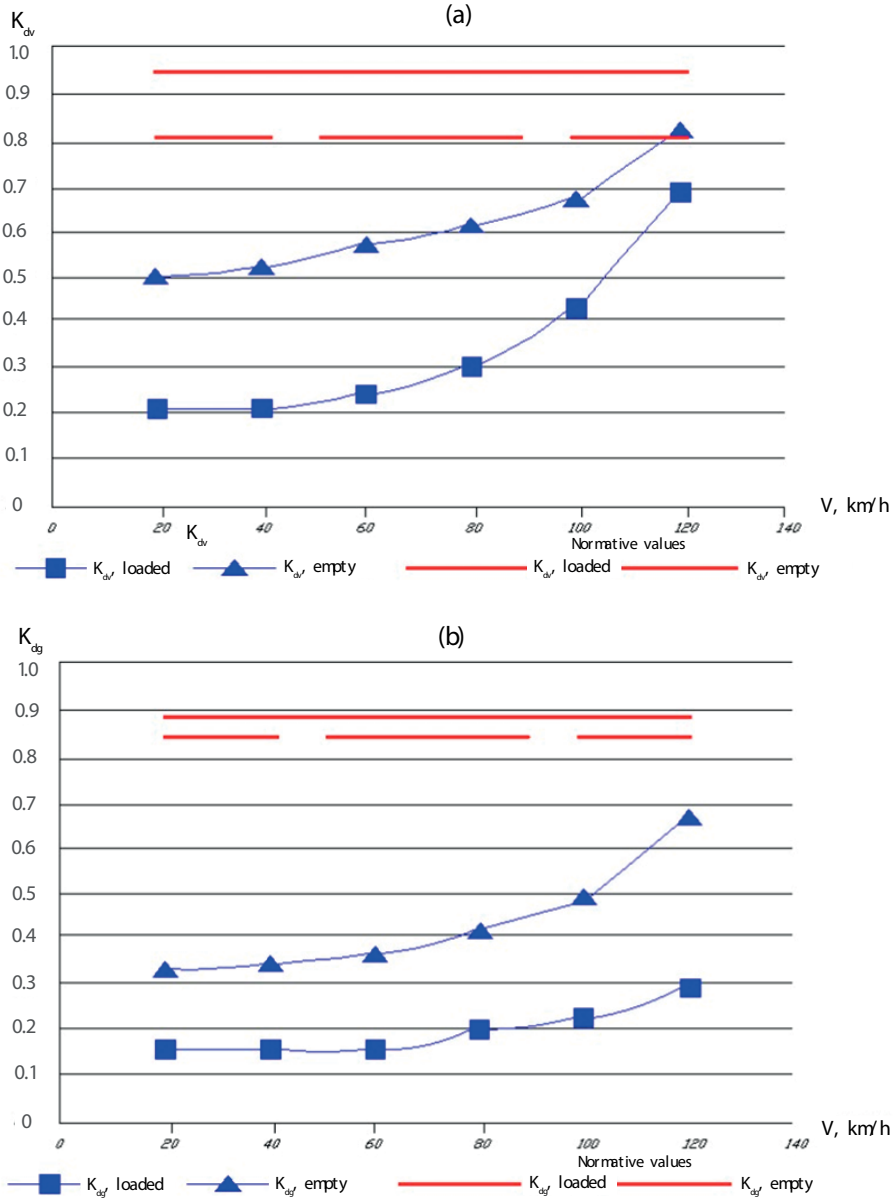

Figure 10 *The dependence of the coefficients of vertical (a) and horizontal (b) dynamics on speed when moving along a straight section of the path*

and speeds of freight wagons to solve the most important problem - increasing the freight and carrying capacity of railways will be cost-effective only if the new freight trucks have a "mild" effect on the track [23].

Among the measures aimed at ensuring the stability of the movement of wagons, and, above all, the most massive - freight, the design and condition of trolleys, especially those equipped with diagonal connections between their sidewalls, play a role. The largest number of patents and articles devoted to these constructions belong to Professor G. Scheffel (see, for example, [20, 24]). Freight wagons have been put into operation in Kazakhstan, the trolleys of which are equipped with diagonal connections.

The wagons of the 12-9920 model were manufactured for the railways of Kazakhstan by the Qiqihar Carriage Company CNPC (People's Republic of China). Their two-axle trolleys of the ZK1 type are designed for an axial load of 25 tons and a speed of 120 km/h in empty and loaded conditions. The design of the trolley with diagonal ties, elastic-roller slides, adapters, rubber shock absorbers and cassette bearings in the axle box is discussed above.

4 Conclusion

Increased axial loads have a significant impact on the dynamic interaction between the wagon wheelsets and the track. Increased weight and force on track elements lead to accelerated wear of rails, joints and ballast base. This is especially evident in high-traffic areas and when operating heavy trains, which requires more frequent maintenance and modernization of the infrastructure.

Modelling of dynamic processes has shown that the interaction of wheel sets with rails causes additional loads on joints and rail connections, increasing the risk of their failure. The rail track is subjected to greater wear and deformation, which may lead to the need for more frequent repair and replacement of elements.

Analyses of the dynamic interaction between the rail track and freight wagons under conditions of increased axial load led to the need to revise existing railway design standards. Recommendations on the use of more durable and wear-resistant materials for rails and other track components, as well as optimisation of wagon design taking into account dynamic characteristics can significantly improve the operational efficiency and safety of transport systems.

The results of this research have an important practical significance for the design, operation and repair of railways. The developed diagnostic and predicting methods can be introduced into the practice of railway companies, which will improve safety and reduce the risks associated with increased axle loads. In the future, it is possible to extend the study to other types of transport tracks and expand the methods to more accurately assess the condition of infrastructure under various operating modes.

The results of dynamic tests have shown sufficiently good driving qualities of the considered wagon, that with an increase in axial loads to 25 t/axle and above, it is necessary to optimize the design of wagon trolleys and strengthen the structure of the railway track by using rails of type R65 and above, reinforced concrete sleepers and crushed stone ballast;

- to reduce the dynamic impact of the wagon on the track, the total static deflection of the spring suspension should be at least 55 mm;
- when comparing trolleys of different designs with an axial load of 25 t/axle, it was found that:

1) the bending moment in the rails at a speed of 100 km/h for trolleys 18-194-1 is 4500 km, for trolleys 18-9996 - 4800 km;
2) the maximum load on the sleeper at a speed of 100 km/h for trolleys 18-194-1 is 60 kN, for trolleys 18-9996 - 68 kN;
3) the maximum deflection of the rail at a speed of 100 km/h for trolleys 18-194-1 is 4 mm, for trolleys 18-9996 - 4.5 mm.

In conclusion, the study has shown that the dynamic interaction of the rail track and freight wagons under increased axial load requires an integrated approach and the introduction of innovative technologies to ensure safe and efficient operation of railway transport.

Acknowledgements

The authors received no financial support for the research, authorship and/or publication of this article.

Conflicts of interest

The authors declare that they have no known competing financial interests or personal relationships that could have appeared to influence the work reported in this paper.

References

[1] ANDERSON, W. F., KEY, A. J. Model testing of two-layer railway track ballast. *Journal of Geotechnical and Geoenvironmental Engineering* [online]. 2000, **126**(4), p. 317-323. ISSN 1090-0241, eISSN 1943-5606. Available from: https://doi.org/10.1061/(ASCE)1090-0241(2000)126:4(317)

[2] ABDULLAYEV, S., TOKMURZINA-KOBERNYAK, N., ASHIRBAYEV, G., BAKYT, G., IZBAIROVA, A. Simulation of spring-friction set of freight car truck, taking into account track profile. *International Journal of Innovative Research and Scientific Studies* [online]. 2024, **7**(2), p. 755-763. eISSN 2617-6548. Available from: https://doi.org/10.53894/ijirss.v7i2.2883

[3] MOLATEFI, H., MAZRAEH, A., SHADFAR, M., YAZDANI, H. Advances in Iran railway wheel wear management: A practical approach for selection of wheel profile using numerical methods and comprehensive field tests. *Wear* [online]. 2019, **424-425**, p. 97-110. ISSN 0043-1648, eISSN 1873-2577. Available from: https://doi.org/10.1016/j.wear.2019.02.016

[4] BAKYT, G., SHALBAYEV, K., ABDULLAYEV, S., MAZHITOV, S., Hydrogen generator for internal combustion engine. *Journal of Applied Research and Technology* [online]. 2023, **21**(4), p. 535-541. ISSN 1665-6423, eISSN 2448-6736. Available from: https://doi.org/10.22201/icat.24486736e.2023.21.4.1963

[5] AZILKIYASHEVA, M. M., SHAYAKHMETOV, S. B., BAKYT, G. B., KOPENOV, B. T., BAUBEKOV, Y. Y., ZHAUYT, A. Development of a method for calculating the degree of use of the plasticity resource (Dupr) when rolling on a new continuous mill. *Metalurgija - Journal of Metallurgy* [online]. 2021, **60**(3-4), p. 362-364. ISSN Metallurgical 0543-5846, eISSN 1334-2576. Available from: https://hrcak.srce.hr/256109

[6] SHITTU, S., LI, G., AKHLAGHI, Y.G., MA, X., ZHAO, X., AYODELE, E. Advancements in thermoelectric generators for enhanced hybrid photovoltaic system performance. *Renewable and Sustainable Energy Reviews* [online]. 2019, **109**, p. 24-54. ISSN 1364-0321, eISSN 1879-0690. Available from: https://doi.org/10.1016/j.rser.2019.04.023

[7] LAU, A., HOFF, I. Simulation of train-turnout coupled dynamics using a multibody simulation software. *Modelling and Simulation in Engineering* [online]. 2018, **2018**, 578272. ISSN 1687-5591, eISSN 1687-5605. Available from: https://doi.org/10.1155/2018/8578272

[8] ABDULLAYEV, S., BAKYT, G., KAMZINA, A., SULEYEVA, N., TOKMURZINA-KOBERNYAK, N. Dynamic interaction of the TE-33A diesel locomotive and the track in a curve with a radius of 600 meters. *International Journal of Mechanical Engineering and Robotics Research* [online]. 2024, **13**(2), p. 205-212. eISSN 2278-0149. Available from: https://doi.org/10.18178/ijmerr.13.2.205-212

[9] GHAZAVI, M. R., TAKI, M. Dynamic simulations of the freight three-piece bogie motion in curve. *Vehicle System Dynamics* [online]. 2008, **46**(10), p. 955-973. ISSN 0042-3114, eISSN 1744-5159. Available from: https://doi.org/10.1080/00423110701730737

[10] PAGAIMO, J., MAGALHAES, H., COSTA, J. N., AMBROSIO, J. Derailment study of railway cargo vehicles using a response surface methodology. *Vehicle System Dynamics* [online]. 2022, **60**, p. 309-334. ISSN 0042-3114, eISSN 1744-5159. Available from: https://doi.org/10.1080/00423114.2020.1815810

[11] ABDULLAYEV, S., BAKYT, G., KAMZINA, A., SARSANBEKOV, K., ABDULLAYEVA, A. Interaction of the TE33a diesel locomotive and the railway track on curved section with radius 290 m. *Communications - Scientific Letters of the University of Zilina* [online]. 2023, **25**(4), p. B315-326. ISSN 1335-4205, eISSN 2585-7878. Available from: https://doi.org/10.26552/com.C.2023.069

[12] HARAK, S. S., SHARMA, S. C., HARSHA, S. P. Structural dynamic analysis of freight railway wagon using finite element method. *Procedia Materials Science* [online]. 2014, **6**, p. 1891-1898. ISSN 2211-8128. Available from: https://doi.org/10.1016/j.mspro.2014.07.221

[13] ABDULLAYEVA, A., KALABAYEVA, A., IVANOV, A., ABDULLAYEV, S., BAKYT, G. Methods for identification of complex industrial control objects on their accelerating characteristics. *Communications - Scientific Letters of the University of Zilina* [online]. 2022, **24**(3), p. B239-B246. ISSN 1335-4205, eISSN 2585-7878. Available from: https://doi.org/10.26552/com.C.2022.3.B239-B246

[14] MUSSABEKOV, M., BAKYT, G., OMIRBEK, A., BRUMERCIKOVA, E., BUKOVA, B. Shunting locomotives fuel and power resources decrease. *MATEC Web of Conferences* [online]. 2017, **134**, 00041. eISSN 2261-236X. Available from: https://doi.org/10.1051/matecconf/201713400041

[15] GAO, M., CONG, J., XIAO, J., HE, Q., LI, S., WANG, Y., YAO, Y., CHEN, R., WANG, P. Dynamic modeling and experimental investigation of self-powered sensor nodes for freight rail transport. *Applied Energy* [online]. 2020, **257**, 113969. ISSN 0306-2619, eISSN 1872-9118. Available from: https://doi.org/10.1016/j.apenergy.2019.113969

[16] BAKYT, G., JAILAUBEKOV, Y., ABDULLAYEV, S., ASHIRBAYEV, G., ASHIRBAYEVA, I. Assessment of carbon dioxide emissions in road transport, using exhaust gas cleaning technology, in the Republic of Kazakhstan. *Vibroengineering Procedia* [online]. 2023, **48**, p. 87-92. ISSN 2345-0533, eISSN 2538-8479. Available from: https://doi.org/10.21595/vp.2023.23163

[17] REZVANI, M. A., MAZRAEH, A. Dynamics and stability analysis of a freight wagon subjective to the railway track and wheelset operational conditions. *European Journal of Mechanics - A/Solids* [online]. 2017, **61**, p. 22-34. ISSN 0997-7538, eISSN 1873-7285. Available from: https://doi.org/10.1016/j.euromechsol.2016.08.011

[18] ABDULLAYEV, S., BAKYT, G., TOKTAMYSSOVA, A., ASHIRBAYEV, G., BAUBEKOV, Y., IMASHEVA, G. Determination of parameters of upper assembly of current collector when it interacts with contact suspension.

Vibroengineering Procedia [online]. 2024, **54**, p. 279-284. ISSN 2345-0533, eISSN 2538-8479. Available from: https://doi.org/10.21595/vp.2024.23917

[19] MASSEL, A. Experimental tracks and their role in testing of rolling stock and railway infrastructure. *Problemy Kolejnictwa /Railway Report* [online]. 2021, **192**, p. 153-170. ISSN 0552-2145, eISSN 2544-9451. Available from: https://doi.org/10.36137/1923E

[20] ABDYKADYROV, A., ABDULLAYEV, S., TASHTAY, Y., ZHUNUSSOV, K., MARXULY, S. Purification of surface water by using the corona discharge method. *Mining of Mineral Deposits* [online]. 2024, **18**(1), p. 125-137. ISSN 2415-3435, eISSN 2415-3443. Available from: https://doi.org/10.33271/mining18.01.125

[21] JAWAHAR, P., GUPTA, K., RAGHU, E. Mathematical modelling for lateral dynamic simulation of a railway vehicle with conventional and unconventional wheelset. *Mathematical and Computer Modelling* [online]. 1990, **14**, p. 989-994. ISSN 0895-7177. Available from: https://doi.org/10.1016/0895-7177(90)90326-i

[22] ABDULLAYEV, S., MUSAYEV, J., CHIGAMBAEV, T., MALYBAYEV, S., BAKYT, G. Optimum distribution of repairs -S-8 of electric locomotives VL80- between repair depots on the Republic of Kazakhstan railway. *Transport Problems* [online]. 2017, **12**(2), p. 19-30. ISSN 1896-0596, eISSN 2300-861X. Available from: https://doi.org/10.20858/tp.2017.12.2.3

[23] ANTOLIN, P., ZHANG, N., GOICOLEA, J. M., XIA, H., ASTIZ, M. A., OLIVERA, J. Consideration of nonlinear wheel-rail contact forces for dynamic vehicle-bridge interaction in high-speed railways. *Journal of Sound and Vibration* [online]. 2013, **332**(5), p. 1231-1251. ISSN 0022-460X, eISSN 1095-8568. Available from: https://doi.org/10.1016/j.jsv.2012.10.022

[24] HAN, Y., ZHANG, X., WANG, L., ZHU, Z., CAI, C.S., HE, X. Running safety assessment of a train traversing a long-span bridge under sudden changes in wind loads owing to damaged wind barriers. *International Journal of Structural Stability and Dynamics* [online]. 2022, **22**, 2241010. ISSN 0219-4554, eISSN 1793-6764. Available from: https://doi.org/10.1142/S0219455422410103

RESEARCH ON THE USE OF BIOGAS AS AN ADDITIVE TO COMPRESSED NATURAL GAS FOR SUPPLYING VEHICLE ENGINES

Oleksandr Kravchenko[1,*], Roman Symonenko[2], Juraj Gerlici[1], Andrii Golovan[3], Serhii Shymanskyi[4], Igor Gritsuk[5], Yuriy Grytsuk[6]

[1]University of Zilina, Zilina, Slovakia
[2]Center for Scientific Research of Complex Transport Problems, State Road Transport Research Institute, Kyiv, Ukraine
[3]Department of Navigation and Maritime Safety, Odesa National Maritime University, Odesa, Ukraine
[4]Sector for Ensuring the Circulation of Cards for Digital Tachographs, State Road Transport Research Institute, Kyiv, Ukraine
[5]Department of Operation of Ship Power Plants, Kherson State Maritime Academy, Odessa, Ukraine
[6]Department of General Engineering Training, Donbas National Academy of Civil Engineering and Architecture, Ivano-Frankivsk, Ukraine

*E-mail of corresponding author: avtoap@ukr.net

Oleksandr Kravchenko 0000-0003-4677-2535,
Juraj Gerlici 0000-0003-3928-0567,
Igor Gritsuk 0000-0001-7065-6820,
Serhii Shymanskyi 0000-0001-5316-2466
Roman Symonenko 0000-0002-4269-5707,
Andrii Golovan 0000-0001-6589-4381,
Yuriy Grytsuk 0000-0003-3389-1172,

Resume

Internal combustion engines, which operate in various load and speed conditions, are significant sources of environmental pollution that affect a vehicle's movement in traffic. Automotive engines typically operate in unsteady-state modes, transitioning cyclically from one operating mode to another during vehicle operation. The potential of using biogas as an additive to compressed natural gas for automotive engines was explored within this research. The results of experimental studies on the fuel efficiency and environmental performance of a vehicle with a petrol engine, converted to run on a mixture of compressed natural gas and biogas, are presented. A comparative analysis was conducted on the fuel and economic performance, as well as environmental indicators of A-92 petrol, compressed natural gas, and a mixture of compressed natural gas and biogas in the European driving cycle modes.

Article info

Received 9 November 2024
Accepted 18 March 2025
Online 14 April 2025

Keywords:

biogas
compressed natural gas
alternative fuel
European driving cycle
harmful substances
internal combustion engine

Available online: https://doi.org/10.26552/com.C.2025.034

ISSN 1335-4205 (print version)
ISSN 2585-7878 (online version)

1 Introduction

The escalating energy demands of humanity result in increased energy consumption, leading to resource depletion and environmental pollution. Currently, the pressing issue is to conserve natural resources and protect the environment while simultaneously increasing energy production to meet human needs. This can be achieved by utilizing alternative fuels derived from renewable sources. Biogas can be produced through the anaerobic decomposition of organic waste.

Fully or partially purified biogas is similar to compressed natural gas (CNG) in terms of its characteristics. As a result, it can be stored and transported in a compressed or liquefied state [1]. Special tankers can deliver it to petrol stations, and it can be supplied through the special gas pipelines.

Biogas is composed of methane (CH_4), carbon dioxide (CO_2), small amounts of carbon monoxide (CO), hydrogen (H_2), nitrogen (N_2), oxygen (O_2), water vapor (H_2O), and hydrogen sulphide (H_2S). When used as a fuel, biogas affects the operation of internal combustion engines differently than the traditional fuels.

According to a literature review, most studies have focused on evaluating the environmental impact, fuel efficiency, and engine performance of biogas [2] and CNG as alternative fuels compared to traditional gasoline. Khan et al. [3] stated that using biogas as an additive to CNG results in the same fuel economy and lower carbon dioxide emissions compared to vehicles fueled solely with CNG. Bordelanne et al. [4] found that vehicles fueled with biomethane-enriched CNG can reduce the greenhouse gas emissions by more than 80% compared to gasoline-powered vehicles. Agbulut et al. [5] discovered that adding biogas to CNG can reduce exhaust emissions and improve performance metrics in gasoline engines. Chandra et al. [6] observed that methane-enriched biogas showed almost similar engine performance compared to compressed natural gas in terms of brake power output, specific gas consumption, and thermal efficiency. Shamekhi et al. [7] stated that CNG, may improve the fuel efficiency and environmental performance of gasoline engines compared to traditional fuels like gasoline. Singhal et al. [8] suggested that biogas is a potential fuel for providing a continuous supply of CNG in the form of bio-CNG, which contains about 95% methane. Lemke et al. [9] found that converting a production vehicle to run on gasoline, CNG, and biomethane shows potential for improving fuel efficiency and environmental performance compared to traditional fuels like A-92 gasoline. Melaika et al. [10] observed that gaseous fuels, such as natural gas and biogas, can improve engine efficiency, reduce standard emissions and particulates, and provide additional benefits like lower particulate numbers compared to gasoline. Wargula et al. [11] observed that CNG-fueled engines reduced fuel consumption by 31% and hourly estimated machine operating costs resulting from fuel costs by 53% compared to traditional gasoline engines. Limpachoti and Theinnoi [12] found that Compressed Biomethane Gas (CBG) fuel in a spark ignition engine has higher thermal efficiency and lower NOx and HC emissions compared to CNG. Pavlovskyi [13] have shown how the use of biodiesel blends with rapeseed oil additives can improve fuel efficiency and reduce emissions in diesel engines, specifically noting a significant reduction in total mass emissions when using three-component biodiesel fuels.

However, the impact of using biogas as an additive to compressed natural gas on the fuel efficiency and environmental performance of gasoline engines has not been extensively researched, particularly when compared to traditional fuels like A-92 gasoline. The gaps in research discussed above motivate us to focus on answering the question - "What is the impact of using biogas as an additive to compressed natural gas on the fuel efficiency and environmental performance of gasoline engines converted to run on this mixture compared to traditional fuels such as A-92 gasoline?" The research question aims to investigate the impact of compressed natural gas and biogas blends on the environmental performance and fuel efficiency of vehicle engines. The study results will provide valuable insights into the potential of biogas as an alternative fuel that can help reduce harmful emissions and increase energy independence.

The paper's structure can be summarized as follows. Section 2 provides a detailed methodology for studying the impact of using biogas as an additive to compressed natural gas on the fuel efficiency and environmental performance of petrol engines. Section 3 presents and discusses the study results. Section 4 presents conclusions and prospects for further research.

2 Research methodology

A methodology for researching the impact of biogas on engine and vehicle performance has been developed for conducting experimental and theoretical studies.

The research methodology comprises theoretical and experimental measures. Conclusions can be drawn about the effectiveness of using a mixture of natural gas and biogas to improve the fuel, economic, and environmental performance of a vehicle in operation [14].

Figure 1 shows the flowchart of this methodology, which comprises eight stages.

The initial stage includes an analysis of previous studies on the use of biogas to reduce pollution from cars and save oil products. This stage requires analyzing research conducted by individual authors and research organizations both in Ukraine and abroad. When analyzing the literature, biogas was evaluated to determine its advantages and disadvantages [15]. Special attention was given to the potential for its widespread use as a motor fuel and its ability to improve the environmental performance of vehicles [16]. According to the analysis in the first section, it is predicted that in the near future, a mixed fuel consisting of CNG, and biogas will likely replace petrol as a fuel for spark-ignition automotive engines, rather than pure biogas.

The second stage entails selecting and justifying a test-driving cycle, conducting experimental research on regulating the car engine power supply system while driving a car in the European urban driving cycle, and improving gas fuel equipment [17].

At the third stage, the permissible content of the inert component (6%) was determined by simulating a mixture of CH_4 and different proportions of CO_2. Based on the characteristics and properties of the available biogas, the ratio between the components of the mixed fuel - CNG 80% and biogas 20% was determined. The similarity between the proposed mixed fuel and the simulated gas was established. Subsequently, due to the lack of an adequate amount of biogas, large-scale experimental studies of the car were carried out when the engine was powered by the simulated gas.

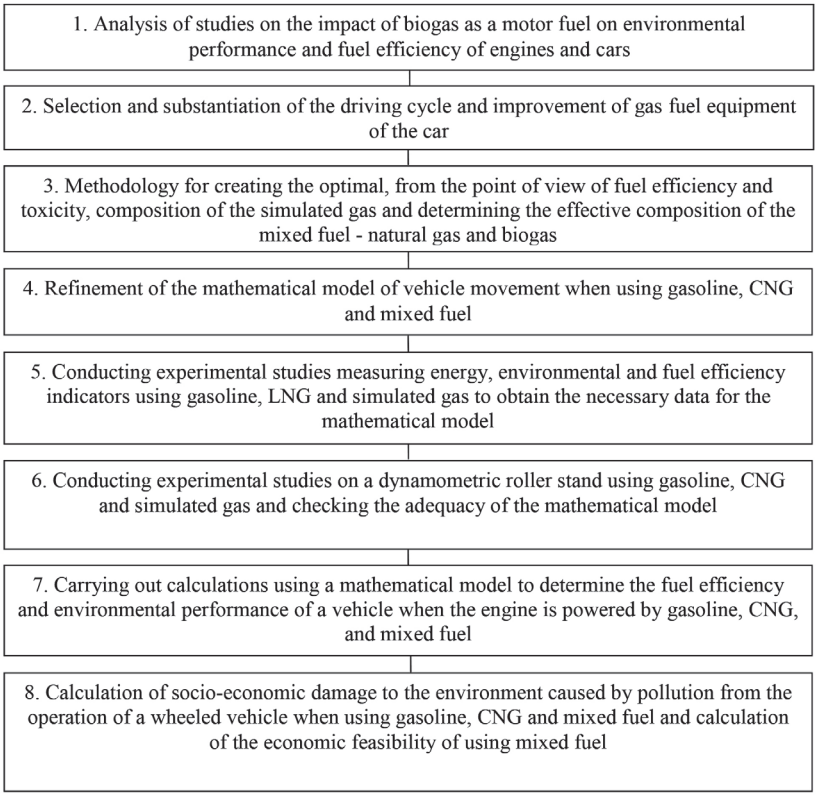

Figure 1 *Flowchart of the general research methodology*

Mathematical modelling is frequently employed to determine engine performance across a wide range of operating conditions, including transient modes [18]. Therefore, it is necessary to refine the existing mathematical model [19] that simulates the movement of a car during test cycle modes to study the efficiency of using different types of fuels, particularly mixed fuels (stage four).

When compiling a mathematical model of vehicle movement according to the European driving cycle modes, seven modes are distinguished, according to the types of their identical mathematical description [20-21]:

- engine operation in idling mode;
- engine acceleration in idling mode;
- vehicle starting from a standstill in the first gear;
- gear shifting from higher to lower and from lower to higher;
- vehicle movement at a constant speed;
- vehicle deceleration with the clutch locked;
- engine deceleration with the clutch disengaged.

Mathematical dependencies describing changes in the main parameters characterizing the engine operation in the study were compiled based on the results of experimental studies. The description of the parameters was carried out by a factorial experiment in a wide range of changes in speed and load modes on a dynamometric roller stand. As a result, hourly fuel and air consumption and concentrations of harmful substances in engine exhaust gases were established [20].

For calculations based on the refined mathematical model, it is necessary to conduct a number of experimental studies to measure the fuel efficiency and environmental performance [22] when the car engine is powered by petrol, CNG and simulated gas (similar to mixed fuel) and to develop polynomial dependencies that describe engine performance in a wide range of speed and load conditions when powered by petrol, CNG and mixed fuel (stage five).

The mathematical model was improved to calculate the fuel consumption and the concentration of harmful substances in engine exhaust gases under different speed and load conditions during the driving cycle. The model was tested using petrol, CNG, and mixed fuel (stage six).

During the seventh stage, experimental tests were conducted on the car using petrol, CNG, and simulated gas to determine its environmental performance and fuel efficiency in different driving modes over the driving cycle. The tests were carried out on a dynamometer roller stand under engine conditions. Additionally, the obtained data from the mathematical model is compared to the experimental data.

At the eighth stage, the socio-economic damage to the environment [23] caused by pollution from the operation of a wheeled vehicle using petrol, CNG and mixed fuel was calculated, and the economic feasibility [24] of using mixed fuel was calculated.

Currently, there are three groups of driving cycles used worldwide to assess the fuel efficiency and environmental performance of vehicles: European, US,

and Japanese driving cycles. For research purposes, it is appropriate to use the European driving cycle of a car, as regulated by UNECE Regulation No. 83. This regulation provides uniform provisions for the approval of vehicles regarding the emission of pollutants in accordance with engine fuel requirements.

The European Driving Cycle, also known as the EU and ECE (European Economic Commission) test cycle, is a program designed to closely simulate urban driving. It was supplemented in 1993 by the Extra Urban Driving Cycle (EUDC), which includes suburban driving at speeds of up to 120 km/h. The New Urban Driving Cycle (NEDC) is a combination of the urban and suburban cycles.

The use of natural and biogas as motor fuels has some disadvantages compared to liquid fuels. These include a low energy concentration in 1 m^3 of the combustible mixture, which results in a decrease in the effective power of the engine. For the spark ignition engines, the decrease is around 11-12% with optimization of the ignition advance angle and 17-19% without optimization.

For combustible mixtures with an excess air ratio of $\alpha = 1$, lower calorific value of 1 m^3 is: petrol-air - $h_H = 3739$ kJ/m^3; gas-air - $h_H = 3404$ kJ/m^3; and biogas-air (with $CH_4 = 62\%$) - $h_H = 2168$ kJ/m^3.

Based on the preliminary calculations, the heat reduction in 1 m^3 of the engine fuel mixture is 8.7% when using natural gas, 42.1% when using biogas, and 15.25% when using a mixture of 80% natural gas and 20% biogas.

To prevent a decrease in engine energy performance and energy losses during the biogas purification when used as a motor fuel, it is recommended to use it as a mixed fuel with natural gas.

Experimental studies were conducted on a vehicle with an external mixture formation engine. (Table 1), which was converted to run on gas fuel. The car was tested using petrol, CNG, and a mixture of CNG and biogas. For petrol, a carburetor-mixer was used, while for CNG, a three-stage reducer, gas metering, and carburetor-mixer were used. The fuel-air mixture in the engine was regulated by the vacuum in the inlet pipeline. Feedback on the oxygen content in the exhaust gases of the engine was not used.

The studies remain relevant as there are still many

Table 1 *Technical characteristics of the car*

Title	Value
Fuel	A-92
Engine displacement, cm^3	1300
Engine power, kW	52
Engine torque, Nm / Engine speed, rpm	96 / 3400
Engine layout / number of cylinders	straight / 4
Maximum speed, km/h	145
Fuel consumption (combined cycle), liters per 100 km.	9
Fuel consumption (urban cycle), liters per 100 km.	11
Fuel consumption (suburban cycle), liters per 100 km.	8
Compression ratio	8.5
Engine crankshaft moment of inertia, kg m^2	0.15
Wheel moment of inertia, kg m^2	0.7
Dynamic wheel radius, m	0.255
Transmission	4 manual transmission (mechanics)
Gearbox ratios	
- 1 gear	3.753
- 2 gear	2.303
- 3 gear	1.493
- 4 gear	1
Final drive ratio	4.3
Drive type	Rear
Front suspension	Independent. Multi-link
Rear suspension	Dependent. On longitudinal levers
Front brake	Disk
Brake rear	Drum
Tire size	155 SR13
Curb weight, kg	955

vehicles in operation that run on both petrol and gas fuels without exhaust gas oxygen feedback.

The experiments were conducted on a simulated roller stand (Figure 2), strictly adhering to the predetermined speeds, to accurately measure the level of harmful substances present in the exhaust gases (CO, NO_x, CH, C_mH_n, CO_2).

Several experimental studies were conducted to determine the feasibility of using the biogas mixed with CNG as a motor fuel. The studies required a substantial amount of biogas.

Large-scale biogas production has not yet been established in Ukraine. Biogas is mainly produced in the industrial and agricultural sectors. In the private sector, biogas is produced in smaller volumes and under non-standardised conditions, resulting in fluctuations in biogas characteristics.

The enterprises use the biogas they produce, but taking constant samples or large volumes of gas would disrupt the closed production cycle. This would not be suitable for the producers as it would interrupt the biogas production process. Consequently, it was not possible to purchase enough biogas for testing.

It is possible to construct a biogas plant independently. However, due to the small size of the plant, the composition of the biogas may vary at the beginning, middle, and end of the production process. A stable biogas composition is crucial for the road transport.

The availability of biogas may change over time if a network of gas filling stations that sell biogas according to the standard is established, or if it is produced in large volumes and is consistent across filling stations from production to consumption. Convincing evidence of the efficiency of biogas production and use as a motor fuel is required for this to occur, which is the focus of this research.

Due to the current shortage of biogas that could be used for experimental studies of automobile engines, a methodology for simulating gas containing methane and carbon dioxide in certain proportions (CH_4 - 94% and CO_2 - 6%) was developed, which corresponds to a mixture of CH_4 - 80% and biogas 20% with a CO_2 content close to 6%.

The required content of the inert component was determined by simulating a mixture of CH_4 with varying proportions of CO_2.

Two methods of adding CO_2 were used in the sequence of experiments:

1) adding CO_2 to the mixture with air, and
2) adding CO_2 to a mixture with CNG.

To determine the optimal dose of CO_2 and the appropriate method of addition, the stand was equipped with a reference volumetric gas meter called “CALIBR”, with factory number 00017. The meter has a measuring range of 0.016 to 10.00 m^3/h with an error of ± 0.3% of the measured value.

The purpose of the set of experimental studies of the car is to determine the effect of using different types of fuels to power the engine: A-92 petrol, CNG and simulated gas (which is close to mixed fuel in its

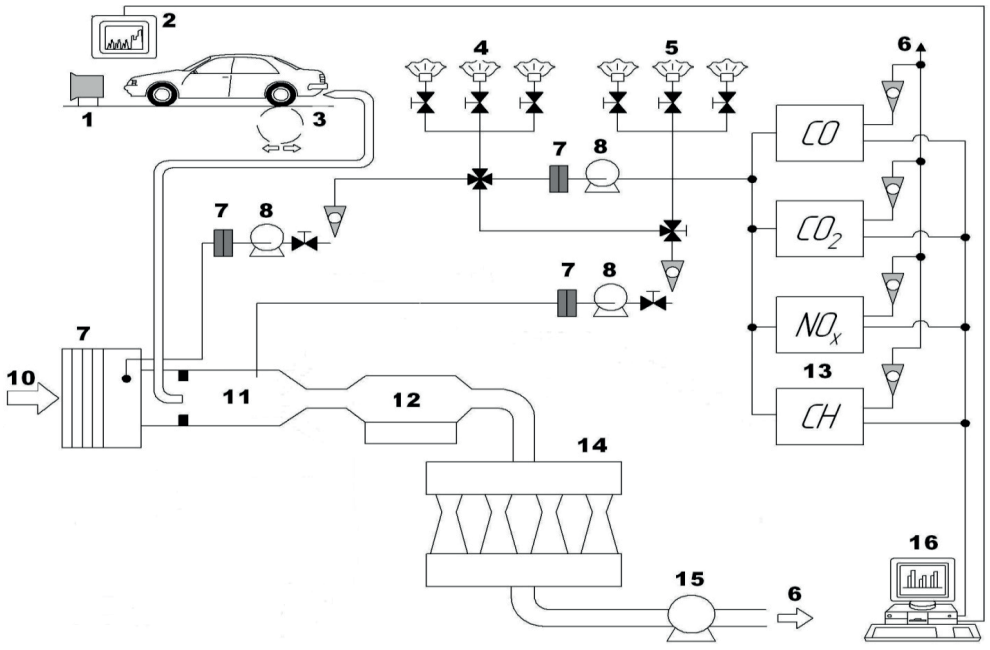

1 - blower; 2 - monitor for displaying the driving cycle; 3 - rollers; 4 - air sampling tanks; 5 - exhaust gas sampling tanks; 6 - exhaust gas outlet; 7 - filter; 8 - vacuum pump; 9 - heater; 10 - air supply; 11 - exhaust gas dilution tunnel; 12 - heat exchanger/heater; 13 - gas analyzers; 14 - venturi nozzles; 15 - centrifugal vacuum pump; 16 - computer for processing results

Figure 2 *Diagram of the simulating roller stand*

composition), on its performance in different load and speed modes and in the modes of the European driving cycle.

To accomplish this objective, the following tasks were completed:

1. Optimal adjustment of gas equipment, considering the improvement of the vehicle's environmental performance and the improvement of gas fuel equipment.
2. Checking the compliance of the simulated gas with the mixed fuel in the modes of the car's movement according to the European driving cycle.
3. Determination of the energy, fuel-economic and environmental performance of the engine when operating in different load and speed modes and active idling mode when powered by different types of fuels.
4. Determining the performance of the car when the engine is powered by A-92 petrol, CNG and simulated gas during the testing on a dynamometer roller stand to verify the adequacy of the refined mathematical model.

A factorial experiment was conducted to assess the economic and environmental performance of the engine using different types of fuels and advanced gas cylinder equipment.

The dynamometer continuously recorded the following parameters during the tests: vehicle speed, total fuel consumption in gallons per mile (G_{pal}), concentrations of carbon monoxide (CO), total hydrocarbons (CH), non-methane hydrocarbons (C_mH_n), nitrogen oxides (NO_x), and carbon dioxide (CO_2) in dilute exhaust gases.

The calculation method was utilised to determine the specific G_{CO} - mass emissions of carbon monoxide per cycle, G_{CO2} - carbon dioxide, G_{CH} - total hydrocarbons, G_{CmHn} - non-methane hydrocarbons, and G_{NOx} - nitrogen oxides.

During the testing, exhaust gases are continuously analysed and sampled using the Constant Volume Sampling method and stored in elastic containers. The emissions of harmful substances are calculated by averaging the concentrations of harmful substances in the exhaust gases. This is obtained by processing a dataset of instantaneous values of concentrations of harmful substances in the exhaust gases, or by averaging the concentrations of harmful substances in diluted exhaust gases sampled into an elastic container.

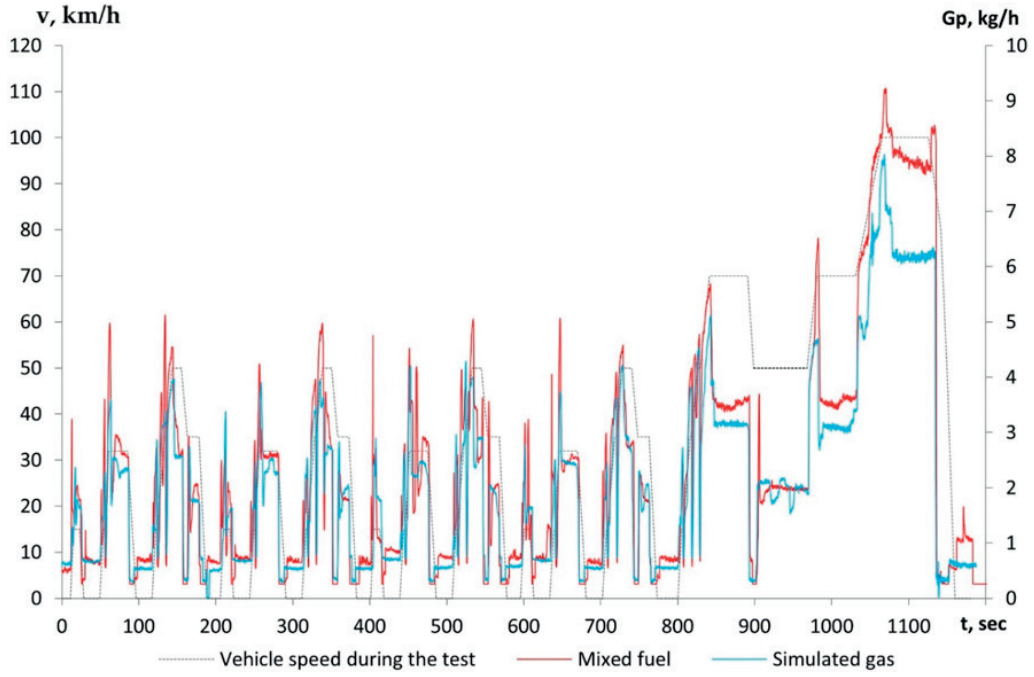

Figure 3 *Instantaneous fuel consumption values (Gp) during the car test on the roller stand in the driving modes according to the European driving cycle*

Table 2 *Fuel consumption and harmful substances emissions during the testing of a car on a dynamometer roller bench in the European driving cycle modes*

Fuels	Fuel consumption, g/cycle	Mass emissions of harmful substances			
		G_{CO}, g/km	G_{NOx}, g/km	G_{CO2}, g/km	G_{CmHn}, g/km
Mixture of natural and biogas	720.56	0.5313	0.4552	113.2	0.3463
Simulated gas	677.35	0.5040	0.4269	106.4	0.3334

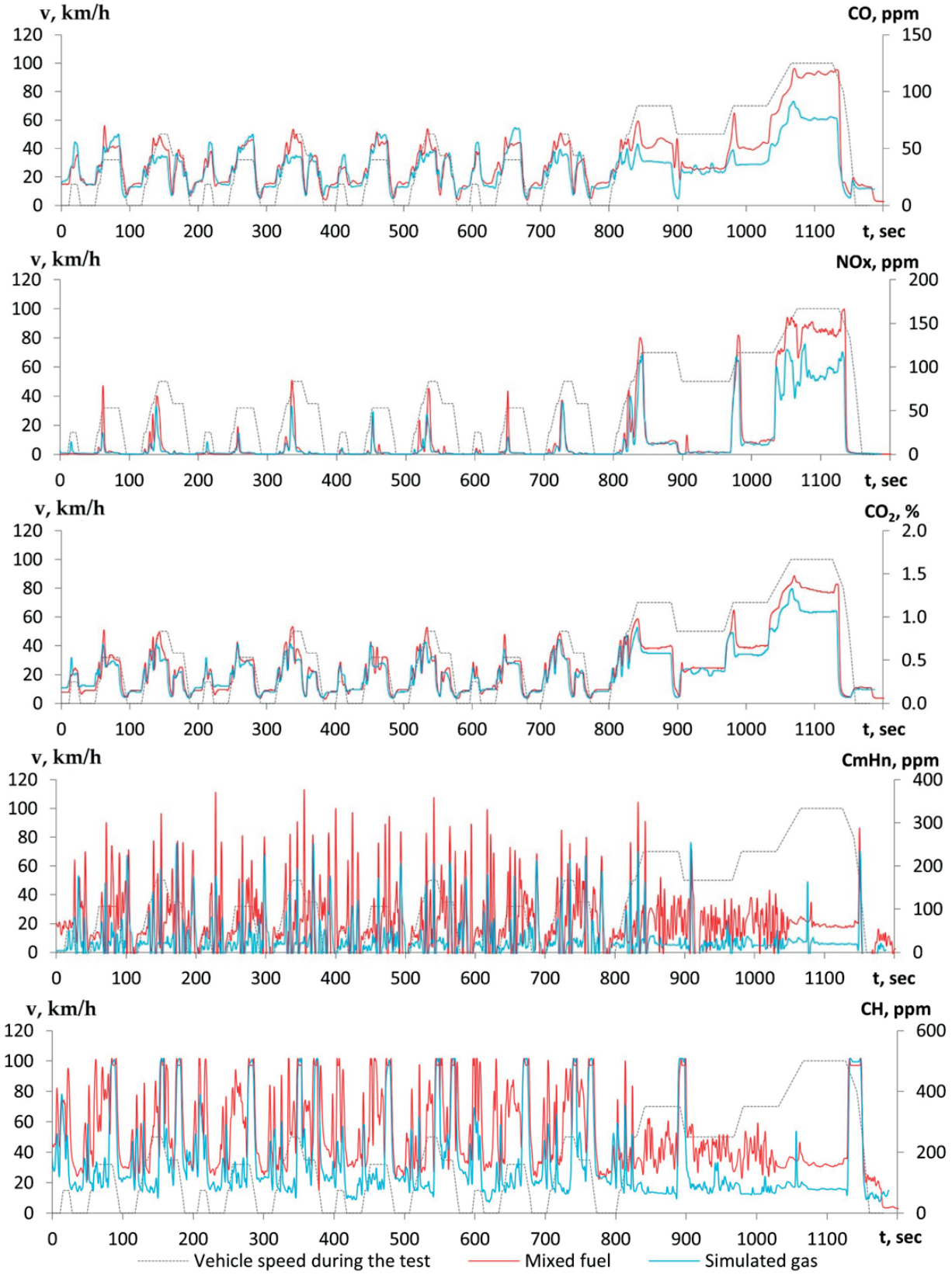

Figure 4 *Instantaneous concentrations of harmful substance oxides in exhaust gases during the test of a car on a dynamometer roller test bench in driving modes according to the European driving cycle*

3 Research results

Tests were conducted to evaluate the environmental performance of the engine using different types of fuel: petrol, CNG, mixed fuel (80% LNG and 20% biogas) and simulated gas (94% LNG and 6% CO_2).

The biogas used in the research has the following composition: CH_4 - 57%, CO_2 - 30%, N_2 - 11%, H_2O - 3%, O_2 - 0%.

The results of the first stage of testing of the vehicle are shown in Figures 3-6.

An excessive level of carbon monoxide CO concentration in exhaust gases, when the car engine is powered by CNG, indicates excessive enrichment of the gas-air mixture. The increase in CO concentration occurs in the engine braking mode.

The level of NO_x concentrations with exhaust gases, when powering an CNG engine, is almost the same as with petrol.

Emissions of total hydrocarbons CH increase in the engine braking mode. The level of concentrations of non-methane hydrocarbons C_mH_n in the exhaust gases of the engine when powered by CNG is reduced compared to petrol.

Figure 3 displays the results of measuring instantaneous fuel consumption during a car test on a roller bench in the European driving cycle modes when the engine is powered by a mixture of fuels (80% CNG and 20% biogas) and simulated gas (94% CNG and 6% CO_2). Figure 4 shows the results of measuring instantaneous concentrations of harmful substances in the exhaust.

The results of the tests of the car, when the engine is powered by mixed fuel and simulated gas, on a dynamometer roller stand in the driving modes according to the European driving cycle, are given in Table 2.

According to the results of tests of the car on a dynamometer roller stand in driving modes according to the European driving cycle, when the engine is powered by mixed fuel, fuel consumption increases by 6% compared to the engine power supply with simulated gas.

The emissions of harmful substances in exhaust gases are reduced when simulated gas is used compared to mixed fuel. Specifically, carbon monoxide (CO) is reduced by 5.1%, nitrogen oxides (NO_x) by 6.2%, carbon dioxide (CO_2) by 6%, and non-methane hydrocarbons (H_{CmHn}) by 3.7%.

The experimental studies confirm that the simulated gas is suitable for large-scale experiments using mixed fuels.

Thus, a simulated gas (CH_4 - 94% and CO_2 - 6%) was used for a large series of experimental studies, which corresponds to a mixture of CH_4 - 80% and biogas 20% with a CO_2 content close to 6%. The biogas used in the research has the composition: CH_4 - 57%, CO_2 - 30%, the rest are gases that do not participate in the combustion process (N_2 - 11% and H_2O - 3%).

Figure 5 displays the instantaneous fuel consumption values obtained during the car test on a roller stand in the European driving cycle.

Figure 6 displays the measurements of harmful substance concentrations in engine exhaust gases during car testing on a dynamometer roller in the European driving cycle.

Tables 3 and 4 present the results of tests conducted on the car using various types of fuel on a dynamometer roller stand in the European driving cycle.

Based on the results of the car's tests on

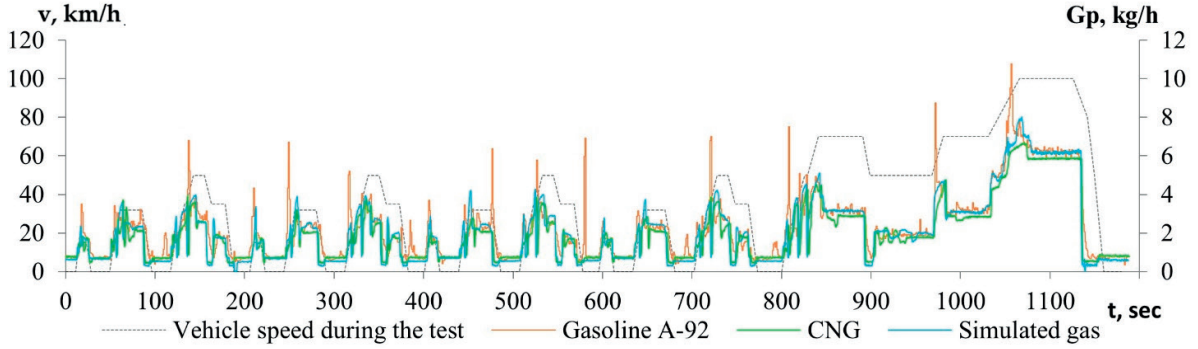

Figure 5 *Instantaneous values of fuel consumption G_{fuel} during the test of the car on the roller stand in the European driving cycle modes*

Table 3 *Fuel consumption during testing of the car on a dynamometer roller bench in driving modes according to the European driving cycle*

Fuels	g/cycle	MJ/cycle	Fuel consumption
A-92 petrol	750.81	33.04	9.17 litters/100 km
CNG	652.61	30.02	7.96 m³/100 km
Simulated gas	677.35	29.26	7.8 m³/100 km

a dynamometer roller under the conditions of the European driving cycle, it was found that the fuel consumption (g/cycle) decreased by 13.1% when powered by CNG and by 9.8% when powered by simulated gas, compared to A-92 petrol.

The experimental studies used fuels with varying

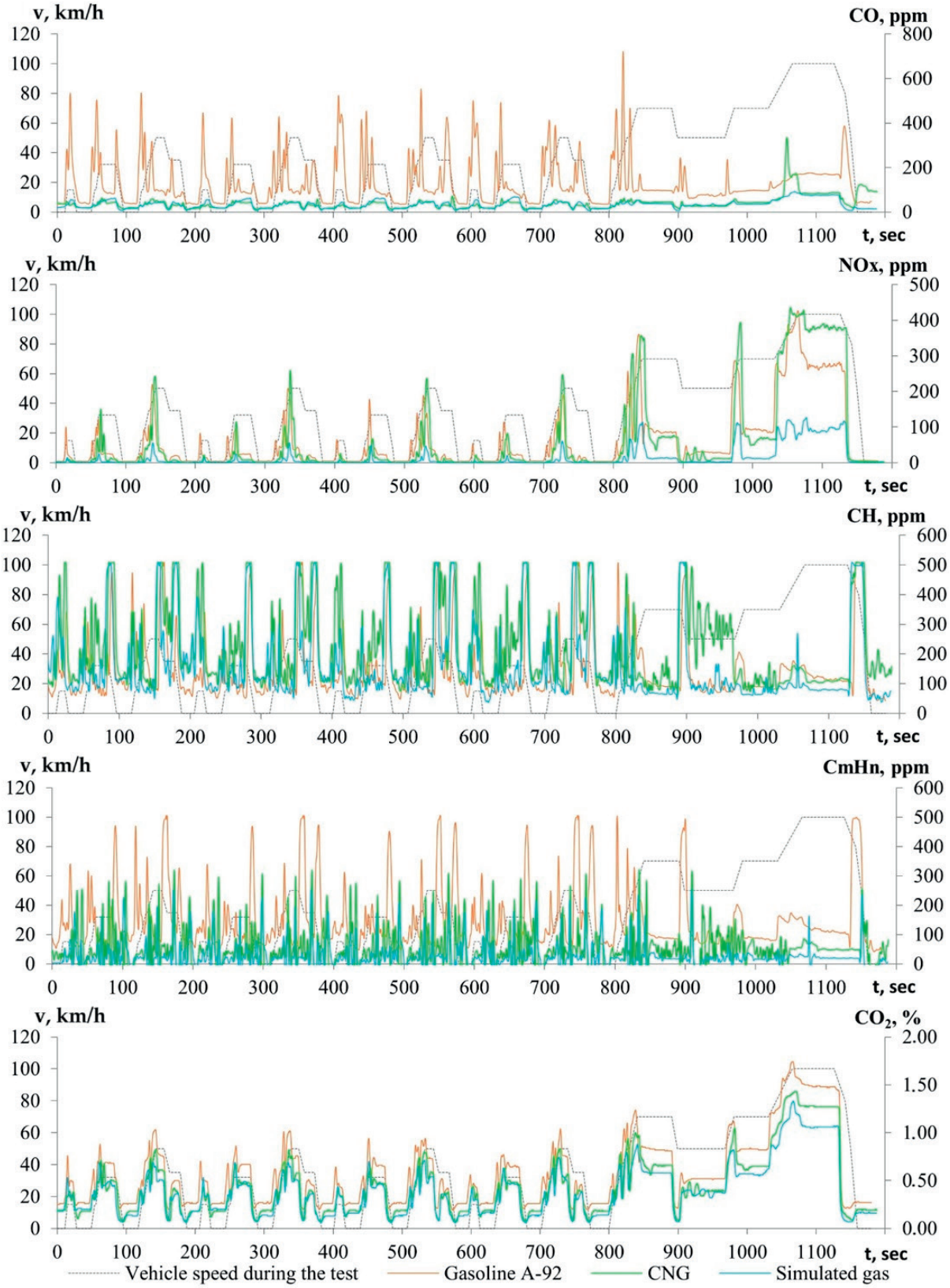

Figure 6 *Instantaneous concentrations of harmful oxides in engine exhaust gases during the test of a car on a dynamometer roller dynamometer in driving modes according to the European driving cycle*

Table 4 *Mass emissions of harmful substances during the testing of a car on a dynamometer roller bench in driving modes according to the European driving cycle*

Mass emissions of harmful substances	A-92 petrol	CNG	Simulated gas
G_{CO}, g/km	2.7743	0.7379	0.5040
G_{CO2}, g/km	180.8	127.3	106.4
G_{CH}, g/km	1.5051	2.7941	1.7749
G_{NOx}, g/km	1.7855	1.7580	0.4269
G_{CmHn}, g/km	1.4502	0.7352	0.3334
$G_{\Sigma CO}$, con. g/km	80.741	75.315	19.103

specific heat of combustion. The quality of heat use was assessed by fuel consumption in energy equivalent (MJ/cycle). The results show that when the engine is powered by CNG (46 MJ/kg), there is a 9.1% reduction in fuel consumption in energy equivalent. Similarly, when powered by simulated gas (43.2 MJ/kg), there is an 11.8% reduction compared to A-92 petrol (44 MJ/kg), which was used in the driving cycle.

Based on the obtained concentrations, the mass emissions of individual components and total mass emissions reduced to CO were calculated (Table 4).

The use of simulated gas in cars improves their environmental performance compared to A-92 petrol. Specifically, when powered by CNG, carbon monoxide (CO) emissions are 73.4% lower, and nitrogen oxides (NO_x) emissions are 1.5% lower. When powered by simulated gas, CO emissions are 81.8% lower, and NO_x emissions are 76.1% lower. Additionally, CO_2 emissions are 29.6% lower when powered by CNG and 41% lower when powered by simulated gas. When powered by simulated gas, emissions are 6% lower compared to non-simulated gas. Additionally, non-methane hydrocarbons (H_{CmHn}) are 49.3% lower with CNG and 77% lower with simulated gas. However, total hydrocarbons (H_{CH}) increase by 46.1% with CNG and by 15.2% with simulated gas.

The facility's environmental assessment calculates the total mass emissions reduced to CO using mass emissions and their relative aggressiveness coefficients (CO = 1, NO_x = 41.1, CH = 3.16).

Table 4 displays the total mass emissions reduced to CO. When powered by CNG, the total mass emissions of harmful substances in exhaust gases, reduced to CO, in the European driving cycle are reduced by 1.1% compared to A-92 petrol. Similarly, when powered by simulated gas, the emissions are reduced by 76.3% compared to A-92 petrol.

The novelty of this study can be summarised in the following aspects:

The study confirms a significant reduction in emissions of harmful substances in exhaust gases when using a mixture of biogas and compressed natural gas compared to traditional petrol.

The results of the study show an improvement in fuel efficiency, which is important for reducing the fuel costs and increasing the energy efficiency of vehicles.

The study's results suggest that a combination of biogas and compressed natural gas could be implemented for everyday use, contributing to the adoption of renewable energy sources in the transport sector.

These aspects underline the significant potential and importance of the research in the context of energy sustainability, environmental safety and innovation in the transportation.

4 Conclusions and prospects for further research

The results of the studies show that the use of mixed fuel (which was replaced by a similar simulated gas during the tests) reduces the concentrations and emissions of harmful substances in the exhaust gases.

Tests of a car equipped with a spark ignition engine, converted to run on CNG, show that mass emissions of harmful substances with exhaust gases, namely CO, G_{CmHn}, and G_{NOx}, decrease when the engine is powered by CNG, and simulated gas, compared to A-92 petrol. However, G_{CH} increases.

The test results showed that when the engine is powered by CNG, the total mass emissions of harmful substances reduced to CO, in the European driving cycle, are reduced by 1.1%, and by simulated gas - by 76.3%, compared to A-92 petrol.

The use of biogas as a motor fuel for car engines can reduce energy dependence on oil fuels and emissions of harmful substances in exhaust gases. Additionally, biogas can be used as an additive to compressed natural gas, eliminating the need for additional resources for purification. The study results can serve as a scientific foundation for developing policies and regulatory standards for alternative fuel use in vehicles. This can aid in transitioning towards a more sustainable transportation system.

Acknowledgment

This research was funded by the Cultural and Educational Grant Agency of the Ministry of Education of the Slovak Republic in the project KEGA 031ZU-

4/2023: Development of key competencies of the graduate study program Vehicles and Engines and KEGA 024ZU-4/2024: Deepening the knowledge of university students in the field of construction of transport means by carrying out professional and scientific research activities in the field; the Slovak Research and Development Agency of the Ministry of Education, Science, Research, and Sport in the project VEGA1/0513/22 "Investigation of the properties of railway brake components in simulated operating conditions on a flywheel brake stand"; the EU NextGenerationEU through the Recovery and Resilience Plan for Slovakia was under the project No. 09I03-03-V01-00129.

Conflicts of interest

The authors declare that they have no known competing financial interests or personal relationships that could have appeared to influence the work reported in this paper.

References

[1] VOLYANSKAYA, Y., VOLYANSKIY, S., ONISHCHENKO, O., NYKUL, S. Analysis of possibilities for improving energy indicators of induction electric motors for propulsion complexes of autonomous floating vehicles. *Eastern-European Journal of Enterprise Technologies* [online]. 2018, **2**(8(92)), p. 25-32 [accessed 2023-11-15]. ISSN 1744-5302. Available from: https://doi.org/10.15587/1729-4061.2018.126144

[2] KOLODNYTSKA, R., KRAVCHENKO, O., GERLICI, JU., KRAVCHENKO KAT. The effects of biodiesel on NOx emissions for automotive transport. *Communications - Scientific Letters of the University of Zilina* [online]. 2022, **24**(1), p. B59-B66. ISSN 1335-4205, eISSN 2585-7878. Available from: https://doi.org/10.26552/com.C.2022.1.B59-B66

[3] KHAN, I. U., OTHMAN, M. H. D., HASHIM, H., MATSUURA, T., ISMAIL, A. F., REZAEI-DASHTARZHANDI, M., AZELEE, I. W. Biogas as a renewable energy fuel - a review of biogas upgrading, utilisation and storage. *Energy Conversion and Management* [online]. 2017, **150**, p. 277-294 [accessed 2023-11-15]. ISSN 0196-8904. Available from: https://doi.org/10.1016/J.ENCONMAN.2017.08.035

[4] BORDELANNE, O., MONTERO, M., BRAVIN, F., PRIEUR-VERNAT, A., OLIVETI-SELMI, O., PIERRE, H., PAPADOPOULO, M., MULLER, T. Biomethane CNG hybrid: a reduction by more than 80% of the greenhouse gases emissions compared to gasoline. *Journal of Natural Gas Science and Engineering* [online]. 2011, **3**, p. 617-624 [accessed 2023-11-15]. ISSN 1875-5100. Available from: https://doi.org/10.1016/J.JNGSE.2011.07.007

[5] AGBULUT, U., AYDIN, M., AGBULUT, U., AYDIN, M., KARAGOZ, M., DENIZ, E. AND CIFTCI, B. An experimental assessment of combustion and performance characteristics of a spark ignition engine fueled with co-fermentation biogas and gasoline dual fuel. *Journal of Process Mechanical Engineering* [online]. 2021, **236**, p. 1330-1339 [accessed 2023-11-15]. ISSN 0954-4089. Available from: https://doi.org/10.1177/09544089211060131

[6] CHANDRA, R., VIJAY, V. K., SUBBARAO, P. M. V., KHURA, T. K. Performance evaluation of a constant speed IC engine on CNG, methane enriched biogas and biogas. *Applied Energy* [online]. 2011, **88**, p. 3969-3977 [accessed 2023-11-15]. ISSN 0306-2619. Available from: https://doi.org/10.1016/J.APENERGY.2011.04.032

[7] SHAMEKHI, A., KHATIBZADEH, N., SHAMEKHI, A. Performance and emissions characteristics investigation of a Bi-Fuel SI engine fuelled by CNG and gasoline. In: Internal Combustion Engine Division Spring Technical Conference: proceedings [online]. 2006. ISBN 0-7918-4206-1, p. 393-400. Available from: https://doi.org/10.1115/ICES2006-1387

[8] SINGHAL, S., AGARWAL, S., ARORA, S., SHARMA, P., SINGHAL, P. Upgrading techniques for transformation of biogas to bio-CNG: a review. *International Journal of Energy Research* [online]. 2017, **41**, p. 1657-1669 [accessed 2023-11-15]. ISSN 1099-114X. Available from: https://doi.org/10.1002/er.3719

[9] LEMKE, B., MCCANN, N., POURMOVAHED, A. Performance and efficiency of a Bi-fuel bio methane/gasoline vehicle. *Renewable Energy and Power Quality Journal* [online]. 2011, **9**(1), p. 208-213 [accessed 2023-11-15]. eISSN 2172-038X. Available from: https://doi.org/10.24084/REPQJ09.289

[10] MELAIKA, M., HERBILLON, G., DAHLANDER, P. Spark ignition engine performance, standard emissions and particulates using GDI, PFI-CNG and DI-CNG systems. *Fuel* [online]. 2021, **293**, 120454 [accessed 2023-11-15]. ISSN 0016-2361. Available from: https://doi.org/10.1016/J.FUEL.2021.120454

[11] WARGULA, L., KUKLA, M., LIJEWSKI, P., DOBRZYNSKI, M., MARKIEWICZ, F. Impact of compressed natural gas (CNG) fuel systems in small engine wood chippers on exhaust emissions and fuel consumption. *Energies* [online]. 2020, **13**(24), 6709 [accessed 2023-11-15]. eISSN 1996-1073. Available from: https://doi.org/10.3390/en13246709

[12] LIMPACHOTI, T., THEINNOI, K. The comparative study on compressed natural gas (CNG) and compressed biomethane gas (CBG) fueled in a spark ignition engine. *E3S Web of Conferences* [online]. 2021, **302**, 01005 [accessed 2023-11-15]. eISSN 2267-1242. Available from: https://doi.org/10.1051/e3sconf/202130201005

[13] PAVLOVSKYI, M. The improvement of fuel efficiency and environmental characteristics of diesel engine by using biodiesel fuels. In: *Modern technologies in energy and transport. Studies in systems, decision and control. Vol. 510* [online]. BOICHENKO, S., ZAPOROZHETS, A., YAKOVLIEVA, A., SHKILNIUK, I. (Eds.). Cham: Springer, 2024. ISBN 978-3-031-44351-0, p. 35-69. Available from: https://doi.org/10.1007/978-3-031-44351-0_4

[14] SYMONENKO, R. V. Improving the operational efficiency of wheeled vehicles based on intelligent telematics technologies. D.Sc. thesis. Kyiv, Ukraine: National Transport University, 2021. Available from: http://diser.ntu.edu.ua/Symonenko_dis.pdf

[15] MELNYK, O., ONYSHCHENKO, S., ONYSHCHENKO, O., LOHINOV, O., OCHERETNA, V. Integral approach to vulnerability assessment of ship's critical equipment and systems. *Transactions on Maritime Science* [online]. 2023, **12**(1), p. 1-10 [accessed 2023-11-15]. Available from: https://doi.org/10.7225/toms.v12.n01.002

[16] GOROBCHENKO, O., FOMIN, O., GRITSUK, I., SARAVAS, V., GRYTSUK, Y., BULGAKOV, M. Intelligent locomotive decision support system structure development and operation quality assessment. In: 3rd International Conference on Intelligent Energy and Power Systems: proceedings [online] [accessed 2023-11-15]. 2018. Available from: https://doi.org/10.1109/ieps.2018.8559487

[17] KURIC, I., GOROBCHENKO, O., LITIKOVA, O., GRITSUK, I., MATEICHYK, V., BULGAKOV, M., KLACKOVA, I. Research of vehicle control informative functioning capacity. *IOP Conference Series: Materials Science and Engineering* [online]. 2020, **776**, 012036 [accessed 2023-11-15]. ISSN 1757-899X. Available from: https://doi.org/10.1088/1757-899x/776/1/012036

[18] PARSADANOV, I., MARCHENKO, A., TKACHUK, M., KRAVCHENKO, S., POLYVIANCHUK, A., STROKOV, A., GRITSUK, I., RYKOVA, I., SAVCHENKO, A., SMIRNOV, O., POSTOL, Y., SAVCHUK, V. complex assessment of fuel efficiency and diesel exhaust toxicity. *SAE Technical Paper* [online]. 2020, 2020-01-2182 [accessed 2023-11-15]. ISSN 0148-7191. Available from: https://doi.org/10.4271/2020-01-2182

[19] VOLODARETS, M., GRITSUK, I., CHYGYRYK, N., BELOUSOV, E., GOLOVAN, A., VOLSKA, O., HLUSHCHENKO, V., POHORLETSKYI, D., VOLODARETS, O. Optimization of vehicle operating conditions by using simulation modeling software. *SAE Technical Paper Series* [online]. 2019, 2019-01-0099 [accessed 2023-11-15]. ISSN 0148-7191. Available from: https://doi.org/10.4271/2019-01-0099

[20] ABRAMCHUK F. I., GUTAREVICH Y. F., DOLGANOV K. E., TIMCHENKO I. I. *Automobile engines*. Kyiv, Ukraine: Aristei, 2004. ISBN 966-8458-26-5.

[21] GOLOVAN, A., GRITSUK, I., POPELIUK, V., SHERSTYUK, O., HONCHARUK, I., SYMONENKO, R., SARAVAS, V., VOLODARETS, M., AHIEIEV, M., POHORLETSKYI, D., KHUDIAKOV, I. Features of mathematical modeling in the problems of determining the power of a turbocharged engine according to the characteristics of the turbocharger. *SAE International Journal of Engines* [online]. 2019, **13**(1), p. 5-16 [accessed 2023-11-15]. ISSN 1946-3936, eISSN 1946-3944. Available from: https://doi.org/10.4271/03-13-01-0001

[22] PODRIGALO, M., KLETS, D., SERGIYENKO, O., GRITSUK, I., SOLOVIOV, O., TARASOV, Y., BAITSUR, M., BULGAKOV, N., HATSKO, V., GOLOVAN, A., SAVCHUK, V., AHIEIEV, M., BILOUSOVA, T. Improvement of the assessment methods for the braking dynamics with ABS malfunction. *SAE Technical Paper* [online]. 2018, 2018-01-1881 [accessed 2023-11-15]. ISSN 0148-7191. Available from: https://doi.org/10.4271/2018-01-1881

[23] MELNYK, O., ONISHCHENKO, O., ONYSHCHENKO, S., GOLIKOV, V., SAPIHA, V., SHCHERBINA, O., ANDRIEVSKA, V. Study of environmental efficiency of ship operation in terms of freight transportation effectiveness provision. *TransNav: International Journal on Marine Navigation and Safety of Sea Transportation* [online]. 2022, **16**, p. 723-722 [accessed 2023-11-15]. ISSN 2083-6473, eISSN 2083-6481. Available from: https://doi.org/10.12716/1001.16.04.14

[24] BUDASHKO, V., OBNIAVKO, T., ONISHCHENKO, O., DOVIDENKO, Y., UNGAROV, D. Main problems of creating energy-efficient positioning systems for multipurpose sea vessels. In: 2020 IEEE 6th International Conference on Methods and Systems of Navigation and Motion Control 2020 MSNMC 2020: proceedings [online]. IEEE. 2020. eISBN 978-1-7281-8135-6, p. 106-109 [accessed 2023-11-15]. Available from: https://doi.org/10.1109/MSNMC50359.2020.9255514

JUSTIFICATION OF THE POSSIBILITY FOR EXTENDING THE SERVICE LIFE OF CAST PARTS OF A THREE-AXLE BOGIE BASED ON RESULTS OF THE RUNNING STRENGTH TESTS TO DETERMINE THEIR LOADING

Rustam Rahimov*, Diyor Zafarov

Faculty of Railway Transport Engineering, Tashkent State Transport University, Tashkent, Republic of Uzbekistan

*E-mail of corresponding author: rakhimovrv@yandex.ru

Rustam Rahimov 0000-0002-5652-2604, Diyor Zafarov 0000-0003-0100-4815

Resume

The article presents the results of research aimed at assessing the residual life and the possibility of extending the service life of cast parts of a UVZ-9M three-axle bogie used in six-axle scale test wagons. The tests have shown that the maximum stresses in the most stressed areas of the side frame, spring and pivot beams are within acceptable values, which indicates the presence of a residual life. The analysis of safety margin coefficients confirmed that the bogie elements have a significant reserve of operational characteristics. Calculations of the full service life of cast parts, performed based on the experimental data, demonstrated a sufficient residual life to prolong their use. It has been scientifically and experimentally proven that the cast parts of the UVZ-9M three-axle bogie can be safely operated for 5 years.

Article info

Received 20 January 2025
Accepted 22 March 2025
Online 16 April 2025

Keywords:

scale test wagon
three-axle bogie
cast parts
stress
residual life
running strength test
safety margin

Available online: https://doi.org/10.26552/com.C.2025.035

ISSN 1335-4205 (print version)
ISSN 2585-7878 (online version)

1 Introduction

Extending the service life of railway wagons and their assemblies in modern conditions is an important element of optimizing the operation of transport infrastructure, which contributes to the effective management of their resources while ensuring the continuity and uninterrupted transportation process. It contributes to a significant reduction in capital costs associated with the acquisition of the new rolling stock, and leads to an optimization of the cost of maintaining a serviceable fleet. At the same time, it also has significant disadvantages associated with increased repair and maintenance costs, a decrease in the repair interval and, in some cases, a deterioration in the operational characteristics of wagons, which directly affects the efficiency of their use. A number of scientists and research centers around the world are working on the issues of determining the remaining resource and the possibility of extending the service life of rolling stock and their components.

The authors of [1] proposed modelling and analysis of the remaining service life of railway wagons in the Swedish mining company LKAB. To achieve this goal, the behavior of critical subsystems in the case of failures was analyzed. Then, taking into account effective operational factors, proportional hazard model (PHM) was applied to calculate reliability functions. Within the framework of this concept, it was possible to obtain and analyze the remaining life of wagons with different initial service life.

Work [2] presents a methodology for predicting the remaining service life of both wheels and freight wagons by combining the data from three types of sensors, including wheel shock sensors, machine vision systems and optical geometry sensors. Many new functions are being created based on the normalization of objects, signal characteristics, and summary statistics for previous periods. Missing data is processed in the missForest environment, using a nonparametric algorithm for calculating missing values. Several data mining methods have been implemented and compared to predict the wheel and truck wear on the Class I railroad network in the United States. Numerical tests have shown that the proposed technique makes it possible to accurately predict the wear of

railway carriage components, especially in the medium term.

In [3], a method was proposed for assessing the fatigue of axles subject to scratches, which can be used for maintenance and evaluation of damaged axles of high-speed railways. Geometric parameters and the type of load were taken into account to assess the safety of operation of axes subject to scratches. The fatigue limit curve of axes prone to scratches was calculated using the Murakami equation. The results of the study show that when the critical scratch depth is exceeded, the fatigue strength decreases with increasing groove depth. Otherwise, the groove depth has no noticeable effect on the fatigue characteristics of EA4T steel. This means that a critical roughness value can be achieved for high-speed axles made of EA4T steel, which can be very important in the production and maintenance of high-speed railway axles.

The authors of [4] have previously proposed a phased fatigue assessment system for a wheelset with internal axle boxes, which includes a safe service life as the first level and damage resistance as the second level. The estimated load range was used to estimate the remaining service life of the damaged axle made of EA4T steel. The calculation results show that the critical safety zone has been moved to the center of the axis, unlike classical axes, where the probability of a 1.0 mm deep crack spreading, which is the limit of control, is lower. In addition, the wheelset with internal axle boxes shows a lower stress value. The analysis, based on the well-known Kitagawa-Takahashi diagram, indicates a safety risk when using only the rated stress method.

Separately, it is worth noting the work [5], which defines the remaining life of the load-bearing structures of platform wagons with a service life of 25 years. The authors conducted the full-scale tests of the technical condition of the load-bearing structures of the platform wagons on the basis of the Southern Railway depot of "Ukrzaliznytsia" JSC. The model 13-401 platform wagon was chosen as the object of the study. It has been established that the estimated service life of the load-bearing structures of the studied platform wagons, taking into account the extension of their service life, is at least 18 years. The strength of the load-bearing structure of the platform wagon was calculated using the finite element method in the environment of the SolidWorks Simulation (COSMOSWorks) software. In the course of the work, the authors found that the maximum equivalent stresses occurring in the area of interaction of the support beam with the pin are 337.5 MPa, which ensures the strength of the load-bearing structure of the platform wagons. Additionally, an assessment of the progress of the platform wagons has been determined, in the MathCad software environment, using the Runge-Kutta method. The calculations performed show that the wagon's rating is "excellent". Thus, the results of the study contribute to improving the efficiency of combined transportation in international traffic.

There is a well-known study [6] in which, to confirm the service life of freight wagons, the authors evaluated and compared the results of durability and running dynamic strength tests of analog wagons, as well as digital modelling in the "Universal Mechanism" software package. As a result of the testing of this technique, the service life of the hopper wagon models 19-1272-01 and 19-1298, manufactured by JSC "Ruzkhimmash", which is 32 years, was confirmed.

2 The status of the issue, goals and objectives of the work

Summarizing the introductory part of the work, the following conclusions can be drawn:

- methods for assessing the residual life of the railway rolling stock and its components are constantly being improved using modern engineering programs and experimental techniques. However, most research focuses on high-speed rolling stock and general-purpose rolling stock (freight and passenger wagons);
- a number of studies have been conducted on the running gear of the rolling stock, where the object of research is often a two-axle three-element bogie due to its widespread use;
- despite the growing demand for three-axle bogies, their cast bearing components (side frame, springboard and pivot beam) have not been subjected to fatigue strength tests. The regulatory framework for three-axle bogies is poorly developed, mainly attention is paid to two-axle bogies of freight wagons.

It is worth noting that many studies have been conducted in world practice [7-11] aimed at determining the load capacity, residual resource, reliability and fatigue resistance of parts and assemblies in mechanical engineering, in particular the railway rolling stock. The main focus of the research was on high-speed rolling stock, general-purpose wagons and their components. In this regard, the ways of solving issues related to the study of the loading of cast parts of three-axle bogies to determine their residual life, have not been sufficiently investigated nor fully formulated. Taking into account the above, the purpose of this work is to scientifically substantiate the possibility of extending the service life of three-axle bogies of the UVZ-9M models to increase the efficiency of using their resource by experimentally examining the loading of cast parts (side frame, springboard and pivot beam) of this bogie and comparing the results obtained experimentally to calculated and normative data. Thus, the object of research in this work is a three-axle bogie model UVZ-9M, manufactured in 1965 and operated under the scale test wagons of type 640-VPV, and the subject of the study is the loading of cast parts of this bogie.

3 The methodology of the experiment

For an experimental study of the loading of cast parts of a three-axle bogie of the UVZ-9M model, the determination of which makes it possible to assess the residual life of these parts and justify the possibility of extending their service life, a Methodology was developed [12] for conducting the running strength tests of a six-axle scale test wagon of type 640-VPV using the strain gauge method. During the tests, the coefficients of dynamic addition of sprang and non-sprang parts of the wagon bogie were also determined [13].

According to the Methodology [12], the running strength tests were carried out on a track of a length of more than 5 km, without precipitation, under climatic conditions from +9 to +15 ° C using a traction locomotive. At the same time, measuring instruments were placed in conditions that ensure their operation within the passport data. Prior to the start of the tests, strain gauges of the BBF200-10AA-A(11)-BX30 type were

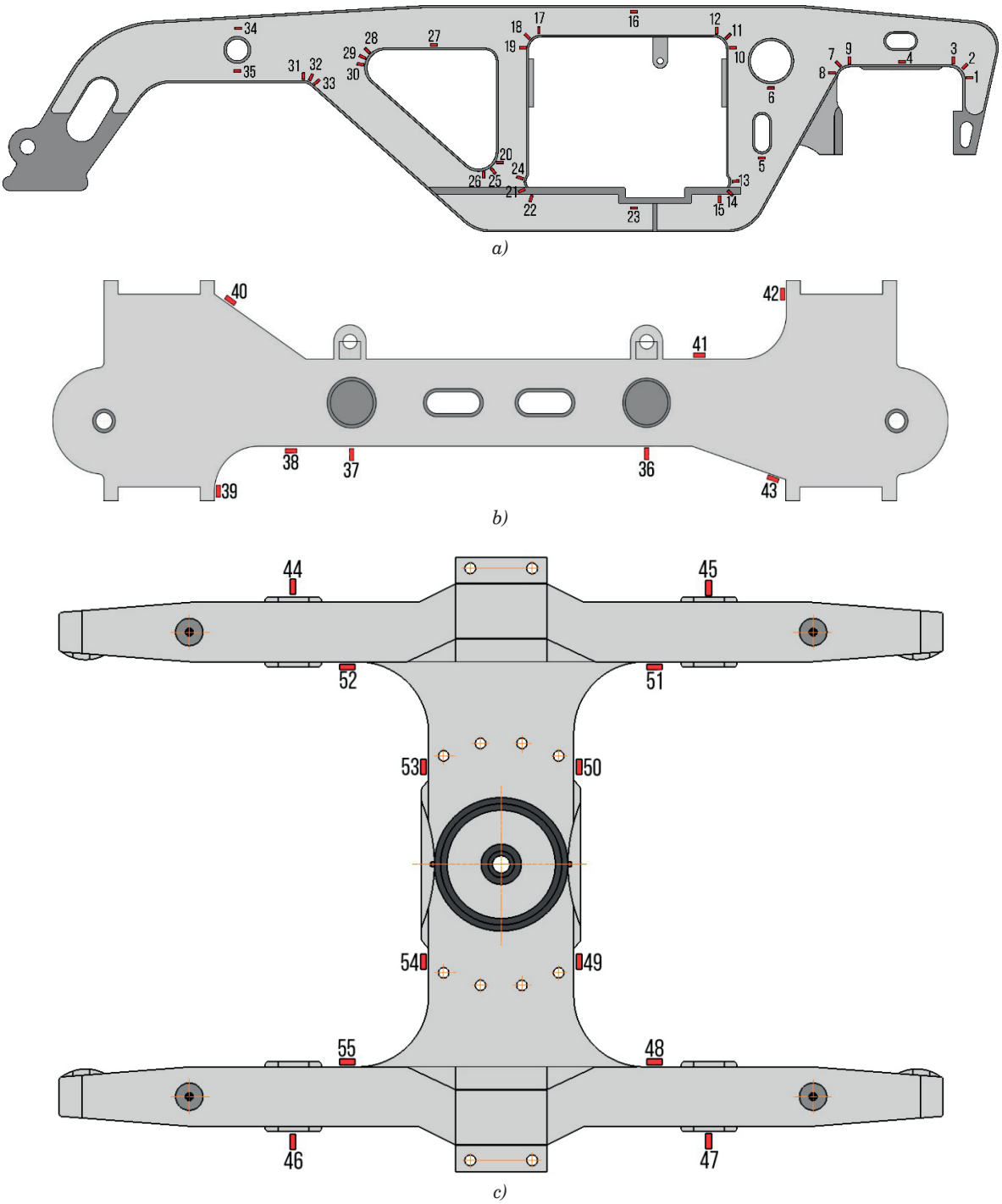

Figure 1 *Scheme of the installation of strain gages on the side frame (a), spring (b) and pivot (c) beam of the bogie model UVZ-9M of six-axle scale test wagon type 640-VPV*

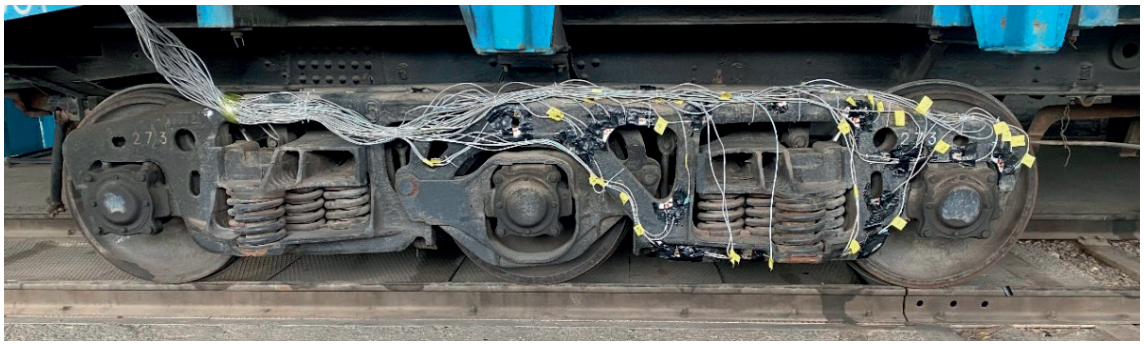

a)

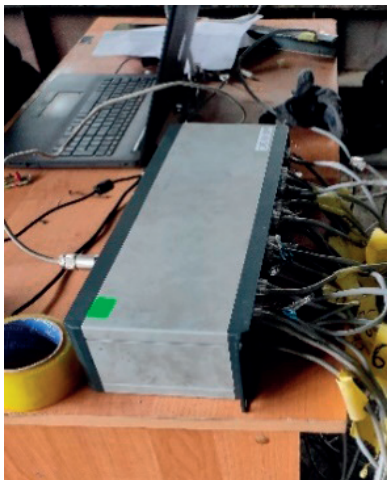

b)

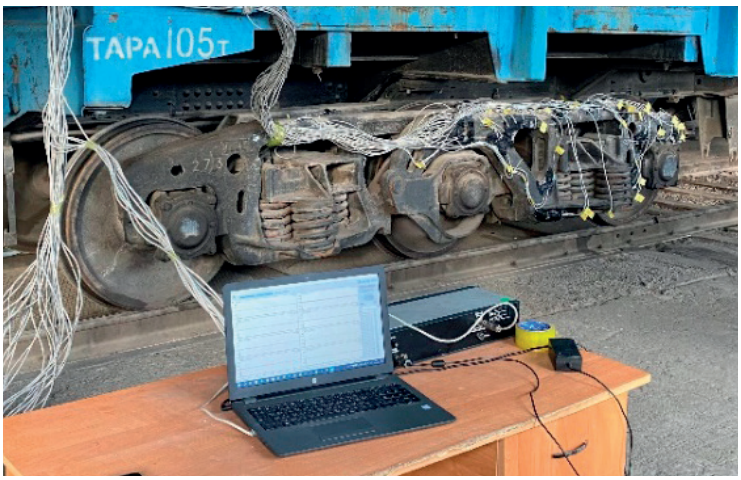

c)

Figure 2 *Installation of strain gauges (a), combining them into channels (b) and connecting to a multi-channel strain measuring system type MIC-185 and a computer (c)*

glued to the control zones of the cast parts of the three-axle bogie according to the scheme recommended in the Methodology (Figure 1). The scheme of installation and connection of strain gauges to determine the coefficient of dynamic addition of sprangunsprang parts on the side frame of the bogie was carried out in accordance with State Standard 33788-2016 [14].

After installing the strain gauges on the elements of the bogie and combining them into working channels, they were connected to a multi-channel strain measuring system of the MIC-185 type, which, in turn, was connected to a computer with the Recorder program installed to receive measuring signals (Figure 2).

The constant calibration coefficients of the strain gauge scheme, necessary to measure the coefficients of dynamic addition of sprang and non-sprang parts of the bogie, were determined by gradually raising and lowering the body of the scale test wagon using jacks.

4 Conducting the running strength tests

To carry out the running strength tests, an experimental trailer was formed (Figure 3), consisting of a scale test wagon and a locomotive (Figure 4).

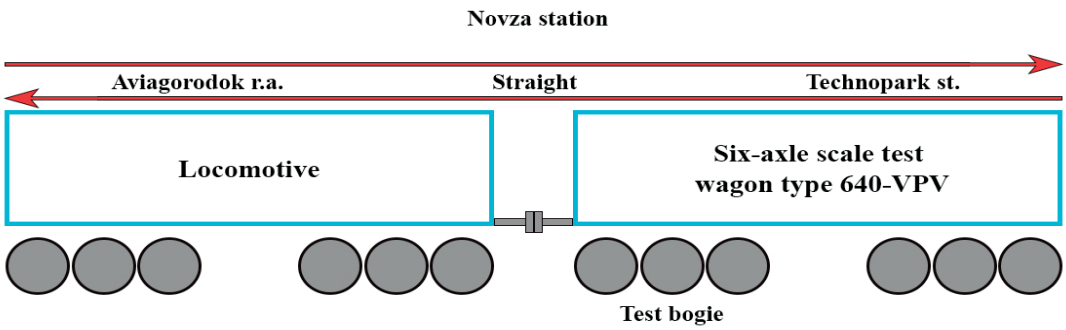

Figure 3 *Experimental trailer scheme*

Figure 4 *Scale test wagon and a locomotive*

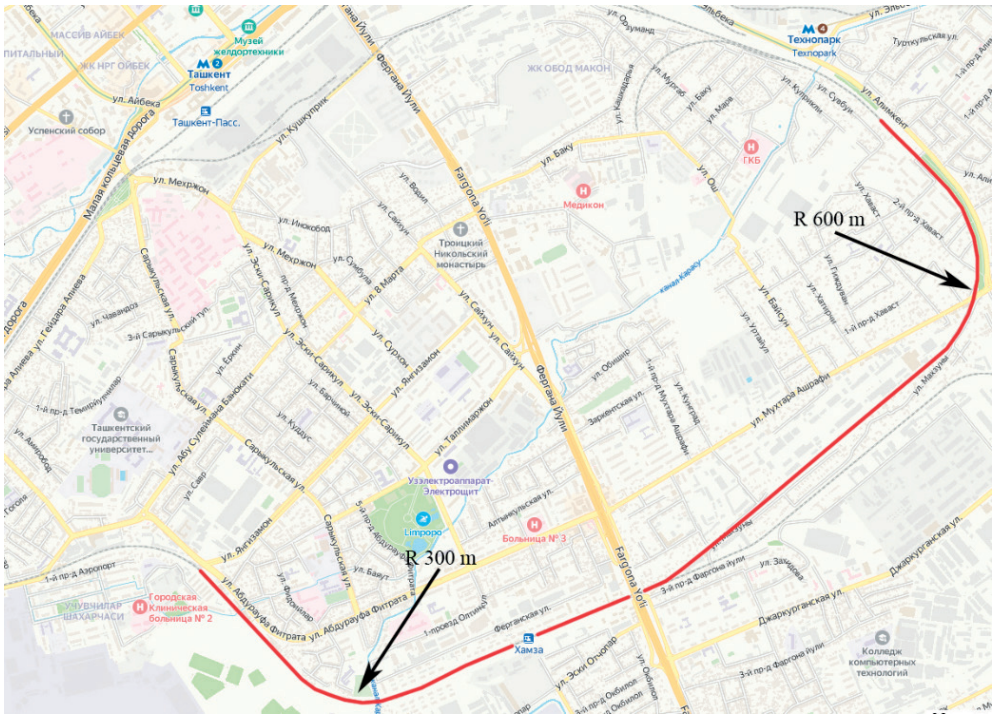

Figure 5 *Diagram of the test section of the railway track*

Table 1 *Conditions for passing the straight and curved sections of railway track during running strength tests*

Track	Speed, km·h^{-1}							
A straight section of the track	10	20	30	40	50	60	70	80
A curved section of the track:								
R = 300 m	10	20	30	40	50	×	×	×
R = 600 m	10	20	30	40	50	60	×	×

The test section of the railway track included curved sections with a radius of R=300 m, R=600 m and a straight section of the railway track according to [12] (Figure 5).

The conditions for passing straight and curved sections of railway track during the running strength tests of cast bogie parts of the UVZ-9M model of six-axle scale test wagons of type 640-VPV are shown in Table 1.

The collection of the necessary and sufficient array of experimental data during the passage of straight and curved sections of the track in each speed range was carried out in three passes according to State Standard 33788-2016 [14]. The average values of the obtained experimental data were selected for subsequent processing and analysis. The results were processed using the WinPOS software.

For the strain gauges installed in orthogonal *x, y* directions and at an angle of 45° to them, measuring

relative deformations, ε_x, ε_y, ε_{45}, the corresponding main relative deformations ε_1, ε_2 were determined by the formulas [14]:

$$\varepsilon_1 = \frac{1}{2}\left(\varepsilon_x + \varepsilon_y + \frac{\varepsilon_x - \varepsilon_y}{\cos 2a}\right),$$

$$\varepsilon_2 = \frac{1}{2}\left(\varepsilon_x + \varepsilon_y + \frac{\varepsilon_x - \varepsilon_y}{\cos 2a}\right), \quad (1)$$

$$tg2a = \frac{2\varepsilon_{45} - (\varepsilon_x - \varepsilon_y)}{\varepsilon_x - \varepsilon_y},$$

where ε_x, ε_y, ε_{45} are the relative deformations for the strain gages installed in orthogonal x, y directions and at an angle of 45° to them.

The equivalent stress, MPa, was determined by the formula:

$$\sigma_e = \sqrt{\sigma_1^2 + \sigma_2^2 - \sigma_1\sigma_2}, \quad (2)$$

where σ_1, σ_2 are the corresponding stresses at the measured relative strain ε.

Table 2 *The results of running strength tests on a straight section (side frame, MPa)*

Strain gauge	Zone	Speed (km·h^{-1})							
		10	20	30	40	50	60	70	80
1	The outer corner of the axle box opening	20.0	24.2	29.3	35.5	42.9	51.9	62.8	73.5
2									
3									
4	The edge of the upper belt above the axle box opening	17.7	21.5	26.0	31.4	38.0	46.0	55.7	67.4
5	The edges of the technical holes	11.3	13.6	16.5	19.9	24.1	29.2	35.3	42.8
6		12.2	14.8	17.9	21.7	26.2	31.7	38.4	46.4
7	The inner corner of the axle box opening	15.1	18.2	22.1	26.7	32.3	39.1	47.3	57.2
8									
9									
10	Upper outer right corner of the spring opening	14.1	17.1	20.6	25.0	30.2	36.5	44.2	53.5
11									
12									
13	Lower outer right corner of the spring opening	17.3	21.0	25.4	30.7	37.1	44.9	54.4	65.8
14									
15									
16	Upper belt above the spring opening	16.4	19.9	24.1	29.1	35.3	42.7	51.6	62.5
17	Upper outer left corner of the spring opening	14.1	17.1	20.7	25.0	30.2	36.6	44.3	53.6
18									
19									
20	The lower edge of the technical hole	16.8	20.3	24.6	29.8	36.0	43.6	52.7	63.8
21	Lower outer left corner of the spring opening	19.2	23.3	28.2	34.1	41.2	49.9	60.4	73.0
22		19.7	23.9	28.9	34.9	42.3	51.1	61.9	72.9
23	Lower belt above the spring opening	20.4	24.6	29.8	36.1	43.6	52.8	63.9	73.1
24	Lower outer left corner of the spring opening	20.1	24.3	29.5	35.6	43.1	52.2	63.1	72.4
25	The lower edge of the technical hole	14.5	17.5	21.2	25.6	31.0	37.5	45.4	54.9
26		14.0	17.0	20.5	24.8	30.1	36.4	44.0	53.2
27	Upper belt above the technical hole	13.4	16.2	19.6	23.7	28.7	34.7	42.0	50.8
28	The edges of the technical holes on the trunk side	14.1	17.1	20.6	25.0	30.2	36.5	44.2	53.5
29									
30									
31	Transitions from the lower surface of the trunk to the inclined belt	16.9	20.5	24.8	30.0	36.3	43.9	53.1	64.3
32									
33									
34	The edges of the technical holes	14.2	17.2	20.8	25.1	30.4	36.8	44.5	53.8
35		13.7	16.6	20.0	24.2	29.3	35.5	42.9	51.9

The results of running strength tests, obtained according to the above formulas, and readings of strain gauges installed in the studied areas, are shown in Tables 2-10, and Figures 6-8 graphically show the stresses occurring in the most stressed areas of the side frame, spring and pivot beams.

The coefficients of vertical dynamics of the sprang and unsprang parts of the bogie were also determined according to [15]. These coefficients are necessary to understand the behavior of sprang and non-sprang parts and allow accurate assessment of their load capacity and service life, which is important for planning the maintenance and repair. The coefficients of vertical dynamics obtained during the running strength tests of a six-axle scale test wagon type 640-VPV are shown in Figure 9.

As can be seen, the coefficient of vertical dynamics of the sprang parts of the bogie, at a maximum speed of 80 km·h^{-1}, is 0.28, which does not exceed the maximum allowable value of 0.65 for the sprang parts, while this coefficient for the non-sprang parts is 0.39, which also does not exceed the maximum allowable 0.9 for the non-sprang parts according to [15].

The analysis and evaluation of the results of running dynamic load tests of cast bogie parts of the UVZ-9M model of six-axle scale test wagons of type 640-VPV

Table 3 *The results of running strength tests on a section with R = 300 m (side frame, MPa)*

Strain gauge	Zone	Speed (km·h^{-1})				
		10	20	30	40	50
1						
2	The outer corner of the axle box opening	20.7	26.3	33.3	42.3	53.7
3						
4	The edge of the upper belt above the axle box opening	19.2	24.4	31.0	39.3	49.8
5	The edges of the technical holes	17.7	22.5	28.5	36.2	46.0
6		17.0	21.5	27.3	34.7	44.0
7						
8	The inner corner of the axle box opening	17.3	22.0	27.9	35.4	44.9
9						
10						
11	Upper outer right corner of the spring opening	15.5	19.6	24.9	31.6	40.1
12						
13						
14	Lower outer right corner of the spring opening	18.7	23.7	30.1	38.2	48.5
15						
16	Upper belt above the spring opening	19.2	24.4	30.9	39.2	49.8
17						
18	Upper outer left corner of the spring opening	17.3	22.0	27.9	35.4	44.9
19						
20	The lower edge of the technical hole	18.6	23.6	30.0	38.1	48.3
21	Lower outer left corner of the spring opening	23.8	30.2	38.3	48.6	61.7
22		25.0	31.7	40.2	51.0	64.7
23	Lower belt above the spring opening	23.4	29.7	37.6	47.8	60.6
24	Lower outer left corner of the spring opening	22.2	28.2	35.8	45.4	57.6
25	The lower edge of the technical hole	16.1	20.5	26.0	33.0	41.9
26		17.1	21.7	27.5	34.9	44.3
27	Upper belt above the technical hole	18.6	23.6	30.0	38.0	48.2
28						
29	The edges of the technical holes on the trunk side	15.5	19.6	24.9	31.6	40.1
30						
31						
32	Transitions from the lower surface of the trunk to the inclined belt	19.7	24.9	31.6	40.2	51.0
33						
34	The edges of the technical holes	16.5	20.9	26.5	33.7	42.7
35		17.0	21.5	27.3	34.7	44.0

Table 4 *The results of running strength tests on a section with R = 600 m (side frame, MPa)*

Strain gauge	Zone	Speed (km·h^{-1})					
		10	20	30	40	50	60
1							
2	The outer corner of the axle box opening	21.2	26.2	32.6	40.4	44.2	50.2
3							
4	The edge of the upper belt above the axle box opening	19.2	23.9	29.6	36.8	40.3	45.7
5	The edges of the technical holes	15.1	18.8	23.4	29.2	32.0	36.5
6		15.2	18.9	23.5	29.3	32.1	36.6
7							
8	The inner corner of the axle box opening	16.8	20.9	26.0	32.3	35.3	40.2
9							
10							
11	Upper outer right corner of the spring opening	15.3	19.0	23.6	29.4	32.1	36.5
12							
13							
14	Lower outer right corner of the spring opening	18.7	23.2	28.8	35.8	39.2	44.5
15							
16	Upper belt above the spring opening	18.6	23.0	28.6	35.6	38.9	44.3
17							
18	Upper outer left corner of the spring opening	16.3	20.2	25.2	31.3	34.2	39.0
19							
20	The lower edge of the technical hole	18.4	22.9	28.4	35.3	38.6	43.9
21	Lower outer left corner of the spring opening	22.4	27.8	34.6	43.0	47.1	51.6
22		23.3	28.9	35.9	44.7	48.9	51.7
23	Lower belt above the spring opening	22.8	28.3	35.1	43.6	47.7	52.3
24	Lower outer left corner of the spring opening	22.0	27.3	33.9	42.2	46.1	52.4
25	The lower edge of the technical hole	15.9	19.8	24.5	30.5	33.4	37.9
26		16.2	20.1	25.0	31.1	34.0	38.7
27	Upper belt above the technical hole	16.6	20.7	25.8	32.1	35.1	40.0
28							
29	The edges of the technical holes on the trunk side	15.3	19.0	23.6	29.4	32.1	36.5
30							
31							
32	Transitions from the lower surface of the trunk to the inclined belt	19.0	23.6	29.3	36.4	39.9	45.3
33							
34	The edges of the technical holes	16.0	19.8	24.6	30.6	33.5	38.1
35		16.0	19.8	24.7	30.7	33.6	38.2

Table 5 *The results of running strength tests on a straight section (spring beam, MPa)*

Strain gauge	Zone	Speed (km·h^{-1})							
		10	20	30	40	50	60	70	80
36	The central belt of the spring beam	14.2	17.2	20.8	25.2	30.4	36.8	44.6	53.9
37		13.5	16.4	19.8	24.0	29.0	35.1	42.5	51.4
38	The transition from the central belt to the ends of the beam	12.3	14.8	17.9	21.7	26.3	31.8	38.5	46.6
39		11.3	13.7	16.6	20.1	24.3	29.4	35.6	43.0
40	Corner belt at the end of the beam	12.8	15.5	18.7	22.6	27.4	33.1	40.1	48.5
41	The transition from the central belt to the ends of the beam	11.3	13.7	16.6	20.1	24.3	29.4	35.6	43.1
42		12.6	15.3	18.5	22.3	27.0	32.7	39.6	47.9
43	Corner belt at the end of the beam	10.1	12.3	14.8	17.9	21.7	26.3	31.8	38.5

Table 6 *The results of running strength tests on a section with R = 300 m (spring beam, MPa)*

Strain gauge	Zone	Speed (km·h^{-1})				
		10	20	30	40	50
36	The central belt of the spring beam	17.4	22.0	27.9	35.5	45.0
37		17.0	21.6	27.4	34.8	44.1
38	The transition from the central belt to the ends of the beam	14.2	18.0	22.8	28.9	36.7
39		14.9	18.9	24.0	30.4	38.6
40	Corner belt at the end of the beam	14.5	18.4	23.4	29.6	37.6
41	The transition from the central belt to the ends of the beam	13.6	17.3	21.9	27.9	35.3
42		15.0	19.0	24.1	30.6	38.8
43	Corner belt at the end of the beam	13.9	17.6	22.4	28.4	36.0

Table 7 *The results of running strength tests on a section with R = 600 m (spring beam, MPa)*

Strain gauge	Zone	Speed (km·h^{-1})					
		10	20	30	40	50	60
36	The central belt of the spring beam	16.4	20.4	25.4	31.5	34.5	39.3
37		15.9	19.8	24.6	30.6	33.5	38.1
38	The transition from the central belt to the ends of the beam	13.7	17.1	21.2	26.4	28.8	32.8
39		13.6	17.0	21.1	26.3	28.8	32.7
40	Corner belt at the end of the beam	14.2	17.6	21.9	27.2	29.8	33.8
41	The transition from the central belt to the ends of the beam	13.0	16.1	20.1	25.0	27.3	31.1
42		14.4	17.8	22.1	27.5	30.1	34.3
43	Corner belt at the end of the beam	12.5	15.6	19.4	24.1	26.4	30.1

Table 8 *The results of running strength tests on a straight section (pivot beam, MPa)*

Strain gauge	Zone	Speed (km·h^{-1})							
		10	20	30	40	50	60	70	80
44	Pivot beam	12.2	14.8	17.9	21.7	26.2	31.7	38.4	46.5
45		12.2	14.7	17.8	21.6	26.1	31.6	38.2	46.2
46		11.5	13.9	16.8	20.3	24.6	29.8	36.0	43.6
47		11.9	14.4	17.4	21.0	25.4	30.8	37.3	45.1
48		13.2	16.0	19.4	23.4	28.4	34.3	41.5	50.2
49		12.8	15.4	18.7	22.6	27.4	33.1	40.0	48.5
50		11.7	14.1	17.1	20.7	25.0	30.3	36.7	44.4
51		12.0	14.6	17.6	21.3	25.8	31.2	37.8	45.7
52		12.8	15.5	18.8	22.7	27.5	33.3	40.3	48.8
53		13.2	16.0	19.3	23.4	28.3	34.2	41.4	50.1
54		14.1	17.1	20.7	25.0	30.2	36.6	44.3	58.9
55		13.1	15.8	19.1	23.2	28.0	33.9	41.0	49.6

were carried out by examining their technical condition and comparing the maximum stresses obtained to the permissible values, according to [15]. Thus, the test results show that the most stressed zones are the lower belt of the spring opening of the side frame, in which the highest stresses are formed, amounting to 73.5 MPa in straight sections of the track, 64.7 MPa in curved sections with a radius of curvature R 300 and 52.4 MPa in curved sections with a radius of curvature R 600.

According to the calculations, the coefficient of safety margin of the side frame was 2, for the spring beam - 2.7 and the pivot beam - 2.5, which is higher than the minimum permissible 1.6 according to [15].

Thus, the stresses obtained in the cast parts of the UVZ-9M three-axle bogie during the running strength tests of the 640-VPV six-axle scale test wagon do not exceed the permissible value of 145 MPa according to [15], which fully meets the established requirements. Therefore, it can be concluded that there is a safety margin (residual life) and the possibility of extending the service life of a three-axle bogie model UVZ-9M six-axle scale test wagon type 640-VPV.

Table 9 *The results of running strength tests on a section with R = 300 m (pivot beam, MPa)*

Strain gauge	Zone	Speed (km·h^{-1})				
		10	20	30	40	50
44	Pivot beam	13.7	17.3	22.0	27.9	35.4
45		14.5	18.4	23.4	29.7	37.7
46		13.8	17.5	22.2	28.2	35.8
47		13.6	17.2	21.8	27.7	35.1
48		16.4	20.8	26.4	33.6	42.6
49		14.8	18.8	23.9	30.3	38.5
50		13.6	17.2	21.9	27.8	35.2
51		14.0	17.8	22.6	28.7	36.4
52		15.3	19.4	24.7	31.3	39.7
53		16.3	20.6	26.2	33.2	42.2
54		17.7	22.4	28.5	36.1	45.8
55		16.9	21.5	27.3	34.6	43.9

Table 10 *The results of running strength tests on a section with R = 600 m (pivot beam, MPa)*

Strain gauge	Zone	Speed (km·h^{-1})					
		10	20	30	40	50	60
44	Pivot beam	13.5	16.7	20.8	25.8	28.2	32.1
45		13.9	17.3	21.4	26.7	29.2	33.2
46		13.1	16.3	20.3	25.2	27.6	31.4
47		13.2	16.4	20.4	25.4	27.7	31.5
48		15.4	19.2	23.8	29.7	32.5	36.9
49		14.4	17.8	22.2	27.5	30.1	34.3
50		13.2	16.3	20.3	25.2	27.6	31.4
51		13.6	16.8	20.9	26.0	28.5	32.4
52		14.7	18.2	22.6	28.1	30.8	35.0
53		15.3	19.1	23.7	29.5	32.2	36.7
54		16.5	20.6	25.6	31.8	34.8	39.6
55		15.6	19.4	24.2	30.1	32.9	37.4

5 Calculation of the remaining service life of cast parts of the UVZ-9M bogie

The determination of the possibility of extending the service life of the cast parts of the UVZ-9M bogie by the residual life was carried out based on the condition of the absence of visible damage to the cast elements (cracks in welds or base metal, violation of geometry, loss of stability of structural elements), as well as stress values in the control zones obtained after the implementation of all modes of running strength tests that should not exceed the values specified in [15].

Thus, based on the results of experimental studies, the service life (residual life) for each cast part was calculated according to [15] using the formula:

$$T_k = \frac{\left(\frac{\sigma_{a,N}}{[n]}\right)^m \cdot N_0}{B \cdot \mu f \sum_{j=1}^{n} K_{yzj} \sum P_{vi} \sum \sigma_{ai}^m P_{\sigma i}}, \quad (3)$$

where: $\sigma_{a,N}$ is the endurance limit (in amplitude) for the control zone with a symmetrical cycle and steady-state loading mode with a base number of cycles $N_0 = 10^7$,

N_0 is the base number of cycles; m is the exponent in the equation of the fatigue curve in amplitudes,

μ is the coefficient obtained from the results of modelling the dynamics of wagons, taking into account the impact of degradation during operation of the wagon structure (friction and corrosion wear),

B is the conversion coefficient of the estimated calendar service life of the beam in years during continuous movement in seconds, s·year^{-1},

f is the frequency of changes in the dynamic additive coefficient,

K_{yzj} is the average fraction of the length of the track sections,

$P_{\sigma i}$ is the probability of occurrence of an amplitude with the level σ_{ai} in the i-th range of carriage speeds,

P_{Vi} is the fraction of time spent on operation in the i-th speed range,

σ_{ai} is the level of stress amplitudes from the action of vertical dynamic forces in the interval i, reduced to an equivalent symmetrical cycle.

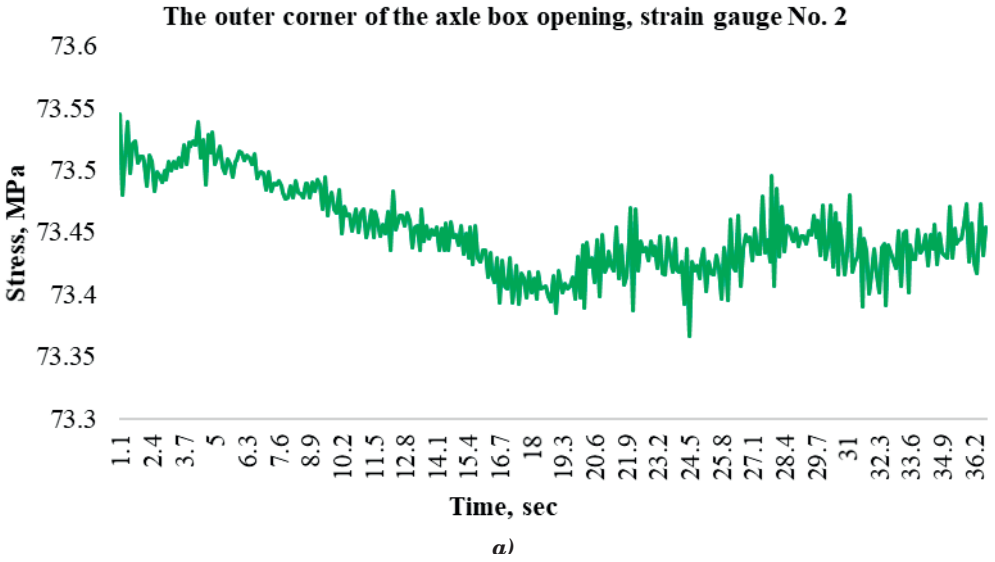

a)

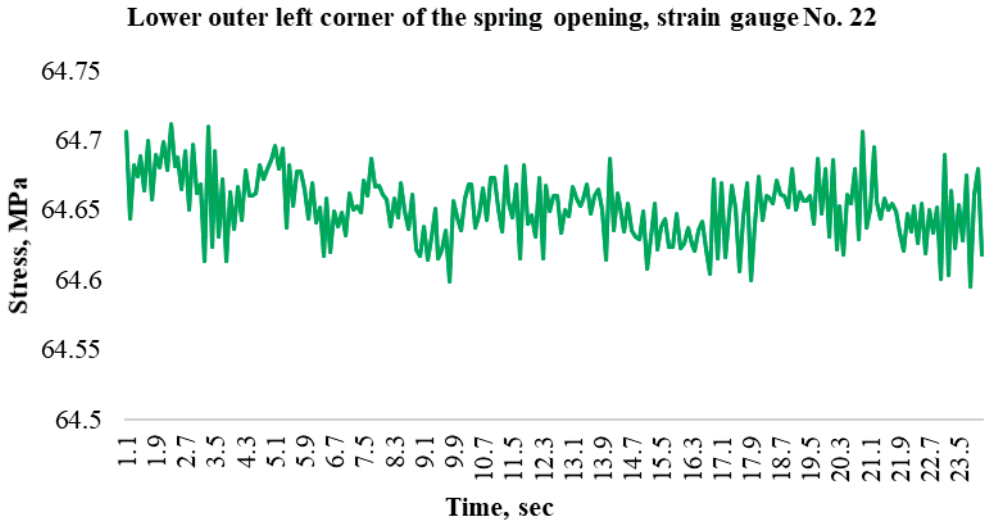

b)

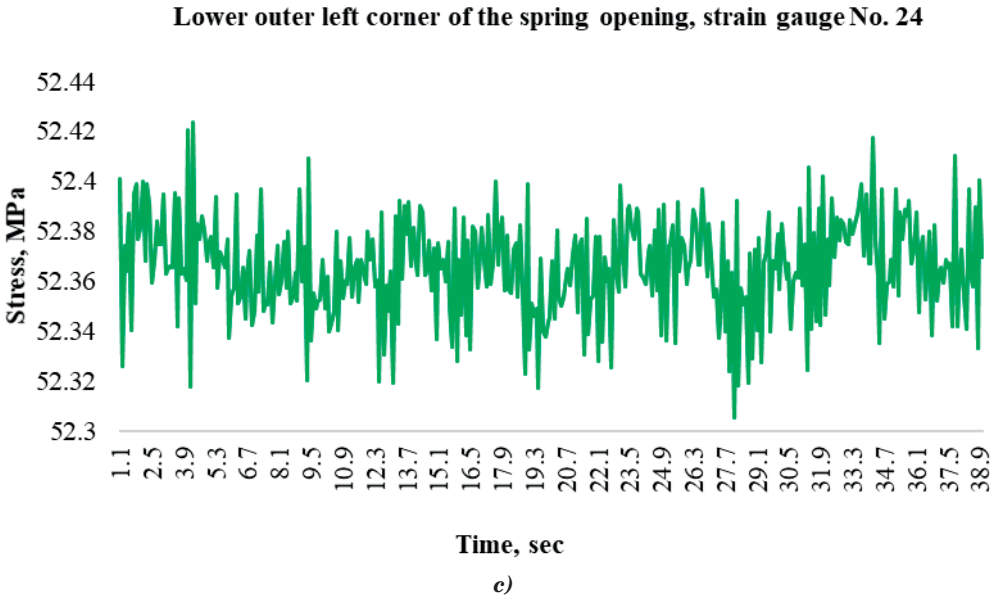

c)

Figure 6 *Stresses obtained on the side frame of the UVZ-9M bogie during the running strength tests of a six-axle scale test wagon type 640-VPV on a straight section of track at a speed of 80 km·h^{-1} (a), on a curved section of track with a radius of R = 300 m at a speed of 50 km·h^{-1} (b) and on a curved section paths with a radius of R = 600 m at a speed of 60 km·h^{-1} (c)*

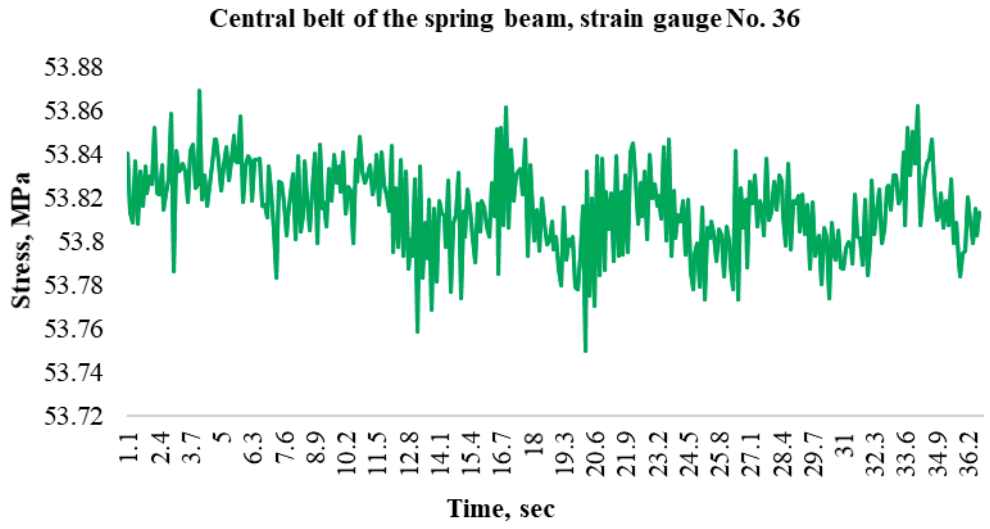

a)

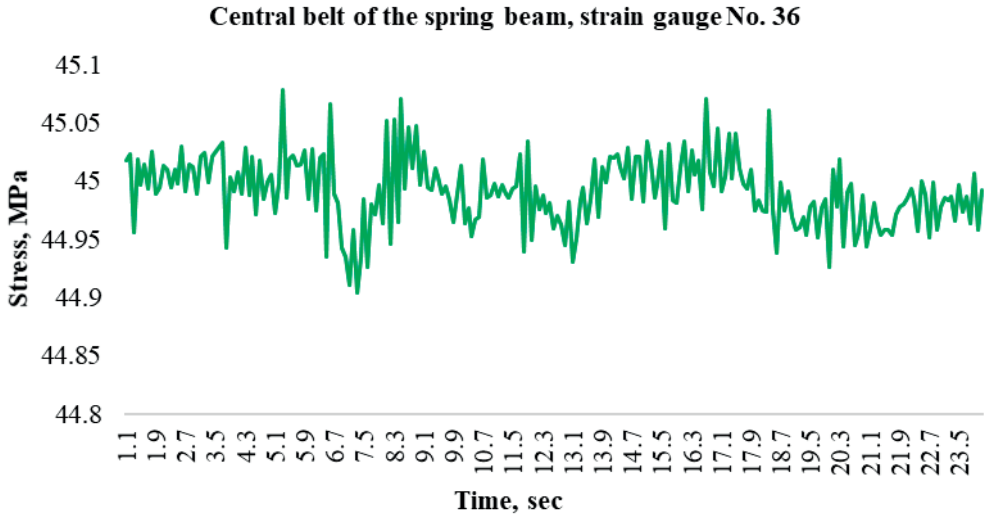

b)

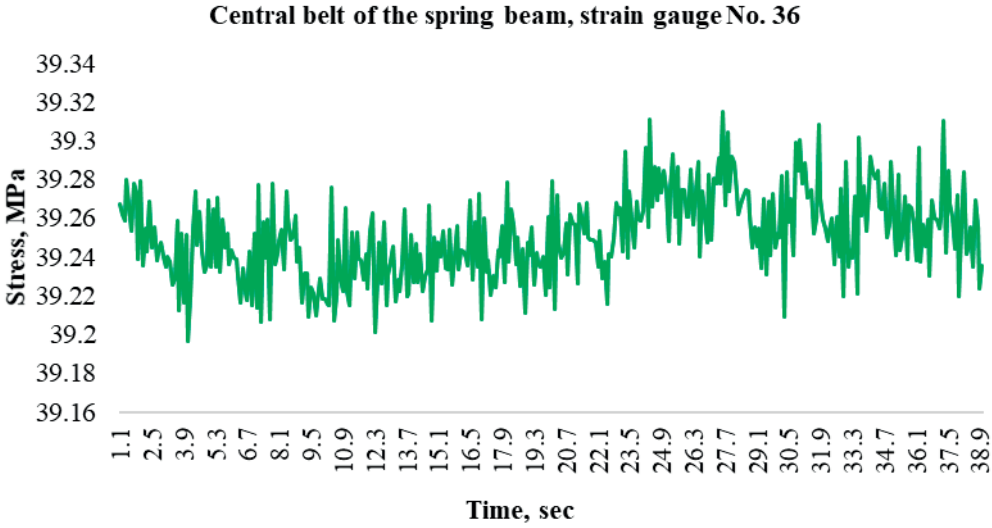

c)

Figure 7 *Stresses obtained on the spring beam of the UVZ-9M bogie during the running strength tests of a six-axle scale test wagon type 640-VPV on a straight section of track at a speed of 80 km·h^{-1} (a), on a curved section of track with a radius of R = 300 m at a speed of 50 km·h^{-1} (b) and on a curved section paths with a radius of R = 600 m at a speed of 60 km·h^{-1} (c)*

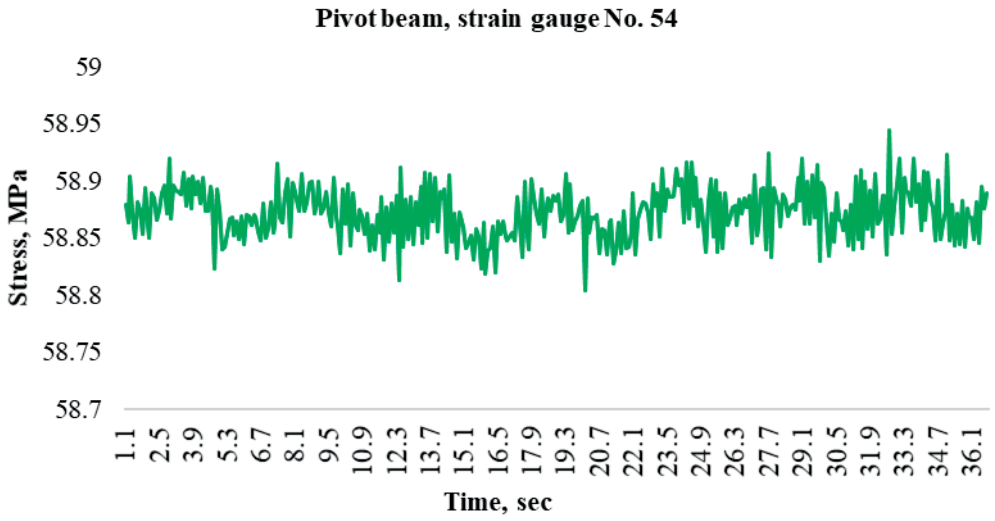

a)

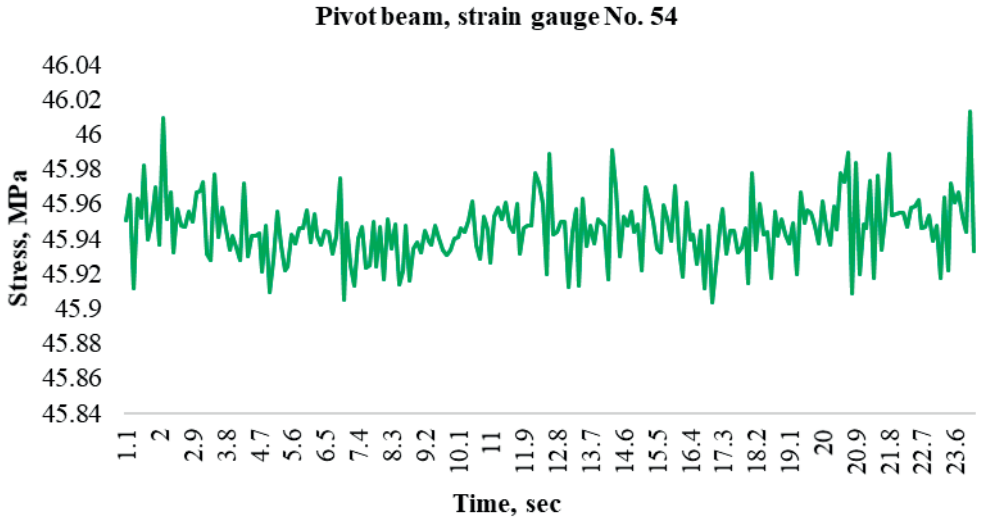

b)

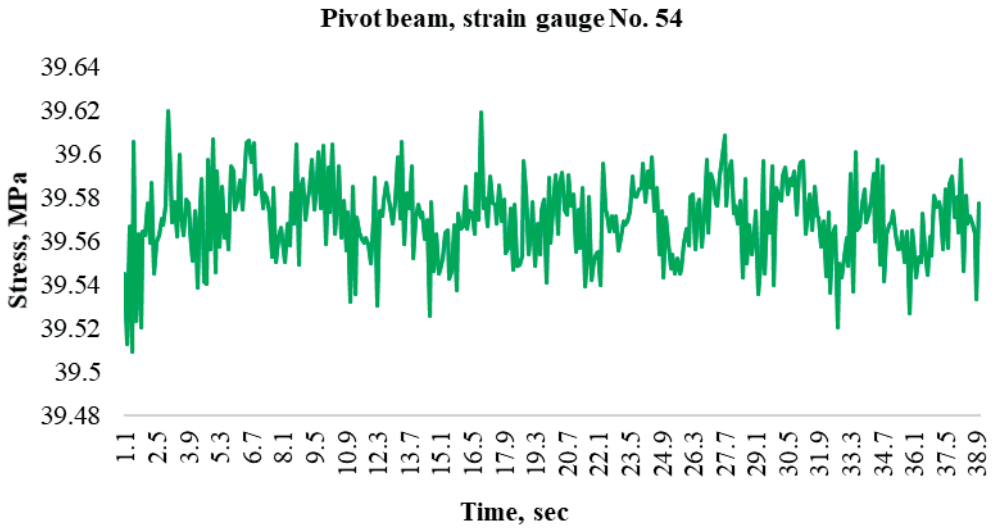

c)

Figure 8 *Stresses obtained on the pivot beam of the UVZ-9M bogie during the running strength tests of a six-axle scale test wagon type 640-VPV on a straight section of track at a speed of 80 km·h^{-1} (a), on a curved section of track with a radius of R = 300 m at a speed of 50 km·h^{-1} (b) and on a curved section paths with a radius of R = 600 m at a speed of 60 km·h^{-1} (c)*

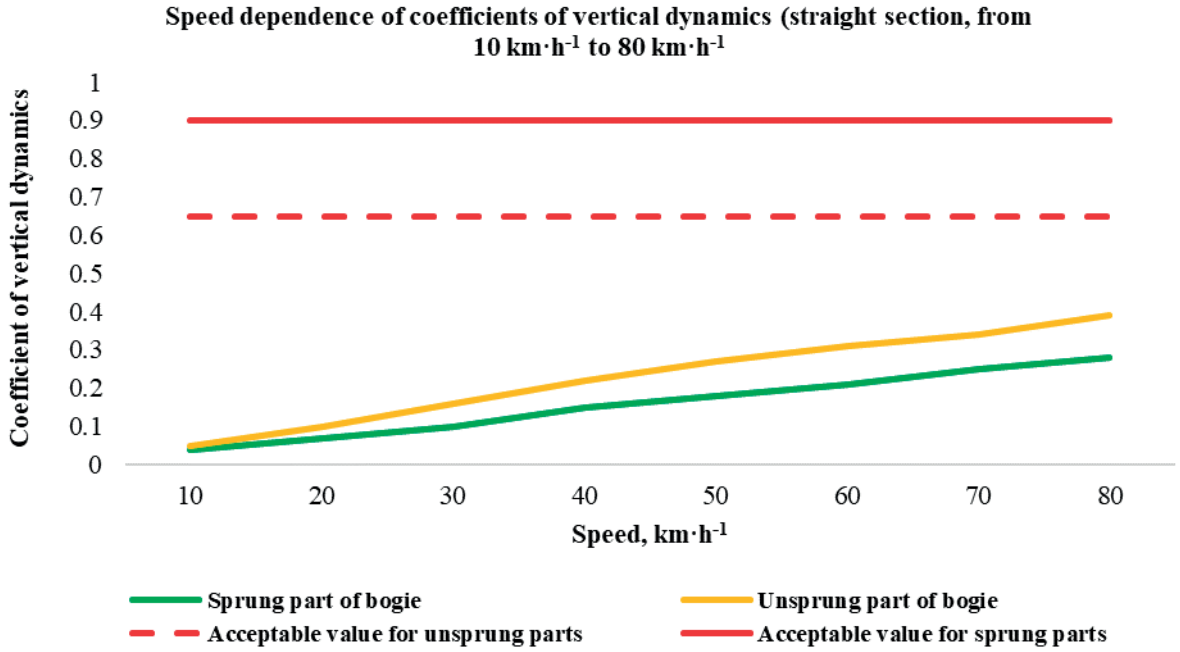

Figure 9 *Coefficients of vertical dynamics of sprang and unsprang parts of the UVZ-9M bogie, obtained during the running strength tests of a six-axle scale test wagon type 640-VPV depending on the speed of movement on a straight section of track*

The calculation results were:

- for the side frame - 64.3 years;
- for the spring beam - 67.8 years;
- for the pivot beam - 66.1 years.

Thus, calculations to determine the full technical service life of the cast parts, based on experimental data, indicate the presence of a residual life of 5.3 years for the side frame, for the spring and pivot beams of 8.5 and 7.1 years, respectively.

6 Results and their significance

As can be seen from the calculation results based on experimentally obtained data, the total life of the cast parts of the UVZ-9M three-axle bogie exceeds their service life by 5.3 years at the moment, taking into account the minimum value obtained (side frame). Therefore, based on the data obtained, it is possible to scientifically substantiate the possibility of extending the service life of cast parts by 5 years.

Based on the results of the work, it is possible to single out a key advantage - the possibility of extending the service life of cast parts of bogies without their premature replacement. This makes it possible to significantly reduce the capital costs for the purchase of new bogies, extend the operation of the rolling stock without reducing its reliability, ensure a more rational use of the resources of railway enterprises, and create a scientifically sound basis for assessing the lifetime of similar units in other types of wagons.

An additional advantage is the reduction of the negative impact on the environment. Extending the service life of existing parts reduces the need to manufacture new cast elements, which in turn reduces CO_2 emissions, reduces consumption of natural resources, and reduces waste from decommissioned parts and structures.

From an economic point of view, extending the service life of parts can significantly reduce the costs of replacing them and purchasing new components for foreign currency. The purchase of new bogies requires large investments, while the operation of existing ones, provided they comply with regulatory requirements, is more profitable and helps to reduce operating costs.

It is important to note that the proposed method of running strength tests can be successfully adapted for other types of wagons, such as dump trucks, platforms, tanks and other industrial units using the three-axle trucks of the UVZ-9M model. This expands the scope of its application, going beyond the weighing industry and making the technique a universal tool for assessing the strength and durability of structures.

In conclusion, it should be emphasized that the studies carried out confirm the strength of cast parts, exclude the presence of critical defects and justify the possibility of extending their service life without the risk of structural failures. Thus, the results obtained not only make it possible to increase the service life of trolleys, but make their use safe and economically justified, as well.

7 Conclusion

Experimental studies conducted using the developed methodology [14] for conducting the running strength tests of a six-axle scale test wagon of type 640-VPV made it possible to determine the dependence of the stress-strain state of cast parts of a three-axle bogie of the UVZ-9M model on the speed of movement of a six-axle scale test wagon of type 640-VPV to substantiate the possibility of extending the service life of these parts, taking into account the assessment of their safety margin and the remaining lifetime.

The following main results were obtained during the running strength tests:

- the maximum stresses generated on the side frame of the bogie are concentrated in the area of radius R55, above the axle box opening, the stresses reach 73.5 MPa;
- on the spring beam of the bogie, maximum stresses are observed in the central belt, the value of which does not exceed 53.9 MPa.
- the maximum stresses on the pivot beam are concentrated in the transverse beam with a support arm, where their stresses reach 58.9 MPa.

As can be seen from the results, all the maximum stresses obtained on individual cast parts do not exceed the maximum value of 145 MPa set by [15].

An analysis of calculations, based on the experimental safety margin data, showed that the full service life of cast parts is 64.3 years for the side frame, and for the spring and pivot beams this figure is 8.5 and 7.1 years, respectively. Thus, the scientific and practical research has substantiated the possibility of extending the service life of cast parts by 5 years, taking into account the minimum total service life of the side frame.

Acknowledgements

The authors received no financial support for the research, authorship and/or publication of this article.

Conflicts of interest

The authors declare that they have no known competing financial interests or personal relationships that could have appeared to influence the work reported in this paper.

References

[1] RAHIMDE, M., GHODRATI, B., TAGHIZADEH VAHED, A. Prediction of mining railcar remaining useful life. In: 28th International Symposium on Mine Planning and Equipment Selection MPES 2019: proceedings [online]. 2020. ISBN 978-3-030-33954-8, p. 281-288. Available from: https://doi.org/10.1007/978-3-030-33954-8_35

[2] LI, Z., HE, Q. Prediction of railcar remaining useful life by multiple data source fusion. *IEEE Transactions on Intelligent Transportation Systems* [online]. 2015, **16**(4), p. 2226-2235. eISSN 1558-0016. Available from: https://doi.org/10.1109/TITS.2015.2400424

[3] XU, Z. W., WU, S. C., WANG, X. S. Fatigue evaluation for high-speed railway axles with surface scratch. *International Journal of Fatigue* [online]. 2019, **123**, p. 79-86. ISSN 0142-1123. Available from: https://doi.org/10.1016/j.ijfatigue.2019.02.016

[4] WU, S. C., LIU, Y. X., LI, C. H., KANG, G. Z., LIANG, S. L. On the fatigue performance and residual life of intercity railway axles with inside axle boxes. *Engineering Fracture Mechanics* [online]. 2018, **197**, p. 176-191. ISSN 0013-7944. Available from: https://doi.org/10.1016/j.engfracmech.2018.04.046

[5] FOMIN, O., VATULIA, G., HORBUNOV, M., LOVSKA, A., PISTEK, V., KUCERA, P. Determination of residual resource of flat wagons load-bearing structures with a 25-year service life. *IOP Conference Series: Materials Science and Engineering* [online]. 2021, **1021**(1), ISSN 1757-899X. Available from: https://doi.org/10.1088/1757-899X/1021/1/012005

[6] SYGANSKAYA, L., HAMRAEVA, E., NARKIZOVA, E. Testing the methodology for justifying the service life of freight cars based on the results of analog car testing. *Bulletin of Scientific Research Results* [online]. 2024, **2024**(4), p. 15-23. ISSN 2223-9987. Available from: https://doi.org/10.20295/2223-9987-2024-04-15-23

[7] LUO, Y., LI, C., KANG, X., HU, Y., WU, S. Fatigue limit and residual life evaluation of railway EA4T axles with artificial surface impacts. *Journal of Materials Engineering and Performance* [online]. 2023, **32**, p. 5167-5175. eISSN 1544-1024. Available from: https://doi.org/10.1007/s11665-022-07447-3

[8] REN, X., WU, S., XING, H., FANG, X., AO, N., ZHU, T., LI, Q., KANG, G. Fracture mechanics based residual life prediction of railway heavy coupler with measured load spectrum. *International Journal of Fracture* [online]. 2022, **234**, p. 313-327. eISSN 1573-2673. Available from: https://doi.org/10.1007/s10704-022-00627-1

[9] WANG, C., ZHU, T., YANG, B., XIAO, S., YANG, G. Remaining useful life for heavy-duty railway cast steel knuckles based on crack growth behavior with hypothetical distributions. *Chinese Journal of Mechanical Engineering* [online]. 2024, **37**, 77. ISSN 2192-8258. Available from: https://doi.org/10.1186/s10033-024-01052-2

[10] ORLOVA, A. M., BABANIN, V. S., TURUTIN I. V. Calculation justification of the assigned service life of the finished axle of a freight wagon wheelset. *Railway Technique*. 2023, **1**(61), p. 22-26. ISSN 1998-9318.
[11] ELYAZOV, I. S., YUSIFZADE, E. N., BAKHSHIEV, A. B., HUSEYNOV, I. D. Method for calculating the durability of a car wheelset. *Bulletin of RGUPS*. 2024, **3**(95), p. 109-118. ISSN 0201-727X.
[12] ZAFAROV, D. Development of a methodology for conducting running strength tests to determine the load of cast parts of a three-axle bogie. *Railway Transport: Topical Issues and Innovations*. 2023, **4**, p. 165-171. ISSN 2181-953X.
[13] BORONENKO, Y., RAHIMOV, R. Experimental determination of forces through measurements of strains in the side frame of the bogie. *Transport Problems* [online]. 2021, **16**(3), p. 199-211. ISNN 1896-0596. Available from: https://doi.org/10.21307/tp-2021-053
[14] State standard 33788-2016. Freight and passenger wagons. Strength and dynamic quality testing methods. Standartinform. 2016.
[15] Norms for the calculation and design of wagons, railways of the MPS track gauge 1520 mm (non-self-propelled) with amendments and additions. GosNIIV-VNIIIZHT. Moscow, 1996.

STATISTICAL RESEARCH ON BRAKING MALFUNCTIONS OF PASSENGER ROLLING STOCK IN OPERATION

Juraj Gerlici[1], Alyona Lovska[1,*], Vasyl Ravlyuk[2], Yaroslav Derevianchuk[2], Oleksandr Derevyanchuk[3]

[1]University of Zilina, Zilina, Slovak Republic
[2]Ukrainian State University of Railway Transport, Kharkiv, Ukraine
[3]Yuriy Fedkovych Chernivtsi National University, Chernivtsi, Ukraine

*E-mail of corresponding author: Alyona.Lovska@fstroj.uniza.sk

Juraj Gerlici 0000-0003-3928-0567,
Vasyl Ravlyuk 0000-0003-4818-9482,
Oleksandr Derevyanchuk 0000-0002-3749-9998
Alyona Lovska 0000-0002-8604-1764,
Yaroslav Derevianchuk 0000-0002-4932-2751,

Resume
In this article are highlighted the results of the research on braking malfunctions of passenger rolling stock identified during the car maintenance. Based on the collected statistical material, the key factors that cause braking malfunctions in operation are highlighted. The main brake equipment units that account for the largest number of malfunctions in operation are determined. The data on the malfunctions of air distributors used in passenger rolling stock was systematized using the STATISTIKA software package. To ensure continuous monitoring and timely detection of defects in the brake system of passenger trains, it is critical to use modern diagnostic tools to predict the technical malfunctions of pneumatic and electropneumatic brake system units of passenger cars. Moreover, this would ensure compliance with the requirements for overhaul periods for passenger cars in accordance with the current standards and technical documents and would guarantee the traffic safety on Ukrainian railways.

Article info
Received 10 December 2024
Accepted 18 March 2025
Online 12 May 2025

Keywords:
brake equipment
diagnostic system
passenger car
pneumatic brakes
statistical analysis
transport engineering

Available online: https://doi.org/10.26552/com.C.2025.038

ISSN 1335-4205 (print version)
ISSN 2585-7878 (online version)

1 Introduction

The operation of Ukrainian Railways (Ukrzaliznytsia, UZ) can be optimized and the high quality of passenger transportation can be ensured by implementing advanced technological solutions aimed at improving the traffic safety [1-6]. One of the research priorities in this regard is to improve the braking system of passenger cars, which plays a key role in the safe operation of rolling stock.

In practice, considerable attention is paid to the system of maintenance and repair of passenger cars, which is aimed at minimizing risks of forced train stops. That requires the systematic detection and elimination of malfunctions at passenger car maintenance depots. A significant amount of rolling stock constantly passes through the rail sections equipped with such maintenance depots at which maintenance staff performs the required technical inspection of railcars and identifies faulty and defective units. This can lead to significant delays in trains or even their stoppage on the rail hauls. Among the critical units that require special attention are brakes.

The brake equipment for passenger cars is a key element in ensuring safety and comfort during the rail transportation. It provides effective braking of the train at different operating modes, including both standard and non-standard traffic conditions. The proper operation and regular maintenance of the brake system is the foundation of reliable passenger car operation, which guarantees the safety of life and health of passengers and staff.

High reliability of the brake system during the operation of passenger trains is defined as one of the key priorities in car maintenance and repair. Potential malfunctions can be predicted by means of an integrated diagnostic system for passenger cars. It would allow monitoring the technical condition of the main elements of the brake system, such as air distributors or electric air distributors of the train in operation. Timely detection and elimination of any defects in these units would help to provide the trouble-free operation of the

brake system and reduce the time required to eliminate faults, which in turn, significantly improve the safety of rail transportation.

Modern brake diagnostic systems for cars are usually labour-intensive and not always highly reliable regarding individual brake units [7]. This poses significant challenges for the railway train traffic safety. Accordingly, there is a growing need to improve diagnostic technologies to optimize maintenance and repair processes and increase the overall reliability of brake systems.

Diagnostic systems can be improved through the development of more efficient monitoring methods that can quickly and accurately identify potential malfunctions and predict potential failures. This approach will not only reduce the time for diagnostics and repairs, but significantly reduce the risks associated with the operation of passenger cars, as well, thereby ensuring a significant level of passenger transportation safety.

Analysis of recent publications. The efficient operation of rolling stock and railway transport equipment is critical for increasing the capacity and safety of rail transportation [8-9]. These aspects are fundamental for all UZ structural divisions. The optimized operation of the rolling stock and railway equipment implies not only maintenance and modernization, but the continual updating of management strategies aimed at improving the operational characteristics of the transportation system, as well.

Many studies have been devoted to analysing the operation of brake systems on railway rolling stock and improving their operating efficiency. Thus, in studies [10-11] are highlighted the peculiarities of the use of vacuum, pneumatic, mechanical, electrodynamic and magnetic rail brakes for railway transport. Their advantages and disadvantages, together with promising application methods to be implemented for any rail vehicle, are considered. However, authors of these studies did not pay attention to the diagnostics of brake equipment units of passenger cars on the train's route.

In study [12] is dealt with the methodology for computational and experimental research into the braking efficiency of passenger cars using mathematical models and computer modelling. However, the authors of the study, which was aimed at improving braking efficiency and train safety, did not pay attention to diagnosing the pneumatic units of railcars that ensure the performance of the whole braking system and the train's route speed.

Authors of study [13] described the operation of the UIC pneumatic brake system used for freight wagons. They emphasized that if a train consists of 10-15 wagons, the air brakes are difficult to control due to the complexity of the air distribution system and its operation processes, which affects the longitudinal forces in the train. The operation of the air distributor at different operational modes was analysed. However, the authors did not address the issues of controlling the pneumatic and electrical parts of the brake equipment along the train's route.

In [14], the authors emphasized that a higher train speed means that the production costs of railcar units that account for the reliable operation of the vehicle will be higher. The requirements for the development of new types of brakes for railway rolling stock with improved performance characteristics are presented. However, the authors did not pay attention to the on-board technical diagnostic tools on passenger rolling stock, the use of which would significantly increase the train speed and ensure railway traffic safety.

In study [15] is described the operation of the pneumatic brake system of rolling stock during rail freight transportation. The authors investigated the complex pneumatic processes in the train braking system. It is determined that a significant amount of compressed air leaks into the atmosphere through the loose brake connections. It is established that the modelling of dynamic processes in a pneumatic network depends on the loading of a vehicle. However, the authors did not consider the diagnostic tools that can better control the technical condition of the brake system when the train is moving.

The pneumatic braking systems of freight trains that guarantee the safe rail transportation are described in [16]. An algorithm is proposed for determining diagnostic features for advanced diagnostic systems to detect malfunctions of pneumatic brakes. It is recommended to accumulate diagnostic values using a laboratory car acting as an experimental platform. The authors used the method that allows detecting maximum values in combination with a first-order difference function to divide and classify time series of air pressure into the phases of braking and lapping. Several algorithms of the modified machine learning method are investigated. This makes it possible to achieve an accuracy of about 99% when detecting faults in the brake line of a rail car, and more than 94% when diagnosing faults in brake equipment units. However, the algorithms of the modified machine learning method proposed in this paper are applicable only to pneumatic brake systems of freight rolling stock.

In study [17] was examined the pneumatic brake system of freight trains used on Chinese Railways. A model of the brake system is analysed based on the equation of gas flow and the equation of air flow rate through the calibration holes in the brake units. The proposed model was tested in experimental conditions on 150 pilot rail vehicles. The tests were conducted at different braking modes: step-by-step braking, full braking and emergency braking. The pressure and the time of filling the brake cylinders, spare tanks, and the time response for air distributors of a freight train were studied. In addition, the switching times of the air distributor elements under the simulation conditions were determined.

The analysis of literature [8-17] has made it possible to establish that the issues of diagnosing inoperative brake systems and their elements on passenger rolling stock are quite relevant and require further development and study.

Purpose and main objectives of the article. The purpose of the article is to highlight the peculiarities of statistical research into malfunctions of brake units of passenger rolling stock in operation.

To achieve this purpose, the following objectives have to be set:

- to analyse the collected statistical data on malfunctions of brake equipment units of passenger cars;
- to systematize the data on malfunctions of brake equipment units using STATISTIKA; and
- to propose a technical diagnostic system to improve the efficiency of braking equipment units of passenger cars.

2 Materials and methods

The study of the technical condition of the brake systems of passenger cars included a comprehensive analysis of braking malfunctions at various operating modes, namely charge and release, service braking, overlapping, full-service braking, and emergency braking [18]. The key brake system components, such as electric air distributors (No. 305), air distributors (No. 292), brake lines with fittings, electric lines, brake cylinders and spare tanks, were given special attention. This technical inspection was carried out in accordance with the requirements of the current regulatory documents [19-22].

Based on the analysis of statistical data, collected during the maintenance of brake equipment of passenger cars, a histogram was constructed (Figure 1). It presents the distribution of malfunctions in the basic units and elements of pneumatic and electrical part of brake equipment collected between 2019 and 2023.

The analysis of this histogram demonstrates that in 2023 the number of malfunctions in the main units of brake systems of passenger cars decreased if compared to 2019. This is due to the decommissioning of many passenger cars that did not meet the technical requirements and the service life of which expired. Those measures helped to improve the overall reliability and efficiency of rolling stock.

The histogram also shows that in recent years, units and elements of the pneumatic and electrical parts of the brake equipment of passenger cars fail in operation primarily due to their inoperable state. Therefore, there exist critical problems that require urgent solutions on how to improve the performance of brake systems and ensure the train safety [23].

Over 2023 the condition of brake equipment was assessed through the systematic technical inspections carried out in the operational and repair depots of the passenger facility. Based on the collected statistical data, the histogram was constructed (Figure 2). It illustrates the distribution of malfunctions of brake equipment units in 2023 by visualizing problematic aspects and their dynamics over the specified period.

The inspection conducted revealed 1,166 malfunctions of pneumatic brake equipment of passenger cars. As seen from the histogram above, electric air distributor malfunctions rank first, among which are inoperable braking and releasing valves, pneumatic relay malfunctions, clogged throttle openings, damaged

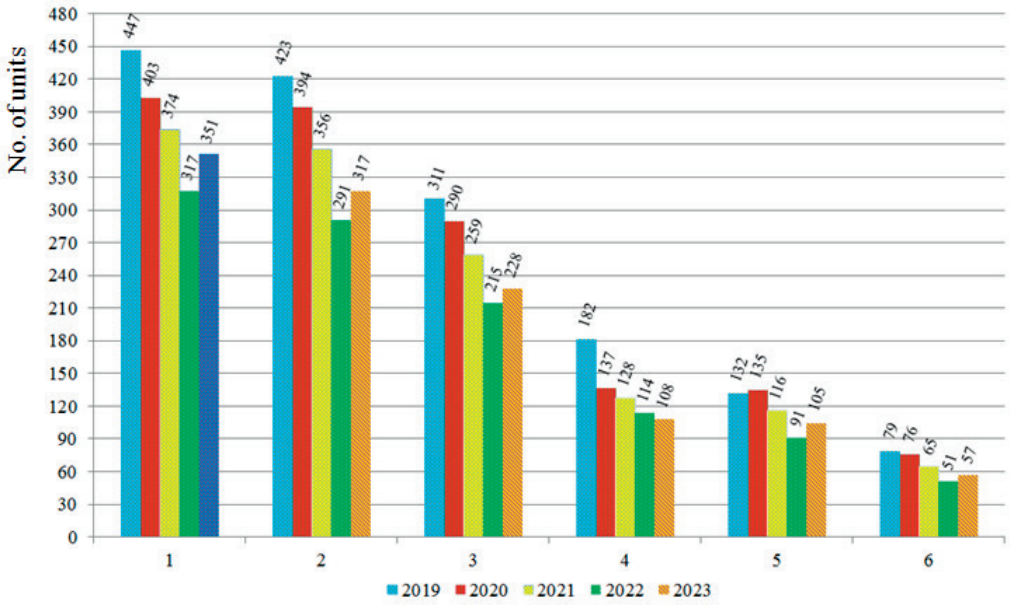

1 - electric air distributor No. 305; 2 - air distributor No. 292; 3 - brake line with fittings; 4 - electric line; 5 - brake cylinder; 6 - spare tank

***Figure 1** Distribution of malfunctions in passenger car brake equipment*

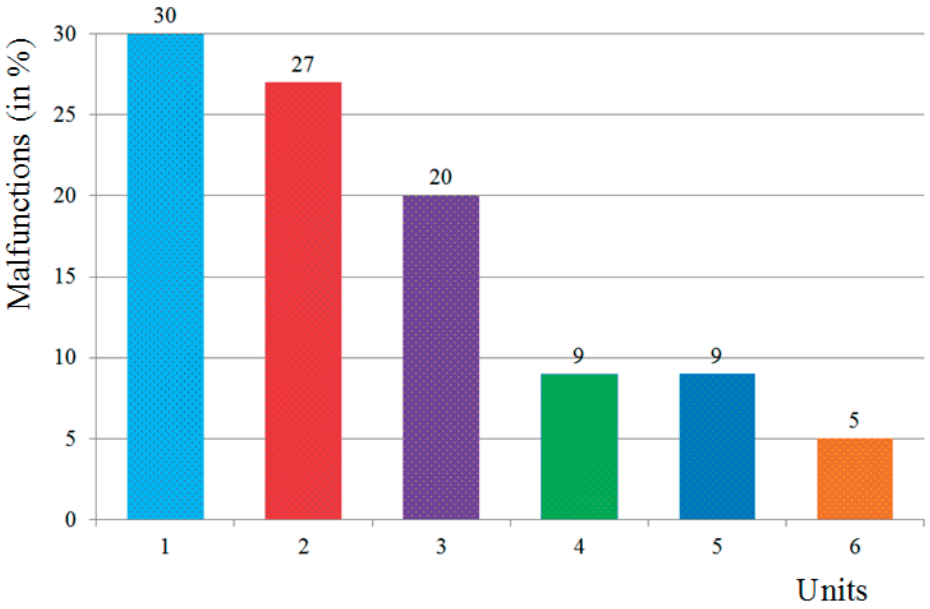

1 - electric air distributor No. 305; 2 - air distributor No. 292; 3 - brake line with fittings; 4 - electric line; 5 - brake cylinder; 6 - spare tank

Figure 2 *Distribution of malfunctions in passenger car brake equipment*

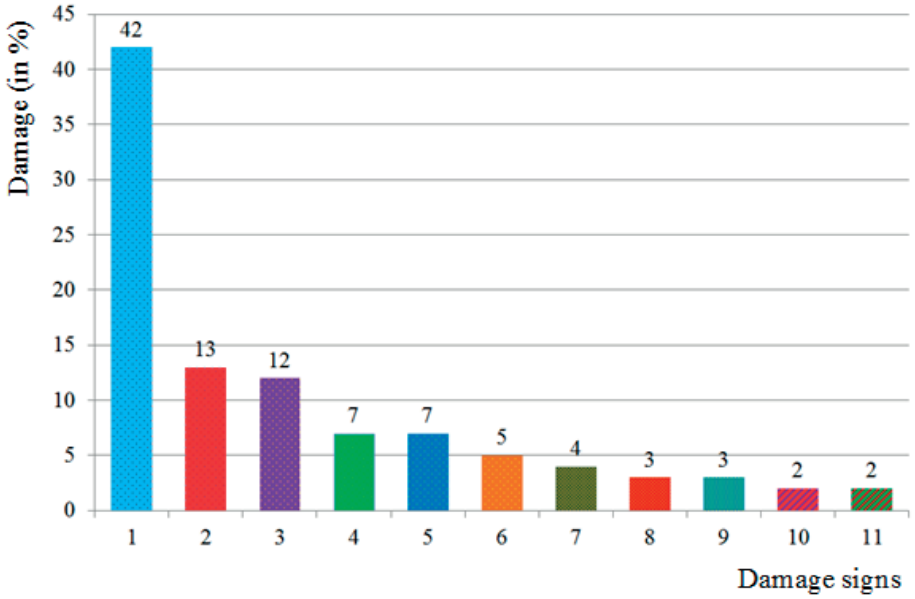

1 - air leakage due to a loose connection of the hoses; 2 - air leakage due to damage to the connecting hose; 3 - air leakage due to a loose threaded connection of the air line; 4 - malfunction of the elements of the end valve; 5 - breakage of the brake line; 6 - malfunction of the elements of the connecting valve; 7 - disconnection of the pipe leading to the air distributor; 8 - rupture of the connecting hoses; 9 - malfunction of the pipe leading to the reserve tank; 10 - malfunction of the stop valve; 11 - other malfunctions of the brake line

Figure 3 *Distribution of malfunctions in the brake line and fittings*

(broken) diodes, lack of electrical contact, etc. They were detected in electric air distributor No. 353 and amounted to 30% of the total number of malfunctions.

The air distributor malfunctions rank second; they include clogged throttle openings and filters, wear of the main and cut-off spools, wear of bushings and the main piston, etc. The inspection revealed them in 317 air distributors, which is 27% of the total number of faults.

Malfunctions of the brake line and valves rank third; they include damaged main and supply pipes, loss of density at coupling joints, inoperable end cranes, stop cranes, disconnecting cranes, etc. As a rule, such malfunctions cause air leakage from the pneumatic part into the atmosphere at all brake operating modes. In addition, the brake can spontaneously activate while the train is moving. These malfunctions were detected in 228 cars, which is 20% of the total number of units inspected.

Electrical line malfunctions rank fourth; they include damage to the contacts of the electrical part

of the connecting hoses, breakdown of the electrical wire to the body, damage or reduction of the insulation resistance of the wires, lack of contact in the terminal boxes, damage or breakage of the wires, etc. Such malfunctions were detected in 108 cars, which is 9% of the total number of malfunctions.

Brake cylinder malfunctions rank fifth and include worn cuffs, weakened or broken return springs, rod wear or bending, loss of seal density between the body and the cover, etc. Those malfunctions lead to a decrease in the efficiency of train braking, they were detected in 105 brake cylinders, which is 9% of the total number of those inspected.

Malfunctions of spare tanks rank sixth and include local abrasions, corrosion and mechanical damage, overdue testing, etc. According to the inspection results, such malfunctions were found in 57 spare tanks, which is 5% of their total number.

Based on the results of the malfunctions found during the car maintenance at the servicing depot, as well as on the route, the distribution of malfunctions in the brake line and valve was obtained (Figure 3).

Based on the results of the diagram analysis, the following main malfunctions in the brake line and fittings were identified (in %):

- air leakage due to lose connection of sleeves 369A (Figure 3, item 1) as a result of damage or wear of the sealing rings, wear of the profile of connecting heads, etc. (42%);
- air leakage due to a damaged connecting hose (Figure 3, item 2) as a result of deficiencies in the operation of individual elements, such as wear of the sealing ring, malfunctions of the tube and connections, etc. (13%);
- air leakage through the loose threaded connection of the air duct (Figure 3, item 3) due to damage or wear of the threaded connection, unsuitable mounting seal, etc. (12%);
- malfunctioning of the end valve elements (Figure 3, item 4) due to cracks in the body, poor installation, thread damage, broken or missing handle, etc. (7%);
- breakage of the brake line (Figure 3, item 5) due to damage or wear of the threaded connection, poor installation of the seal, fastening faults, etc. (7%);
- malfunctioning of the connecting valve elements (Figure 3, item 6) due to damaged threads, broken or missing switching handle, air leakage from the body, poor quality installation of the seal, etc. (5%);
- disconnection of the pipe supplied to the air distributor (Figure 3, item 7) due to defects in the operation of individual elements, such as wear of the threaded connection, damage to the threaded fasteners, poor-quality installation of the seal on the pipeline, etc. (4%);
- rupture of the connecting hoses (Figure 3, item 8) due to damage to the tube, wear of the hose head and ferrule thread, poor-quality installation of the seal, deformation of the clamp fastening, etc. (3%);
- malfunctions of the pipe leading to the spare tank (Figure 3, item 9) due to wear or damage to the threaded connection, poor quality of the seal, deformation or damage to their fastenings, etc. (3%);
- malfunction of the stop valve (Figure 3, item 10) due to poor installation of the seal, damaged threads, broken or missing switching handles, cracks in the body, etc. (2%);
- other malfunctions of the brake line (Figure 3, item 11) due to defects in the operation of individual elements; these defects include damage or breakage of threads, abrasions, corrosion and mechanical damage, air leakage through the threaded connections, poor installation of the seal, etc. (2%).

Of special attention is the fact that the largest number of malfunctions identified during the car maintenance was in the elements of electric and pneumatic air distributors. This is due to the complexity of their structural elements manufactured with high precision, and a significant number of calibration holes in spools and bushings [18].

Based on the statistical material collected during the maintenance of passenger cars carried out at the service depot, as well as on the route, the distribution histogram of malfunctions of air distributor No. 292 was drawn (Figure 4).

Based on the results of the histogram analysis, the following main types of air distributor malfunctions were identified (in %):

- slow charging of the reserve tank (Figure 4, item 1) due to clogged calibration holes and filters, slow movement of the main piston and spools as a result of increased resistance in the charging position, contamination or increased viscosity of the lubricant, etc. (27%, the largest number);
- air distributor does not work during the service braking (Figure 4, item 2) due to a slow movement of the main piston and spools as a result of increased resistance in the braking position, contamination or increased viscosity of the lubricant, etc. (17%);
- reduced pressure of the brake cylinder in the Lap position (Figure 4, item 3), which leads to air leakage from the pneumatic cylinder due to damaged threaded connections, poor seals and wear of the cuffs (14%);
- increased pressure of the brake cylinder in the Lap position (Figure 4, item 4), accompanied by a slow movement of the main piston and air distributor spools in the braking mode (13 %);
- the accelerator does not trigger at emergency braking (Figure 4, item 5) due to insufficient pressure in the accelerator chamber, failure to connect the accelerator chamber to the brake cylinder, and in the accelerator-off mode (9%);
- the accelerator is triggered at service braking (Figure 4, item 6) due to a slight moving effort of the main piston and air distributor spools as a result of triggering or weakening of the buffer spring (8%);

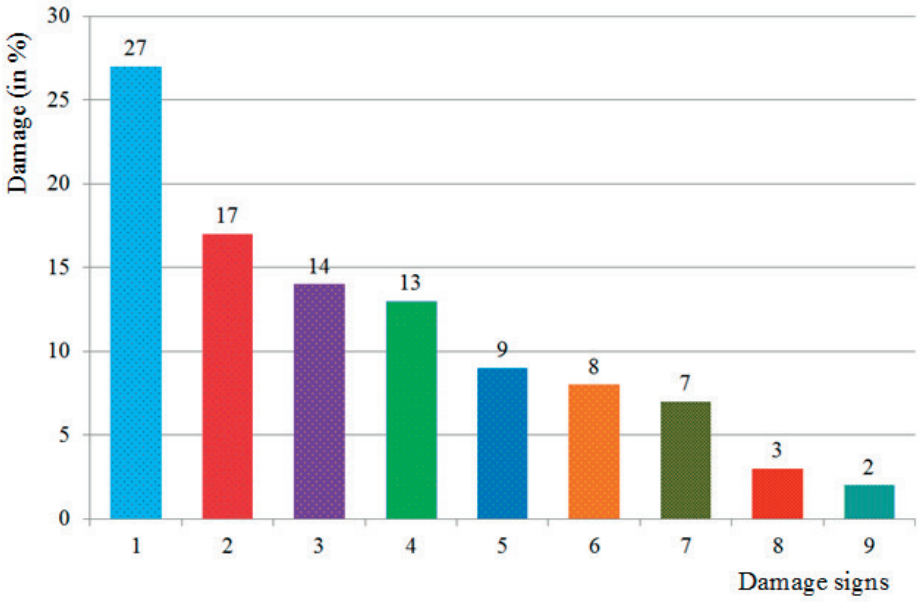

1 - slow charging of the reserve tank; 2 - air distributor does not operate at service braking; 3 - lower pressure in the brake cylinder in the Lap position; 4 - higher pressure in the brake cylinder in the Lap position; 5 - accelerator does not operate at emergency braking; 6 - accelerator operates at service braking; 7 - malfunction of an emergency braking accelerator; 8 - brakes are released unauthorizedly in the Lap position; 9 - brakes are released unauthorizedly after emergency braking

Figure 4 *Distribution of malfunctions of air distributor No. 292*

- malfunction of the emergency brake accelerator (Figure 4, item 7) is the cause of its actuating during the charging of the brake line due to a small moving force of the accelerator piston (7%);
- unauthorized release of brakes in the Lap position (Figure 4, item 8) caused by air leakage from the brake cylinder as a result of poor-quality installation of threaded connection seals or damaged release valve (3%);
- unauthorized release of brakes after emergency braking of the train (Figure 4, item 9) due to significant air leakage from the brake cylinder caused by damaged release valve of the reserve tank (2 %).

3 Results

The collected statistical data on the detected malfunctions of air distributors No. 292, for different passenger car mileages during their maintenance, are shown in Table 1.

The optimal number of experimental data n, required to verify that the sampling-normal distribution is consistent, can be determined by the ratio of the mean value of the modulus of deviation of the random variable x_i from its sample mean $\bar{x}$ to the standard deviation σ [24-25].

Provided that the following inequality is satisfied:

$$\left| \frac{\left| \sum |x_i - \bar{x}| \right|}{\sigma} - \sqrt{\frac{2}{\pi}} \right| < \frac{0.4}{\sqrt{n}}, \tag{1}$$

the sample size is considered sufficient for further research. The number $\sqrt{2/\pi}$ defines this ratio for a normally distributed random variable.

The average mileage of a passenger car after the maintenance service (MS-3) was 78,600 km, and after depot repair (DR) it was 146,900 km [26].

The data analysis was based on mathematical statistics methods for determining the variance of the population and the standard deviation, which is an estimate of the standard deviation based on the unbiased estimate of the variance [27]. The key statistical indicators were calculated using the following formulae:

- average sample value of a random variable

$$\bar{x} = \frac{\sum_{i=1}^{n} x_i}{n}; \tag{2}$$

- variance σ^2 of a random variable calculated by the formula

$$\sigma^2 = \frac{\sum_{i=1}^{n} (x_i - \bar{x})}{n-1}, \tag{3}$$

where n is the size of a given sample; x_i is the i-th sample element. It was found, that $\bar{x} = 31.655$, and $\sigma^2 = 31.107$.

The experimental dependence of the frequency of malfunctions in air distributor No. 292, detected during the maintenance service and on the route of passenger cars, relates to the number of observations. At the same time, the distribution function of this random variable $F(x)$ of the sample is unknown [26].

The H_0 hypothesis is formulated by the following definition: the distribution function of a random variable is described by the normal distribution law $F_0(x)$

Table 1 *Statistical data on the total number of malfunctions in air distributor No. 292*

Month of observation	No. of malfunctions	Average car mileage interval after MS-3, N, km	Average car mileage interval after DR, N, km	Month of observation	No. of malfunctions	Average car mileage interval after MS-3, N, km	Average car mileage interval after DR, N, km	Month of observation	No. of malfunctions	Average car mileage interval after MS-3, N, km	Average car mileage interval after DR, N, km
1	30	77.530	47.790	29	24	104.710	208.530	57	34	63.490	145.610
2	29	72.420	156.750	30	26	71.320	123.50	58	36	89.840	223.160
3	25	45.260	104.750	31	27	97.950	138.380	59	39	88.160	243.100
4	26	98.870	165.540	32	28	39.100	56.460	60	41	32.760	201.840
5	25	94.130	119.870	33	29	102.360	179.170	61	42	97.130	74.870
6	23	116.410	93.760	34	31	120.180	243.750	62	39	71.150	53.590
7	22	99.560	178.940	35	32	52.480	170.180	63	37	95.140	207.890
8	24	81.090	84.990	36	33	120.460	177.430	64	36	33.170	49.270
9	23	99.300	176.140	37	36	117.370	146.510	65	34	79.280	195.020
10	27	98.260	64.710	38	34	33.550	201.030	66	31	112.830	171.940
11	28	117.000	194.430	39	33	70.930	196.060	67	33	109.410	174.100
12	30	41.020	77.570	40	32	69.640	59.120	68	34	106.220	170.990
13	27	66.480	246.140	41	30	67.120	144.960	69	35	104.390	230.160
14	26	98.350	54.690	42	29	69.640	77.540	70	36	58.250	120.220
15	25	77.260	129.930	43	30	116.90	244.490	71	39	62.790	120.610
16	23	65.790	45.450	44	31	33.760	60.990	72	41	62.610	175.010
17	23	38.330	90.700	45	32	33.460	152.310	73	43	41.570	86.710
18	22	99.680	206.060	46	34	100.230	127.280	74	42	115.500	136.860
19	21	71.610	151.430	47	36	30.100	115.880	75	40	69.390	241.690
20	23	36.370	118.330	48	37	96.530	157.550	76	39	76.340	107.770
21	24	48.540	135.300	49	40	51.840	110.750	77	35	51.750	85.250
22	25	47.450	149.230	50	36	115.030	127.360	78	31	37.650	224.540
23	25	88.960	198.500	51	35	34.260	240.840	79	32	66.250	66.490
24	28	87.290	180.340	52	34	100.260	213.840	80	36	117.830	178.920
25	33	110.860	114.630	53	32	71.940	185.620	81	34	63.070	154.760
26	31	74.410	231.540	54	31	52.170	186.620	82	37	88.180	185.070
27	30	83.040	142.150	55	32	87.950	235.740	83	39	121.840	137.100
28	29	83.760	44.250	56	33	94.450	142.280	84	40	111.880	49.180

$$F_0(x) = \frac{1}{\sqrt{2\pi\sigma^2}} e^{-\frac{(x-\bar{x})^2}{2\sigma^2}}. \quad (4)$$

The function $F_0(x)$ is fully defined for the given $\bar{x}$ and σ.

The alternative hypothesis H_1: the distribution function does not follow the normal distribution law.

That is, H_0: $F(x)=F_0(x)$, H_1: $F(x)\neq F_0(x)$.

Test the hypothesis H_0.

The purpose of that is to check whether the sample is consistent with the assumption that the distribution function of the aggregate is $F_0(x)$.

Further, the consistency criterion χ^2 is used and the frequency of occurrence of a random variable included in the sample in a given interval is calculated. Based on the results of car maintenance, it was found that the number of all observations was *n=84*.

Finally, the range of sample data 20-44 is divided into 12 intervals with a step equal to two (Figure 5) and the frequency of observations, with which random variable falls into each interval is determined.

Based on the analysis of statistical data on malfunctions of air distributors No. 292 of passenger cars for 2023, the information was systematized and processed in STATISTIKA.

The results of the processing are shown in Figure 5, which presents the empirical data on the faults of this unit.

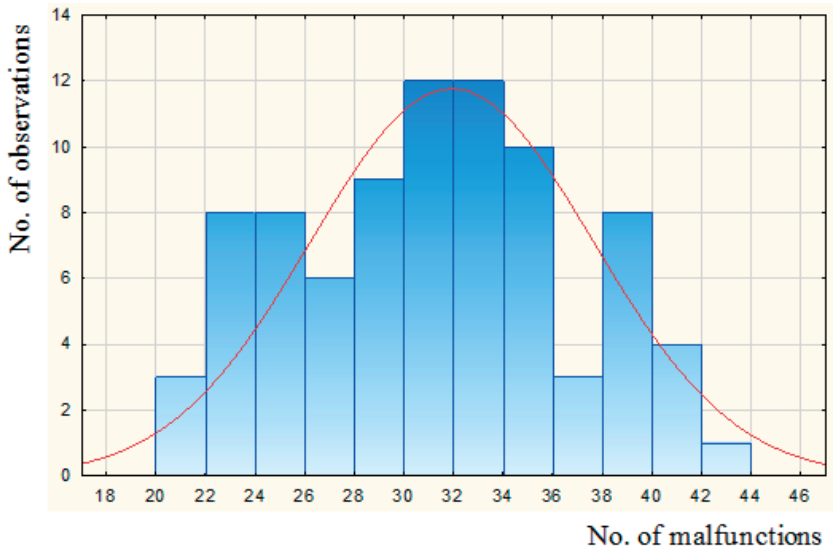

Figure 5 *Results of processing the statistical data on malfunctions of air distributor No. 292*

The solid line in Figure 5 describes the theoretical frequency of occurrence of a malfunction if the sampling distribution function follows a normal distribution law.

This statement can be confirmed or denied with the use of the χ^2 criterion (Pearson's criterion) of consistency of the distribution function $F(x)$ of the sample with the normal distribution $F_0(x)$.

Pearson's theorem states that if the hypothesis H_0 is realized, then the experimental values $\chi^2(n)$ converge to the critical value χ^2_{n-1} for the n-1 degree of freedom.

Therefore, the new random variable χ^2 of statistics $\frac{(n_i - np_i)^2}{np_i}$ for the i-th interval is introduced where np_i is the corresponding value of the theoretical frequency.

Before constructing a random variable, its theoretical probability must be determined using the following formula:

$$p_i = P(x_1 \le x_i \le x_2) = F\left(\frac{x_2 - \bar{x}}{\sigma}\right) - F\left(\frac{x_1 - \bar{x}}{\sigma}\right), \quad (5)$$

where $F(x)$ is the Laplace function;
x_1, x_2 are the left and right boundaries of the *i-th* interval.

The experimental value $\chi^2(n)$ is determined by the formula

$$\chi^2(n) = \sum_{i=1}^{m} \frac{(w_i - p_i)^2}{p_i} = \sum_{i=1}^{m} \frac{(n_i - np_i)^2}{np_i}, \quad (6)$$

where m is the number of intervals;
n_i is the *i-th* experimental frequency;
p_i is the theoretical probability of a random variable falling into the i-th interval;
w_i is the experimental probability of a random variable falling into a given interval;
np_i is the theoretical frequencies of a random variable falling into the i-th interval.

For the given level of significance α (probability γ) and the known degree of freedom k, find the critical value of the parameter x_α.

Since the degree of freedom $k = m - 1 = 12 - 1 = 11$, for the value $k = 11$ and the significance level $\alpha = 0.05$ according to the table [23, 26], the critical value of this parameter is found, it is $x_\alpha = 19.7$.

It should be noted, that at this stage of the study, the parameter α equals to the value of 0.05 as an example. At subsequent stages of the study, it is planned to adopt this parameter at a level lower than 0.05. In this case, the same methodology will be used as described in this presented research. This will allow to compare the obtained result and to draw a conclusion about the appropriateness of using this parameter in the corresponding range.

According to the criterion χ^2, the hypothesis H_0 is accepted if the following inequality is fulfilled

$$P(\chi^2_{n-1} - x_\alpha) < 1 - \alpha, \quad (7)$$

or it is equivalent to the inequality $\chi^2(n) < x_\alpha$. Otherwise, if the parameter $\chi^2(n) \ge x_\alpha$ or inequality in Equation (7) is not satisfied, the alternative hypothesis H_1 is accepted.

The experimental value of the parameter determined by Equation (6) is $\chi^2(n) = 7.55$.

According to the results of the calculations, it was found that the inequality $P(\chi^2_{n-1} - x_\alpha) < 1 - \alpha$, written in the form $\chi^2(n) < x_\alpha$, is fulfilled, since 7.55 < 19.7.

This means that the hypothesis H_0 is accepted. Therefore, the distribution function of this sample is normal.

The technical inspection of the brake equipment units of passenger cars, conducted in 2023, demonstrated that air distributors accounted for the largest share of malfunctions (27%). These results correlate with the interim findings of the study, according to which the failure rate of air distributors No. 292 depends on seasonal temperature fluctuations. In particular, there

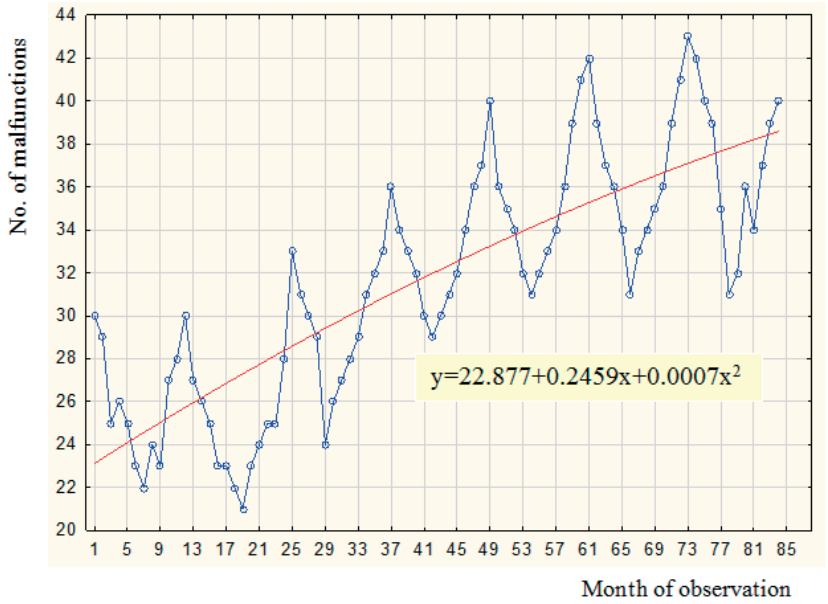

Figure 6 *Graphical distribution of malfunctions of air distributors No. 292 by month*

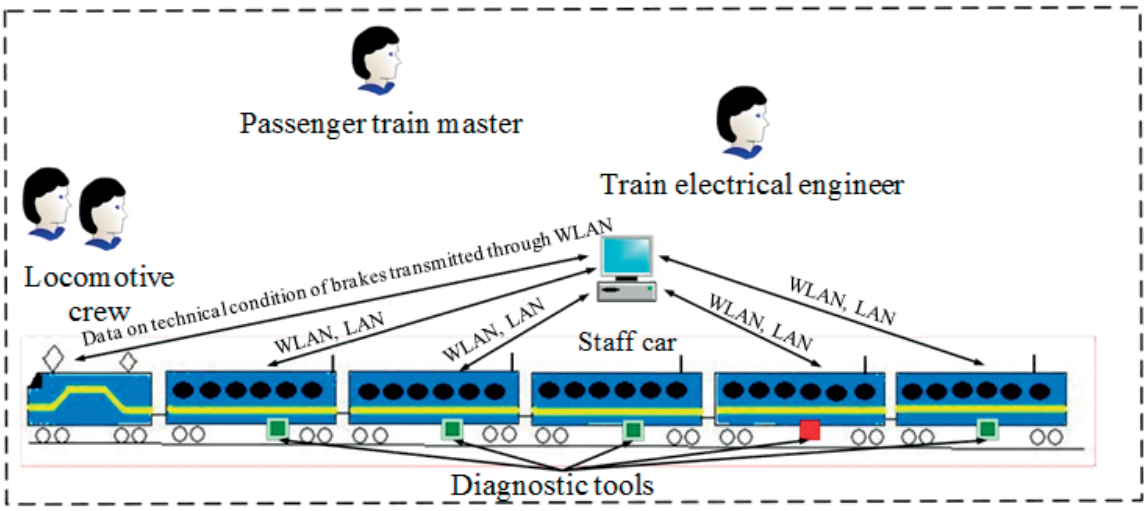

Figure 7 *The technical diagnostic system for the brake equipment of the passenger rolling stock*

is a significant increase in the number of malfunctions during the cold season (Figure 6) due to deteriorating operating conditions.

Low temperatures negatively affect the condition of air distributor components such as valves, bushings, spools, rubber cuffs and gaskets, thus causing their premature wear. The winter temperature conditions also cause a decrease in lubricant quality, destruction of valve seats and damage to other critical components, which increases the number of malfunctions in the brake system while the train is in motion. In addition, the breach of tightness in rubber cuffs and gaskets, as well as in valve seats, increases the risk of air leakage, which further degrades the performance of the brake system of passenger cars.

Based on the malfunction data and the analytical study of the operation of air distributors No. 292 under operating conditions, a number of negative factors affecting the performance of these elements were identified. They do not only cause unstable operation of the air distributors, but they do lead to increased operating costs, longer train travel times, and reduced traffic safety, as well [7, 23, 26].

It is critical to use the modern diagnostic tools to reduce the frequency of railway transport accidents caused by malfunctions in the braking equipment of passenger cars [28-29]. This would allow for timely detection and elimination of potential malfunctions in advance and, thus, ensure traffic safety.

The technical diagnostic system is based on the processes running in the brake equipment of the passenger rolling stock (Figure 7) [28].

They are also used for determining the operability of units. Diagnostic tools are used for building and analyzing mathematical models describing the operation of the brake system of a rail car. The reliable operation

of the diagnostic system would ensure the maintenance of the passenger train schedule.

The main criteria of an efficient diagnostic system are the reliability and efficiency of obtaining information on the technical condition of the brake equipment of passenger cars, the speed of processing and transmission of diagnostic information, the degree of autonomy and protection against natural and human-induced interference.

The structure of the brake system of a passenger car is characterized by quantitative parameters that represent different physical variables. Their values can be initial, permissible or boundary. During the operation structural parameters change; that leads to deterioration in the technical condition of brake equipment units of passenger cars.

The condition of the brake system a passenger train can be approximately estimated using direct and indirect characteristics (diagnostic parameters). They reflect the most probable defects associated with a decrease in performance and the occurrence of brake system malfunctions.

The requirements for the system of technical diagnostics of brake units of passenger cars are to approximate the maximum compliance with the controlled parameters. They should include the following stages:

- to determine the boundary values of the criteria by which malfunctions are graded;
- to determine the list of malfunctions of the brake system units of passenger cars that need to be diagnosed;
- to develop a diagnostic model to provide information on the degree of danger of the passenger car brake system units to be diagnosed, as well as information for maintenance personnel;
- to develop diagnostic software that, at the user interface level, should formalize the process of diagnosing the units of the passenger car brake system and provide its better functionality;
- to develop the necessary measuring devices for monitoring the brake system units of passenger cars and design a data collection system for them;
- to conduct testing and assess the reliability according to the list of malfunctions of passenger car brake system units, taking into account the statistical data on operation; and
- to develop the standard technical documents, programs and methods for diagnosing the brake system units of passenger cars, and operating documentation for diagnostic equipment.

4 Conclusions

1. A technical inspection of the brake systems of passenger cars under operating conditions was carried out; the collected statistical data were systematized. It has been established that the number of malfunctions of the main units of the brake system has decreased significantly in recent years due to has decreased significantly in recent years due to the fact that a significant number of passenger cars was decommissioned due to outdated technical conditions

A detailed analysis of the statistical data revealed that the main units of brake equipment have most of the faults. Air distributors No. 292 account for a significant number of malfunctions due to their unsatisfactory performance in operation, which is caused by the complexity of their design, strict maintenance requirements and the poor-quality repair carried out at car repair facilities. In particular, it was found that 21% of the malfunctions of air distributors No. 292 resulted from excessive brake cylinder filling time during the full-service braking, 19% was the result of excessive start-up time after full-service braking, and 15% were related to a slow increase in brake cylinder pressure in the Lap mode. These malfunctions have a significant impact on the brake system efficiency and train safety.

2. Mathematical statistical methods were used to determine the distribution of faults in air distributors No. 292 used in the brake system of passenger cars. The collected data on malfunctions were processed and systematized in STATISTIKA. The analysis showed that the distribution of malfunctions was described by a normal law.

It was found that the dynamics of changes in the malfunctions of the air distributor correlated with seasonal factors that affected their occurrence. The results of the calculations showed that χ^2=7.55. This suggests that the normal distribution of the data is adequate. The variance of malfunctions was defined as σ^2= 31.107; the arithmetic mean of the number of malfunctions was $\bar{x} = 31.655$. These results help better understand the impact of external factors on the reliability of brake systems and plan the measures for their optimization.

3. A technical diagnostic system for the brake equipment of passenger rolling stock has been proposed for improving the traffic safety. This system enables effective monitoring of key parameters of the braking system of passenger cars and controlling the air pressure in the brake line and pneumatic cylinder, which varies depending on the operating mode of the brake equipment. It will also monitor how often the pneumatic brakes are applied while the train is in motion.

The use of these diagnostic tool would accurately monitor the condition of equipment in real time, predict the service life of the equipment and optimize the overhaul periods based on the up-to-date data on the technical condition of the units. Such an approach can significantly improve the traffic safety and reduce the risk of rail accidents, thus ensuring the stable and reliable operation of the brake systems of passenger cars.

Acknowledgment

This publication was supported by the Cultural and Educational Grant Agency of the Ministry of Education of the Slovak Republic under the project KEGA 024ZU-4/2024: Deepening the knowledge of university students in the field of construction of means of transport by carrying out professional and scientific research activities in the field. It was also supported by the Slovak Research and Development Agency of the Ministry of Education, Science, Research and Sport under the project VEGA 1/0513/22: Investigation of the properties of railway brake components in simulated operating conditions on a flywheel brake stand. Funded by the EU NextGenerationEU under the Recovery and Resilience Plan for Slovakia under the project No. 09I03-03-V01-00131.

Conflicts of interest

The authors declare that they have no known competing financial interests or personal relationships that could have appeared to influence the work reported in this paper.

References

[1] DIZO, J., BLATNICKY, M., HARUSINEC, J., SUCHANEK, A. Assessment of dynamics of a rail vehicle in terms of running properties while moving on a real track model. *Symmetry* [online]. 2022, **14**(3), 536. ISSN 2073-8994. Available from: https://doi.org/10.3390/sym14030536

[2] SOUKUP, J., SKOCILAS, J., SKOCILASOVA, B., DIZO, J. Vertical vibration of two axle railway vehicle. *Procedia Enginering* [online]. 2017, **177**, p. 25-32. ISSN: 1877-7058. Available from: https://doi.org/10.1016/j.proeng.2017.02.178

[3] PANCHENKO, S., GERLICI, J., VATULIA, G., LOVSKA, A., RYBIN, A., KRAVCHENKO, O. Strength assessment of an improved design of a tank container under operating conditions. *Communication - Scientific Letters of the University of Zilina* [online]. 2023, **25**(3), p. B186-B193. ISSN 1335-4205, eISSN 2585-7878. Available from: https://doi.org/10.26552/com.C.2023.047

[4] DIZO, J., BLATNICKY, M. Evaluation of vibrational properties of a three-wheeled vehicle in terms of comfort. *Manufacturing Technology* [online]. 2019, **19**(2), p. 197-203. ISSN 1213-2489, eISSN 2787-9402. Available from: https://doi.org/10.21062/ujep/269.2019/a/1213-2489/mt/19/2/197

[5] VATULIA, G., LOVSKA, A., PAVLIUCHENKOV, M., NERUBATSKYI, V., OKOROKOV, A., HORDIIENKO, D., VERNIGORA, R., ZHURAVEL, I. Determining patterns of vertical load on the prototype of a removable module for long-size cargoes. *Eastern-European Journal of Enterprise Technologies* [online]. 2022., **6/7**(120), p. 21-29. Available from: https://doi.org/10.15587/1729-4061.2022.266855

[6] GERLICI, J., LOVSKA, A., PAVLIUCHENKOV, M. Study of the dynamics and strength of the detachable module for long cargoes under asymmetric loading diagrams. *Applied Sciences* [online]. 2024, **14**, 3211. eISSN 2076-3417. Available from: https://doi.org/10.3390/app14083211

[7] RAVLYUK, V. G. Determining the technical condition of rolling stock bushings by means of vibration diagnostics. *Eastern European Journal of Advanced Technologies* [online]. 2015, **2/7**(74), p. 11-15. ISSN 1729-3774, eISSN 1729-4061. Available from: https://doi.org/10.15587/1729-4061.2015.39036

[8] Analysis of the state of train traffic safety on the railways of Ukraine for 2022 - Joint-stock company "Ukrainian railway", Department of traffic safety [online]. 2022. Available from: https://old.dsbt.gov.ua/sites/default/files/imce/Bezpeka_DTP/2023/analiz_avariynosti_2022_1.pdf

[9] Brake failures have been a problem for trains - since the 1880s - Bangor Daily News [online]. 2013. Available from: https://www.bangordailynews.com/2013/07/11/news/brake-failures-have-been-a-problem-for-trains-since-the-1880s/

[10] GUNA, Y. M., KORKMAZ, M. E., OZMEN, R. An investigation on braking systems used in railway vehicles. *Engineering Science and Technology, an International Journal* [online]. 2020, **23**(2)**,** p. 421-431. eISSN 2215-0986. Available from: https://www.researchgate.net/publication/339036207_An_investigation_on_braking_systems_used_in_railway_vehicles

[11] SHARMA, R. CH., DHINGRA, M., PATHAK, R. K. Braking systems in railway vehicles. *International Journal of Engineering Research and Technology (IJERT)* [online]. 2015, **4**(01), p. 206-211. ISSN 2278-0181. Available from: https://www.ijert.org/research/braking-systems-in-railway-vehicles-IJERTV4IS010360.pdf

[12] GORBUNOV, M. I., GERLITSY, Y., KRAVCHENKO, K. O., LAK, T., PROSVIROVA, O. V. Evaluation of methods of improving the operational characteristics of railway braking systems. *Bulletin of the Volodymyr Dahl East Ukrainian National University*. 2017, **4**(234), p. 81-85. ISSN 1998-7927.

[13] PUGI, L., PALAZZOLO, A., FIORAVANTI, D. Simulation of railway brake plants: an application to SAADKMS freight wagons. *Proceedings of the Institution of Mechanical Engineers, Part F: Journal of Rail*

and Rapid Transit [online]. 2008, **222**(4), p. 321-329. ISSN 0954-4097, eISSN 2041-3017. Available from: https://doi.org/10.1243/09544097JRRT118

[14] ETWELL, M. W. J. Advances in rail wagon design. *Proceedings of the Institution of Mechanical Engineers, Part F: Journal of Rail and Rapid Transit* [online]. 1990, **204**(1), p. 45-54. ISSN 0954-4097, eISSN 2041-3017. Available from: https://doi.org/10.1243/PIME_PROC_1990_204_185_02

[15] WU, Q., COLE, C., SPIRYAGIN, M., WANG, Y., MA, W., WEI, C. Railway air brake model and parallel computing scheme. *Journal of Computational and Nonlinear Dynamics* [online]. 2017, **12**(5), 051017. ISSN 1555-1415, eISSN 1555-1423 Available from: https://doi.org/10.1115/1.4036421

[16] WANG, Q., GAO, T., TANG, H., WANG, Y., CHEN, Z., WANG, J., WANG, P., HE, Q. A feature engineering framework for online fault diagnosis of freight train air brakes. *Measurement* [online]. 2021, **182**, 109672. ISSN 0263-2241, eISSN 1873-412X. Available from: https://doi.org/10.1016/j.measurement.2021.109672

[17] JIANG, F., LI, K., WU, H., LUO, S. Freight train air brake modelling with emergency valves. *Advances in Mechanical Engineering* [online]. 2024, **16**(4), p. 1-9. ISSN 0954-4097, eISSN 2041-3017. Available from: https://doi.org/10.1177/16878132241242953

[18] BABAEV, A. M., DMYTRIEV, D. V. *The principle of action, calculations and basics of operation of railway rolling stock brakes* (in Ukrainian). Kyiv: DETUT, 2007. ISBN 978-966-2197-03-7.

[19] Instructions for the repair of brake equipment of wagons: CV-CL-0013. 2004.

[20] Instructions for the use of rolling stock brakes on the railways of Ukraine: CT-CV-CL-0015. 2004.

[21] Freight cars. Maintenance and repair system according to technical condition: STP 04 - 010:2018. 2018.

[22] Rules of technical operation of railways of Ukraine. 2002.

[23] PANCHENKO, S., LOVSKA, A., RAVLYUK, V., BABENKO, A., DEREVYANCHUK, O., ZHAROVA, O., DEREVIANCHUK, Y. Detecting the influence of uneven loading of the brake shoe in a freight car bogie on its strength. *Eastern-European Journal of Enterprise Technologies* [online]. 2023, **5**(7(125)), p. 6-13. ISSN 1729-3774, eISSN 1729-4061. Available from: https://doi.org/10.15587/1729-4061.2023.287791

[24] KYRYLENKO O. P., PYSMENNYI V. V. Fundamentals of scientific research in diagrams and tables. 2013. ISBN 978-966-654-328-1.

[25] SLIUSARCHUK, Y. M., KHROMIAK, Y. Y., DZHAVALA, L. L., TSYMBAL, V. M. Probability theory, mathematical statistics and probabilistic processes. 2015. ISBN 978-617-607-775-6.

[26] PANCHENKO, S., GERLICI, J., LOVSKA, A., RAVLYUK, V. The service life prediction for brake pads of freight wagons. *Communications. Scientific Letters of the University of Zilina* [online]. 2024, **26**(2), p. B80-B89. ISSN 1335-4205, eISSN 2585-7878. Available from: https://doi.org/10.26552/com.C.2024.017

[27] GERYCH, M. S., SINYAVSKA, O. O. Mathematical statistics [online]. 2021. Available from: https://dspace.uzhnu.edu.ua/jspui/handle/lib/34910

[28] RAVLUYK, V., DEREVIANCHUK, I., AFANASENKO, I., RAVLUYK, N. Development of electronic diagnostic system for improving the diagnosis reliability of passenger car brakes. *Eastern-European Journal of Enterprise Technologies* [online]. 2016, **2**(9(80)), p. 35-41. ISSN 1729-3774, eISSN 1729-4061. Available from: https://doi.org/10.15587/1729-4061.2016.66007

[29] KUMBHAR, S. G., SUDHAGAR, P. E. Fault diagnostics of roller bearings using dimension theory. *Journal of Nondestructive Evaluation, Diagnostics and Prognostics of Engineering Systems* [online]. 2021, **4**(1), 011001. ISSN 2572-3901, eISSN 2572-3898. Available from: https://doi.org/10.1115/1.4047102

INFLUENCE OF LASER ABLATION TREATMENT ON ELECTROCHEMICAL CHARACTERISTICS OF AZ80 MAGNESIUM ALLOY

Daniel Kajánek[1,*], Luboš Halimovič[1], Martina Jacková[1], Leoš Doskočil[2], Ingrid Zuziaková[1], Branislav Hadzima[1]

[1]Research Centre, University of Zilina, Zilina, Slovak Republic
[2]Materials Research Centre, Faculty of Chemistry, Brno University of Technology, Brno, Czech Republic

*E-mail of corresponding author: daniel.kajanek@uniza.sk

Daniel Kajánek 0000-0002-5005-8740,
Leoš Doskočil 0000-0002-9584-9191,
Martina Jacková 0000-0003-1625-6847,
Branislav Hadzima 0000-0002-8201-905X

Resume

In this study was investigated the effect of a novel surface treatment technique, called laser ablation or laser surface cleaning (LSC), on the electrochemical properties of AZ80 magnesium alloys. Its effect on corrosion resistance was compared to conventional techniques represented by grinding and polishing. The corrosion stability of the produced surfaces was determined by potentiodynamic (PD) polarization tests and electrochemical impedance spectroscopy in 0.1M NaCl. The results showed that the LSC process produced a regular, uniform surface morphology. Although the LSC treatment led to the passivation of the AZ80 surface, the overall corrosion resistance was compromised compared to surfaces treated by grinding and polishing.

Article info

Received 27 February 2025
Accepted 14 April 2025
Online 30 April 2025

Keywords:

magnesium alloy
corrosion
laser ablation
laser surface cleaning

Available online: https://doi.org/10.26552/com.C.2025.039

ISSN 1335-4205 (print version)
ISSN 2585-7878 (online version)

1 Introduction

Magnesium is one of the most abundant elements on earth, which led to the idea of using magnesium as an engineering metal [1-2]. However, the mechanical properties of magnesium are not very favourable due to its hexagonal lattice [3]. The main advantage of using magnesium as an engineering material is its low density, which is 1.74 g.cm^{-3}. Other positive properties of magnesium are its ratio of tensile strength to density (specific strength) and its non-toxicity, which allows it to be used as a biodegradable implant [4-6]. Magnesium alloys, due to their low density, can reduce the weight of a vehicle, which in turn lowers fuel consumption. This can be achieved by replacement of commonly used materials such as steels. Using of magnesium alloys can subsequently have a positive impact on greenhouse gas emissions. Currently, components made of magnesium alloys, such as engine blocks, central control panels, door frames, steering wheels, etc., are already in use. However, most of these components can be found only in high-end cars like Porsche or Jaguar due to higher economical demands [4].

Despite its promising properties, magnesium and therefore its alloys have a major disadvantage represented by their high electrochemical reactivity in most practical environments [7-8]. This behaviour is mainly indicated by the low standard electrode potential of magnesium (-2.36 vs. SHE). This is the lowest value of the commonly used metals, with the exception of lithium. Another problem with the corrosion resistance of magnesium is the non-protective surface film formed when exposed to the environment. This quasi-passive film is only protective in highly alkaline environments. To overcome this problem, extensive efforts are being made to improve the corrosion resistance of magnesium alloys. One of the ways to improve the corrosion resistance is to alloy magnesium with corrosion resistant materials. However, alloying magnesium with other metals is often unfavourable due to the occurrence of microgalvanic corrosion leading to dissolution of the Mg matrix [8-9]. The more favourable and effective approach is to apply a proper surface treatment. Grinding, polishing or milling and turning are typical representatives of the category of conventional surface treatment methods [10-12]. On the other hand, there are unconventional surface treatment methods whose influence is still the subject of research by many scientific teams. This

category is represented by various coating processes, such as plasma-electrolytic oxidation, chemical vapour deposition (CVD) and physical vapour depositions (PVD) methods, treatments based on the application of laser beams, etc. [13-18].

Laser surface cleaning (LSC), commonly known as laser ablation, is one of the unconventional and novel laser-based surface modification methods for metallic materials. The main difference between LSC and laser surface melting (LSM) is the careful selection of processing parameters to avoid melting of the surface layer [16-18]. The LSC is a non-contact technique that aims to clean and decontaminate the surface from impurities by carefully setting up the laser beam. During the LSC treatment, the concentrated laser beam is generated by the power supply. When the treated surface is hit by the laser beam, energy absorption begins. The removal of impurities or other layers depends on the ability of the surface layer to absorb the energy transferred by the laser beam. In practice, the higher the ability of the surface to absorb energy, the higher the efficiency of the removal process [19]. This method is used when a clear, oxide-free surface is required. The positive effect on surface properties is reported on metallic materials, such as various types of steel, titanium alloys, aluminium alloys, etc. One of the most important advantages of LSC compared to common chemical cleaning of metals is the high environmental friendliness of the whole process [15-16]. Studies on the effect of the LSC on the corrosion resistance of materials have confirmed that in the case of stainless steels or aluminium alloys, e.g. materials that can be passivated, the LSC method proved to be beneficial in improving the corrosion resistance in aggressive environments [20-21]. On the other hand, the application of this method to materials with low melting points, such as zinc, did not have a positive effect on corrosion stability. The researchers stated that the zinc was melted before the oxides were successfully removed [22]. Few studies can be found on the LSC treatment of magnesium alloys. For example, the study by Zhu et al., 2024 dealt with the application of laser cleaning as a pre-treatment to the micro-arc oxidation (MAO) coatings. Although the authors found a positive effect on the corrosion resistance of AZ31 alloy, only a 20 W laser treatment without coating was tested for a short exposure time of 30 minutes [23]. In contrast to this study, Xiong et al., 2024 found that the application of 6.5 W laser treatment had a negative effect on short-term corrosion resistance [24].

There is an evident lack of knowledge about the impact of the LSC on the electrochemical characteristics of magnesium alloys mainly during prolonged exposure periods. Moreover, presented studies used low-powered laser cleaning and reached conclusions opposite to each other. The purpose and novelty of this study are provided by the evaluation of the LSC impact performed using a 100 W power source on corrosion resistance of AZ80 magnesium alloy during the prolonged exposure period in an aggressive chloride environment.

2 Experimental material and methods

The AZ80 magnesium alloy was produced by continuous casting using a heated mould. The chemical composition of AZ80Mg alloy (Table 1) was obtained by EDXRF analysis using ARL QUANT'X EDXRF spectrometer. To observe the microstructure of AZ80, the samples were ground by the SiC papers up to p4000 and polished by polishing cloth using 3 μm and 1 μm polishing emulsions composed of diamond suspension

Table 1 *Chemical composition of AZ31 magnesium alloy obtained by EDXRF analysis*

Component	Al	Zn	Mn	Mg
wt. %	8.99	0.45	0.24	balance

Figure 1 *Pulse laser P-laser, model QFC-100*

and isopropyl alcohol. The samples were then etched for 5 seconds with an etchant consisting of picric acid, acetic acid and ethanol [25]. Microstructural analysis was performed using a Zeiss Axio Imager.A1 optical microscope and corresponding software.

The laser surface cleaning (LSC) treatment was performed using a pulse laser P-laser machine, model QFC-100 (Figure 1). The working distance during the treatment was set at 320 mm. The pulse frequency was 60 Hz and the laser power was 100 W. The pulse duration was 180 ns and the pulse wavelength was λ = 1064 nm. The LSC was applied to the surface for a period of 120 seconds. Each specimen was polished prior to the LSC treatment using the above-mentioned procedure for metallographic analysis to ensure a homogeneous surface before the treatment.

The Alicona InfiniteFocus G5 measuring system was used to evaluate the effect of the LSC treatment and other investigated techniques on morphology and surface roughness. Surface scanning of treated samples was performed within an area of 5 x 5 mm at 10x magnification. The cross-sectional morphology of the treated surfaces was observed using the Zeiss Axio Imager.A1. Moreover, wettability testing was performed using SITA SurfaSpector device.

The electrochemical characteristics of the studied samples were determined by potentiodynamic polarisation (PD) and electrochemical impedance spectroscopy (EIS) using a VSP Biologic VSP 300 laboratory potentiostat, accompanied by EC Lab V11.50 software. Both PD and EIS tests were performed in 0.1 M NaCl solution at the laboratory temperature of 22 ± 2 °C. During the exposures, the samples were stored in corrosion cells as shown in Figure 2. A three-electrode system was used, with the sample acting as the working electrode, the Pt electrode as the auxiliary electrode and the saturated calomel electrode as the reference electrode (+0.2446 V vs. SHE). The PD measurements were started after 10 min of open circuit potential (OCP) stabilisation. In the case of the EIS measurements, the polarisation resistance measurements were made after different OCP stabilization times: 1 h, 2 h, 4 h, 8 h, 12 h, and 24 h in order to observe the electrochemical behaviour during the prolonged exposures.

During the PD tests, samples were polarised in the range -200 mV to +500 mV vs. OCP at a polarisation step rate of 1 $mV.s^{-1}$. The Tafel analysis of the measured PD curves was used to obtain values of corrosion potential (E_{corr}), corrosion current density (i_{corr}), cathodic and anodic coefficients (βc, βa). Corrosion rate values (r_{corr}) were calculated using proper software.

The measured frequencies during the EIS were in the range of 100 kHz to 10 mHz. The amplitude of the applied signal was set at 5 mV with the mean value identical to the OCP value after each exposure period. The measured electrochemical data were plotted as Nyquist plots. These plots were analysed by the equivalent circuit method using two types of equivalent circuit. The first circuit (Figure 3 left) was used to evaluate a simple Nyquist plot with one capacitive loop. The second circuit (Figure 3 right) determined the electrical parameters of the Nyquist diagrams consisting of two capacitive loops. These circuits are used to simulate surface conditions during exposure [16]. The R_{Ω}

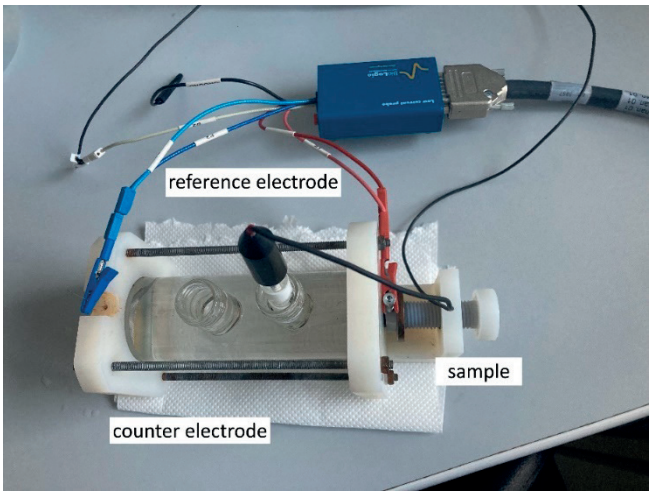

Figure 2 *Corrosion cell*

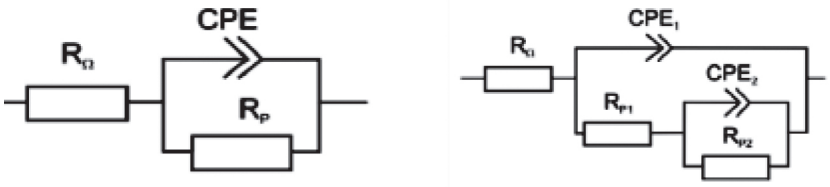

Figure 3 *Equivalent circuits for analysis of Nyquist diagrams with one capacitance loop (left) and two capacitance loops (right)*

component in the circuits is the resistance of the solution and the R_P component determines the polarisation resistance of the surface. Note that the higher the R_P value of the surface, the higher the corrosion resistance. Therefore, this study is mainly oriented to evaluate the corrosion resistance based on the evolution of R_p values during the exposure period. The constant phase element (CPE) represents a heterogeneity of the working electrode (sample) surface. In the case where the Nyquist plot is composed of two capacitance loops, the total polarization resistance is given as the sum of the partial resistances R_{p1} and R_{p2} [26-28].

3 Results and discussion

The microstructure (Figure 4) of the magnesium alloy AZ80 is formed by dendrites of the α-phase. Intermetallic phases were identified based on literature review [26, 29]. The intermetallic phase $Mg_{17}Al_{12}$ is present at the boundaries of dendrites and in interdendritic spaces. The α-phase is a solid solution of aluminium, zinc and manganese in magnesium. An Al_6Mn intermetallic is also present due to the low solubility of manganese in Mg.

The variation of the Sa parameter (arithmetic mean height of the surface) was chosen to determine the roughness after the surface treatments [30]. Table 2 shows that the roughness gradually increased from polished to ground to LSC surface. Note that the roughness values of the polished and ground surfaces were in the same order of magnitude. The roughness value of the surface treated by the LSC method was significantly higher than those of the conventional surface treatments. The LSC surface achieved almost 4 times higher value compared to the polished counterpart.

Figure 5 shows that the polished surface has a typical appearance of a surface treated by mechanical polishing, i.e., it is flat with a low number of heterogeneities such as scratches and pits (Figure $5a_1$). On the ground surface, linear scratches can be seen in the direction of grinding, especially on the top surface view (Figure $5b_1$). The surface roughness was visibly increased compared to polishing, which is well documented in Figure $5b_2$ as well. The appearance of the surfaces treated by LSC is different with respect to those treated by previous methods. When looking at the surface from above (Figure $5c_1$), it is clear that it is directed and regular, corresponding to a pulse laser beam impact applied to the material. Table 2 also shows that as the surface roughness increases, so does the wettability represented by the lower water contact angle values.

The cross sections (Figure 5) show that the surface after the LSC application has not undergone significant melting, as is usually the case with other laser surface treatments such as laser surface melting of magnesium alloys [14]. Therefore, the microstructural appearance of the base material is not visibly affected by this process. On the other hand, the surface is much more heterogeneous compared to the polished and ground counterparts. In addition, the thick porous oxide layer is visible on the surface (Figure $5c_2$) after the LSC application. The oxides formed were heterogeneous and are probably products of the increased reactivity of magnesium with atmospheric oxygen. This is a direct result of the increased temperature of the magnesium base material during the laser treatment.

Potentiodynamic polarisation curves are shown in Figure 6. The electrochemical characteristics were obtained by table analysis of the PD plots (Table 3). Potentiodynamic polarisation curves clearly show that surface roughness and wettability play an important role

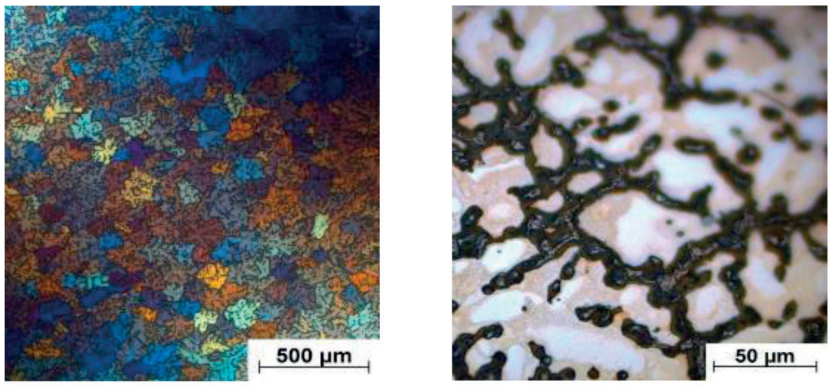

Figure 4 *Microstructure of AZ80 alloy: overview (left) and detail (right)*

Table 2 *Values of the surface roughness and water contact angle of treated samples*

Treatment method	S_a	Contact angle θ, °
Grinding	598.88 nm	52.5 ± 2.6
Polishing	156.49 nm	93.1 ± 1.3
LSC	11.52 µm	42.1 ± 8.8

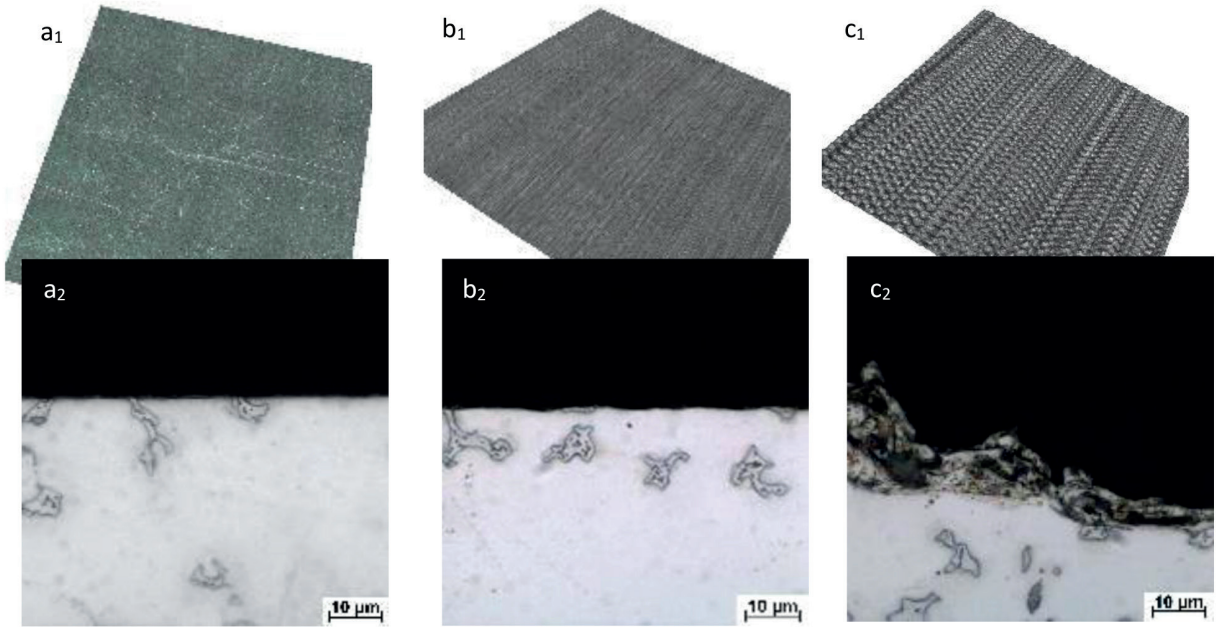

Figure 5 *Surface view (subscript 1) and cross sections (subscript 2)*
a - polishing, b - grinding, c - LSC

Table 3 *Electrochemical characteristics obtained by PD of treated surfaces of AZ80 alloy in 0.1M NaCl*

Treatment method	E_{corr} (mV)	i_{corr} (µA/cm²)	β_a (mV/dec.)	β_c (mV/dec.)	r_{corr} (mm/year)
Grinding	-1525 ± 13	8 ± 1	57 ± 13	157 ± 6	0.19 ± 0.02
Polishing	-1509 ± 19	7 ± 1	128 ± 19	153 ± 1	0.16 ± 0.01
LSC	-1568 ± 3	13 ± 1	82 ± 6	139 ± 4	0.29 ± 0.03

in the corrosion behaviour [7, 30]. The surface treated by the LSC method showed the lowest values of corrosion potential (E_{corr}), indicating the lowest thermodynamic stability of the surface. The most thermodynamically stable surface was the one treated by polishing. In terms of corrosion current density (i_{corr}) and corrosion rate (r_{corr}), the LSC treated samples reached the highest values of these electrochemical characteristics. Note that these characteristics represent corrosion kinetics in such a way that the higher these values are, the more intense the corrosion degradation is [31]. On the other hand, the i_{corr} and r_{corr} for polished and ground surfaces were not significantly different. The main reason for the reduced corrosion resistance of the LSC samples is the presence of the increased electrochemically active area in contact with aggressive environment confirmed by roughness measurement (Table 2). In addition, the porous and non-compact oxide layer formed on the surface (Figure $5c_2$) does not provide a sufficient barrier effect. The effect of surface roughness on the corrosion resistance has been investigated by several authors [7, 30]. In the first case, Reddy et al., 2021 investigated the effect of milling feed rate on roughness and corrosion behaviour of magnesium alloy. The authors found that an increase in surface roughness promoted corrosion degradation [7]. In a second study, the authors demonstrated that decreasing the surface roughness led to the more noble values of corrosion potential [30]. The Figure 6 shows that the potentiodynamic curves for polished and lasered surfaces are of similar shape, which means that the surface reacts similarly to polarisation. However, the values of E_{corr} are different. In accordance with the above-mentioned study of Walter et al., 2011 [30], the rougher surface after LSC resulted in more negative values of E_{corr}, meaning worse thermodynamic stability. It can be assumed that the surface film containing oxides (MgO), hydroxides ($Mg(OH)_2$ and $MgCl_2$ was formed on all tested surfaces during exposure to 0.1M NaCl solution [1, 13]. The factor that made the difference between the samples is the initial roughness of the surface on which this film is formed. The rougher the surface, the more difficult it is to form a compact homogeneous surface film. This phenomenon contributed to the higher corrosion resistance of the polished surface [7, 30, 32].

Another factor to consider when talking about corrosion resistance is the surface wettability. Table 2 shows that high roughness values are associated with increased surface wettability. It can be seen that as the roughness increases the water contact angle decreases. It can be seen that this fact results in an enhanced retention of a water/electrolyte drop on the surface and such surface conditions are favourable for corrosion initiation [1-2, 7, 33].

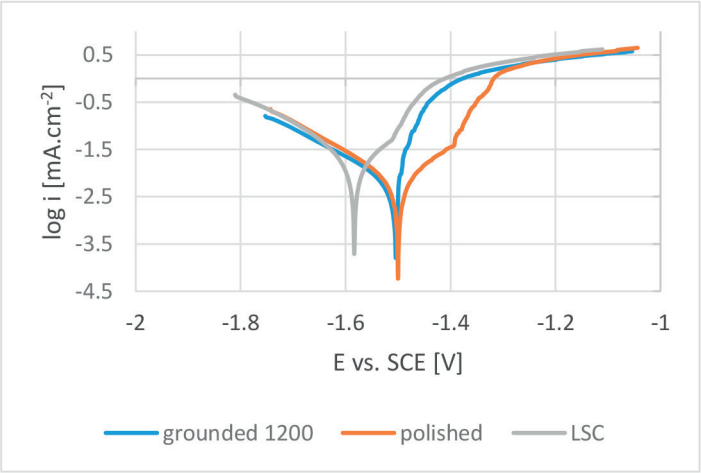

Figure 6 *Representative potentiodynamic polarization curves of treated surfaces of AZ80 alloy tested in 0.1M NaCl solution*

Table 4 *Polarization resistance of treated surfaces of AZ80 alloy in 0.1M NaCl*

Treated method	R_p (Ω.cm²)					
	1 h	2 h	4 h	8 h	12 h	24 h
Grounded	3817	3410	2577	2268	2210	1769
Polished	13770	9376	9070	7544	7191	6961
LSC	655	671	650	740	682	549

For the EIS test, a prolonged exposure of up to 24 hours was set to observe the corrosion behaviour of the treated surfaces in an aggressive corrosive environment represented by 0.1M NaCl. The R_p values (Table 4), obtained by equivalent circuit analysis of the Nyquist plots (Figure 7), describe the electrochemical stability of the surface, as these values are directly proportional to the corrosion resistance of the corresponding surface. The Nyquist plots show that only the polished surface is represented by the two capacitance loops, corresponding to the formation of a more compact oxide/hydroxide surface layer compared to ground and LSC samples. These oxides formed a film that suppressed the corrosion process in the first hour of exposure (Table 4). However, such surface film did not play a significant role in the overall corrosion resistance. This oxide/hydroxide film is not able to slow down the corrosion process as these substances are only stable in alkaline environments [1, 12, 30].

It is clear that after the first hour of exposure, the most resistant surface was the polished surface and the lowest corrosion resistance was measured in the case of the LSC treated surface. This result is in good agreement with the presented results of the PD tests (Figure 6, Table 2). On the other hand, the LSC treated surface was the only one to show an increase of the R_P during the prolonged exposure. This improvement in corrosion resistance over time can be explained by the local sealing of the porous oxidic film formed during the laser treatment (Figure $5c_2$) by the products of the corrosion reactions. The maximum R_P was obtained after 8 hours of exposure, followed by a continuous decrease in corrosion resistance due to the instability of the porous layer of corrosion products mentioned above. In contrast, the polished and ground samples showed a decrease in corrosion resistance throughout the exposure period, indicating continuous corrosion degradation. Note that the two conventional treatments reached higher corrosion resistance compared to LSC, with the polished surface showing the highest electrochemical stability throughout the exposure.

Based on the principle of the LSC method, it can be assumed that the lasered surface layer exhibited increased internal energy leading to a promoted surface reactivity. Consequently, the creation of oxides/hydroxides by reaction with the surrounding atmosphere leading to the formation of surface film and corrosion products during exposure, was catalysed. Sealing of the oxide/hydroxide surface film happened more easily on heterogeneous surface due to the presence of capillaries and irregularities within the original surface film on the LSC surface (Figure $5c_2$) [1, 13, 34]. Similarly, to the previous case, the created film and products of corrosion reactions are not protective in neutral pH environment for longer period and will naturally deteriorate, which is demonstrated by decreasing trend of the R_p values after 12 h of exposure [1]. The obtained LSC results can be compared to another unconventional method of surface treatment such as shot peening. Although this method works on different principles, the resulting surface is similar when speaking about heterogeneity of surface and corrosion behaviour. Comparably to the LSC, the oxide film is formed on the surface during the shot peening treatment. Internal energy of the surface is

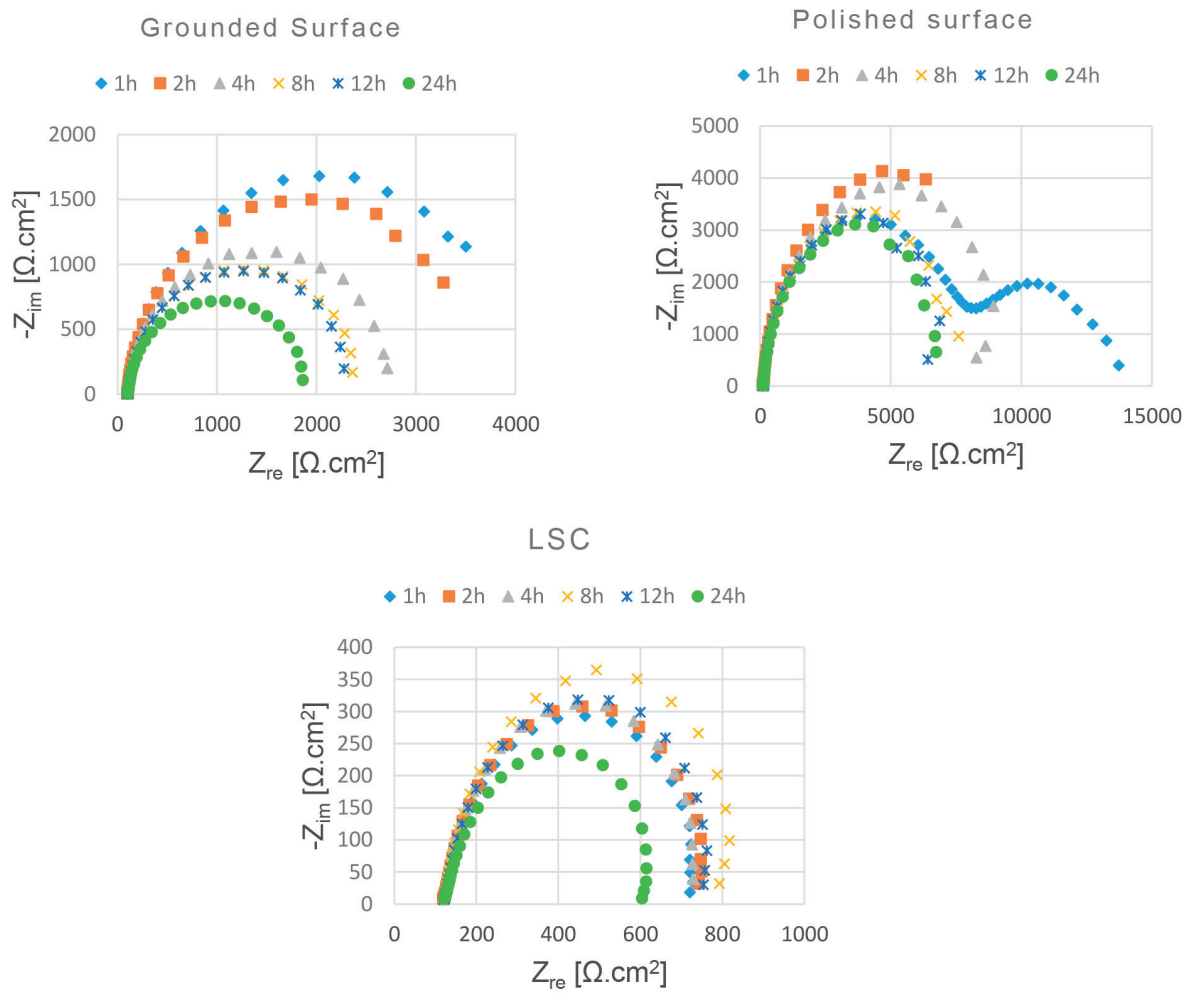

Figure 7 *Nyquist diagrams of treated surfaces of AZ80 alloy tested in 0.1M NaCl*

amplified by the intensive plastic deformation resulting in promoted oxidation of substrate and decreased corrosion resistance [30-31, 35].

Although the LSC method at selected parameters did not improve the corrosion resistance of the AZ80 magnesium alloy in the desired way, there is considerable scope for developing this method in terms of its optimization. The modification of the ablation process is possible on multiple levels - adjusting the device's power, defocusing the laser beam to achieve lower beam intensity to achieve more uniform 100% coverage with lower roughness. On the other hand, obtained results can be exploited for further research connected with coatings as the rough and reactive surface provides suitable thermodynamic conditions for the formation of oxide protective layers such as plasma electrolytic oxidation or anodization [13].

4 Conclusions

The performed experiments were designed to compare conventional and unconventional surface treatment methods. The following conclusions were drawn from the obtained results:

The highest roughness and promoted wettability were obtained by the LCS treated surface. Microscopic observations revealed that the LSC surface showed an oxidised heterogeneous layer after the treatment.

Potentiodynamic polarization experiments confirmed the relationship between the surface roughness, wettability and corrosion resistance. The lowest corrosion resistance was measured on the LSC treated surface; the highest corrosion resistance was recorded on the polished surface.

Electrochemical impedance spectroscopy experiments confirmed the results of the PD tests. After the first hour of exposure, the difference between the LSC surface and the polished surface was significant. The EIS tests also showed that the LSC surface exposed to an NaCl solution underwent passivation leading to an increase of the R_p up to 8 hours of exposure. However, the highest R_p values during the exposure period were obtained from the polished surface. The LSC surface showed the lowest corrosion resistance after 24 hours of exposure.

Acknowledgement

The research was funded by the EU NextGenerationEU through the Recovery and Resilience Plan for Slovakia under the project No. 09I03-03-V03-00036.

Conflicts of interest

The authors declare that they have no known competing financial interests or personal relationships that could have appeared to influence the work reported in this paper.

References

[1] SONG, G. L. *Corrosion of magnesium alloys*. 1. ed. Philadelphia: Woodhead Publishing, 2011. ISBN 978-1-84569-708-2.

[2] JIANG, J., GENG, X., ZHANG, X. Stress corrosion cracking of magnesium alloys: a review. *Journal of Magnesium and Alloys* [online]. 2023, **11**(6), p. 1906-1930. eISSN 2213-9567. Available from: https://doi.org/10.1016/j.jma.2023.05.011

[3] SANDLOBES, S., FRIAK, M., KORTE-KERZEL, S., PEI, Z., NEUGEBAUER, J., RAABE, D. A rare-earth free magnesium alloy with improved intrinsic ductility. *Scientific Reports* [online]. 2017, **7**, 10458. eISSN 2045-2322. Available from: https://doi.org/10.1038/s41598-017-10384-0

[4] LIU, B., YANG, J., ZHANG, X., YANG, Q., ZHANG, J., LI, X. Development and application of magnesium alloy parts for automotive OEMs: a review. *Journal of Magnesium and Alloys* [online]. 2022, **11**(1), p. 15-47. eISSN 2213-9567. Available from: https://doi.org/10.1016/j.jma.2022.12.015

[5] WHITE, L., KOO, Y., YUN, Y., SANKAR, J. TiO2 deposition on az31 magnesium alloy using plasma electrolytic oxidation. *Journal of Nanomaterials* [online]. 2013, **2013**, 19437. ISSN 1687-4110, eISSN 1687-4129. Available from: https://doi.org/10.1155/2013/319437

[6] DING, Y., WEN, C., HODGSON, P., LI, Y. Effects of alloying on corrosion behavior and biocompatibility of biodegradable magnesium alloys: a review. *Journal of Materials and Chemistry B* [online]. 2014, **2**, p. 1912-1933. ISSN 2050-750X, eISSN 2050-7518. Available from: https://doi.org/10.1039/C3TB21746A

[7] REDDY, U., DUBEY, D., PANDA, S. S., IREDDY, N., JAIN, J., MONDAL, K., SINGH, S. S. Effect of surface roughness induced by milling operation on the corrosion behavior of magnesium alloys. *Journal of Materials Engineering and Performance* [online]. 2021, **30**, p. 7354-7364. ISSN 1059-9495, eISSN 1544-1024. Available from: https://doi.org/10.1007/s11665-021-05933-8

[8] ATRENS, A., SONG, G.-L., LIU, M., SHI, Z., CAO, F., DARGUSH, M. S. Review of recent developments in the field of magnesium corrosion. *Advanced Engineering Materials* [online]. 2015, **17**(4), p. 400-453. ISSN 1438-1656, eISSN 1527-2648. Available from: https://doi.org/10.1002/adem.201400434

[9] FINTOVA, S., DRABIKOVA, J., PASTOREK, F., TKACZ, J., KUBENA, I., TRSKO, L., HADZIMA, B., MINDA, J., DOLEZAL, P., WASSERBAUER, J., PTACEK, P. Improvement of electrochemical corrosion characteristics of AZ61 magnesium alloy with unconventional fluoride conversion coatings. *Surface and Coatings Technology* [online]. 2019, **357**, p. 638-650. ISSN 0257-8972, eISSN 1879-3347. Available from: https://doi.org/10.1016/j.surfcoat.2018.10.038

[10] YOUSSEF, H., EL-HOFY, H. *Traditional machining technology* [online]. Boca Raton: CRC Press, 2020. ISBN 9781003055303. Available from: https://doi.org/10.1201/9781003055303

[11] CZAN, A., JOCH, R., SAJGALIK, M., HOLUBJAK, J., HORAK, A., TIMKO, P., VALICEK, J., KUSNEROVA, M., HARNICAROVA, M. Experimental study and verification of new monolithic rotary cutting tool for an active driven rotation machining. *Materials* [online]. 2022, **15**, 1630. eISSN 1996-1944. Available from: https://doi.org/10.3390/ma15051630

[12] VICEN, M., BOKUVKA, O., SKOVAJSA, M., NOVY, F., FLORKOVA, Z. Energy-efficient application of CrN coating on low-alloy tool steel: comparative analysis of technological processes. *Production Engineering Archives* [online]. 2024, **30**(3), p. 406-412. ISSN 2353-5156, eISSN 2353-7779. Available from: https://doi.org/10.30657/pea.2024.30.39

[13] KAJANEK, D., PASTOREK, F., HADZIMA, B., BAGHERIFARD, S., JAMBOR, M., BELANY, P., MINARIK, P. Impact of shot peening on corrosion performance of AZ31 magnesium alloy coated by PEO: comparison with conventional surface pre-treatments. *Surface and Coatings Technology* [online]. 2022, **446**, 128773. ISSN 0257-8972, eISSN 1879-3347. Available from: https://doi.org/10.1016/j.surfcoat.2022.128773

[14] HU, R., ZHANG, S., BU, J.-F., LIN, CH.-J., SONG, G.-L. Recent progress in corrosion protection of magnesium alloys by organic coatings. *Progress in Organic Coatings* [online]. 2012, **73**(2-3), p. 123-141. ISSN 0300-9440, eISSN 1873-331X. Available from: https://doi.org/10.1016/j.porgcoat.2011.10.011

[15] ZHANG, F. D., LIU, H., SUBKA, C., LIU, Y. X., LIU, Y., GUO, W., CHENG, Y. M., ZHANG, S. L., LI, L. Corrosion behaviour of laser-cleaned AA7024 aluminium alloy. *Applied Surface Science* [online]. 2018, **435**, p. 452-461. ISSN 0169-4332. ISSN 0169-4332, eISSN 1873-5584. Available from: https://doi.org/10.1016/j.apsusc.2017.11.141

[16] DOBREV, T., PHAM, D. T., DIMOV, S. S. Laser polishing. In: Second International Conference on Multi-Material Micro Manufacture: proceedings[online]. Elsevier Science. 2019. ISBN 978-0-08-045263-0. Available from: https://doi.org/10.1016/B978-0-08-045263-0.X5000-4

[17] GUAN, Y. C., ZHOU, W., ZHENG, H. Y. Effect of laser surface melting on corrosion behaviour of AZ91D Mg alloy in simulated-modified body fluid. *Journal of Applied Electrochemistry* [online]. 2009, **39**, p. 1457-1464. ISSN 0021-891X, eISSN 1572-8838. Available from: https://doi.org/10.1007/s10800-009-9825-2

[18] TAN, Y. C., WEN, C., ANG, H. O. Influence of laser parameters on the microstructures and surface properties in laser surface modification of biomedical magnesium alloys. *Journal of Magnesium and Alloys* [online]. 2024, **22**(1), p. 72-97. eISSN 2213-9567. Available from: https://doi.org/10.1016/j.jma.2023.12.008

[19] HEIDELMANN. G. Surface cleaning with laser technology. *Plating and Surface Finishing*. 2009, p. 38-41. ISSN 03603164.

[20] HYOUNGWON, P., YOO, H. J., PARK, CH. Wear and corrosion behaviors of high-power laser surface-cleaned 304L stainless steel. *Optics and Laser Technology* [online]. 2024, **168**, 109640. ISSN 0030-3992, eISSN 1879-2545. Available from: https://doi.org/10.1016/j.optlastec.2023.109640

[21] WANG, W., LI, X., LIU, W., XING, F., WANG, J., ZHANG, K. Experimental study on hydrophobic properties and corrosivity of laser cleaned 7075 aluminum alloy anodized film surface. *Optics and Laser Technology* [online]. 2023, **166**, 109615. ISSN 0030-3992, eISSN 1879-2545. Available from: https://doi.org/10.1016/j.optlastec.2023.109615

[22] PROKURATOV, D., SAMOKHVALOV, A., PANKIN, D., VERESHCHAGIN, O., KURGANOV, N., POVOLOTCKAIA, A., SHIMKO, A., MIKHAILOVA, A., BALMASHNOV, R., SMOLYANSKAYA, O., REDKA, D., SALGALS, T., BOBROVS, V. Laser irradiation effects on metallic zinc and its corrosion products. *Journal of Cultural Heritage* [online]. 2023, **61**, p. 13-22. ISSN 1296-2074, eISSN 1778-3674. Available from: https://doi.org/10.1016/j.culher.2023.02.003

[23] ZHU, H., WU, CH., XUE, L., YANG, L., LIU, Y., WANG, D., LIANG, Y., PENG, Z. Effect of laser cleaning on the growth and properties of micro-arc oxidation layers of AZ31 magnesium alloy. *Surface and Coatings Technology* [online]. 2024, **488**, 131051. ISSN 0257-8972, eISSN 1879-3347. Available from: https://doi.org/10.1016/j.surfcoat.2024.131051

[24] XIONG, W., FU, J., LIU, CH., LI, L., WANG, H., ZHANG, M., GE, Z., ZHANG, T., WANG, Q. Laser-chemical surface treatment for enhanced anti-corrosion and antibacterial properties of magnesium alloy. *Coatings* [online]. 2024, **14**(3), 287. eISSN 2079-6412. Available from: https://doi.org/10.3390/coatings14030287

[25] MOFID, M. A., LORYAEI, E. Investigating microstructural evolution at the interface of friction stir weld and diffusion bond of Al and Mg alloys. *Journal of Materials and Research and Technology* [online]. 2019, **8**(5), p. 3872-3877. ISSN 2238-7854, eISSN 2214-0697. Available from: https://doi.org/10.1016/j.jmrt.2019.06.049

[26] KAJANEK, D., HADZIMA, B., PASTOREK, F. Electrochemical characterization of AZ31 magnesium alloy treated by ultrasonic impact peening (UIP). *Communications - Scientific Letters of the University of Zilina* [online]. 2018, **20**(3), p. 24-29. ISSN 1335-4205, eISSN 2585-7878. Available from: https://doi.org/10.26552/com.C.2018.3.24-29

[27] PASTOREK, F., STRBAK, M., KAJANEK, D., JACKOVA, M., PASTORKOVA, J., FLORKOVA, Z. Corrosion behaviour of preserved PEO coating on AZ31 magnesium alloy. *Communications - Scientific Letters of the University of Zilina* [online]. 2021, **23**(2), p. B76-B88. ISSN 1335-4205, eISSN 2585-7878. Available from: https://doi.org/10.26552/com.C.2021.2.B76-B88

[28] KAJANEK, D., HADZIMA, B., BREZINA, M., JACKOVA, M. Effect of applied current density of plasma electrolytic oxidation process on corrosion resistance of AZ31 magnesium alloy. *Communications - Scientific Letters of the University of Zilina* [online]. 2019, **21**(2), p. 32-36. ISSN 1335-4205, eISSN 2585-7878. Available from: https://doi.org/10.26552/com.C.2019.2.32-36

[29] ESMAILY, M., SVENSSON, J. E. FAJARDO, S., BIRBILIS, N., FRANKEL, G. S., VIRTANEN, S., ARRABAL, R., THOMAS, S., JOHANSSON, L. G. Fundamentals and advances in magnesium alloy corrosion. *Progress in Materials Science* [online]. 2019, **89**, p. 92-193. ISSN 0079-6425, eISSN 1873-2208. Available from: https://doi.org/10.1016/j.pmatsci.2017.04.011

[30] WALTER, R., KANNAN, M. B. Influence of surface roughness on the corrosion behaviour of magnesium alloy. *Materials and Design* [online]. 2011, **32**(4), p. 2350-2354. ISSN 0261-3069. Available from: https://doi.org/10.1016/j.matdes.2010.12.016

[31] KHOSHNAW, F., GUBNER, R. Corrosion atlas case studies part i: general aspects of corrosion, corrosion control, and corrosion prevention. In: *Corrosion atlas series* [online]. Elsevier, 2020. ISBN 9780128187609. Available from: https://doi.org/10.1016/B978-0-12-818760-9.02002-X

[32] PASTOREK, F., HADZIMA, B., KAJANEK, D. *Preparation and corrosion properties of structural materials with refined grain structure*. Harlow: Person, 2019. ISBN 978-8396-1054-7.

[33] BERTOLINI, R., BRUSCHI, S., GHIOTTI, A., PEZZATO, L., DABALA, M. The effect of cooling strategies and machining feed rate on the corrosion behavior and wettability of AZ31 alloy for biomedical applications. *Procedia CIRP* [online]. 2017, **65**, p. 7-12. eISSN 2212-8271. Available from: https://doi.org/10.1016/j.procir.2017.03.168

[34] LI, W., LI, D. Y. Influence of surface morphology on corrosion and electronic behavior. *Acta Materialia* [online]. 2006, **54**(2), p. 445-452. ISSN 1359-6454, eISSN 1873-2453. Available from: https://doi.org/10.1016/j.actamat.2005.09.017

[35] BAGHERIFARD, S., HICKEY, D. J., FINTOVA, S., PASTOREK, F., FERNANDEZ-PARIENTE, I., BANDINI, M., WEBSTER, T. J., GUAGLIANO, M. Effects of nanofeatures induced by severe shot peening (SSP) on mechanical, corrosion and cytocompatibility properties of magnesium alloy AZ31. *Acta Biomaterialia* [online]. 2018, **66**, p. 93-108. ISSN 1742-7061. ISSN 1742-7061, eISSN 1878-7568. Available from: https://doi.org/10.1016/j.actbio.2017.11.032

PREDICTING RESIDUAL LIFE OF TORO-40D UNITS USING THE OIL SPECTRAL ANALYSIS METHOD

Bakytzhan Kyrgyzbay[1], Mergen Zhumanov[2], Yerbol Kaliyev[1], Nurbol Kamzanov[3], Nursat Baikenzhe[3], Rustem Kozbagarov[1,*]

[1]Mukhametzhan Tynyshbayev ALT University, Almaty, Republic of Kazakhstan
[2]Al Farabi Kazakh National University, Almaty, Republic of Kazakhstan
[3]Satbayev University, Almaty, Republic of Kazakhstan

*E-mail of corresponding author: ryctem_1968@mail.ru

Bakytzhan Kyrgyzbay 0009-0004-0317-7917,
Yerbol Kaliyev 0000-0002-1961-4809,
Nursat Baikenzhe 0009-0000-0290-9056,
Mergen Zhumanov 0009-0006-2977-6971,
Nurbol Kamzanov 0000-0002-2420-8362,
Rustem Kozbagarov 0000-0002-7258-0775

Resume

At the underground mines of Kazakhmys Corporation, where different types of highly productive self-propelled equipment with different types of pneumatic wheel drive are operated, there are significant downtime of technological equipment. As practice has shown, application of repair system with use of old methods and means, at operation of underground self-propelled equipment appeared to be ineffective. One of the main reasons of low efficiency of self-propelled machines operation is the absence of the system of continuous monitoring of technical condition of each machine and its aggregates with application of methods and means of diagnostics. To avoid failure, it is necessary to establish the predicted and residual resource at a certain operating time of the machine according to the diagnostics data. This paper outlines the results of research on predicting the residual life of machine units used in the conditions of the mine corporation “Kazakhmys”.

Available online: https://doi.org/10.26552/com.C.2025.040

Article info

Received 20 February 2025
Accepted 17 April 2025
Online 30 April 2025

Keywords:

diagnostics
dump truck
wheel gearbox
spectral analysis
aggregate repair method
resource
transmission

ISSN 1335-4205 (print version)
ISSN 2585-7878 (online version)

1 Introduction

At present, the giant mines No. 55, 57, 65, 67 of Kazakhmys Corporation, where ore is extracted, are mines of a new type. Different types of highly productive self-propelled equipment with different types of drive on pneumatic wheels and caterpillars are operating in the faces of these mines. Most of the machines have diesel drive and articulated frame.

As practice has shown, the application of the repair system using old methods and means in the operation of underground self-propelled equipment proved to be ineffective. At the underground mines of Kazakhmys Corporation there are significant downtime of technological equipment. The duration of downtime ranges from 12% to 30% of the total time. From 20% to 30% of the total fleet of machines is constantly in repair, annual consumption of spare parts is from 15% to 20%, and materials - from 8 to 10% of the total costs of machinery and equipment; the number of repairmen is from 20 to 25% of the total number of underground workers [1-5].

One of the main reasons for low efficiency of self-propelled machines operation is the lack of a system of constant control of technical condition of each machine and its units with the use of diagnostic methods and means. Due to the fact that the value of working life before failure of the machine (unit) fluctuates within certain limits, there is a probability of failure during this period. To avoid failure, it is necessary to determine the predicted and residual resource at a certain operating time of the machine (unit) according to diagnostics data [6-8]. According to these data the terms of removal of aggregates or stopping the machine for repair are planned. This avoids emergency repairs and increases uptime of machine operation. Thus, increasing the failure-free operation of each machine unit with the use of methods and means of diagnostics, increases the performance of the machine as a whole.

Related to that, the research works directed on

Figure 1 *TORO-40D dump truck*

increase of workability of the machine by increase of failure-free operation of its aggregates with application of modern methods and means of resource diagnostics are current.

The planetary wheel reducers were selected as an object of research in this work. this is explained by the fact that each machine has four of them, and at the mines of Zhezkazgan work 68 dump trucks TORO-40D (Figure 1) and loading and transporting machines TORO-501 - 20 units. In addition, parts and assemblies of these gearboxes operate under sharply dynamic loads and are often overloaded. They have a relatively low durability, which makes it possible to quickly collect statistical material for calculations of resource parameters, labor intensity and cost of repair actions necessary for the development of repair standards and operational schedules of wheel gearboxes repair.

2 Materials and methods

Research in the field of maintenance of machines and equipment in serviceable condition, by means of methods and means of diagnostics, is carried out in aviation, railway and automobile transportation, machine-building plants.

Such studies for mining machinery and equipment have not been carried out. The transfer of developments from the above industries to the mining industry is impossible due to special operating conditions and distinctive features of the design of these machines [4-5].

In this paper, are given the results of researchers' works on increase of serviceability of self-propelled diesel machines on pneumatic-wheeled way by means of application of methods and means of diagnostics of removable units and theory of management of stocks of turnover fund.

The object of research is a wheel reducer of dump trucks TORO-40D, as a typical representative of units with a common oil bath and a considerable (over 240 pieces) number of them on dump trucks and loaders. Numerous researchers' experience showsexperience shows that the introduction of diagnostics processes of machines and equipment is one of the most important means of increasing their serviceability. Timely prevention of failures leads to reduction of their number and, as a consequence, to reduction of machine downtime; their inter-repair resource is more fully utilized.

Technical diagnostics allows to increase productivity and efficiency of machine operation due to timely performance of adjustment, adjustment, repair and other preventive works.

It is known that the availability of complex systems deteriorates not only with the growth of failure rate, but with the increase in the duration of restoration of technical devices and, in particular, machines, as well. Considering that, the task of increasing the serviceability of machines as a result of improving the characteristics of recoverability: the time of searching for the failed element and the time of eliminating the failure is of great relevance. As it is known, modern repair systems are based on the aggregate repair method (ARM). The main condition for transfer of the main technological equipment to ARM is practical dismemberment of machines into interchangeable removable units, assembly units [7-9].

Machine parsing is aimed at developing such a nomenclature of removable elements, which would provide the most economical way of restoring the serviceability of machines in operating conditions.

Consequently, an optimal nomenclature of detachable units must be formulated for each machine (Figure 2). The main advantage of ARM is that the removable units are not repaired on the machine. Instead of defective ones, the machine is equipped with units from the revolving fund. Consequently, by improving the quality of manufacturing and repair of individual units, it is possible to increase the serviceability of the machine.

Structural parameters of each part working in

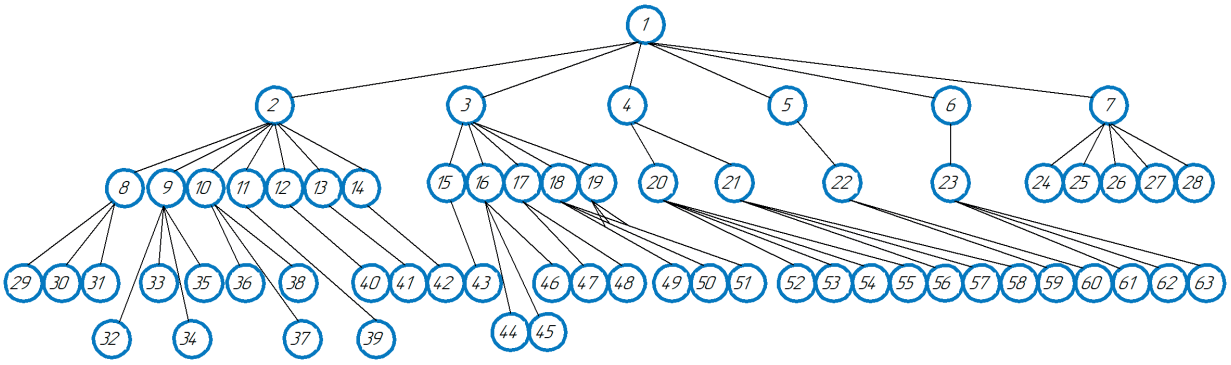

1 - road train; 2 - engine; 3 - transmission; 4 - control mechanism; 5 - frame; 6 - body control mechanism; 7 - electrical equipment; 8 - lubrication system; 9 - power system; 10 - cooling system; 11 - catalytic converter; 12 - cylinder-piston group; 13 - crank mechanism; 14 - gas distribution mechanism; 15 - gearbox; 16 - torque converter; 17 - cardan transmission; 18 - front axle; 19 - rear axle; 20 - steering control; 21 - brake system; 22 - halves articulation joint; 23 - hydraulic system of the body control; 24 - generator; 25 - starter; 26 - accumulator battery; 27 - voltage regulator; 28 - headlights; 29 - cleaning filters; 30 - hydraulic pump; 31 - oil radiator; 32 - high-pressure fuel pump; 33 - fuel pump; 34 - fuel filters cleaning; 35 - air cleaner; 36 - water pump; 37 - radiator; 38 - thermostat; 39 - catalytic cleaning unit; 40 - cylinder block; 41 - crankshaft, complete; 42 - camshaft, complete; 43 - frictions; 44 - pump wheel; 45 - turbine wheel; 46 - reactor; 47 - intermediate cardan shaft; 48 - drive axles cardan shaft; 49 - differential; 50 - wheel spur gear; 51 - wheel hub; 52 - hydraulic pump; 53 - steering cylinders; 54 - main steering distributor; 55 - "orbitrol" unit; 56 - hydraulic accumulators; 57 - brake valves; 58 - parking brake cylinders; 59 - front half-frame; 60 - rear half-frame; 61 - hydraulic pump; 62 - body lift cylinders; 63 - main distributor of the body hydraulic system

Figure 2 *Structural and functional diagram of the TORO-40D dump truck*

Table 1 *Chemical composition of TORO-40D dump truck wheel gearbox parts*

Ńo.	Name parts	Quantity	Average elemental content, %					
			C	Mn	Cr	Cu	Si	Ni
1	Solar gear	1	0.5	0.6	0.2	0.3	0.3	0.3
2	Idler gear	1	0.4	0.6	0.6	0.3	0.3	1.2
3.	Satellite	3	0.5	0.6	-	-	0.3	0.3
4	Satellite pin	3	0.4	0.6	0.9	0.3	0.3	0.3
5	Half-axle	1	0.5	0.6	0.2	0.3	0.3	0.3
6	Stocking	1	0.1	0.4	0.7	2.9	-	-
7	Driver	1	0.3	0.6	0.2	0.3	0.3	-
8	Half axle ring	1	0.4	0.6	0.5	0.3	0.3	0.3

a common oil bath are selected, when reaching the limit values of which the gearbox is removed for overhaul and a rational method of diagnostics.

The dominant method for diagnostics of units, the majority of parts and assembly units of which work in oil, is the spectral analysis of oil.

At AMR the degree of wear is established only for that part and mating parts of assembly units, at the limit wear of which the unit is removed for overhaul [10].

In experimental studies, the chemical composition of each part of the wheel reducer working in the same oil bath was carefully studied (Table 1).

When using the spectral analysis of oil, oil sampling is a very important operation. The standards for analysis were prepared based on the fresh engine oil used in the units of the TORO-40D dump truck (hydromechanical gearbox, axles, wheel reducers, etc.).

Oil samples were taken at critical times for the gearbox: after the running-in, refilling, oil change, at minimum values of technical life of parts working in a common bath before the gearbox removal [11-12]. The oil samples were analyzed in a special laboratory equipped with the MFS-7 unit and sample preparation units complete with an alternating current arc generator, tripod, semi-chromator and electronic recording unit, laboratory microanalytical type scales, etc.

3 Results and discussions

Implementation of diagnostics by spectral analysis of oil required a lot of preparatory work on measurements of worn surfaces of parts, processing of measurement data to obtain the wear from the total operating time $\delta = f(\sum R)$ and the mass of worn material of the part in the oil from the linear value of wear $m = F(\delta)$.

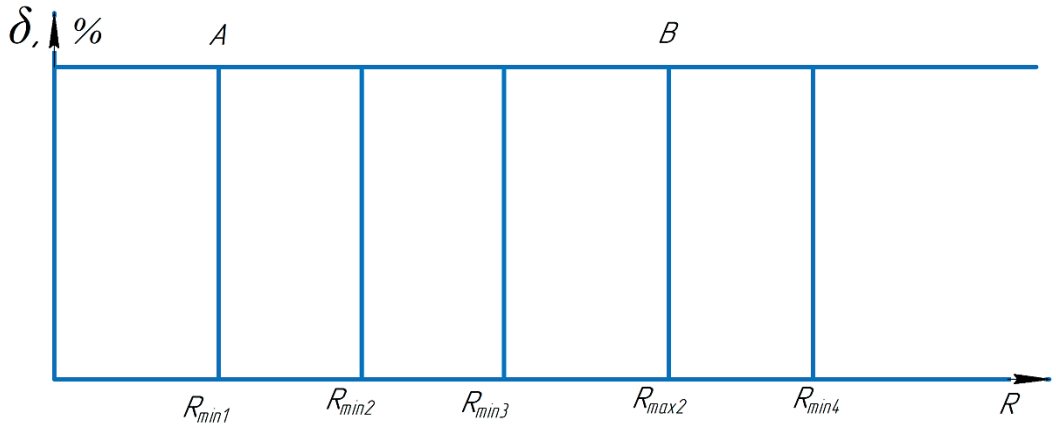

Figure 3 *Selection of parts to obtain service life parameters*

Table 2 *Average chemical composition of TORO-40D dump truck wheel gearbox parts*

No.	Name of parts	Quantity	Average elemental content, %					
			C	Mn	Cr	Cu	Si	Ni
1	Solar gear	1	0.5	0.6	0.2	0.3	0.3	0.3
2	Idler gear	1	0.4	0.6	0.6	0.3	0.3	1.2
3	Satellite	3	0.5	0.6	-	-	0.3	0.3
4	Satellite pin	3	0.4	0.6	0.9	0.3	0.3	0.3

To obtain these dependencies as quickly as possible, it was necessary to carry out a minimum number of measurements, i.e., to obtain data only for those parts for which the gearbox is removed for overhaul. In the work the probabilistic theory of resource distribution is accepted, in which each repair unit has minimum $(R_{\min})$, average $(\bar{R})$ and maximum $(R_{\max})$ values of resource, law and parameters of its distribution. The parts, because of which the gearbox is removed for overhaul, include parts that have a minimum value of the service life $R_{\min} \le R_{\max}^{\min}$, where $R_{\max}^{\min}$ - the minimum value of the maximum service life. Figure 3 shows the graph of locations of $R_{\min i}$ and $R_{\max i}^{\min}$ for parts 1, 2, 3, 4 [13].

In the range from A $(R_{\min 1})$ to B $(R_{\min 2})$, there is a probability that parts 1, 2, 3 will fail and the gearbox will be removed for repair. When operating time $R_{\min 2}$ is reached, there is a 100% probability that part 2 will fail and the gearbox will be removed for repair. For parts with $R_{\min 1} \le R_{\max 1}^{\min}$, instrumented measurements are used to calculate $\delta \le (\sum R)$ and $\delta = F(m)$. In Figure 3 this applies to parts 1, 2, 3.

With the probabilistic theory of the service life value distribution, the wear limit may occur at different operating hours within the range of $R_{\min i}$ to $R_{\max i}$. In this case, for the selected group of gearbox parts it is necessary to set the alloying additives, the content of which in the oil will be used to judge the degree of wear of each part.

The most time-consuming task is the distribution of alloying additives in the gearbox crankcase among the parts depending on the degree of wear. In this case it is necessary to find the distinctive features for each part, by which it is established that it belongs to one or another of the components contained in the oil [14-15].

Table 2 shows the chemical composition of four parts of the gearbox, because of which the gearbox is removed for repair.

Based on Table 2, it can be stated that the amount of each additive is related to the number and amount of other additives. Using this relationship, a system of equations is developed. Mn is taken as the main alloying material, as it is contained in the materials of parts in greater values and equal quantities. For simplicity of calculation the equations are made for four components (Mn, Cr, Ni, Cu) and their masses are equated to the equivalent of Mn.

$$\sum Mn_j = Mn_1 + Mn_2 + Mn_3 + Mn_4, \quad (1)$$

where Mn_j, Mn_1, Mn_2, Mn_3, Mn_4 - amount of manganese in oil due to wear of parts 1, 2, 3, 4, g, respectively.

$$\sum Mi_j = Mi_1 + Mi_2 + Mi_3 + Mi_4, \quad (2)$$

where $\sum Mi_j$ - is the total mass of nickel contained in the gearbox crankcase at the time of sampling, g; Mi_1, Mi_2, Mi_3, Mi_4 - amount of nickel in oil due to wear of parts 1, 2, 3, 4, g, respectively.

Next, Mi is replaced by the equivalent Mn. According to Table 2, part 1 has 2 times more content than Mn, parts 3 and 4 have 2 times less content than Mn. Then, Equation (2) takes the following form

$$\sum N_1 = 0.5Mn_1 + 2Mn_2 + 0.5Mn_3 + 0.5Mn_4. \quad (3)$$

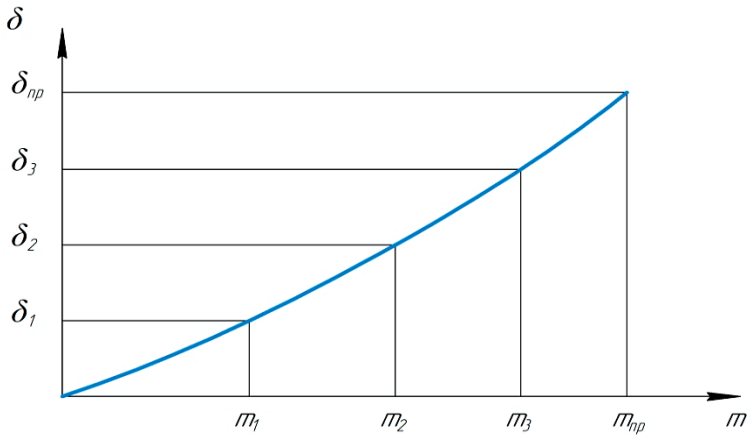

Figure 4 *Dependence of the wear rate* δ *on the worn metal weight m*

In the same way the equations for ΣCr and ΣCu are formed:

$$\sum Cr = 0.33Mn_1 + 2Mn_2 + 1.5Mn_4\,, \tag{4}$$

$$\sum Cu = 0.5Mn_1 + 0.5Mn_2 + 0.5Mn_4\,. \tag{5}$$

Spectral analysis data: ΣMn=240g; ΣNi=140g; ΣCr=80g; ΣCu=80g. From Equation (3) one finds $Mn_1 = 2\sum N_i - 4Mn_2 - Mn_3 - Mn_4$. From Equation (1) one obtains:

$$Mn_2 = \frac{2\sum Ni - \sum Mn}{3} = 13\text{g}\,. \tag{6}$$

In the same way is found ΣMn_1=132g; ΣMn_3=79g; ΣMn_4=16g. Using this data and the dependence $\delta = F(m)$ one can determine the amount of wear δ of each part after the next diagnostics.

All the instrumental measurements were carried out in the mining equipment plant (MEP) when disassembling the gearbox for repair and during the defective parts inspection. Measurement of linear dimensions of worn surfaces is carried out using the technological charts developed by the authors of the work. Measurement of the mass of the worn material m is carried out mainly by weighing the examined part. The mass of the worn material of the part mi; was found by the formula $m_i = m_H - m_B$, - then where m_H - the mass of a new part, taken from the working drawings; m_H - the weighed mass of the same part. Measurement data are processed and dependences $\delta = F(m), \delta = F(R)$ for each of 8 parts are obtained (Figure 4).

The wear limit $\delta_{\max}$ was taken from the manufacturer's data. According to $\delta_{\max}$ and the value of wear δ at operating time R, obtained by diagnostics, the predicted service life was found by the formula

$$R_{for} = R \cdot \sqrt[n]{\frac{\delta_{\max}}{\delta}}\,, \text{ machine hours}, \tag{7}$$

where R - the operating time for the measurement period; n - coefficient, the value of which depends on the type of depreciation, is given in reference books.

On the example of satellites, the dependences of δ on alloying additives $\delta = f(m_{Cr}), \delta = f(m_{Cu}), \delta = f(m_{Ni})$ etc. were obtained. The sums $\sum m_{Cr}, \sum m_{Ni}, \sum m_{Mn}$ etc. were found for each operating time and at known values of wear.

$$\begin{aligned}
&\sum m_{Cr} = m_{Cr1} + m_{Cr2} + \ldots + m_{Crn};\\
&\sum m_{Ni} = m_{Ni1} + m_{Ni2} + \ldots + m_{Nin};\\
&\ldots\ldots\ldots\ldots\ldots\ldots\ldots\ldots\ldots\ldots\ldots\ldots\\
&\sum m_{Mn} = m_{Mn1} + m_{Mn2} + \ldots + m_{Mnn};
\end{aligned} \tag{8}$$

where $m_{Ni1}, \ldots, m_{Nin}, m_{Cr1}, m_{Crn}, m_{Mn1}, \ldots, m_{Mnn}$ - mass of nickel, chromium, manganese and other alloying additives at wear of $\delta_1, \delta_2, \delta_m$ from 1 to n-th parts, respectively.

Thus, for each operating time, it is calculated how much of each component should be in the oil from wear of all 8 parts. Using this data, the service life values, distribution laws and their parameters for each part of the wheel gearbox are established.

A method for determining the total mass of alloying additives that are contained in the drained and working crankcase oils has been proposed. This mass should correspond to the mass of worn material of the gearbox parts. The essence of the method is as follows [1-3]:

1. When the minimum oil level in the crankcase is reached, a sample is taken;
2. After taking the sample, top up to the maximum mark;
3. Oil refill volume is $V_y = V_{\max} - V_{\min}$, where $V_{\max}$, $V_{\min}$ - is the maximum and minimum crankcase oil volumes;
4. The total mass of components in the oil due to component wear and removed from the gearbox together with the leaked oil is calculated according to the formula:

$$\begin{aligned}
&\sum m_{Cr} = m_{Cr1} + m_{Cr2} + \ldots + m_{Crn};\\
&\sum m_{Mn} = m_{Mn1} + m_{Mn2} + \ldots + m_{Mnn}\ \text{etc.},
\end{aligned} \tag{9}$$

where $m_{Cr1}, m_{Cr2}, \ldots, m_{Crn}$, $m_{Mn1}, m_{Mn2}, \ldots, m_{Mnn}$ - mass of Cr, Mn and other components, respectively, removed

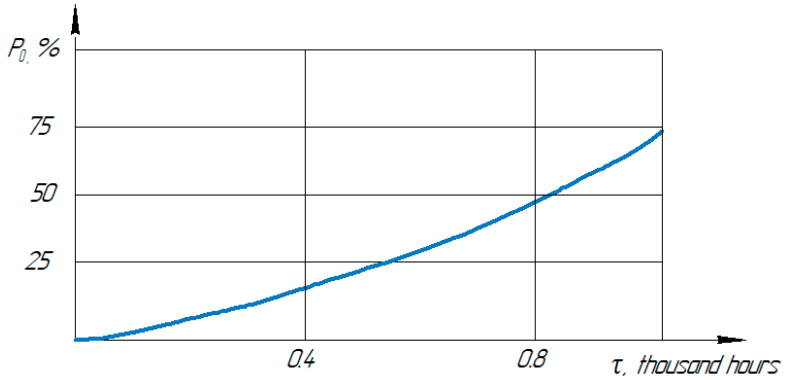

Figure 5 *Dependence of probability of emergency repair on the frequency of diagnostics*

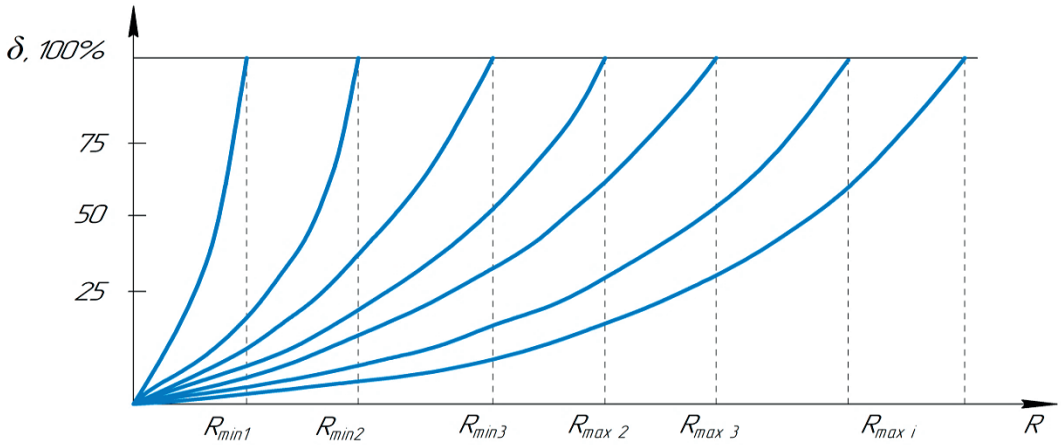

Figure 6 *Setting the optimal timing of diagnosis and the number of samples taken*

from the crankcase by the leaked oil and obtained after 1, 2 ... n topping up;

5. The total mass of each of the alloying additives that should be taken into account to obtain the dependencies $\delta = f(m_i)$, is found from the equation

$$\sum M_i = M_i^z + M_i^d + M_i^b, \quad (10)$$

where M_i^z, M_i^d - total mass of the i-th alloying additive removed from the crankcase during the replacement and leakage; M_i^b - mass of the i-th alloying additive at the last sampling from the oil running in the crankcase. Then, $\delta = f(\sum M_{Cr})$

The diagnostic intervals (τ) should be chosen so that the unit costs of diagnostics and repairs are minimized. The diagnostic intervals in general terms are determined by the formula

$$\tau = \mu \cdot R, \text{ machine hours}, \quad (11)$$

where μ - optimality coefficient showing how many times the optimal periodicity is greater or smaller than the mean time between failures.

At exponential law of developments distribution, the optimality equation will have the form

$$e^{-\lambda\tau} - \lambda\tau - 1 - \frac{c_d}{d_d} = 0, \quad (12)$$

where $\lambda = \frac{1}{R}$ - failure rate parameter.

Under the Weibull distribution law

$$\frac{\alpha\beta \cdot \tau^{\beta-1}}{e^{-\alpha \cdot \tau\beta}} \int e^{\alpha R^\beta} dR + \alpha\tau^\beta - \frac{C_{d.o}}{C_A} = 0, \quad (13)$$

where α, β - distribution parameters.

Figure 5 shows the increase in the probability of emergency repair depending on the frequency of diagnostics for a certain mode of operation and operating conditions.

Oil samples are taken from the crankcase in the following cases: after the end of running-in of the product, each refilling and changing of oil, as well as to determine the degree of wear of individual parts working in an oil bath.

Periodicity of running-in, topping up and oil change is specified in the operating instructions. The sampling intervals and the number of samples to be taken can be optimized.

First of all, the gearbox parts and assemblies for which it is necessary to calculate the predicted service life R_{npi} are installed. For this purpose, the parts and assemblies with the shortest maximum life $R_{\max}^{\min}$ are selected (Figure 6).

On the graph (see Figure 6) δ, % - wear of parts; R - machine operating time in machine hour; $R_{\min 1}, R_{\min 2}$,

R_{min3} - minimum values of service life of 1st, 2nd and 3rd parts, R_{max1}, R_{max2}, R_{max3} - their maximum values, respectively.

When unit R_{max2} has reached the end of its service life, it must be removed and sent for overhaul. The range from R_{min1} to R_{max2} includes values R_{min1}, R_{min2}, R_{min3}.

4 Conclusions

Increase of serviceability of self-propelled mining machines at the aggregate method of repair is achieved by increasing the failure-free operation of their aggregates by methods and means of resource diagnostics. This is achieved by reducing the costs of emergency repairs and losses from machine downtime in these repairs, thanks to the prevention of failures by methods and means of spectral analysis of oil, which allows to establish the predicted and remaining life of the unit before its removal.

Acknowledgements

The authors received no financial support for the research, authorship and/or publication of this article.

Conflicts of interest

The authors declare that they have no known competing financial interests or personal relationships that could have appeared to influence the work reported in this paper.

References

[1] KLORIKYAN, S. H., STARICHNEV, V. V., SREBNY, M. A. *Machinery and equipment for mines and mines: a reference book.* Moscow: MSUH, 2002. ISBN 5-7418-0173-0.

[2] KAZACHENKO, G. V., PRUSHAK, V. Y., BASALAI, G. A. *Mining machines. Part 2. Machines and complexes for mining: a textbook*. Minsk: Higher school, 2018. ISBN 978-985-06-2982-1.

[3] GOLIK, V. I. *Underground mining of ore deposits*. Vologda: Infra-Engineering, 2022. ISBN 978-5-9729-0793-9.

[4] ANUSHENKOV, A. N., AKHPASHEV, B. A., VOLKOV, E. P. *Underground geotechnology.* Krasnoyarsk: Siberian Federal University, 2017. ISBN 978-5-7638-3725-4.

[5] KHOMENKO, O. E., KONONENKO, M. M., MALTSEV, D. V. *Mining equipment for underground mining of ore deposits: a reference guide.* Donetsk: National Mining University, 2010. ISBN 978-966-350-240-3.

[6] KOZBAGAROV, R. A., ZHIYENKOZHAYEV, M. S., KAMZANOV, N. S., TSYGANKOV, S. G., BAIKENZHEYEVA, A. S. Design of hydraulic excavator working members for development of mudslides. *News of the National Academy of Sciences of the Republic of Kazakhstan, Series of Geology and Technical Sciences* [online]. 2023, **2**(458), p. 134-141. ISSN 2224-5278, eISSN 2518-170X. Available from: https://doi.org/10.32014/2023.2518-170X.288

[7] KOZBAGAROV, R., KAMZANOV, N., AMANOVA, M., BAIKENZHEYEVA A., NAIMANOVA G., Justification of the cam roller parameters for destruction of the road coatings for obtaining the lumpy asphalt scrap. *Communications - Scientific Letters of the University of Zilina* [online]. 2023, **25**(2), p. 103-109. ISSN 1335-4205, eISSN 2585-7878. Available from: https://doi.org/10.26552/com.C.2023.028

[8] KOZBAGAROV R., AMANOVA M., KAMZANOV N., BIMAGAMBETOVA L., IMANGALIYEVA, A. Investigation of wear of cutting part of polygonal knife car graders in different ground conditions. *Communications - Scientific Letters of the University of Zilina* [online]. 2022, **24**(4), p. 229-238. ISSN 1335-4205, eISSN 2585-7878. Available from: https://doi.org/10.26552/com.C.2022.4.D229-D238

[9] SHAKENOV, A., SLADKOWSKI, A., STOLPOVSKIKH, I. Haul road condition impact on tire life of mining dump truck. *Scientific Bulletin of the National Mining University / Naukovyi Visnyk Natsionalnoho Hirnychoho Universytetu* [online]. 2022, **6**, p. 25-29. ISSN 2071-2227, eISSN 2223-2362. Available from: https://doi.org/10.33271/nvngu/2022-6/025

[10] SLADKOWSKI, A., UTEGENOVA, A., KOLGA, A. D., GAVRISHEV, S. E., STOLPOVSKIKH, I., TARAN, I. Improving the efficiency of using dump trucks under conditions of career at open mining works. *Naukovyi Visnyk Natsionalnoho Hirnychoho Universytetu* [online]. 2019, **2**, p. 36-42. ISSN 2071-2227, eISSN 2223-2362. Available from: https://doi.org/10.29202/nvngu/2019-2/8

[11] TARAN, I., KLYMENKO, I. Analysis of hydrostatic mechanical transmission effciency in the process of wheeled vehicle braking. *Transport Problems* [online]. 2017, **12**, p. 45-56. ISSN 1896-0596, eISSN 2300-861X. Available from: https://doi.org/10.20858/tp.2017.12.se.4

[12] BURMISTROV, K. V., OSINTSEV, N. A., SHAKSHAKPAEV, N. A. Selection of open-pit dump trucks during quarry reconstruction. *Procedia Engineering* [online]. 2017, **206**, p. 1696-1702. ISSN 1877-7058. Available from: https://doi.org/10.1016/j.proeng.2017.10.700

[13] RAKHMANGULOV, A., BURMISTROV, K., OSINTSEV, N. Multi-criteria system's design methodology for selecting open pits dump trucks. *Sustainability* [online]. 2024, **16**(2), 863. eISSN 2071-1050. Available from: https://doi.org/10.3390/su16020863

[14] KOZBAGAROV, R., ZHUSSUPOV, K., KALIYEV, Y., YESSENGALIYEV, M., KAMZANOV, N. Energy intensity study for soil transportation by inertial rotor. *Vibroengineering Procedia* [online]. 2023, **48**, p. 93-99. ISSN 2345-0533, eISSN 2538-8479. Available from: https://doi.org/10.21595/vp.2023.23086

[15] BODZIONY, P., KASZTELEWICZ, Z., SAWICKI, P. The problem of multiple criteria selection of the surface mining haul trucks. *Archives of Mining Sciences* [online]. 2016, **61**(2), p.223-243. ISSN 0860-700, eISSN 1689-0469. Available from: https://doi.org/10.1515/amsc-2016-0017

INFLUENCE OF THE CUTTING ANGLE ON THE RESISTANCE OF BULLDOZER WORKING EQUIPMENT BLADE BURIAL WHEN THE MACHINE IS MOVING

Nursat Baikenzhe[1], Shynbolat Tynybekov[1], Bakytzhan Kyrgyzbay[2], Kazyna Ashim[3], Nurbol Kamzanov[1], Rustem Kozbagarov[2,*]

[1]Satbayev University, Almaty, Republic of Kazakhstan
[2]Mukhametzhan Tynyshbayev ALT University, Almaty, Republic of Kazakhstan
[3]Nazarbayev Intellectual Schools of Chemistry and Biology, Almaty, Republic of Kazakhstan

*E-mail of corresponding author: ryctem_1968@mail.ru

Nursat Baikenzhe 0009-0000-0290-9056,
Bakytzhan Kyrgyzbay 0009-0004-0317-7917,
Nurbol Kamzanov 0000-0002-2420-8362,
Shynbolat Tynybekov 0009-0002-6146-2076,
Kazyna Ashim 0009-0002-1496-1278,
Rustem Kozbagarov 0000-0002-7258-0775

Resume

The influence of the cutting angle on the resistance to the bulldozer blade burial during its movement, taking into account the one-sided stressed state of the soil, was studied in the research results of which are presented in this paper. It is established that the resistance to deepening is significantly reduced when the machine is moving, which allows using smaller cutting angles without increasing the energy consumption. Constructive features and kinematics of the working equipment are considered, including a promising parallelogram scheme, which provides automatic reduction of the cutting angle during deepening. Calculations of the resistance of the blade penetration into the ground, and experimental data confirming the cutting force reduction up to 7%, for each degree of angle reduction, are given. It is determined that the optimum cutting angle is 30-40°. The obtained results can be used to increase the productivity of bulldozers and optimize the design of their working equipment.

Article info

Received 6 March 2025
Accepted 25 April 2025
Online 14 May 2025

Keywords:

bulldozer
blade
knife
cutting angle
soil

Available online: https://doi.org/10.26552/com.C.2025.041

ISSN 1335-4205 (print version)
ISSN 2585-7878 (online version)

1 Introduction

The study and systematization of the results of conducted research on bulldozer equipment allows to identify trends in their development and establish directions for further research. The generalizing work [1-6] indicates that a promising direction of research in the field of universal earthmoving machines, including bulldozers, is the creation of working bodies with the properties of wide adaptation to external conditions and types of work performed.

In the case of bulldozers, this trend is manifested in the creation of designs of working equipment that allow for transverse skewing of the blade and changing the cutting angle, as well as equipping the moldboards with a jaw grip, protruding middle blade. Improving the efficiency of bulldozer is largely associated with improving the design of working equipment, its kinematic and force parameters. At the same time, the working equipment schemes used in practice are usually structurally similar regardless of the layout of the basic machine. However, the efficiency of the bulldozer is influenced not only by the parameters of the working equipment and the base machine taken separately, but by the consistency of their mutual work, as well. Thus, there is a question of choosing a rational scheme of working equipment.

To determine the ways of solving this issue, authors considered the impact on the efficiency of the working process of the bulldozer, as a result of research on the features of the working equipment and its links with the base machine. It is known that in the process of bulldozer operation most of its power is spent on cutting the soil and moving it along the working body - blade. Since the process of soil cutting is carried out as a result of force interaction with it as a result of both the working equipment and the running system of the base tractor, it

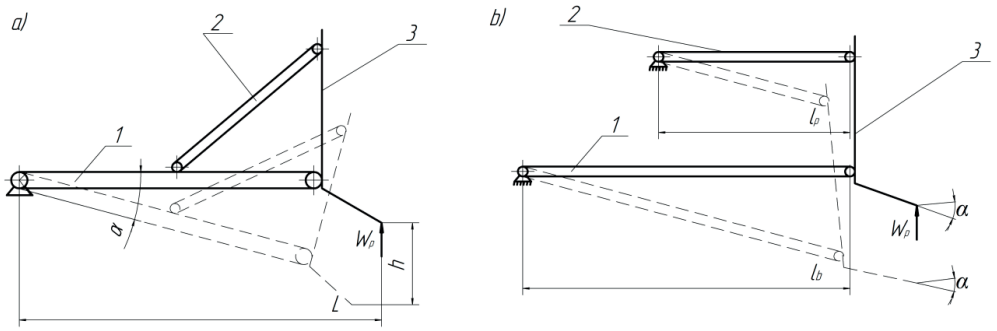

Figure 1 *Scheme of burial into the ground of the blade of the working equipment of the bulldozer: a) scheme "traditional"; b) scheme "parallelogram"; 1- strut, 2 - push bar, 3 - moldboard*

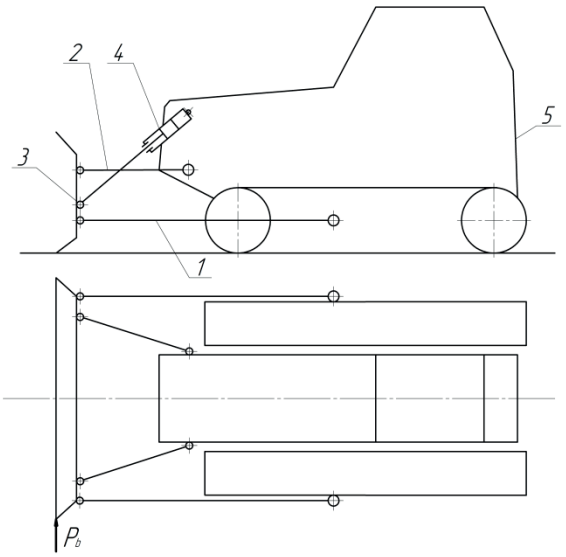

Figure 2 *Kinematic diagram of bulldozer working equipment: 1 - push bar; 2 – strut; 3- moldboard; 4 - hydraulic cylinder; 5 - tractor base*

is necessary to identify the influence of their parameters on its efficiency.

There are known designs of working equipment having a traditional scheme, in which both skews are made in the form of hydraulic cylinders, serving both for realization of blade skew and for controlled change of cutting angle in the process of cutting W_p [5-7]. However, they have not become widespread due to the increased cost of construction. Therefore, a promising way to improve this function should be recognized as the creation of a scheme of working equipment that reduces the blade cutting angle as it is embedded in the ground due to its own kinematics. The changes in the cutting angle α depending on the digging depth h in the traditional bulldozer scheme were considered, [8-10]. In accordance with the notations in Figure 1, and taking into account that $h << L$, one obtains the relationship between the changes in cutting angle α and h

$$\alpha = 57.7\frac{h}{L}. \quad (1)$$

As can be seen from Equation (1), the cutting angle at $h << L$ is linearly related to the digging depth h. From the point of view of kinematics, this dependence is determined by the impossibility to rotate the moldboard 3 relative to the push bars 1, which is prevented by the presence of links between the struts 2 and the bars. Therefore, in this case, the pushing bars and struts cannot be connected to each other, for example, in a "parallelogram" pattern (Figure 1, b).

If the condition $l_p << l_b$ is provided in this mechanism, the cutting angle decreases as the blade penetrates the ground. Such technical solution is known (Figure 1, b), however, it has not been practically realized on industrial bulldozers, which is explained by peculiarities of basic tractors design. In particular, in tractors with semi-rigid suspension, the frame is not rigid enough in the horizontal plane and is not designed to absorb lateral forces. In the scheme of the bulldozer shown in Figure 2, when it is loaded with force P_b applied to the moldboard 3, its lateral stability is provided by struts 2, which leads to loading of the tractor frame 5 by a bending moment in the horizontal plane.

Related to this, it seems reasonable, using the advantages of the "parallelogram" scheme, to ensure loading of the tractor frame by forces lying only in its

vertical-longitudinal plane, due to redistribution of forces acting on the tractor between the crawler tracks designed to absorb complex loading (forces lying in three planes can act on them simultaneously). Another advantage of this scheme of blade connection with bars and struts is the fact that bending moments in the vertical plane do not act on the pushing bars. This makes it possible to significantly reduce the metal consumption of the structure, it is possible to manufacture pushing bars from pipes and thereby reduce the cost and labor intensity of their manufacture.

2 Materials and methods

From the above considerations follows the requirement for the design of the working equipment: to reduce the energy intensity of digging, reduce the metal intensity of the working equipment and its production costs, the scheme of blade connection with struts and push bars should be made according to the scheme "parallelogram" with the absence of links between the push bars and struts, ensuring that the tractor frame can absorb the forces lying in its longitudinal plane of symmetry.

Deepening of the working tool into the ground [8, 11] is the initial and important stage of digging, which has a significant impact on the working process of the earthmoving machine. To create the conditions for optimal kinematic mode of the blade penetration into the ground, it is necessary to know the magnitude of forces acting on the blade during the process of burrowing when calculating the control mechanism of the working tool. When the knife penetrates into the ground, a stress state of the second type is created in front of it, the so-called limit stress state.

The scheme of the bulldozer working equipment suspension is represented as a flat mechanism consisting of links connected by joints. In this case, the suspension is an articulated four-link *EFGH* (Figure 3, a) in the form of a closed four-link chain with one degree of freedom, which has a leading link *EF* (strut), connecting rod *FG* distance between the attachment points of the strut and push bar on the moldboard) and a fixed link *EH* (distance between the attachment points of the strut and push bar on the base machine). In single degree of freedom mechanisms, one generalized coordinate completely determines the position of all links in the mechanism. By changing the angle φ of inclination of the driving link *HG*, one can determine the angle ψ of inclination of the driven link EF, and vice versa, knowing the position of the driving link *HG* and driven link *EF*, one can determine the angle λ of rotation of the connecting rod link *FG*. For this purpose, in the scheme of the four-link mechanism, conditionally is distinguished the parallelogram $EFF'H$. From FGF' and HGF', one determines the length *GF* by the cosine theorem:

$$|GF| = R^2 + r^2 - 2Rr\cos(\varphi - \psi), \quad (2)$$

where *L*- length of the fixed link *EH*; *l*- length of connecting rod *FG*; λ - angle of rotation of the connecting rod link *FG* to the fixed link *EH*; *R* - drive link length *HG*; *r* - slave length *EF*; φ - angle of inclination of drive link *HG* to the vertical axis; ψ - inclination angle of the driven link *EF* to the vertical axis.

Equating the values of $/FG/$ and transforming the resulting expression one finds the value of angle λ:

$$\lambda = arccos\left(\frac{L^2 + l^2}{2Ll} - \frac{R^2 + r^2}{2Li} + \frac{Rr}{Ll}\cos(\varphi - \psi)\right). \quad (3)$$

The angle of rotation of the connecting rod link *FG*, in the articulated four-link diagram, corresponds to the

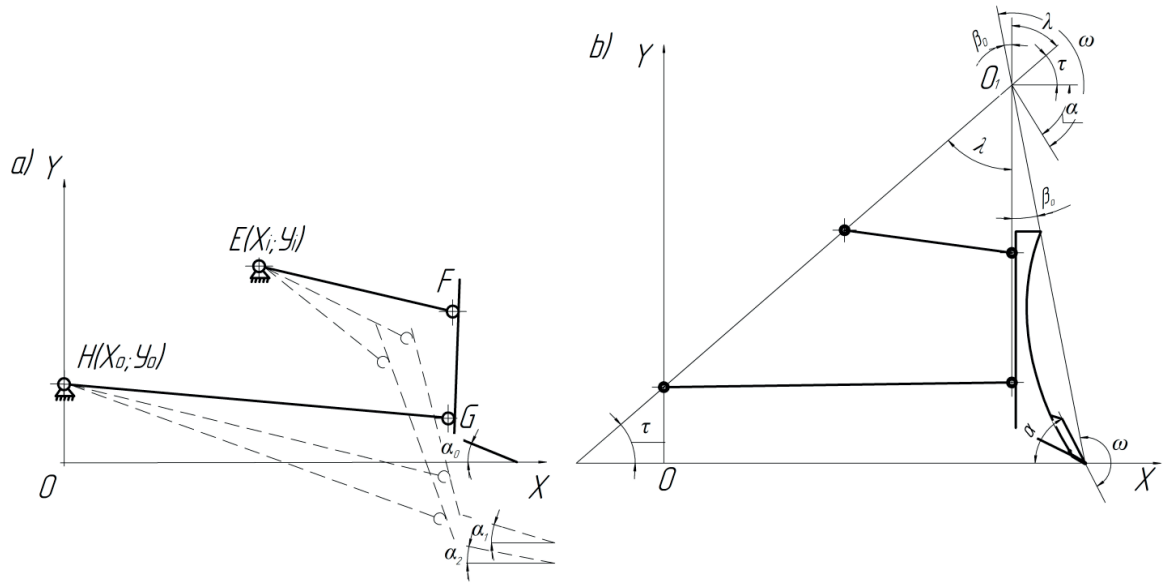

Figure 3 *Schematic diagram of the bulldozer attachment suspension: a) parallelogram scheme; b) cutting angle determination scheme*

angle of rotation of the dozer blade in real conditions when its position is changed.

The main angles $\lambda, \omega, \tau, \beta_0$, characterizing the suspension of attachments and the blade design will be transferred to the point O_1 of intersection of the line connecting the fixing points of the pusher bar and strut on the base machine with the line of fixing the same elements on the blade (Figure 3, b). The cutting angle will be equal to:

$$\alpha = \omega - \beta_0 - \tau - \lambda, \tag{4}$$

where ω - angle between the line connecting the upper edge of the moldboard surface with the cutting edge of the moldboard blade and the moldboard cutting element, $\omega = 160^\circ$; τ - angle between the line connecting the fixing points of the strut and push bar on the tractor base and the horizontal axis:

$$\tau = arctg\left(\frac{Y_i - Y_0}{X_i - X_0}\right), \tag{5}$$

where X_i, Y_i - coordinates of point E; X_0, Y_0 - coordinates of point H; β_0 - the angle between the line connecting the strut and push bar attachment points on the moldboard and the line connecting the upper edge of the moldboard surface with the cutting edge of the moldboard middle blade, $\beta_0 = 19 - 21^\circ$.

The values of angles $\lambda, \omega, \tau, \beta_0$ are entered into Equation (3) and one obtains:

$$\alpha = 141^\circ - arctg\left(\frac{Y_i - Y_0}{X_i - X_0}\right) - \\ - arccos\left(\frac{L^2 + l^2}{2Ll} - \frac{R^2 + r^2}{2Ll} + \frac{Rr}{Ll}\cos(\varphi - \psi)\right). \tag{6}$$

The value of the cutting angle α according to the Equation (6) is determined by the points of fixing the strut on the tractor base and on the moldboard, i.e., the length of the strut, as well as the moldboard depth (values φ and ψ). Thus, the obtained expression allows determining the cutting angle of the bulldozer working equipment for all the intermediate values (thickness of the cut chips).The rigorous solution of the problems on the ground limit state is given in analytical form in [12-13] and graphically in [8-9]. The interaction of the working body with the soil is considered from the point of view of those provisions of the theory of limit equilibrium, which are related to the definition of passive soil pressure on retaining walls.

The process of deepening is considered as periodically repeated chipping of the elements of the cut chip, caused by the introduction of a knife with a broken front edge into the slope of the massif formed during the previous chipping by a value of h_3. The calculation consists of two stages:

I - determination of sliding surfaces in the soil massif using characteristic circles in works [8-11];

II - analytical determination of pressures perceived by the knife faces. When calculating the passive

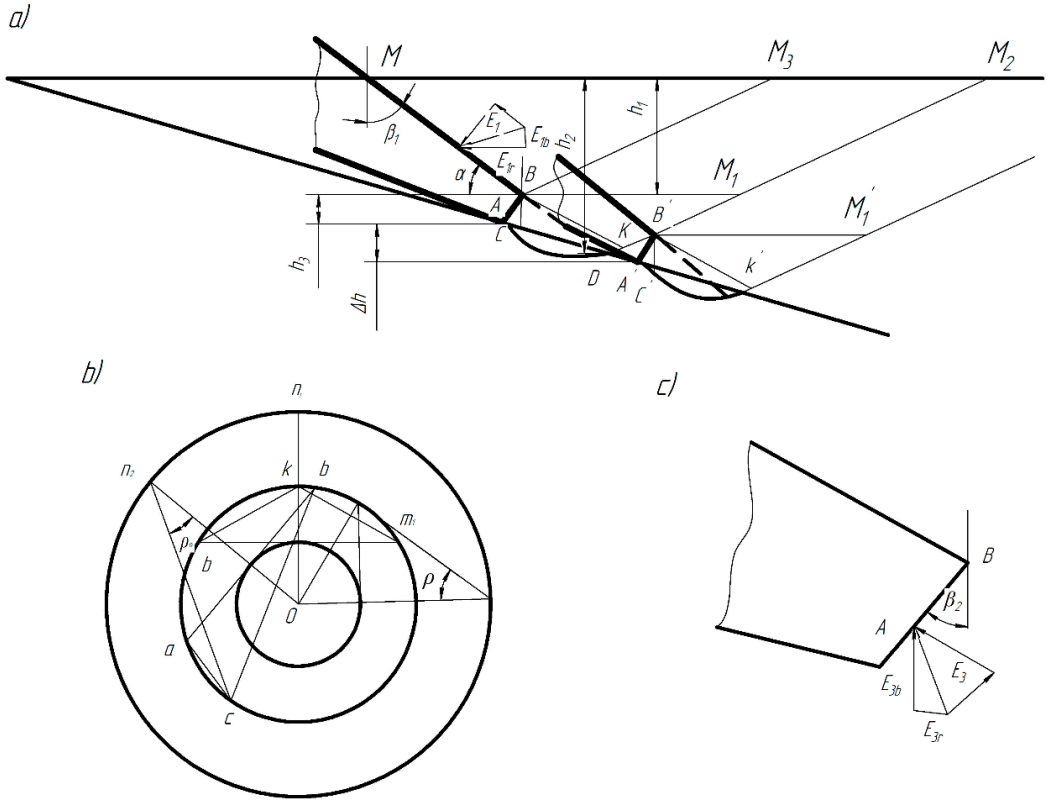

Figure 4 *Scheme for determining the resistances acting on the knife during burial: a - design scheme, b - system of characteristic circles, c - scheme of forces acting on edge AB*

ground pressure acting on the knife faces, one uses the method proposed in [5].

When the knife is buried in the ground, there is actually a resistance of the ground to cutting, since the amount of ground on the working body is insignificant and other resistances to digging are relatively small. To determine the total resistance of the knife penetration into the ground, it is necessary to determine the cutting resistance of each edge of the knife. The cutting resistance is first determined for a knife of a width of 1 m, without taking into account the resistance to chipping on the side edges [14-15].

The soil pressure on the *MB* face (Figure 4, a) is defined as the pressure of a loose body on the retaining wall, since the MM_3B soil prism was punched out earlier and now only its displacement is carried out.

The horizontal component of pressure on the *MB* face will be determined by the formula:

$$E_{1r} = M_1 K_1 \frac{\gamma h_1^2}{2}, \tag{7}$$

where M_1, K_1 – coefficient depending on the angle β_1 of *BM* face inclination to the vertical; γ - volumetric weight of soil; h_1 - digging depth at 1 position.

The vertical component is found by the formula:

$$E_{1B} = M_2 K_1 \frac{\gamma h_1^2}{2}, \tag{8}$$

where M_2 - coefficient depending on the angle β_1.

The values of the coefficients M_1, M_2, K_1 are determined depending on the angle β_1 of inclination of the *BM* face to the vertical [13].

To determine the pressure on the knife edge *AB*, the directions of the sliding surfaces are found by the characteristic circles (Figure 4, b), taking the horizontal plane drawn through point *B* as the ground surface.

The value of the final radius of the logarithmic spiral is determined by the formula:

$$\overline{BK} = \overline{BC} e^{\theta tg\rho}, \tag{9}$$

where θ - angle of *CBK*; *e* - base of natural logarithms.

The sliding plane KM_1 is extended up to the ground surface (point M_2). Three zones appear in the ground in front of the sloping face *AB*: BKM_1, *BKC*, *ABC*. The pressure on the face *AB* is determined in the following way. Due to the smallness of the protrusion prism KBM_1, without much damage to accuracy, the pressure on the face *BK* can be assumed to be approximately equal to the pressure on the plane *BD*, which is a continuation of the knife *BM*. The horizontal and vertical components of the pressure on the plane *BD* are defined as the difference of pressures on the faces *MD* and *MB*:

$$\begin{aligned} E'_{2r} &= M_1\left\{K_1\left[\frac{\gamma}{2}(h_2^2 - h_1^2) + ch_2 ctg\rho\right] - ch_2 ctg\rho\right\}, \\ E'_{2B} &= M_2\left\{K_1\left[\frac{\gamma}{2}(h_2^2 - h_1^2) + ch_2 ctg\rho\right] - ch_2 ctg\rho\right\}, \end{aligned} \tag{10}$$

where ρ - angle of internal ground friction; *c* - soil coefficient.

To obtain the required solution in closed form, the actions of the horizontal and vertical components E'_{2r} and E'_{2B} are transferred to the plane BM_1 and for that some corrections to the obtained values of the components had to be done. We subtract from the obtained values the mass of the prism BM_1D of the coupling force along the plane M_1D.

The horizontal component of the coupling force C_r is equal to:

$$C_r = \overline{DM}_1 c \cos\left(\frac{\pi}{4} - \frac{\rho}{2}\right). \tag{11}$$

The vertical component of the coupling force C_B is equal to

$$C_B = \overline{DM}_1 c \sin\left(\frac{\pi}{4} - \frac{\rho}{2}\right). \tag{12}$$

The mass of the prism BM_1D is equal to:

$$G_B = \frac{\overline{BM}_1 \gamma h_4}{2}, \tag{13}$$

where

$$\overline{BM}_1 = h_4\left[ctg\alpha + ctg\left(\frac{\pi}{4} - \frac{\rho}{2}\right)\right];\ \overline{DM}_1 = \frac{h_4}{\sin\left(\frac{\pi}{4} - \frac{\rho}{2}\right)};$$

$$h_4 = \frac{\overline{AB}\sin\alpha'\sin\alpha}{\cos\beta_1} e^{\theta_1 tg\rho};$$

$$\alpha'_1 = \frac{1}{2}\left[\frac{\pi}{2} + \rho + \rho_0 + \arcsin\frac{\sin\rho_0}{\sin\rho}\right];$$

$$\theta_1 = \frac{\pi}{2} - \frac{1}{2}\left[\frac{\pi}{2} + \rho - \rho_0 - ar\sin\frac{\sin\rho_0}{\sin\rho}\right],$$

where ρ_0 - angle of friction of the ground against the blade; α'_1 = *BAC* angle; θ = *CBD* angle.

The value of *AB* can be determined directly on the machine or set.

Finally, for the forces acting on the plane BM_1

$$E_{2r} = E'_{2r} - C_r; \qquad E_{2B} = E'_{2B} - C_B - G. \tag{14}$$

Then, the vertical uniformly distributed load acting on the plane BM_1 is equal to:

$$q = \frac{E_{2B}}{\overline{BM}_1}. \tag{15}$$

The pressure on the face *AB*, under conditions where the boundary of the bulk solid is a horizontal surface with a confinement of intensity q, can be defined in a closed form:

$$\begin{aligned} E_{3r} &= M_3\left\{K_2\left[\frac{\gamma h_3^2}{2} + qh_3 + Ch_3 ctg\rho\right] - Ch_3 ctg\rho\right\}; \\ E_{3B} &= M_4\left\{K_2\left[\frac{\gamma h_3^2}{2} + qh_3 + Ch_3 ctg\rho\right] - Ch_3 ctg\rho\right\}. \end{aligned} \tag{16}$$

The coefficients M_3, M_4, M_2 are determined depending on the angle β_2 of inclination of the face *AB*

to the vertical (Figure 4, c).

The distance between the two consecutive spalls h is defined as

$$h = \frac{\overline{BM_1}\sin\delta\sin\left(\frac{\pi}{4}-\frac{\rho}{2}\right)}{\sin\left(\delta+\frac{\pi}{4}-\frac{\rho}{2}\right)}, \quad (17)$$

where $\delta = arctg\frac{v_2}{v_1}$ - v_2 - implemented lowering speed; v_1 - forward speed of the machine.

The total cutting resistance by *MBA* edge at cutting width b:

$$W_p = (W_p' + W_p'')\cdot b, \quad (18)$$

where $W_p' = E_{1r}$ - cutting resistance by *BM* edge; $W_p'' = E_{3r} + E_{2r}$ - resistance to cutting with edge *AB*.

The additional vertical pressure on the blade required for stable penetration of the blade into the ground will be equal to:

$$\sum E_B = (E_{3B} - E_{1B})\cdot b. \quad (19)$$

When the bulldozer blade is embedded into the ground, while the machine is moving in front of the cutting blade, the ground is stressed only on one side, located in front of the blade in the direction of travel. Therefore, the resistance to the blade sinking when the machine is moving is smaller than when it is embedded in the ground when the machine is stationary. This allows the blade to be driven into the ground at lower cutting angles.

3 Results and discussions

The cutting angle determines the ratio of machine operating speeds and rational trajectories, but the study of the effect of the cutting angle cannot yet be considered complete. The authors measured the force separating the chip from the furrow wall with a sharp knife with a vertical cutting edge (such cutting is close to semi-free cutting) [8, 16-17].

Measurements were made in a soil channel (Figure 5) on medium loam with moisture content from 9.4 to 10.8% and density by statistical density meter from 13.1 to 13.2 N/cm. The width of the cut was equal from 165 to 178 mm, thickness - 100 and 50 mm. It was found that as the cutting angle changed from 20 to 38°, the cutting force increased by an average of 1.7% for each degree of increase in the cutting angle. When changing the cutting angle from 40 to 90°, the average increase in cutting force is 6% per degree.

The change of cutting force is not the same at different cutting angles. It decreases intensively with decreasing of cutting angle up to 35÷40°, but at cutting angle less than 35÷40° the intensity of its decrease slows down. According to some data, the dependence has a minimum in the area of small values of the cutting angle. The study of the considered dependence was carried out by means of dynamometric stands. The results of the experiments confirmed the general character of the dependence established by the previous studies. Decrease of cutting angle up to 35÷40° is accompanied by intensive decrease of cutting force for the majority of soils. With further reduction of the cutting angle the decrease of cutting force slows down, and for some soils (loam, weak sandstone when cutting along the layers, sulfur earth merilic clay) in the area of small values of the cutting angle the cutting force increased again.

The assumption of independence of cutting force from the cutting angle of the part of the cutting force that is spent on overcoming the resistance of the ground on the sides of the knife, allowed along with the conclusion and practical proportionality, to directly compare the measurement data on different soils and to obtain a general experimental picture of the effect of the cutting angle on the cutting force. Comparison of the experimental values of the blocked cutting force excluded a part of it, which is used to overcome the resistance of the soil on the sides of the knife at a given thickness of the cut, thus determining the part of the cutting force that depends on the cutting angle. This part of the cutting force at a cutting angle of 45° was taken as one, and its value at all other values of

Figure 5 *Stand for physical modeling of bulldozer working processes*

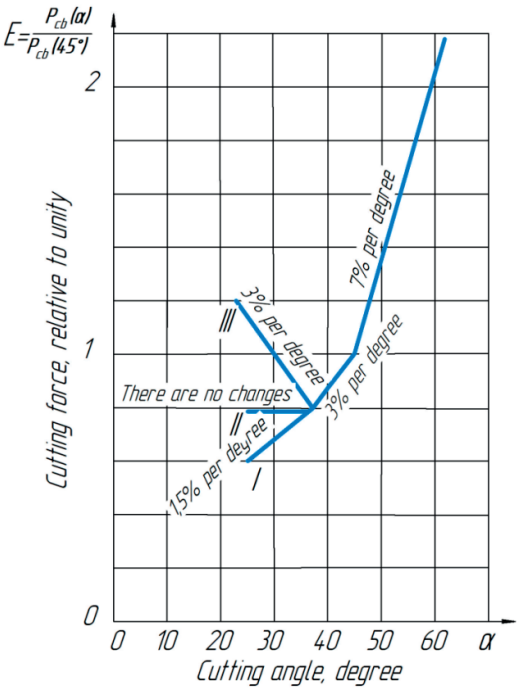

Figure 6 *Graph proposed for characterization of the frontal resistance force to the knife dependence on the cutting angle of soils: I - plastic clay soils; II - layered, cutting along layers; III - other sandy-clay soils*

cutting angle was determined in relation to this value. As a result of such an analysis, a graph (Figure 6) was obtained, proposed to characterize the changes in the part of the cutting force that goes to overcome the frontal resistance of the knife.

Based on the obtained data, it can be noted that at the cutting angle value over 45° there is an intensive change in the part of the cutting force, which goes to overcome the frontal resistance to the knife (on average 7% per degree of cutting angle, but in relation to the value at a cutting angle of 45°). In the cutting angle range 37÷30° the reduction of the mentioned part of the cutting force slows down. At further reduction of the cutting angle for some soils there is sometimes an increase in the soil resistance. Thus, when changing the cutting angle of the soil with the bulldozer attachment, it is necessary to provide the possibility of its reduction to 20÷30°.

Comparison of the results of mathematical modelling to the data of physical experiments confirmed the adequacy of the developed model to describe the process of burial of the bulldozer's working body into the soil. It was found that the model accurately reflects the nature of the dependence of the cutting force on the cutting angle, including the presence of the minimum force value at an angle of 35-40°, which coincides with the results of the bench tests. The obtained analytical expressions allow us to quantitatively evaluate the influence of kinematic and design parameters of the suspension of the working equipment on the change of the cutting angle and the corresponding force of interaction with the ground. Thus, the developed model can be used in engineering practice to optimize the design of working equipment and to select a rational blade trajectory minimizing the energy intensity of the cutting process.

4 Conclusions

In the course of the research, it has been established that the process of burrowing the bulldozer's working body into the ground is characterized by a one-sided stress state arising in front of the cutting blade along the machine's movement. This allows the blade to penetrate into the ground at lower values of the cutting angle, which contributes to reduction of the cutting resistance. The optimal trajectory of the blade movement from the energy point of view is recognized as such a trajectory of the blade movement, at which the cutting angle at the moment of penetration into the ground is maximum, with its subsequent reduction. The developed mathematical model adequately describes this process, confirming both qualitative and quantitative dependencies established in the course of physical experiments. In particular, the presence of minimum cutting resistance at cutting angle of 35-40° is confirmed, and the sensitivity of cutting force to changes in structural and kinematic parameters of the moldboard suspension is revealed. The model can be recommended for practical application in the design and optimization of bulldozer working equipment to improve its efficiency and reduce the energy consumption of earthmoving operations.

Acknowledgements

The authors received no financial support for the research, authorship and/or publication of this article.

Conflicts of interest

The authors declare that they have no known competing financial interests or personal relationships that could have appeared to influence the work reported in this paper.

References

[1] VOLKOV, D. P., KRIKUN, V. Y., TOTOLIN, P. E., GAEVSKAYA, K. S. *Machines for earthworks.* Moscow: Mechanical Engineering, 1992. ISBN 5-217-01973-5.

[2] DOTSENKO, A. I., KARASEV, G. N., KUSTAREV, G. V., SHESTOPALOV, K. K. *Machines for earthworks.* Moscow: Bastet, 2012. ISBN 978-5-903178-28-5.

[3] LUKASHUK, O. A., KOMISSAROV, A. P., LETNEV, K. Y. *Machines for soil development. Design and calculation*. Ekaterinburg: Ural University Publishing House, 2018. ISBN 978-5-7996-2386-9.

[4] FEDOROV, D. I. *Working bodies of earth-moving machines*. Moscow: Mechanical Engineering, 1977. ISBN 5-217-00490-8.

[5] BALOVNEV, V. I. *Modelling of interaction processes with the environment of working bodies of road construction machines*. Moscow: Higher School, 1981, ISBN 5-217-02343-0.

[6] DOVGYALO, V. A., BOCHKAREV, D. I. *Road construction machines. Part I: Machines for earthworks.* Gomel: Belarusian state University of Transport, 2010. ISBN 978-985-468-741-4.

[7] SHERBAKOV, A. P., PUSHKAREV, A. E., MAKSIMOV, S. E. Replacement working body material as a way to increase reliability of road construction machines. *The Russian Automobile and Highway Industry Journal* [online]. 2021, **18**(6), p. 646-661. ISSN 2658-5626. Available from: https://doi.org/10.26518/2071-7296-2021-18-6-646-661

[8] KOZBAGAROV, R. A., ZHUSSUPOV, K. A., KALIYEV, E. B., YESSENGALIYEV, M. N., KOCHETKOV, A. V., KAMZANOV, N. C. Development of control suspension of attachment of a bulldozer. *News of the National Academy of Sciences of the Republic of Kazakhstan, Series of Geology and Technical Sciences* [online]. 2020, **4**(442), p. 166-174. ISSN 2224-5278, eISSN 2518-170X. Available from: https://doi.org/10.32014/2020.2518-170X.97

[9] GUO, Z., DU, G., LI, Z., LI, X. Orthogonal experiment on resistance reduction by soil-engaging surfaces of bulldozer blade. *Nongye Jixie Xuebao / Transactions of the Chinese Society of Agricultural Machinery* [online]. 2015, **46**(7), p. 372-378. ISSN 1000-1298. Available from: https://doi.org/10.6041/j.issn.1000-1298.2015.07.053

[10] KOZBAGAROV, R., AMANOVA, M., KAMZANOV, N., BIMAGAMBETOVA, L., IMANGALIYEVA A. Investigation of wear of cutting part of polygonal knife car graders in different ground conditions. *Communications - Scientific Letters of the University of Zilina* [online]. 2022, **24**(4), p. D229-D238. ISSN 2585-7878, eISSN1335-4205. Available from: https://doi.org/10.26552/com.C.2022.4.D229-D238

[11] KOZBAGAROV, R., KAMZANOV, N., AMANOVA, M. BAIKENZHEYEVA, A., NAIMANOVA, G. Justification of the cam roller parameters for destruction of the road coatings for obtaining the lumpy asphalt scrap. *Communications - Scientific Letters of the University of Zilina* [online]. 2023, **25**(2), p. 103-1097. ISSN 2585-7878, eISSN 1335-4205. Available from: https://doi.org/10.26552/com.C.2023.028

[12] TROYANOVSKAYA, I., GREBENSHCHIKOVA, O. Optimization of technical productivity of a bulldozer unit in terms of traction and speed parameter. *The Russian Automobile and Highway Industry Journal* [online]. 2025, **21**(6), p. 844-851. ISSN 2071-7296, eISSN 2658-5626. Available from: https://doi.org/10.26518/2071-7296-2024-21-6-844-8517

[13] AUKENOVA, B., RADENKOV, R., SAVELIEV, A., DOUDKIN, M. Investigation of the Interaction Process with the Environment of a Bulldozer Bladow with Variable Geometry. *Trudy Universiteta / Proceedings of the University* [online]. 2023, **2**(91), p. 67-73. ISSN 1609-1825, eISSN 2710-3382. Available from: https://doi.org/10.52209/1609-1825_2023_2_67

[14] MIAO, CH. Modeling and simulation research on the hydraulic system of the blade of an unmanned bulldozer. *Frontiers in Computing and Intelligent Systems* [online]. 2025, **11**(2), p.78-82. ISSN 2832-6024. Available from: https://doi.org/10.54097/n8pphn83

[15] YULIUS, M., NURBAITI, SARMIDI, MUHAMMAD, I. G. Usage Procedure of Liebherr 756 Bulldozer Unit in Live Stockpile OPB 4 PT Bukit Asam Tbk / Prosedur penggunaan unit bulldozer liebherr 756 di live stockpile OPB 4 PT. Bukit Asam, Tbk (in Indonesian). *Jurnal Ilmiah Teknik dan Sains / Scientific Journal of Engineering and Science* [online]. 2025, **2**(1), p. 117-123. eISSN 3025-8871. Available from: https://doi.org/10.62278/jits.v2i1.50

[16] AKANKSHA, M., VIKAS, K. S., SHIVAM, VIPUL, C. A comprehensive review of bulldozers in modern construction. *Journal of Scientific Research and Reports* [online]. 2024, **30**(5), p. 337-342. ISSN 2320-0227 Available from: https://doi.org/10.9734/JSRR/2024/v30i51949

[17] SHARMA, D., BARAKAT, N. Evolutionary bi-objective optimization for bulldozer and its blade in soil cutting. *Journal of The Institution of Engineers (India): Series C* [online]. 2019, **100**(2), p. 295-310. ISSN 2250-0545, eISSN 2250-0553. Available from: https://doi.org/10.1007/s40032-017-0437-z

DETERMINATION OF THE OPTIMUM COMBINATION OF PARAMETERS OF SPECIALIZED BLADES FOR THE SHANTUI SD 32 BULLDOZER WHEN MOVING LOW-DENSITY MATERIALS

Tavbay Khankelov[1,*], Maloxat Abdukadirova[2], Otabek Ochildiev[3], Zebo Alimova[4], Gulxayo Niyazova[4], Anvar Kadirov[5]

[1]Department of Engineering of Technological Machines, Tashkent State Transport University (TSTU), Tashkent, Uzbekistan
[2]Department of Ecology and Water Resources Management, Tashkent Institute of Irrigation and Agricultural Mechanization Engineers, National Research University, Tashkent, Uzbekistan
[3]Departments of Health, Safety and Environment, Termez Institute of Engineering and Technology, Termez, Uzbekistan
[4]Department of Transport Power Plants, Tashkent State Transport University (TSTU), Tashkent, Uzbekistan
[5]Department of Applied Mechanics, Tashkent State Transport University (TSTU), Tashkent, Uzbekistan

*E-mail of corresponding author: xankelovt9@gmail.com

Tavbay Khankelov 0000-0002-4653-4679,
Otabek Ochidiev 0000-0002-9573-5979,
Gulxayo Niyazova 0009-0008-8673-0560,
Maloxat Abdukadirova 0000-0003-1188-2662,
Zebo Alimova 0000-0002-6711-5318,
Anvar Kadirov 0000-0002-9773-7249

Resume
Recommendations are given on combinations of parameters of box-shaped and "dump" types of dumps for the SHANTUI SD 32 bulldozer, which provide the highest technical characteristics of the bulldozer when moving low-density materials. The optimal dimensions of a box blade for equipping the SHANTUI SD32 bulldozer are a grasp width of up to 3730 mm, radius of curvature of up to 1700 mm, width of the cutting edge of up to 460 mm, canopy width of up to 140 mm, flap length of up to 860 mm. The optimal dimensions of a "landfill" blade for equipping the SHANTUI SD32 bulldozer are a grasp width of up to 3900 mm, radius of curvature of up to 460 mm, width of the cutting edge of up to 124 mm, canopy width of up to 610 mm.

Article info
Received 10 February 2025
Accepted 14 April 2025
Online 10 June 2025

Keywords:
dozing prism
technical performance
box blade
"landfill" blade
material
efficiency,
optimization

ISSN 1335-4205 (print version)
ISSN 2585-7878 (online version)

Available online: https://doi.org/10.26552/com.C.2025.042

1 Introduction

Bulldozers are widely used in construction. Currently, there are about as many of them in operation as there are excavators. Bulldozers account for about 35-40% of the total volume of earthworks performed in construction. Bulldozers work in road-building, reclamation, irrigation, construction, and in quarries of the mining industry. They carry out leveling work, constructing road and railway embankments from lateral reserves, transporting soil over a distance of up to 100 m, digging canals and pits, filling trenches and holes, clearing roads and construction sites of snow, felling trees and uprooting stumps. They are used as pushers when working with scrapers [1]. It is known that there are materials (snow, wood chips, coal, etc.), which in some cases are most convenient to move with bulldozers, but the capacities of blades designed for working with soils do not ensure full use of the machine traction and power. For such situations, bulldozer blades of high capacity were developed, called specialized blades. For this study, the term "specialized blades" refers to bulldozer blade-type working bodies of high capacity, for which the large-scale excavation is neither the only nor primary nor the preferred area of application. These include [2]: U-dozer blades for moving light materials, box blades for moving light, bulk, liquefied and coarse materials, "landfill" blades for moving household waste. The work is devoted to finding the optimal combination of blade parameters for the SHANTUI SD 32 bulldozer. Mathematical modelling of the working process of a bulldozer was taken as

a research method, and the technical performance of the bulldozer was chosen as a criterion for the quality of blade parameters, providing a reliable assessment of the results of parametric synthesis of blades [3].

2 Literature sources review and problem statement

Many structural, technological, and ergonomic factors influence the performance of a bulldozer. In addition, some researchers in their works also take into account the position that with the maximum set of the soil drag prism in front of the dump, its area of contact with the frontal surface is determined by the position of the dump in the cross section determined by the chip formation trajectory of the soil layer [4]. For example, in [5-7], the issues of the influence of the cutters' design and the properties of materials on the performance of a bulldozer were studied, and losses from the dozing prism were taken into account only by introducing a loss factor. In [8-10], formulas for determining the productivity consider not only the design but the technological parameters of a bulldozer, as well. It should be noted that some publications [11-15] also take into account the driver's qualifications by introducing a correction factor. Issues related to the calculation of the main parameters of earth-moving machines are addressed in [16-19]. References [20-23] take into account the influence of developed areas' properties on the efficiency of the digging, leveling, and transportation processes. Currently, a large number of studies [24-31] are devoted to the issues of automation of work processes, unmanned control of earthmoving equipment, and the influence of unmanned control on the efficiency of machines. Despite the numerous studies aimed at determining the performance of a bulldozer, the issues of considering the losses of transported materials from the dozing prism and choosing the optimal combination of bulldozer blades based on the properties of the transported materials, are relevant.

3 Purpose and objectives of the study

In the structure of generalized indices assessing the efficiency of the road-building machines (mainly, energy and mass indices), productivity occupies a special place. Performance evaluation provides a basis for assessing the suitability of a machine for its functional purpose. To find the optimal combination of parameters of box and "landfill" types of blades for the SHANTUI SD 32 bulldozer when developing various materials of reduced density and cohesion that provide the greatest technical performance. To achieve this goal, the following tasks were solved:

- establishing the patterns of the processes of prism formation, considering their discrete phases;
- development of a mathematical model of the performance of a bulldozer equipped with any type of blade, considering the losses from the dozing prism;
- classification and quantitative description of probable production situations;
- development of recommendations for combinations of parameters of the box and "landfill" types of blades for the SHANTUI SD 32 bulldozer.

3.1 The process of prism formation considering the losses

For this study, the maximum volume of material that can be removed by a blade is considered as the blade capacity.

Analysis of the relationships proposed in [4-12] for determining the capacity of the blade made it possibly to conclude [18] that the formula proposed by Balovnev et al. [1] and the model proposed by Karasev et al. [19,] are the closest to the generally accepted concepts about the mechanism of prism formation, experimental data and the objectives of this study. The disadvantage of the former is that it describes the maximum volume of the dozing prism, while, in reality, the performance of the bulldozer depends on the level of losses from the dozing prism during its formation and movement. Below is outlined the methodology for considering such losses when calculating the dozing capacity.

4 Materials and methods

It is accepted that the material being moved can either be stored in heaps or presented as a layer along the ground line.

When moving a pile (a heap) of material, losses begin from the time when the entire volume of material captured by the blade begins to move along the ground line, i.e. when the formation of the dozing prism is completed. Here:

$$Q = Q_{\max}, \tag{1}$$

where Q is the dozing capacity, m^3; Q_{max} is the maximum value of the dozing capacity, m^3.

The current value of the dozing capacity is

$$Q_i = Q_{i-1} + dQ, \tag{2}$$

where Q_i is the dozing capacity Q at the end of the i-th section of the bulldozer path of dl_t length, m^3; Q_{i-1} is the dozing capacity Q at the beginning of the i-th section of the bulldozer path of length dl_t, m^3; dQ is the capacity of loosened material entering the dozing prism on the i-th section of the bulldozer path of length dl_t, m^3.

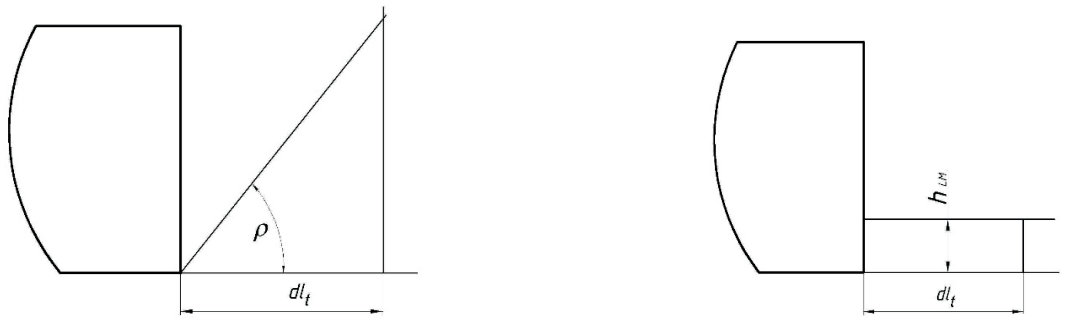

a) b)

Figure 1 *Volume of material entering the dozing prism: a) when collecting from a heap; b) during the layered cutting, where ρ is the angle of natural repose of material; dl_t is the incremental step length of the bulldozer path, mm; h_{LM} is the thickness of the layer of material cut by the blade, mm*

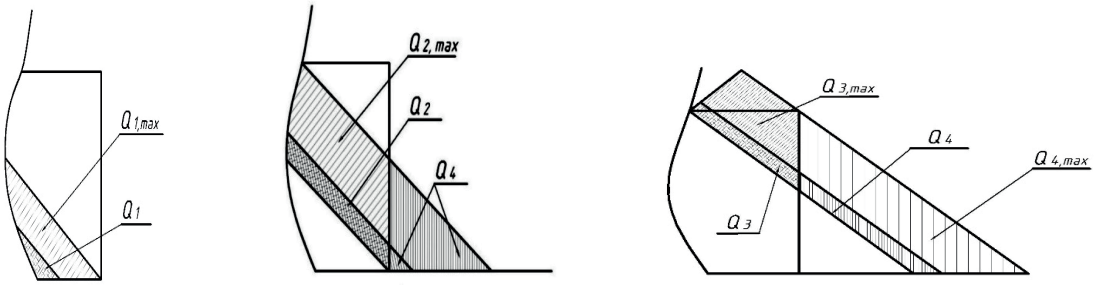

a) b) c)

Figure 2 *Phases of dozing prism formation: a) 1st phase; b) 2nd phase; c) 3rd phase*

$$dQ = (i - 0.5) \cdot dl_t^2 \cdot tg\rho \cdot L \cdot f_r\text{, (Figure1),} \quad (3)$$

where dl_t is the incremental step length of the bulldozer, m; $(i - 0.5)$ is the represents a coefficient that determines the amount of material entering the drag prism; $tg\rho$ is the tangent of the angle of inclination of the drag prism; ρ is the angle of natural repose of the material, degree; L is the grasp width of the blade, m; f_r is the loosening coefficient of the material. The volume of material entering the dozing prism is shown in Figure 1.

When forming a dozing prism from a layer of material, it is assumed that the process goes through three phases (Figure 2).

Phase 1 - the dozing prism grows from zero to capacity $Q_{1,max}$ due to the growth of component Q_1. (Figure 2, a); there are no losses from the dozing prism;

Phase 2 - the dozing prism grows from capacity $Q_{1,max}$ to $(Q_{1,max} + Q_{2,max} + Q_4)$ due to the growth of components Q_2 and Q_4 (Figure 2, b); the volume of losses is proportional to capacity Q_4;

Phase 3 – the dozing prism grows from capacity $(Q_{1,max} + Q_{2,max} + Q_4)$ to due to the growth of components Q_3 and Q_4 (Figure 2, c); the volume of losses is proportional to capacity Q_4; where Q_1,Q_2,Q_3,Q_4 are the components of the dozing prism, m^3; $Q_{1,max},Q_{2,max},Q_{3,max},Q_{4,max}$ are the maximum values of capacities Q_1,Q_2,Q_3,Q_4 respectively.

The phase ends with the end of the growth of the dozing prism. For the current value of dozing capacity Q, the following is true:

$$Q_i = Q_{i-1} + dQ - Q_L\text{,} \quad (4)$$

(Figure 1, b): Q_L is the volume of losses on the i-th section of the bulldozer path of dl_t, m^3 long.

$$dQ = h_{LM} \cdot L \cdot dl_t \cdot f_r\text{,} \quad (5)$$

where f_r is the loosening coefficient of the material.

The proportionality of losses to the part of dozing capacity that is not limited on the sides by the blade flaps (Q_4 in Figure 2) is expressed by the following formula:

$$Q_L = Q_4 \cdot K_L \cdot dl_t\text{,} \quad (6)$$

where K_L is the loss coefficient from the dozing prism. Thus, the task of considering losses from a dozing prism when calculating its capacity comes down to determining the value of Q_4 in discrete sections of the bulldozer path from the point of the beginning of prism formation to the point of its completion. Along this path, the pattern of the volume formation process will change at points (Figure 2) corresponding to the following boundary conditions:

$$Q_1 = Q_{1,\max} \quad (7)$$

is the beginning of the process of Q_4 formation (volume Q_4 forms as soon as Q_1 reaches its maximum value,

$$Q_2 = Q_{2,\max} \tag{8}$$

is the change in the pattern of Q_4 formation (pattern of Q_4 formation changes as soon as Q_2 reaches its maximum value),

$$Q_3 = Q_{3,\max} \tag{9}$$

is the end of the dozing prism growth process (the dozing prism growth stops as soon as Q_3 reaches its maximum value).

Another condition for stopping the growth of the dozing prism is that the losses are equal to the volume of material entering the blade:

$$Q_L = dQ. \tag{10}$$

Moreover, the condition in Equation (10) takes precedence over condition in Equation (9), because when it occurs, the growth of the dozing prism stops, although Q_3 has not yet reached its maximum value.

4.1 Dozing capacity considering the losses

According to the accepted assumptions and corresponding boundary conditions in Equations (7)-(10), design schemes shown in Figures 3-6 were taken for calculating capacities Q_1, $Q_{1,max}$, Q_2, $Q_{2,max}$, Q_3, $Q_{3,max}$, Q_4 and $Q_{4,max}$. To simplify the analysis, the cylindrical surfaces of the blade sections were replaced by vertical planes. In the final determination of the dozing capacity, the allowed error was corrected by adding to the prism the capacity proportional to the part of the segment formed by the surface of the blade and the vertical plane (Figure 3).

$$Q_{me} = (F_1 + F_2)[L + 2W(1 - \cos\mu)], \tag{11}$$

$$F_1 = 0.5R^2(\alpha - \sin\alpha), \tag{12}$$

$$F_1 = \frac{H}{2}\sqrt{\begin{bmatrix}2(1-\cos\alpha)+\\ +k_a^2 + 2k_a \cdot \sin\alpha\end{bmatrix}R^2 - H_0^2}, \tag{13}$$

$$H_0 = H/[1 + k_b \cdot \sin(\alpha + \gamma + \delta)], \tag{14}$$

where F_1, F_2 are the cross-sectional areas of cylindrical segments, m^2; R is the radius of curvature of the cross profile of the blade, m; H is the height of the blade with a canopy, m; k_α is the ratio of the width of the cutting edge to the radius of curvature; k_b is the ratio of the width of the canopy to the radius of curvature; H_0 is the height of the blade without canopy, m.

Checking the fulfillment of condition in Equation (7) involves calculating the maximum capacity value (Figure 4).

$$Q_{1,\max} = W^2 \sin^2\mu \cdot tg\beta\begin{bmatrix}(L - 2W\cos\mu)/\\ 2 + (2W\sin\mu/3)\end{bmatrix} \tag{15}$$

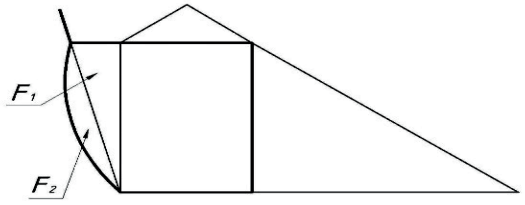

Figure 3 *Additional volume formed by the curvature of the blade and its digging angle inclination*

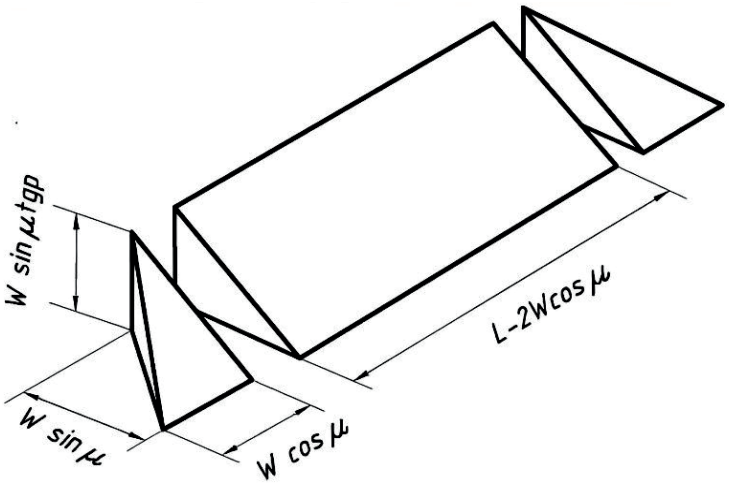

Figure 4. *Scheme for calculating the volume of a drawing prism at the end of the 1st phase of its growth*

In the second phase of filling the blade, the dozing prism grows due to Q_2 and Q_4 related by the following equation:

$$Q_{2,i} + Q_{4,i} = Q_{2,(i-1)} + Q_{4,(i-1)} + dQ\,. \tag{16}$$

From which follows:

$$dQ_2 + dQ_4 = dQ\,, \tag{17}$$

$$dQ_2 = Q_{2,i} - Q_{2,(i-1)}\,, \tag{18}$$

$$dQ_4 = Q_{4,i} - Q_{4,(i-1)}\,, \tag{19}$$

From the design diagram (Figure 5), it follows that:

$$dQ_2 = W\sin\mu(L - W\cos\mu)dz_2\,, \tag{20}$$

$$dQ_4 = L \cdot dz_2 \cdot (2z_2 + dz_2)/2tg\rho\,, \tag{21}$$

$$dz_2 = \left[-c_2 + \sqrt{(c_2^2 + 4b_2 dQ)}\right]/2b_2 \tag{22}$$

$$b_2 = L/2tg\rho\,, \tag{23}$$

$$c_2 = (L - W\cos\mu)W\sin\mu + z_2 L/tg\rho\,, \tag{24}$$

$$z_{2,i} = z_{2,(i-1)} + dz_2\,, \tag{25}$$

where dz_2 is the projection of the layer thickness dQ_2 onto the OZ vertical axis; z_2 is the projection of the layer thickness Q_2 onto the OZ vertical axis.

Q_2 and Q_4 are calculated by the following formulas:

$$Q_{2i} = Q_{2(i-1)} + dQ_2\,, \tag{26}$$

$$Q_{4,i} = Q_{4(i-1)} + dQ_4\,. \tag{27}$$

Checking condition is

$$Q_2 \le Q_{2,\max}\,, \tag{28}$$

where:

$$Q_{2,\max} = (H - W\sin\mu tg\rho)\cdot W \cdot \cdot \sin\mu \cdot (L - W\cos\mu), \tag{29}$$

In the third phase of filling the blade, the dozing prism increases due to Q_3 and Q_4 (Figure 2, c), related by:

$$Q_{3,i} + Q_{4,i} = Q_{3(i-1)} + Q_{4(i-1)} + dQ\,. \tag{30}$$

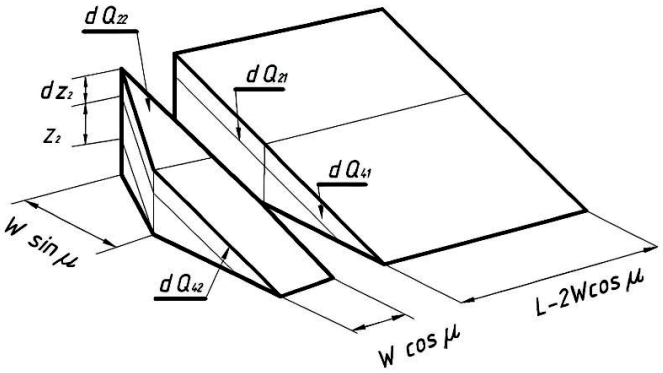

Figure 5 *Scheme for calculating the capacities that determine the growth of the dozing prism in the second phase*

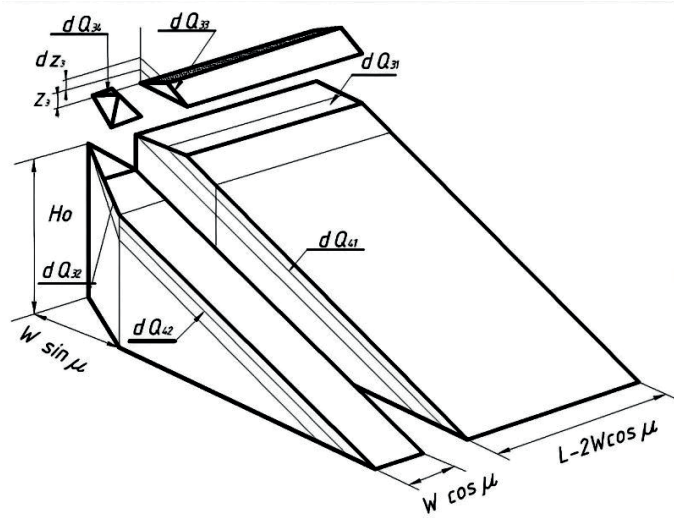

Figure 6 *Scheme for calculating the capacities that determine the growth of the dozing prism in the third phase*

From which follows:

$$dQ_3 + dQ_4 = dQ\,, \tag{31}$$

$$dQ_3 = Q_{3,i} - Q_{3(i-1)}\,, \tag{32}$$

$$dQ_4 = Q_{4,i} - Q_{4(i-1)}\,. \tag{33}$$

Calculation schemes of the capacities that determine the growth of dozing prisms in the second and third phases are shown in Figures 5 and 6.

From the calculation scheme in Figure 6, it follows that

$$dQ_3 = a_3 dz_3^3 + (b_3 - L/2tg\rho)dz_3^2 + \\ +(c_3 - L(z_2 + z_3)/)dz_3, \tag{34}$$

$$dQ_4 = (L/2tg\rho)dz_3^2 + (L(z_2 + z_3)/tg\rho)dz_3\,. \tag{35}$$

The value of dz_3 is found from the following equation:

$$a_3 dz_3^3 + b_3 dz_3^2 + c_3 dz_3 = dQ\,, \tag{36}$$

$$a_3 = -1/(6tg^2\rho tg\mu)\,, \tag{37}$$

$$b_3 = z_3/(2tg^2\rho \cdot tg\mu) + (L - 2W\cos\mu)\cdot \\ \cdot z_3/(2tg\rho) + L/2tg\rho, \tag{38}$$

$$c_3 = z_3^2/2tg^2\rho \cdot tg\mu + (L - 2W\cos\mu)z_3/2tg\rho + \\ +(L - 2W\cos\mu)z_3/2tg\rho + (L - 2W\cos\mu)\times \\ \times W\sin\mu + L(z_2 + z_3)/tg\rho \tag{39}$$

$$z_{3,i} = z_{3(i-1)} + dz_3\,, \tag{40}$$

Q_3 and Q_4 are calculated by the following formulas:

$$Q_{3,i} = Q_{3(i-1)} + dQ_3\,, \tag{41}$$

$$Q_{4,i} = Q_{4(i-1)} + dQ_4\,, \tag{42}$$

checking conditions are

$$Q_3 \le Q_{3,\max} \text{ and } Q_4 \le Q_{4,\max}\,, \tag{43}$$

where:

$$Q_{3,\max} = (W\sin^2\mu)tg\rho(3L - 4W\cos\mu)/4\,, \tag{44}$$

$$Q_{4,\max} = H_0^2 L/2tg\rho\,, \tag{45}$$

For the path traveled by the blade, at any point in the current section it is equal to

$$l_{t,i} = l_{t,(i-1)} + dl_t\,, \tag{46}$$

4.2 Nomenclature and characteristics of the removed materials

In accordance with the technical specifications, the materials for which specialized blades are intended to be processed include packed snow, municipal solid waste, liquefied soil, wood chips. Physical properties of these materials, characterizing them as removed media and ground line, were established by analysis of literary sources [21-24] and are summarized in Table 1.

4.3 Technological options for performing work with specialized blades

Analysis of probable options for using specialized blades made it possible to classify and quantitatively describe several cases characterized by a standard set of parameters:

1. Moving the heap without cutting and without distributing it at the end of the passage.
2. Moving the heap with cutting, without distributing it as a layer at the end of the passage.

Table 1 *Physical properties of materials*

Properties of materials	Packed snow	Municipal waste	Liquified soil	Wood chips
Cohesion index*	1	1	2	1
Coefficients:				
Metal friction	0.06	0.55	0.13	0.4
Material friction	0.51	1.00	0.18	1.05
Loosening the material	1.2	1.4	1.0	1.2
Resistance to motion	0.1	0.12	0.1	0.12
a_u	0.05	0.05	0.05	0.05
b_u	1.76	1.76	1.76	1.76
n	12	8	12	8
Cutting resistance, kN/m^2	21.6	20.0	17.8	30.0
Angle of repose, degrees	60	55	10	50
Volumetric mass, t/m^3	0.40	0.43	1.8	0.35

*1- cohesive material, 2- non-cohesive material

3. Moving the heap without cutting, distributing it as a layer at the end of the passage.
4. Collecting a dozing prism by cutting without distributing it as a layer at the end of the passage.
5. Collecting a dozing prism by cutting, distributing it as a layer at the end of the passage.
6. Moving the heap without cutting, distributing it along the length of the passage.

The values of parameters characterizing technological options for using specialized blades are given in Table 2.

5 Results

5.1. Bulldozer performance when calculating blade capacity using the T. Khankelov model

Below tables 3, 4, 5 and 6 present the results of calculations of bulldozers' performance equipped with specialized blades Straight blade, Half U-dozer, U-dozer, Box-blade, Landfill blade when developing the following materials, such as Packed snow, Municipal solid waste, Liquefied soil, Wood chips for the main technological variants of works presented in paragraph 4.3.

Table 2 *Characteristics of technological options*

Properties characterizing the option	Technological option					
	1	2	3	4	5	6
Allowable maximum slipping, %	100	100	100	100	100	100
Thickness of the material layer to be removed, m	0.0	0.2	0.2	0.2	0.2	0.0
Layer of leveling material, m	0.0	0.3	0.3	0.0	0.3	0.3
Total length of the machine's working stroke, m	80	80	80	80	80	80
Time for auxiliary operations, s	26	26	26	26	26	26
Blade position at*:						
collection	2	2	2	3	3	2
displacement	2	3	3	3	3	3
unloading	0	0	1	0	1	1

*0 - no operation, 1 - the blade does not touch the surface, 2 - the blade is in a "floating" position, 3 - the blade is pressed to the surface

Table 3 *Bulldozer capacity for packed snow, m^3/h*

Technology option number	1	2	3	4	5	6
Straight blade	232	208	207	203	202	233
Half U-dozer	236	208	206	201	208	242
U-dozer	240	207	211	199	200	238
Box blade	225	210	210	202	205	233
Landfill blade	362	315	313	317	317	371

Table 4 *Bulldozer capacity for municipal solid waste, m^3/h*

Technology option number	1	2	3	4	5	6
Straight blade	223	192	191	192	198	224
Half U-dozer	221	195	192	199	197	221
U-dozer	225	195	192	197	197	220
Box blade	226	194	197	194	194	221
Landfill blade	312	279	273	275	279	323

Table 5 *Bulldozer capacity for liquefied soil, m^3/h*

Technology option number	1	2	3	4	5	6
Straight blade	622	598	609	569	594	624
Half U-dozer	621	598	601	558	618	633
U-dozer	615	613	611	568	588	617
Box blade	615	620	612	576	605	633
Landfill blade	363	331	329	322	329	365

Table 7 presents the results of calculations of 6-hour and 48-hour total output of bulldozers equipped with specialized blades Straight blade, Half U-dozer, U-dozer, Box-blade, Landfill blade at the development of the above-mentioned materials under the main technological options.

5.2. Bulldozer performance when calculating blade capacity according to G. N. Karasev

Tables 8, 9, 10 and 11 below present the results of calculations of bulldozer productivity of bulldozers equipped with specialized blades Straight blade, Half U-dozer, U-dozer, Box-blade, Landfill blade when developing the following materials Packed snow, Municipal solid waste, Liquefied soil, Wood chips for the main technological variants of works presented in section 4.3.

Table 12 presents the results of calculations of 6-hour and 48-hour total output of bulldozers equipped with specialized blades Straight blade, Half U-dozer, U-dozer, Box-blade, Landfill blade at development of the above-mentioned materials under the main technological variants.

6 Discussion of results

By assuming an equal probability of bulldozer operation under different operating conditions, it is possible to compare blades in terms of their total output. The total output for 6 hours (Tables 7 and 12) is the sum of the hourly productivity of the bulldozer, calculated for one material and each of the 6 technological options. For example, number 1285 in Table 7 (straight blade, material No. 1) is the sum of numbers from the "straight blade" line of Table 3 (packed snow).

Table 6 *Bulldozer capacity for wood chips, m^3/h*

Technology option number	1	2	3	4	5	6
Straight blade	259	216	214	213	218	252
Half U-dozer	253	216	217	212	215	254
U-dozer	253	214	219	208	216	252
Box blade	255	217	216	209	217	250
Landfill blade	356	304	304	306	307	369

Table 7 *Total output, m^3*

In 6 hours					
Number of material	1	2	3	4	In 48 hours
Blades:	1285	1220	3616	1372	7493
Straight					
Half U-dozer	1301	1225	3629	1367	7522
U-dozer	1295	1228	3612	1362	7497
Box	1285	1226	3661	1364	7536
Landfill	1995	1741	2039	1946	7721

Table 8 *Bulldozer capacity for packed snow, m^3/h*

Technology option number	1	2	3	4	5	6
Straight blade m3/h	286	247	246	247	250	288
Half U-dozer, m3/h	283	250	251	247	251	280
U-dozer, m3/h	277	245	246	240	243	281
Box blade, m3/h	282	250	251	243	246	284
Landfill blade, m3/h	492	445	450	438	441	491

Table 9 *Bulldozer capacity for municipal solid waste, m^3/h*

Technology option number	1	2	3	4	5	6
Straight blade m3/h	278	250	249	247	244	278
Half U-dozer, m3/h	278	253	254	244	252	272
U-dozer, m3/h	273	252	248	244	253	275
Box blade, m3/h	274	255	252	249	252	284
Landfill blade, m3/h	424	389	399	380	392	430

Table 10 *Bulldozer capacity for liquefied soil, m^3/h*

Technology option number	1	2	3	4	5	6
Straight blade m3/h	785	961	952	734	955	990
Half U-dozer, m3/h	785	956	967	735	962	999
U-dozer, m3/h	784	964	948	736	960	998
Box blade, m3/h	785	962	957	733	954	994
Landfill blade, m3/h	779	965	959	736	954	918

Table 11 *Bulldozer capacity for wood chips, m^3/h*

Technology option number	1	2	3	4	5	6
Straight blade m3/h	334	285	285	279	285	336
Half U-dozer, m3/h	337	291	284	288	279	291
U-dozer, m3/h	336	291	287	276	283	340
Box blade, m3/h	332	284	290	281	289	341
Landfill blade, m3/h	507	473	488	452	475	518

Table 12 *Total output, m^3*

	In 6 hours				
Number of material	1	2	3	4	In 48 hours
Blades: Straight	1564	1546	5377	1804	9291
Half U-dozer	1562	1553	5404	1770	10289
U-dozer	1532	1545	5390	1813	9280
Box	1980	1566	5385	1817	9748
Landfill	2757	2414	4352	2913	12436

The total output for 6 hours indicates that regardless of operating conditions (except for liquefied soil) and the method of calculating the blade capacity, the best performance for a bulldozer is provided by a straight blade with an enlarged lattice canopy (the so-called "landfill"). When working with liquefied soil, the greatest productivity is achieved using a box blade.

The total output for 48 hours (i.e., the sum of the hourly productivity of the bulldozer for all materials and for all technological options), assuming the equal probability of the bulldozer operation with any materials according to any technological options, indicates (see Tables 7 and 12) that the greatest efficiency can be expected from a bulldozer equipped with a "landfill" type of a blade. The next largest total output, which is 16-24% less (depending on the method of calculating the blade capacity) is provided by a box blade. The outputs of straight, half U-dozer, and U-dozer blades differ slightly (by 0.2% regardless of the method of calculating the blade capacity), which indicates their approximately equal efficiency under the operating conditions considered. Thus, we can conclude that given the equal probability of the considered operating conditions, the greatest efficiency is ensured by equipping the bulldozer with a "landfill" type of blade, and when operating predominantly with liquefied soil, cement concrete mortars, and other such materials, the greatest efficiency is ensured by a box blade.

The feasibility of installing one of the two types of blades on a bulldozer is determined by the probability of its operating on a particular material since the total output of a bulldozer over a fixed time is a probabilistic value:

$$C_{48} = \sum (C_{6i} \cdot p_i), \tag{47}$$

where C_{48} is the total output of the bulldozer in 48 hours using all materials and all technological options, m^3; C_{6i} is the total output of the bulldozer for 6 hours on the i-th material for all technological options, m^3; p_i is the probability of the bulldozer operating on the i-th material; i is the number of the material for which the output is calculated.

If we assume an equal probability of bulldozer operation for any technological options on any material (except the liquefied soil), then from the data in Tables 3, 7, and 12, it follows that the box blade and the "landfill" blade provide the same total output of the bulldozer; while for its operation on liquefied soil (or similar materials) total output is from 0.27 to 0.5 depending on the method of calculating the blade capacity. If there is a greater probability of the bulldozer operating

Table 13 *Optimized dimensions of a box blade*

Optimized blade parameter		Liquefied soil
Grasp width, m	according to Khankelov	3.83-3.93
	according to Karasev	3.55-3.73
Radius of curvature, m	according to Khankelov	1.58-1.66
	according to Karasev	1.43-1.70
The ratio of the flap length to the grasp width	according to Khankelov	0.22-0.23
	according to Karasev	0.22-0.23

Table 14 *Optimized parameters of a "landfill" blade*

Optimized parameters of a blade		Snow, waste
Grasp width, m	according to Khankelov	3.77-3.92
	according to Karasev	3.63-3.90
Radius of curvature, m	according to Khankelov	0.44-0.46
	according to Karasev	0.41-0.62

on liquefied soil, the high output will be ensured by installing a box blade, and if the probability is less - by installing a "landfill" blade. The dimensions of the box and "landfill" blades optimized for operating with the corresponding materials are given in Tables 13 and 14.

It follows from the data that, depending on the method of calculating the blade capacity, the ranges of optimal values for its dimensions can vary significantly. In particular, this applies to a box blade; its ranges of the grasp width and radius of curvature, calculated by different methods do not overlap (Table 13). In principle, experimental testing of each calculated model to determine the most correct one can eliminate this discrepancy. The difficulties of such testing due to material and financial costs are obvious, and the unambiguity of its results (as evidenced by many years of experience in experimental research) is not guaranteed. Therefore, for practical purposes, authors can recommend:

a) for a box blade:
- set the grasp width to no more than 3750 mm to prevent a possible decrease in bulldozer performance due to increased slippage;
- set the curvature radius to no more than 1700 mm so as not to limit the view from the bulldozer driver's cab;
- set the cutting edge width to no more than 460 mm;
- set the canopy width to no more than 140 mm;
- set the flap length to no more than 860 mm.

b) for a "landfill" blade:
- take the grasp width in the range of 3770-3900 mm;
- take the radius of curvature in the range of 440-460 mm;
- take the width of the cutting edge in the range of 118-124 mm;
- take the width of the canopy in the range of 580-610 mm.

7 Conclusion and future work

An analysis of the effectiveness of equipping the SHANTUI SD32 bulldozer with specialized high-capacity blades showed that the work of the bulldozer on materials that differ in their characteristics from ordinary loamy soil (snow, household waste, liquefied soil, coal, wood chips) could be performed with the highest productivity using the box and "landfill" blades. Moreover, the performance feasibility is determined by the probability of the bulldozer operating on liquefied soil (or similar materials) or other materials (snow, waste, coal, wood chips). The undeniable effectiveness of equipping a bulldozer with a box blade is expected when the probability of the machine operating on liquefied soil (or similar materials) is 0.5 or more.

The optimal dimensions of a box blade for equipping the SHANTUI SD32 bulldozer are a grasp width of up to 3730 mm, radius of curvature of up to 1700 mm, cutting edge width of up to 460 mm, canopy width of up to 140 mm, flap length up to 860 mm. The optimal dimensions of a "landfill" blade for equipping the SHANTUI SD32 bulldozer are a grasp width of up to 3900 mm, radius of curvature of up to 460 mm, cutting edge width of up to 124 mm, canopy width of up to 610 mm. Future work may be aimed at introducing artificial intelligence into the development of various materials with lower specific gravity. Provided that the developed mathematical models are supplemented with parameters describing their properties, as well as the operating conditions of the machines, it will be possible to significantly increase the efficiency of these machines with the least energy and material costs.

Acknowledgements

The authors received no financial support for the research, authorship and/or publication of this article.

Conflicts of interest

The authors declare that they have no known competing financial interests or personal relationships that could have appeared to influence the work reported in this paper.

References

[1] BALOVNEV, V., GLAGOLEV, S., DANILOV, R., KUSTAREV, G., SHESTOPALOV, K., GERASIMOV, M. *Machines for excavation work: design, calculation, consumer properties*. Minsk: BSTU Publishing House, 2012. ISBN 978-985-525-899-6.

[2] DUDKIN, M., KIM, A., AUKENOVA, B., RADENKOV, R., SAVELIEV, A., ANDRYUKHOV, N. Theoretical investigations of the process of interaction with environment of a bulldozer blade with variable geometry. *Journal of Applied Engineering Science* [online]. 2022, **20**(3), p. 798-807. ISSN 1451-4117, eISSN 1821-3197. Available from: https://doi.org/10.5937/jaes0-37210

[3] ASLONOV, N., IRISOV, K. Mathematical model of resistance to spreading forces using a bulldozer blade. *E3S Web of Conferences* [online]. 2023, **390**, 01032. eISSN 2267-1242A. Available from: https://doi.org/10.1051/e3sconf/202339001032

[4] SURASHOV, N., ASMATULLAEV, R., TOLYMBEK, D. Determination of the rational shape of a bulldozer blade, taking into account the soil background of the Republic of Kazakhstan. *Bulletin of SibADI* [online]. 2021,**18**(6), p. 662-677. ISSN 2071-7296, eISSN 2658-5626. Available from: https://doi.org/10.26518/2071-7296-2021-18-6-662-677

[5] KHMARA, L. Scientific support of construction and road machines: research, calculation, creation, selection, use. *Bulletin of the Pre-Dnieper State Academy of Construction and Architecture*. 2019, **209**(7-8), p. 48-69. ISSN 2312-2676.

[6] RAKSHA, S., GLAVATSKY, K., GREBENKO, Y. Study of the process of digging soil with a physical model of bulldozer equipment with a fixed blade and a replaceable blade system. *Bulletin of the Kharkov National Automobile and Highway University* [online]. 2020, **88**(2), p. 86-92. ISSN 2219-5548, eISSN 2521-1773. Available from: https://doi.org/10.30977/BUL.2219-5548.2020.88.2.86

[7] SELECH, J., ULBRICH, D., WLODARCZYK, K., STASZAK, Z., MARCINKIEWICZ, J., RAMEK, D., BARAN, B. A working design of a bulldozer blade as additional equipment of a compaction drum roller. *MATEC Web of Conferences* [online]. 2019, **254**, 04005. eISSN 2261-236X. Available from: https://doi.org/10.1051/matecconf/201925404005

[8] BARAKAT, N., SHARMA, D. Evolutionary multi-objective optimization for bulldozer and its blade in soil cutting. *International Journal of Management Science and Engineering Management* [online]. 2019, **12**(4), p. 102-112. ISSN 1750-9653, eISSN 1750-9661. Available from: https://doi.org/10.1080/17509653.2018.1500953

[9] KHANKELOV, T., ASKARKHODZAEV, T., ASLANOV, N. Modeling of segmental excavator working tool for soil compaction. *E3S Web of Conferences* [online]. 2023, **401**, 826. eISSN 2267-1242A. Available from: https://doi.org/10.1051/e3sconf/202340102052

[10] HIRAYAMA, M., GUIVANT, J., KATUPITIYA, J., WHITTY, M. Path planning for autonomous bulldozer. *Mechatronics* [online].2019, **58**, p. 20-38. ISSN 0957-4158, eISSN 1873-4006. Available from: https://doi.org/10.1016/j.mechatronics.2019.01.001

[11] KIM, S. K., LEE, Y. S., SUN, D. I., LEE, S. K., YU, B. H., JANG, S. H., KIM, W., HAN, C. S. Development of bulldozer sensor system for estimating the position of blade cutting edge. *Automation in Construction* [online]. 2019, **106**, 102890. ISSN 0926-5805, eISSN 1872-7891. Available from: https://doi.org/10.1016/j.autcon.2019.102890

[12] KHANKELOV, T. Results of experimental studies of the process of sorting elastic components of municipal solid waste. *Academic Journal of Manufacturing Engineering*. 2021, **19**(4), p. 97-102. ISSN 1583-7904, eISSN 2601-3045.

[13] KHANKELOV, T., ASKARHODZHAEV, T., MUKHAMEDOVA, N. Determination of key parameters of a device for sorting municipal solid waste. *Journal of Critical Reviews* [online]. 2020, **7**, p. 27-28. eISSN 2394-5125. Available from: https://doi.org/10.31838/jcr.07.04.07

[14] NAVON, R., GOLDSCHMIDT, E., SHPATNISKY, Y. A concept proving prototype of automated earthmoving control. *Automation in Construction* [online]. 2003, **13**(2), p. 225-239. ISSN 0926-5805, eISSN 1872-7891. Available from: https://doi.org/10.1016/j.autcon.2003.08.002

[15] FERNANDO, A., CHEEIN, A., GUIVANT, J. SLAM-based incremental convex hull processing approach for treetop volume estimation. *Computers and Electronics in Agriculture* [online]. 2014, **102**, p. 19-30. ISSN 0168-1699, eISSN 1872-7107. Available from: https://doi.org/10.1016/j.compag.2014.01.002

[16] PENG, G., DUAN, H., TAN, Z., ZHOU, Y., LI, J., HU, B., ZHOU, CH. Construction path tracking and unmanned bulldozer. *Automation in Construction* [online]. 2023, **154**, p. 1-17. ISSN 0926-5805, eISSN 1872-7891. Available from: https://doi.org/10.1016/j.autcon.2023.105015

[17] KHANKELOV, T., AKOBIR MUKHITDINOV, A., IBROKHIMOV, S., ASLONOV, N., MIRKHOLIKOV, S. Determination of the lengths of rebounds of elastic components of solid municipal waste. *AIP Conference Proceedings* [online]. 2022, **2432**, 030028. ISSN 0094-243X, eISSN 1551-7616. Available from: https://doi.org/10.1063/5.0089528

[18] KOSIMBETOV, B., KHANKELOV, T. Usage advanced technological methods for the recovery of cone crusher equipment. *E3S Web of Conferences* [online]. 2021, **264**, 02063. eISSN 2267-1242A. Available from: https://doi.org/10.1051/e3sconf/202126402063

[19] KARASEV, G., DOTSENKO, A., KUSTAREV, G. *Machines for earthworks*. Moscow: Bastet Publishing House, 2012. ISBN 978-5-903178-28-5.

[20] KHANKELOV, T., MUKHAMEDOVA, M. Choice of garbage trucks with rational parameters according to criterion of minimum operation cycle time. *E3S Web of Conferences* [online]. 2023, **401**, 02053. eISSN 2267-1242A. Available from: https://doi.org/10.1051/e3sconf/202340102053

[21] KHANKELOV, T., SARMONOV, A., KADIROV, A. The analytical dependence of the resistance force to digging with a bulldozer blade on the main influencing factors. *E3S Web of Conferences* [online]. 2023, 458, 10001. eISSN 2267-1242A. Available from: https://doi.org/10.1051/e3sconf/202345810001

[22] KHANKELOV, T., MAKSUDOV, Z., MUKHAMEDOVA, N., TURSUNOV, S. Crushing and screening complex for the production of compost from organic components of municipal solid waste. *E3S Web of Conferences* [online]. 2021, **264**, 01026. eISSN 2267-1242A. Available from: https://doi.org/10.1051/e3sconf/202126401026

[23] KHANKELOV, T. A theory of sorting solid domestic waste. *Construction and road Mashinery*. 2001, **5**, p. 34-36. ISSN 0039-2391.

[24] TURGUMBAEV, S., KABASHEV, R. Results of experimental studies of the process of digging soils with a modernized working body under hydrostatic pressure. *Bulletin of SibADI* [online]. 2017, **2**(54), p. 36-42. ISSN 2071-7296, eISSN 2658-5626. Available from: https://doi.org/10.26518/2071-7296-2017-2(54)-36-42

[25] KHAN, S., GUIVANT, J., LI, X. Design and experimental validation of a robust model predictive control for the optimal trajectory tracking of a small-scale autonomous bulldozer. *Robotics and Autonomous System* [online]. 2022, **147**, 103903. ISSN 0921-8890, eISSN 1872-793X. Available from: https://doi.org/10.1016/j.robot.2021.103903

[26] NEZHADALI, V., ERICSSON, L. Wheel loader optimal transient in the short loading cycle. *IFAC Proceedings Volumes* [online]. 2014, **47**(3), p. 7917-7922. ISSN 1474-6670. Available from: https://doi.org/10.3182/20140824-6-ZA-1003.02419

[27] LEE, Y. S., KIM, S. H., SEO, J., HAN, J., CHANG-SOO HAN, C. S. Blade control in Cartesian space for leveling work by bulldozer. *Automation in Construction* [online]. 2020, **118**, 103264. ISSN 0926-5805, eISSN 1872-7891. Available from: https://doi.org/10.1016/j.autcon.2020.103264

[28] HARADA, J., ISHIBASHI, E. ICT bulldozer D61EXi/PXi-24 automatic dozing control improved technology. *Komatsu Technical Report*. 2018, **64**(171), p. 1-18. ISSN 1344-8641.

[29] KE, Y., LIEYUN, D., CHENG, Z., QUANLI, D., XUEPENG, W., BIN, H. 5G-bazed earthwork monitoring system for an unmanned bulldozer. *Automation in Construction* [online]. 2021, **131**, 013891. ISSN 0926-5805, eISSN 1872-7891. Available from: https://doi.org/10.1016/j.autcon.2021.103891

[30] DADHICH, S., BODIN, U., ANDERSSON, U. Key challenges in automation of earth-moving machines. *Automation in Construction* [online]. 2016, **68**, p. 212-222. ISSN 0926-5805, eISSN 1872-7891. Available from: https://doi.org/10.1016/j.autcon.2016.05.009

[31] KHANKELOV, T., RUSTAMOV, K. J., IRISBEKOVA M., SOBIROVA D. K. Substantiation of a hammer crusher for grinding municipal solid waste. *E3S Web of Conferences* [online]. 2024, 515, 03019. eISSN 2267-1242A. Available from: https://doi.org/10.1051/e3sconf/202451503019.

THE RESEARCH OF THE ENGINE-REDUCER ASSEMBLY IN THE TRACTION TRANSMİSSİON SYSTEM

Ayaz Abdullaev[1], Ilham Huseynov[2], Israil Elyazov[3,*], Elchin Yusifzade[3], Ramin Abdullaev[2], Allahverdi Sharifov[2]

[1]Department of Mechatronics and Machine Design, Azerbaijan Technical University, Baku, Azerbaijan
[2]Department of Transport Logistics and the Spirit of Safety, Azerbaijan Technical University, Baku, Azerbaijan
[3]Department of Transport and Logistics, Azerbaijan University of Architecture and Construction, Baku, Azerbaijan

*E-mail of corresponding author: elyazov1962@gmail.com

Ayaz Abdullaev 0000-0003-2243-2712,
Israil Elyazov 0000-0002-7690-9996,
Ramin Abdullaev 0000-0003-1202-7123,
Ilham Huseynov 0000-0001-8294-8521,
Elchin Yusifzade 0000-0002-6902-6781,
Allahverdi Sharifov 0009-0004-7358-9909

Resume

During the movement of the train in various operational regimes, a series of deficiencies arise in the mechanical components, which depend on kinematic and parametric factors affecting the working conditions of the traction drive. An innovative traction drive is discussed in this article, which prevents the non-uniform distribution of parametric factors, as well as dissipative, inertial, and elastic characteristics along the length of the track.

Article info

Received 21 February 2025
Accepted 5 June 2025
Online 26 June 2025

Keywords:

traction transmission
reducer
gear wheel
train
locomotive
mechanical system
dynamic characteristics

Available online: https://doi.org/10.26552/com.C.2025.045

ISSN 1335-4205 (print version)
ISSN 2585-7878 (online version)

1 Introduction

An innovative traction drive is proposed for railway vehicles, comprising a three-stage cylindrical gear transmission that minimizes parametric errors and is symmetrically arranged relative to the wheel pair, based on a detailed analysis of traction drives to eliminate the aforementioned deficiencies. The research was focused on studying the dynamic characteristics of the traction drive, developing a descriptive model, conducting verification calculations for the proposed traction drive, designing the placement scheme of the innovative gearbox, and evaluating the reliability of the proposed traction drive. To enhance the reliability of the traction drive, the selection of the motor-gearbox connection has been examined, and a dual-sided coupling has been deemed appropriate. In the dual-sided transmissions, uneven stress distribution does not occur, which significantly improves the reliability of the traction drive. According to statistical data, design considerations, and some test bench results, it is evident that compared to single-sided transmissions, dual-sided transmissions can improve the reliability of the traction drive by up to 15%. Another indicator is the determination of reliability based on the coefficient of variation and the reliability factor depending on the gear diameter, for which the graphical representations are provided.

Recently, the rapid development of science and technology in the world has necessitated researchers to actively participate in this dynamic progress and constantly create and design new constructions based on innovative thinking. The implementation of the innovative reducer, designed and patented as a result of the scientific activities of the staff of the “Mechatronics and Machine Design” department of the Azerbaijan Technical University [1-3], in various technical fields is of a great importance. A newly designed traction reducer has been developed as an analogue to these reducers, reducing overall dimensions and mechanical system weight to simplify maintenance, lower production costs, and improve the train’s technical characteristics, enhancing reliability through even load distribution, shortening the lever arm, and decreasing the number

of sequentially connected components and increasing efficiency, while saving electrical energy by minimizing the impact of meshing on the side surfaces of co-rotating gears on the shaft and utilizing double-sliding friction bearings [4].

Traction transmissions have been extensively studied by researchers worldwide, leading to commendable work in the modeling of transmissions and their components. The key outcome of these studies is the identification of issues within the transmission and the clarification of trends in the development of new transmission models.

In [5], the author developed an electromechanical coupling dynamic model by explicitly incorporating electrically induced traction force for railway vehicles to study the impact of traction drives on vehicle vibrations. The dynamic responses of vertical, lateral, and longitudinal accelerations in the axle box and bogie components were quantitatively analyzed.

In the research study [6], an optimized design scheme is proposed to reduce the noise in traction drives under operating conditions. Using the parametric model of the traction drive's gears, a modification plan for both the tooth profile and direction was developed. After the modification, the noise of the gear transmission system was analyzed under various operating conditions using the acoustic boundary element method. Subsequently, an optimal design scheme was obtained by combining the working duration under different conditions with the multi-condition modification parameters of the acoustic indicator.

In the article [7], an electromechanical coupling model for the high-speed trains is proposed. The model considers the interaction of the gear pair, the equivalent coupling mechanism of the transmission system, the equivalent circuit of the traction motor, and the direct torque control strategy. Additionally, the numerical simulation of the high-speed train model includes constant speed, traction, and braking conditions, and the impact on system reliability is analyzed.

A 3D model of the transmission system of the locomotive's traction reducer was created to verify the rationality of its design based on a computer software, and a dynamic model of the transmission system was developed. The model was then integrated into the simulation program, and the obtained simulation values were compared to theoretical values. The results indicate that the simulation outcomes fluctuate around the theoretical values, confirming the superior design of the traction reducer's transmission system [8].

Investigating fatigue damage, the most critical failure in the traction drive of urban railway transport vehicles, it has been determined that the passenger capacity is a crucial factor affecting the dynamic load characteristics of the traction transmission system. Therefore, in this study a dynamic model of the traction drive was developed and numerical simulations were conducted under various speeds and curve radii to analyze the impact of passenger capacity on fatigue life. The research results indicate that the passenger capacity is a significant factor influencing the fatigue life of mechanical components [9].

The safety, comfort, and reliability of traction drives are analyzed by integrating theoretical methods, analysis, numerical simulation, and optimization design theory. In the study [10], the focus was on developing a parameterized gear modification model, rational shape modification schemes, parameter design, dynamic characteristics, vibration response, and the acoustics of gear meshing under high-speed traction conditions.

Authors of [11] proposed innovative traction transmissions consisting of a gearbox that increases reliability by reducing the overall dimensions and weight of the mechanical system, optimizing load distribution, and improving the technical level of the traction drive. This is achieved through a reduction in the number of structural elements and the application of double sliding bearings, which also contribute to energy savings.

The traction transmission of modern STADLER KISS trains was examined in [12] and the impact of the technical level of the traction drive on the train's braking characteristics was discussed. The application of an innovative traction gearbox was proposed that can increase the outcome indicators in line with the unit consumption. The key factors, influencing the braking system, include the reduction of the mass of the proposed traction gearbox, the reduction of the inertia coefficient of rotating parts, and the technical parameters considered in the train's motion equation. Based on the braking distance calculation method, the braking distance is calculated for different speed ranges in a practical example, and it is shown that the braking distance can be reduced by 5%, with a proportional reduction in braking time.

Authors of articles [13] and [14] explored the issue of investigating the factors affecting the operating modes of railway vehicles. By examining the factors influencing the movement of trains, they identified the key solution principles that enable improvements, reduction in consumption indicators, or achieving better results without changing the consumption. The optimal approach based on these principles is the reduction of the mass of rotating parts. The application of an innovative multi-stage gear reducer for traction transmission in railway vehicles is considered, and the operating modes of the trains are studied. The main parameters for traction, braking, and free movement modes of Stadler electric trains are identified.

The traction transmissions of railway vehicles, which are an important component of the transportation industry, were explored in [15]. The structural condition of the main parts of the mechanical system was examined, identifying dynamic events in the functional chain as key factors ensuring the system's longevity. Effective measures for improving system performance, enhancing the operation of structures, and upgrading maintenance and repair technologies are discussed. The importance

of evaluating technical quality is substantiated through the development of an innovative model. The current status, design, and operation of modern traction systems are explained.

In study [16] authors investigated the effect of the torsional stiffness of the coupled shafts, couplings, and the machine's working body, as well as the damping capacity of the coupling, on the torsional shock moment generated during the machine's transmission.

To explore the application possibilities of innovative gearboxes, the development trends of traction drives for railway vehicles have been investigated, and 12 key findings have been obtained [17]:

- The issue of developing the required traction drive remains unresolved, which is why frequent structural changes occur in the transmission;
- Traction drives operate in significantly more difficult and especially complex conditions compared to the majority of transmissions in other vehicles;
- Sometimes, production capacity may conflict with operational requirements, and in such cases, operational requirements take precedence, as the technical-economic efficiency of the transmission is determined by the service life and the efficient use of energy resources;
- The traction drive has no reserve, and its failure practically leads to the failure of the train;
- Since the entire useful power flow of the train passes through the traction drive, the transmission must have high efficiency.
- Efforts are made to reduce energy loss, material consumption, and labor intensity during maintenance work;
- Structural and technological solutions are considered appropriate to ensure a high level of standardization and unification of parts and components, as well as their suitability for maintenance and inspection;
- During the production stage of the transmission, a reduction in labor, energy, and material consumption is also required;
- The requirements for the traction drive are primarily operational in nature;
- Typically, only verification calculations are performed during the development of the transmission, as dimensions are determined based on specific alignment conditions rather than project calculations;
- The key outcome for engineers and researchers is conducting effective studies aimed at reducing metal consumption, improving efficiency, and increasing reliability.
- The literature review reveals that the development trends of traction drives, the research results of various authors, as well as the fundamental design, manufacturing, and operational flaws identified during the studies, demonstrate that the investigation of the motor-gearbox connection in traction drives is highly relevant.

The correct structural selection of the motor-gearbox connection would help to solve many problems related to the transmission in the future. To achieve this, the research focuses on the following issues:

Studying the dynamic characteristics of the traction drive and developing a descriptive model;

- Conducting verification calculations for the proposed traction drive;
- Developing the placement scheme of the innovative gearbox;
- Evaluating the reliability of the proposed traction drive.

2 Methods and materials

The research was conducted using a heuristic method based on exploration and design. The tasks set forth were solved through theoretical and experimental studies conducted under laboratory and industrial conditions.

2.1 Study of the dynamic characteristics of the traction drive and development of a descriptive model

Like any mechanical system, railway vehicles are affected by numerous excitation factors. These can be classified into two categories: external and internal. External factors are those that are independent of the characteristics of the traction system, while internal factors are those directly related to the properties of the traction system. Additionally, force, kinematic, and parametric excitations are distinguished. External force excitations arise when there is a change in the resistance to the movement of the train (locomotive). Kinematic excitations are caused by deformations of the rail profiles, such as subsidence and bulging, as well as by local defects in the upper layer of the track, resulting in non-linearity in the track profile. Parametric factors are associated with the uneven distribution of the dissipative, inertia, and elasticity characteristics of the track along its length [18].

Internal force excitations are caused by the electromagnetic torque of traction motors and the imbalance of rotating parts. Due to the non-ideal circularity and conicity of the wheel's rolling surface relative to the geometric axis of the wheelset, as well as the kinematic errors of gear meshing and the traction coupling, internal kinematic excitations arise. These include changes in the radial stiffness of the coupling along a given coordinate (where the inclination of the elastic elements in the environment changes during rotation) and parametric excitations due to changes in the adhesion conditions between the wheel and the rail.

When studying traction drives, the kinematic diagram must be examined first. Based on the

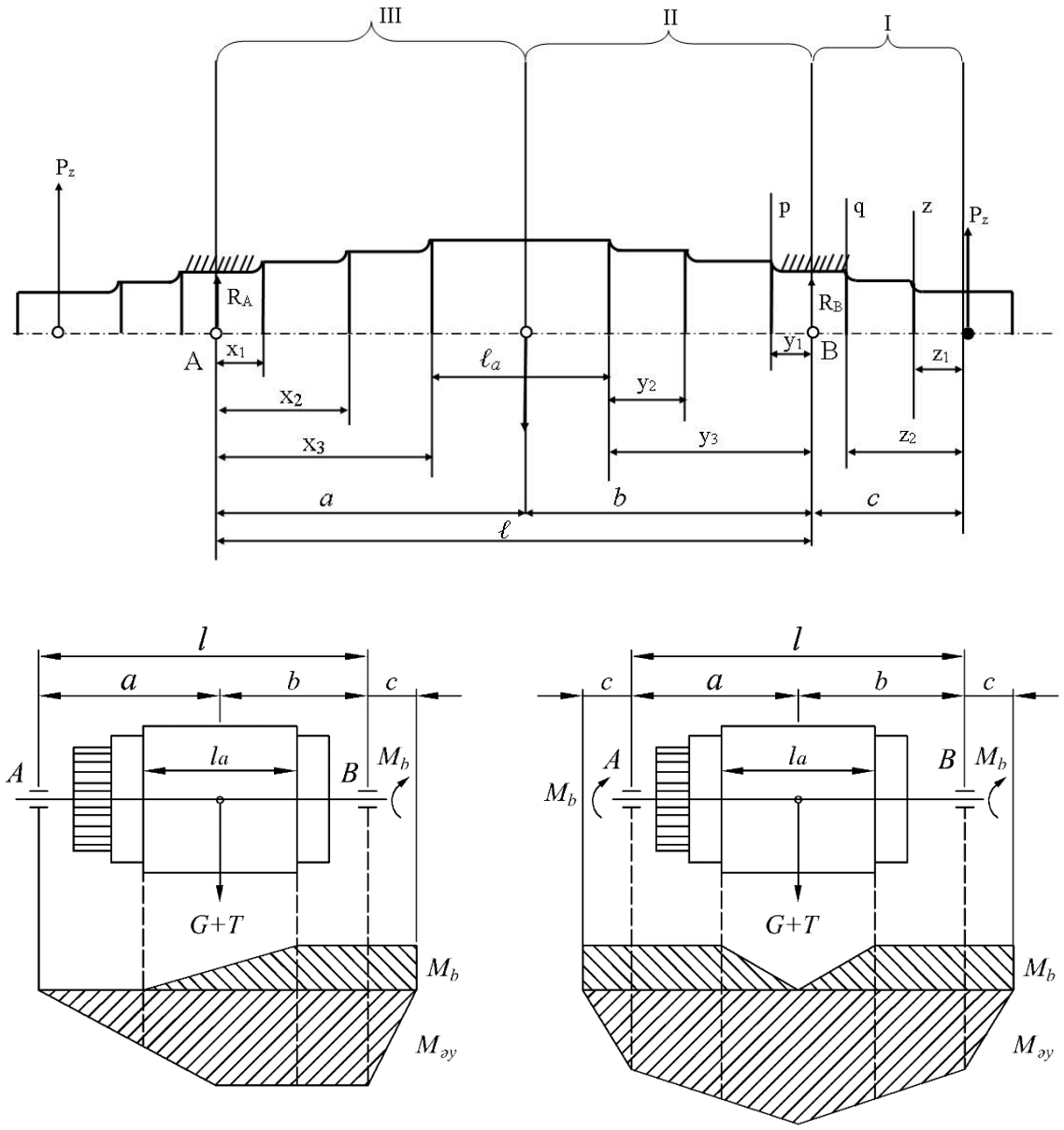

a) Single-sided transmission *b) Dual-sided transmission*

Figure 1 *Load distribution scheme on the motor shaft*

arrangement of the reducers, there are two main types of motor-gearbox connections.

In a single-sided transmission, the force is applied from one side of the motor. In this case, uneven effects occur in the system, leading to negative impacts on the reliability of the drive. To increase the reliability in such designs, additional elastic elements and increased mass are applied, which require extra costs and reduce the technical level of the transmission.

In a dual-sided transmission, the force is applied symmetrically from both sides of the motor to the wheelset. In this case, the reduction of parametric effects, an increase in reliability, and an improvement in the technical level are ensured.

Figure 1 presents a distribution model (diagram) illustrating the load distribution in single-sided and dual-sided traction drive designs.

The calculation of shaft strength consists of comparing the effects acting on its individual sections to their limit values. The shafts are analyzed based on the evaluation of torsional and bending moments. These calculations are carried out based on the traction force of a single axle of a vehicle. The traction force must correspond to the maximum value of the wheel-rail adhesion.

The traction motor shaft is usually made of 20XH3A grade steel (with a fatigue limit of σ_{-1} = 330 MPa). In double-sided transmissions, this stress value can be reduced by 15–20%. This is because, in double-sided transmissions, uneven stress distribution does not occur, which significantly positively affects the reliability of traction shafts [19].

2.2. Verification calculation of the traction transmission

When designing the gears of the reducers, two types of calculations are carried out - verification and design calculations [19-20]. In traction transmissions of railway vehicles, design calculations are usually not required because the sizes of the transmission elements are determined based on adaptation to a specific installation condition. When the dimensions and transmitted load are known, the goal of the verification calculation is to determine the mechanical system's durability limit under the given conditions. During the verification calculation, the calculated stresses are determined, and a comparison is made to the allowable stress. The following sequence of calculations is carried out for this purpose.

The circumferential force of the gear reducer is found by Equation (1);

$$F_{Ft} = \frac{2T_3}{d_1} = \frac{2 \cdot 6050 \cdot 10^3}{496} = 24.39 \cdot 10^3 \ \ N, \tag{1}$$

here: T_3 - the torque of the most loaded gear, N·m; d_1 - the diameter of the gear, mm.

The load applied to the contact line of the tooth is found by Equation (2);

$$W_{Ft} = \frac{F_{Ft} \cdot k_{F\alpha} \cdot k_{F\beta} \cdot k_{Fv}}{b_\omega} = \\ = \frac{24.39 \cdot 10^3 \cdot 1 \cdot 1.5 \cdot 1}{80} = 475 \ \frac{N}{mm}, \tag{2}$$

here: $k_{F\alpha}$ is the coefficient that accounts for the uneven load distribution between the teeth, and for the straight-cut gears, the value is $k_{F\alpha} = 1$, $k_{F\beta}$ is the coefficient that accounts for the uneven distribution of the load along the tooth contact line, and for the straight-cut gears, the value is $k_{F\beta} = 1.5$; k_{Fv} is the internal dynamic load coefficient; for double-sided transmissions $k_{Fv} = 1$; b_ω is the width of the gear, mm.

The bending stress of the teeth is determined by the Equation (3);

$$\sigma_F = \frac{Y_F \cdot Y_{F\varepsilon} \cdot Y_{F\beta} \cdot W_{Ft}}{m} = \\ = \frac{3.75 \cdot 1 \cdot 1 \cdot 457}{8} = 214 MPa, \tag{3}$$

here: Y_F - Tooth form factor, which is selected based on the number of teeth; Y_{Fe}=1 - Coefficient that accounts for the contact ratio of the teeth.

The specific load applied to the center of the tooth is determined by Equation (4);

$$W_{Ht} = \frac{2000 T_3 \cdot k_{H\alpha} \cdot k_{H\beta} \cdot k_{Hv}}{b_\omega \cdot d_{\omega 1}} = \\ = \frac{2000 \cdot 6050 \cdot 1 \cdot 1.7 \cdot 1.03}{80 \cdot 496} = 534 \frac{N}{mm}, \tag{4}$$

here: $k_{H\alpha}$ - Coefficient that accounts for the uneven distribution of load between the teeth; for spur gears, $k_{H\alpha} = 1$; $k_{H\beta}$ - Coefficient that considers the uneven distribution of contact stress along the tooth length; for traction reducers, $k_{H\beta} = 1.7$; k_{Hv} - Internal dynamic coefficient; for traction reducers, $k_{Hv} = 1.03$.

The contact voltage is calculated by Equation (5);

$$\sigma_H = 275 Y_H \cdot Y_{H\varepsilon} \cdot \left[\frac{W_{Ht} \cdot (u_3 + 1)^{0.5}}{u_3 \cdot d_{\omega 1}} \right] = \\ = 275 \cdot 1.76 \cdot 0.867 \cdot \left[\frac{534 \cdot (1.771 + 1)}{1.771 \cdot 280} \right] = \\ = 725 \ MPa, \tag{5}$$

here: Y_H - Coefficient that accounts for the shape of the tooth, determined based on the total number of teeth; $Y_{H\varepsilon}$ - Coefficient that considers the total length of the contact line,; $d_{\omega 1}$ - Base circle diameter of the gear, mm; u - Transmission ratio; W_{Ht} - Specific load applied to the middle of the tooth, N/mm.

Bending and contact stresses are compared to the permissible calculated stresses. The approach here is that the center distance is chosen not according to the contact stress, but according to the design and location possibilities. The bending and contact stresses are calculated according to the obtained center distance and compared with the allowable stress values of the material. The values of the bending and contact stresses of the material are taken from the report of the classic gearbox example.

$$\begin{matrix} \sigma_F = 214 MPa \le \sigma_{Fh} = 236 MPa \\ \sigma_H = 725 Mpa \le \sigma_{Hh} = 900 MPa \end{matrix}. \tag{6}$$

2.3 Development of the layout scheme of the innovative traction reducer

One of the key parameters that shapes the traction characteristics of railway vehicles and ensures that the traction reducer fits within the required dimensional framework in both vertical and horizontal directions is the transmission ratio of the reducer. To determine the transmission ratio, it is sufficient to know the engine shaft speed, wheel diameter, and maximum operating speed. According to Equation (7), the suitability of the transmission ratio within the given parameters is checked and the transmission ratio is determined for each stage of the three-stage innovative reducer.

$$u_{\max} = \frac{n_{\max} \cdot D_{to}}{5.3 \cdot \upsilon_{\max}} \cdot 10^{-3} = \frac{5831 \cdot 880}{5.3 \cdot 160} = \\ = 6.055 > u_\Sigma = \frac{n_1}{n_2} = \frac{2074}{359.4} = 5.557, \tag{7}$$

here: D_{to} - mean diameter of the wheel; u_{max} - maximum speed of the train; n_{max} - maximum rotational speed of the engine shaft, rpm.

The selection and calculation of the main parameters of the traction reducer are based on determining the maximum value of the transmission ratio [21].

The elements of the traction drive must be positioned at a distance from the rail head in such a way that, in

the vertical direction, the wheelset axle remains within the smallest possible radius around its axis. In the transverse direction, they must be placed within the distance between the wheels, ensuring maximum ease of installation while considering manufacturability. Thus, the value of the transmission ratio is determined based on the condition that the safety clearance between the traction reducer housing and the track superstructure conforms to the design dimensions that characterize the reducer's structural features. The maximum outer diameter of the gears is determined by the Equation (8).

$$d_{a2} = D_k - 2 \cdot (\delta_1 + \delta_2 + \delta_3), \tag{8}$$

here: $\delta_1 = (120 \div 140)$ mm - distance from the rail head to the reducer housing; $\delta = (4 \div 12)$ mm - thickness of the bottom wall of the traction reducer housing; $\delta_3 = (8 \div 10)$ mm - distance between the gear and the reducer housing.

The placement of the traction drive within the dimensions limited by the distance between the wheels is determined as follows: B_D - length of the motor housing; b_1 - distance from the reducer housing to the wheel and traction motor, at least 30 mm; b_2 - thickness of the side wall of the reducer, selected based on whether the housing is load-bearing or non-load-bearing, 10 mm; b_3- distance between the side of the gear and the inner wall of the reducer housing, 10 mm; b_{w1}, b_{w2} b_{w3} - widths of the gears of the first, second, and third stages, respectively. Based on the above dimensions, the width of the traction reducer is determined by Equation (9).

$$b_k = b_{w1} + b_{w2} + b_{w3} + 2b_2 + 2b_3 = 20 + 40 + \\ + 80 + 20 + 20 = 180. \tag{9}$$

An outline diagram is prepared according to the selected and calculated dimensions of the traction drive (Figure 2).

2.4 Reliability of the innovative traction transmission

The reliability level defines the safety of railway vehicles. Enhancing reliability is regarded as one of the key requirements in the design and development of the transmission system.

Ensuring the maximum value of the reliability level must occur under conditions where the strength safety factors take their minimum values. The reliability level of all the structural elements of the traction drive must be equal and should approach the upper limit.

$$Q_1(t) = Q_2(t) = \ldots = Q_i(t) = \ldots = Q_n(t) \Rightarrow \sup Q(t), \tag{10}$$

Here, $Q_i(t)$ - is the failure probability of the traction transmission components, in other words, the reliability of the components.

The strength safety factors of the structural elements of the traction drive must be consistent with each other and should approach the lower limit.

$$S_i \Leftrightarrow S_2 \Leftrightarrow \ldots \Leftrightarrow S_i \Leftrightarrow \ldots \Leftrightarrow S_n \Leftrightarrow \inf S = 1, \tag{11}$$

Here, S_i - is the strength safety factor of individual parts of the traction drive. Table 1 presents the required parameters and their values for determining the reliability of the drive system [22].

The reliability of traction devices is formed on the basis of the reliability coefficients of the individual structural elements that make them up and is calculated by Equation (12).

$$Q = Q_1 \cdot Q_2 \cdot Q_3 \cdot \ldots \cdot Q_n = \prod_k^n Q_i, \\ Q_{ir} = Q_1^6 \cdot Q_2^2 \cdot Q_3^4 \cdot Q_4^2 = 0.99^6 \cdot 0.995^2 \cdot 0.96^4 \cdot \\ \cdot 0.95^2 = 0.7144, \tag{12}$$

here, Q_1, Q_2, Q_3, Q_4 - are the reliability levels of the gear transmission, shaft, a pair of rolling bearings, and sliding bearing, respectively.

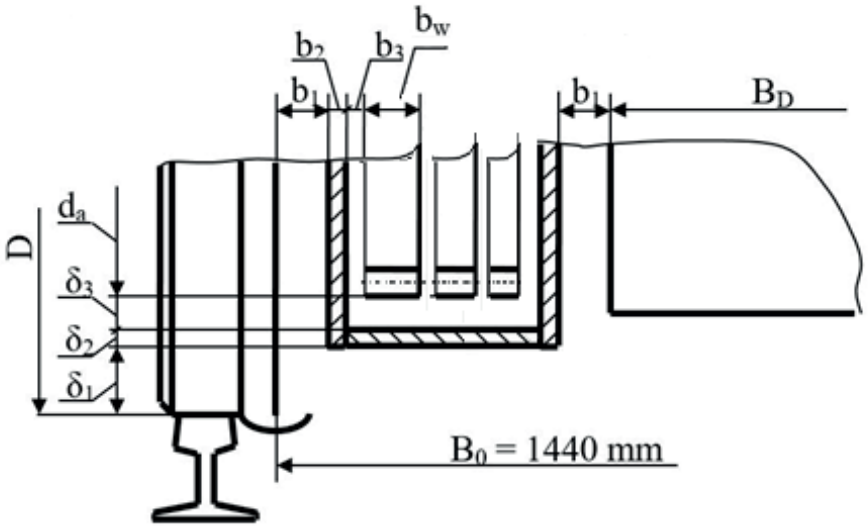

Figure 2. *Layout scheme of the innovative traction reducer*

Table 1 *Quantities required for determining reliability*

s/s	Parameter	Symbol	value
1	Number of gears	$n_{dç}$	6
2	Number of the rolling bearings	n_{dy}	4
3	Number of the shafts	n_u	2
4	Number of sliding bearings	n_{sy}	2
5	Number of sides	K	2
6	Reliability level of the gear	$Q_{dç}$	0.99
7	Reliability level of a pair of rolling bearings	Q_{dy}	0.9
8	Reliability level of the shaft	Q_V	0.995
9	Asymmetry coefficient due to supports	K_{qs}	1
10	Reliability level of sliding bearings	Q_{sy}	0.95

Table 2 *Results of stand tests for determining vibrations at different rotational speeds of the motor shaft in electric locomotives*

Number of measurements	Vibration measurement, mm/s			
	Frequency, rpm		Frequency, rpm	
1	2800	1.6	1.0	37.5
	2000	1.4	1.2	14.3
	1000	0.6	0.5	16.7
2	2800	1.5	1.2	20
	2000	1.9	0.9	52.6
	1000	1.8	0.7	61
3	2800	1.0	0.7	30
	2000	0.8	0.5	37.5
	1000	0.5	0.4	20
4	2800	2.0	1.6	20
	2000	1.6	1.2	25
	1000	1.0	0.8	20
5	2800	1.4	0.9	35.7
	2000	1.9	1.0	47.4
	1000	1.0	0.8	20
6	2800	1.4	1.2	14.3
	2000	1.3	0.8	38.5
	1000	1.1	0.7	36.4
7	2800	1.6	0.8	50
	2000	1.4	0.7	50
	1000	1.2	0.8	33.4
8	2800	1.3	0.7	46.1
	2000	0.9	0.6	33.4
	1000	0.6	0.5	16.7
9	2800	1.4	0.6	57.1
	2000	0.6	0.4	33.4
	1000	0.6	0.4	33.4
10	2800	1.4	0.7	50
	2000	1.6	0.7	56
	1000	1.6	1.0	37.5
Average value K_{qs}=1.32				32.2

3 Discussions and conclusions

A detailed analysis of the traction drives of railway vehicles has been conducted, and an innovative three-stage cylindrical gear traction drive has been proposed to eliminate several known shortcomings by minimizing parametric errors and ensuring symmetric placement relative to the wheelset. The design solution has been accepted and approved by the Eurasian Patent Organization with a corresponding decision [4].

Considering that the reducers are placed in parallel, the asymmetry coefficient will be K_{qsi}=1. If the transmission is asymmetrically positioned relative to the supports, its value can be determined through the experimental and analytical methods. The stand tests have been conducted on traction reducers of railway vehicles with asymmetrically positioned transmissions relative to the supports at different rotational speeds, measuring the effects of vibrations (Table 2).

It was found that the impact of vibrations on the side where the reducer is mounted on the engine shaft is up to 30% lower compared to the opposite side. Various structural solutions have been developed to neutralize these negative effects of vibration. One of the most widely applied methods in recent years is the placement of a hollow shaft over the wheelset axle and utilizing its elasticity properties to reduce vibration effects. However, based on structural considerations and experimental results, it can be concluded that, despite all these measures, when reducers are asymmetrically positioned, the asymmetry coefficient takes a value greater than one. On the other hand, increasing the mass of rotating components negatively affects the technical characteristics of the train.

The reliability level of a typical traction reducer is compared with the reliability level of the innovative traction reducer, and the results are presented in Table 3. As can be seen the application of innovative reducers significantly increases the reliability of the transmission.Thus the low reliability of the traction drive not only reduces production but increases the number of repairs as well, which in turn leads to high maintenance costs. In many cases the repair costs of the transmission exceed its production costs several times. A comparison of existing and innovative traction drives shows that the reliability has increased by up to 13%

Table 3 *Comparison of existing and innovative traction drives*

Characteristic parameters	Types of traction drives	
	Existing	Innovative
Number of shafts	4	6
Number of rolling bearings	3	2
Number of sliding bearings	6	4
Reliability level of gear transmissions. Q1	-	2
Reliability level of shafts. Q2	0.99	0.99
Reliability level of rolling bearings. Q3	0.995	0.995
Reliability level of sliding bearings. Q4	0.96	0.96
Asymmetry coefficient. K_{qs}	0.95	0.95
Reliability level of the traction functional chain. Q(t)	1.12	1
Increase in the reliability level of the traction functional chain. %	0.6352	0.7144
Characteristic parameters	$Q = \frac{Q_i - Q_m}{Q_m} \cdot 100\% = 12.5\%$	

Table 4 *Indicators of Reliability Level*

	Diameter of the driving gear in the heavily loaded stage. d. mm				Factor ensuring reliability. U_p	No.
Reliability Level Q(t)	0.9999	290.92	301.84	312.76	3.9	1
	0.999	290.64	301.128	311.92	3.8	2
	0.99	286.44	292.88	299.32	2.3	3
	0.95	284.592	289.184	293.776	1.64	4
	0.9	283.5	287	290.5	1.25	5
	0.85	282.912	285.824	288.736	1.04	6
	0.8	282.352	284.704	287.056	0.84	7
	Coefficient of Variation V_t					
		0.01	0.02	0.03		

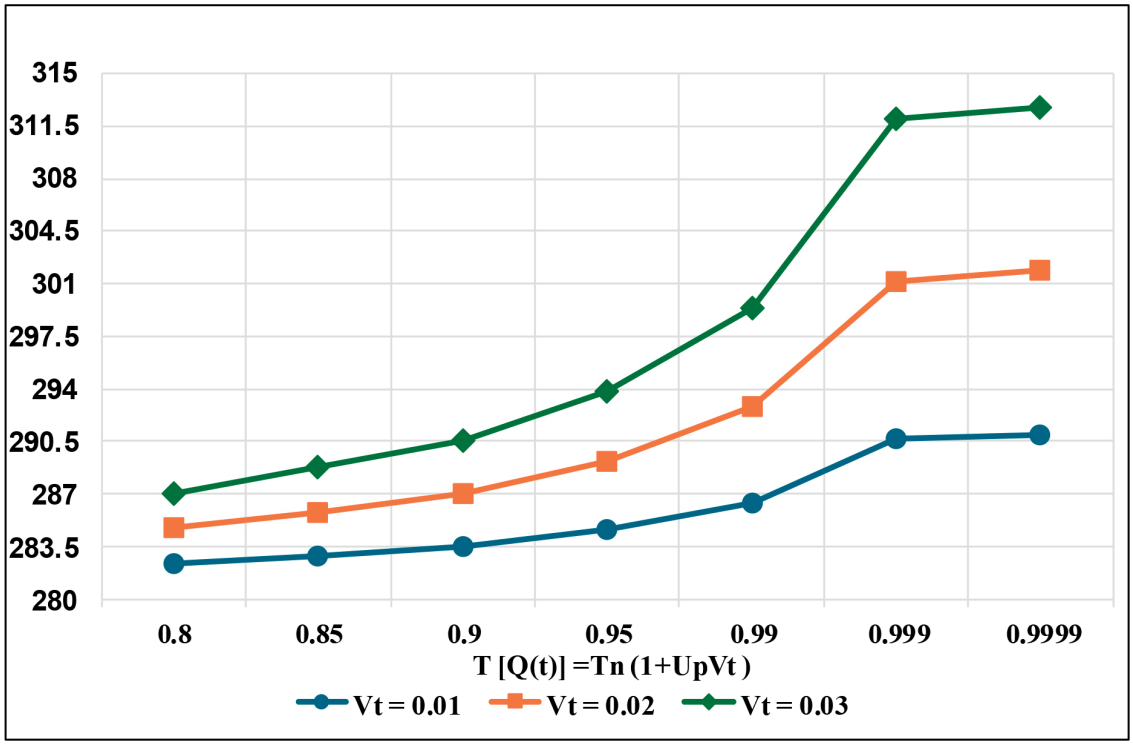

Figure 3. *Dependence of reliability degree on gear wheel diameter*

which is an indicator of an improvement in the technical level of the transmission.

Another indicator for increasing reliability is ensuring the minimum difference between the outer and inner diameters of the gears. In other words an increase in the inner diameter of the gear is directly proportional to an increase in reliability. As seen this condition is met in the innovative traction drive.

The reliability of gears depending on their diameter is determined based on the factor u_p - which ensures the required level of reliability and the coefficient of variation. The reliability level values are presented in Table 4 and Figure 3.

4 Conclusion

In this research study the application possibilities of an innovative traction transmission system for railway vehicles were explored. The dynamic characteristics of the traction transmission are analyzed and along with the development of its descriptive model methodological steps are taken to conduct verification calculations develop the placement scheme of the innovative gearbox and assess its reliability.

By conducting the verification calculations of the traction transmission the permissible stress value of the gear transmission is determined and compared with the calculated value. The selection of the main parameters of the traction motor is based on the maximum transmission ratio of the gearbox (U_m=6.055). An optimal placement scheme for the innovative traction gearbox within the traction transmission system is developed. and installation dimension parameters are determined accordingly.

The correctness of the transmission design and the choice of the constructive scheme are validated by ensuring a 13% increase in reliability and achieving parametric compliance through verification calculations.

Acknowledgements

The authors received no financial support for the research, authorship and/or publication of this article.

Conflicts of interest

The authors declare that they have no known competing financial interests or personal relationships that could have appeared to influence the work reported in this paper.

References

[1] ABDULLAEV, A. I., NADZHAFOV, A. M. Three-stage two-flow cylindrical gearbox (in Russian). Patent for invention No. 17053B1. Russian Federation, 2012.

[2] ABDULLAEV, A. I., CHELEBİ, I. G., ISMAİLOV, O. F., RASULOV, G. N. Hoisting mechanism of bridge, tower and gantry cranes (in Russian). Patent for invention No. 045270. Russian Federation, 2023. Available from: http://www.eapatis.com/Data/EATXT/eapo2023 /PDF/045270.pdf
[3] ABDULLAEV, A. I., ALİFOV, A. A., AKHMEDOV, B. B., CHALABİ, I. G. Single-flow three-stage gear transmission mechanism of point electric drives (in Russian). Patent for invention No. 040109. Russian Federation, 2022. Available from: http://www.eapatis.com/Data/EATXT/eapo2022/PDF/040109.pdf
[4] ABDULLAEV, A. I., NADZHAFOV, A. M., GUSEİNOV, I. D., CHELEBİ, I. GTraction drive of rolling stock (in Russian). Patent for invention No. 043160. Russian Federation, 2023. Available from: http://www.eapatis.com/Data/EATXT/eapo2023/PDF/043160.pdf
[5] WANG, X., PENG, T., WU, P., CUI, L. Influence of electrical part of traction transmission on dynamic characteristics of railway vehicles based on electromechanical coupling model. *Scientific Reports* [online]. 2021, **11**, 18409. eISSN 2045-2322. Available from: https://doi.org/10.1038/s41598-021-97650-4
[6] TANG, Z., LU, M., WANG, M., SUN, J. Research on modification and noise reduction optimization of Electric Multiple Units traction gear under multiple working conditions. *PLoS One* [online]. 2024, **19**(2), e0298785. eISSN 1932-6203. Available from: https://doi.org/10.1371/journal.pone.0298785
[7] ZHANG, K., YANG, J., LIU, C., WANG, J., YAO, D. Dynamic characteristics of a traction drive system in high-speed train based on electromechanical coupling modeling under variable conditions. *Energies* [online]. 2022, **15**, 1202. eISSN 1996-1073. Available from: https://doi.org/10.3390/en15031202
[8] LEI, L., SUI, Y., TIANMIN, G. Dynamic analysis of gearbox transmission system based on ADAMS traction locomotive. *IOP Conference Series: Earth and Environmental Science* [online]. 2019, **330**, 052049. ISSN 1755-1315. Available from: https://doi.org/10.1088/1755-1315/330/5/052049
[9] HUANG, X., WANG, J., YANG, J., ZHAO, Y., WANG, Y. Influence of passenger capacity on fatigue life of gearbox suspender of the traction transmission system in urban railway vehicles. *Sustainability* [online]. 2023, **15**(5), 4338. eISSN 2071-1050. Available from: https://doi.org/10.3390/su15054338
[10] TANG, Z., WANG, M., HU, Y., MEI, Z., SUN, J., YAN, L. Optimal design of traction gear modification of high-speed EMU based on radial basis function neural network. *IEEE Access* [online]. 2020, **8**, p. 134619-134629. eISSN 2169-3536. Available from: https://doi.org/10.1109/ACCESS.2020.3007449
[11] ABDULLAEV, A., HUSEYNOV, I., ELYAZOV, I., ABDULLAEV, R. The technical assessment of the level of innovativetraction transmission of railway vehicle. *EUREKA: Physics and Engineering* [online]. 2023, **3**, p. 40-51. ISSN 2461-4254, eISSN 2461-4262. Available from: https://doi.org/10.21303/2461-4262.2023.002823
[12] ABDULLAEV, A., HUSEYNOV, I., ELYAZOV, I., ABDULLAEV, R. Study of the influence of the technical level of railway vehi-cles on braking characteristics. *EUREKA: Physics and Engineering* [online]. 2024, **1**, p. 59-69. ISSN 2461-4254, eISSN 2461-4262. Available from: https://doi.org/10.21303/2461-4262.2024.003251
[13] HUSEYNOV, I. D. Study of the influence of the innovative reduced traction transmission of railway vehicles on trains'traffic modes. *Journal of Scientific Works / Elmi Eserler*. 2023, **1**, p. 100-108. ISSN 2222-5013.
[14] HUSEYNOV, I. Analysis of taction transmission of railway vehicles and their dynamic characteristics. *Machine Science Journal* [online]. 2023, **1**(1), p. 87-98. ISSN 2227-6912, eISSN 2790-0479. Available from: https://doi.org/10.61413/ssgt4613
[15] PANCHENKO, S., VATULIA, G., LOVSKA, A., RAVLYUK, V., ELYAZOV, I., HUSEYNOV, I. Influence of structural solutionsof an improved brake cylinder of a freight car of railway transport on its load in operation. *EUREKA: Physics and Engineering* [online]. 2022, **6**, p. 45-55. ISSN 2461-4254, eISSN 2461-4262. Available from: https://doi.org/10.21303/2461-4262.2022.002638
[16] KHALILOV I. A., SOFIYEV A. H. Dynamic behavior of shafts, couplings and working body of the machineunder torsional impact moment. *Journal of Applied and Computational Mechanics* [online]. 2024, **10**(4), p. 842-852. eISSN 2383-4536. Available from: https://doi.org/10.22055/jacm.2024.46217.4482
[17] HUSEYNOV, I. D. Development and technical assessment of the level of innovative traction transmission of railway vehicles. Dissertation. Baku: Azerbaijan Technical University, 2025. Available from: https://doi.org/10.13140/RG.2.2.18776.00007
[18] AHMADOV, H. M. The influence of defects in wheels and rails during operation on the dynamic characteristics of trains (in Azerbaijani). Textbook. Baku: 2005.
[19] BİRYUKOV, I. V., BELYAEV, A. I., RYBNİKOV, E. K. Traction transmissions of electric rolling stock of railways (in Russian). Textbook. Moscow: Transport, 1986.
[20] BAKHSHİYEV, I. I., MAMMADOV, S. B., HABİBOVA, E. M. Machine design. Course project and work (in Azerbaijani). Textbook. Baku: 2021.
[21] Traction transmissions of rolling stock [online]. Available from: https://studfile.net/preview/7871891/page:13/
[22] NADZHAFOV A. M. Search design of mechanical drive of sucker rod pumps (in Azerbaijani). Baku: ELM, 2008.

UNIVERSITY
OF ŽILINA

In its over 70 years of successful existence, the University of Žilina (UNIZA) has become one of the top universities in Slovakia.

The journal Komunikácie - vedecké listy Žilinskej univerzity v Žiline / Communications - Scientific Letters of the University of Žilina, Slovakia, began publication in 1999 with the expectation that it would provide sufficient space for presentation of the latest scientific knowledge and trends in the field of transport, telecommunications, and information technology. The scientific scope of the journal was mainly focused on the issues of transport, telecommunications, structures, materials, technologies and new areas of the university development. As of September 2018, the journal has been profiled as a scientific journal focusing on the topic of transportation.

The journal Communications - Scientific Letters of the University of Žilina is now an established open access scientific journal focusing primarily on topics related to the field of transport. The main areas, related to transport, include Civil Engineering, Electrical Engineering, Management and Informatics, Mechanical Engineering, Operations and Economics, Safety and Security, Travel and Tourism Studies. Research in the field of education also falls under these categories.

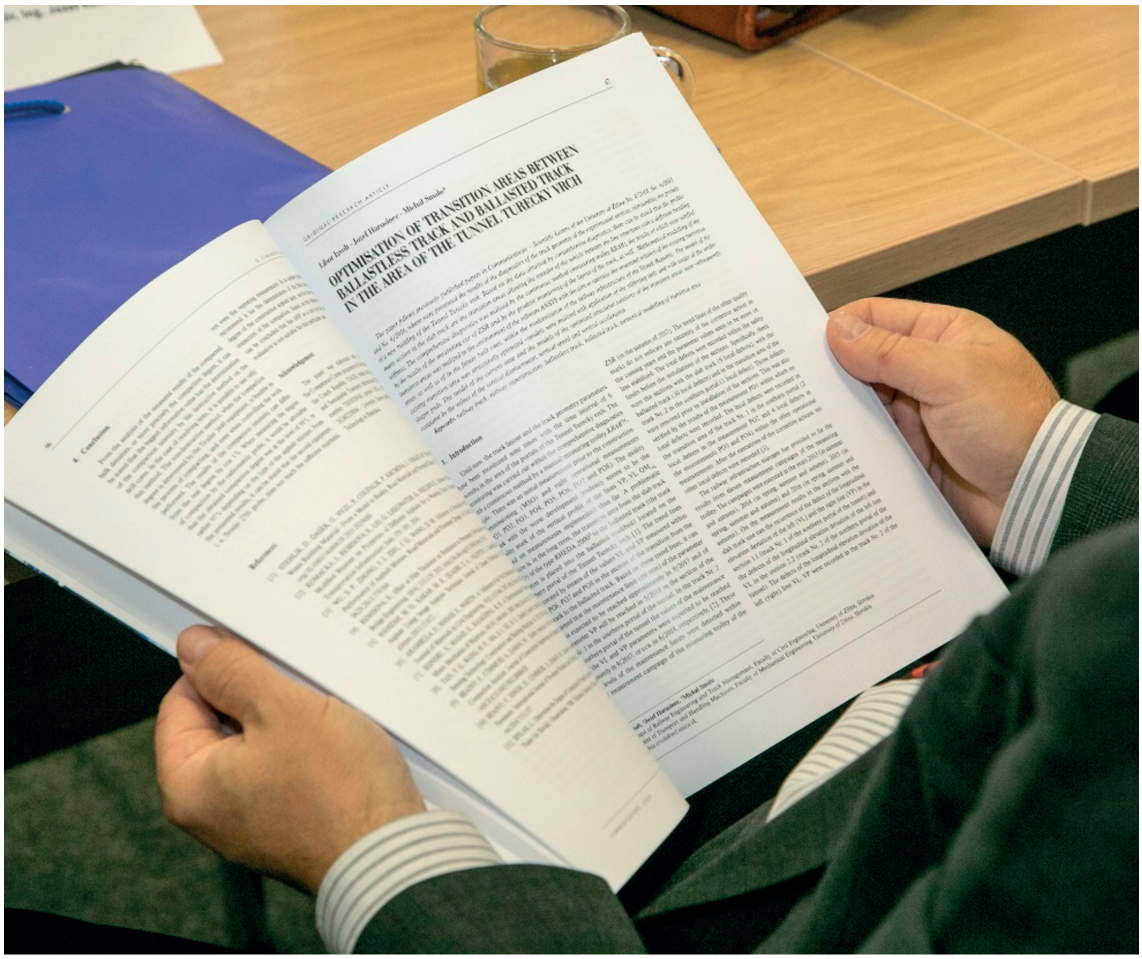

UNIVERSITY OF ŽILINA
Science & Research Department

Univerzitná 8215/1,
010 26 Žilina,
Slovakia

Ing. Janka Macurová
tel.: +421 41 513 5143
e-mail: janka.macurova@uniza.sk

IMPROVING THE METHODOLOGY OF ADAPTIVE TRAFFIC CONTROL AT PEDESTRIAN CROSSWALKS

Yuriy Royko, Oleh Hrytsun, Romana Bura*, Roman Rohalskyi, Yurii Yevchuk

Department of Transport Technologies, Lviv Polytechnic National University, Lviv, Ukraine

*E-mail of corresponding author: romana.r.bura@lpnu.ua

Yuriy Royko 0000-0003-0055-9413,
Romana Bura 0000-0003-1027-8367,
Yurii Yevchuk 0000-0002-8705-3791
Oleh Hrytsun 0000-0001-8391-9642,
Roman Rohalskyi 0000-0001-8223-2320,

Resume

The paper presents the results of an experimental study carried out at signalized intersections and pedestrian crosswalks in Lviv (Ukraine). The study covered intersections with different traffic conditions. Therefore, the intersections were classified into three types. It was found that the share of pedestrians who cross the road on the prohibitive traffic signal varies from 7% in the central areas to 13% near transport hubs. A methodology, which predicts the pedestrian behavior when they make decisions about crossing the roadway, is proposed. Recommendations were developed for choosing the optimal traffic light control modes. It was found that increasing the duration of the restrictive signal for pedestrians increases the probability of crossing the road during the restrictive signal of the traffic light. It emphasizes the need to adjust the duration of the traffic light cycle in areas with heavy pedestrian traffic.

Available online: https://doi.org/10.26552/com.C.2025.037

Article info

Received 8 November 2024
Accepted 26 March 2025
Online 12 May 2025

Keywords:

traffic flow
pedestrian flow
signalized pedestrian crosswalk
traffic light cycle duration
traffic delay

ISSN 1335-4205 (print version)
ISSN 2585-7878 (online version)

1 Introduction

Traffic delays on the road network are one of the main problems of modern cities, leading to time loss, environmental pollution, and excessive fuel consumption. This problem is exacerbated by the constant growth in the number of vehicles and the inefficiency of traffic management [1]. Traffic lights that control traffic at intersections should ensure a balance of traffic and pedestrian flow without increasing the waiting times, queues, and traffic density [2]. However, due to irrational signaling, traffic lights sometimes become bottlenecks in the road network.

Most traffic lights operate in modes with a predefined duration or using detectors. Control with a predefined duration uses fixed intervals of the permissive signals, while control with detectors adapts the phases depending on the detection of vehicles and/or pedestrians [3]. However, due to the high uncertainty in the arrival of vehicles and pedestrians, it is difficult to determine the long-term optimal values of the phases or their extension. As a result, this can lead to queues and excessive stops due to irrationally configured signals of traffic lights.

The latest technologies, such as adaptive traffic management systems, can be used to solve this problem. These systems can analyze data in real-time, predict changes in traffic volumes, and automatically adjust traffic lights to optimize the traffic and pedestrian flow [4]. Using detectors and cameras to collect flow data can also help to create more efficient and flexible control systems.

2 Literature review

Pedestrian crosswalks are one of the most dangerous places on the road network. Most road traffic accidents occur here. In urban centers, pedestrians crossing the road significantly impact the traffic flow. For this reason, several approaches have been developed to detect traffic and pedestrian flows before traffic lights [5-7]. In general, pedestrians should be given priority for various reasons. However, as emphasized in [8], the high priority for pedestrians at pedestrian crosswalks significantly affects the road network's capacity. The researchers evaluated different distances between pedestrian crosswalks, considering their variable nature.

The analysis in [9] shows that increasing number of pedestrians use mobile phones daily. It distracts them when they are getting ready to cross the roadway. Research [10] points to pedestrians as one of the most dangerous road users, with the highest probability of severe or fatal injuries in road accidents. That is why, there is a need to introduce new adaptive traffic control systems at pedestrian crosswalks, which are crucial for improving the pedestrian safety [11].

In [12], an algorithm for detecting traffic lights and pedestrian crosswalks was developed that successfully operates on embedded devices with limited computing resources in real time. This approach is based on image processing and is characterized by high recognition accuracy, although the quality of the results obtained may depend on the quality of the input images.

A high-resolution video surveillance system that collects vehicle and pedestrian traffic data at intersections is presented in paper [13]. This solution is characterized by high accuracy and the ability to collect essential data necessary to maintain safety and mobility in an urban environment.

Such systems are becoming an important component of modern adaptive traffic management systems. However, they do not consider the number of pedestrians waiting at the crosswalk [14].

For example, detectors to detect pedestrians on sidewalks and signalized crosswalks is proposed to use in [15]. Using detectors on sidewalks is challenging because it is crucial to ensure the correct shape and size of the pedestrian detection area. It is essential to identify pedestrians standing along the edge of the sidewalk, where an oval shape may be acceptable, as well as those approaching or standing on the approaches to the sidewalk.

To achieve this, more sophisticated detectors can be used to adapt the shape and size of the detection zone to suit specific conditions. It can be implemented using two beams directed at the pedestrian waiting area [16-18]. The first beam passes along the edge of the sidewalk, and the second beam is perpendicular to the road, covering the approach area. This allows to create a detection zone that better meets the needs of use on sidewalks.

This principle of operation allows the detectors to detect pedestrians both in the crossing area (detectors at the intersection) and in the waiting area on the sidewalk (detectors on the curb). Detectors placed on the sidewalk can track the presence of pedestrians and cancel crossing requests if a pedestrian has already started crossing the roadway [19]. This helps to avoid unnecessary delays and increases pedestrian safety [20].

In addition, particular detectors are used at crosswalks that automatically adjust the duration of the pedestrian phase. This allows sufficient time for safe crossing, especially when many pedestrians move slowly [21-23]. Using such detectors optimizes traffic lights' operation and increases pedestrian traffic efficiency and safety.

This configuration provides more accurate detection of pedestrians on the edge of the sidewalk and in the approach zone, significantly increasing the traffic safety and efficiency. This approach minimizes waiting time for pedestrians, providing them with comfortable road crossing conditions. In addition, using such systems helps to reduce the number of accidents, as drivers receive more accurate data on the presence of pedestrians at the crosswalk [24-25].

In [26], an algorithm for the traffic control at a signalized intersection using fuzzy logic was developed. This algorithm allows reducing the delay of traffic and pedestrian flows by adapting the parameters of traffic light control to traffic and pedestrian flows` volumes.

This study is aimed at determining the indicators or features of traffic flows and pedestrian behavior to substantiate the methodology for adaptive traffic control at pedestrian crosswalks.

It is necessary to perform the following tasks to achieve the objective of the work:

- to analyze the patterns and the main methods of studying the indicators of road users used to adjust the modes and parameters of traffic signal control systems;
- to conduct field studies of road users and analyze the behavioral characteristics of pedestrians at different types of intersections with traffic lights;
- to substantiate the mode of adaptive traffic control at pedestrian crosswalks, taking into account the characteristics of traffic flows and pedestrian behavior based on fuzzy logic;
- to develop recommendations for selecting the effective traffic signal control modes for different types of signalized intersections.

3 Materials and methods

Following the research objective, a number of measurements were made on the streets of Lviv (Ukraine) using the technical means of traffic management of the Lviv municipal enterprise "Lvivavtodor". The experimental study was conducted at signalized intersections and a signalized pedestrian crosswalk outside the intersection (Figure 1). Active motion detectors for both vehicles and pedestrians were used for this study.

During the measurements, the following indicators were determined: width of the pedestrian crosswalk (B_{ped}), length of pedestrian crosswalks (street width, B_{rw}); actual traffic flow volume through the crosswalk (N_a), pedestrian flow volume (N_{ped}), the duration of the traffic signal control cycle at intersections and pedestrian crosswalks and its components (duration of restrictive and permissive signals); the number of pedestrians gathered before the crosswalk; the number of people who crossed the roadway during the restrictive (t_r) and permissive (t_p) traffic signal.

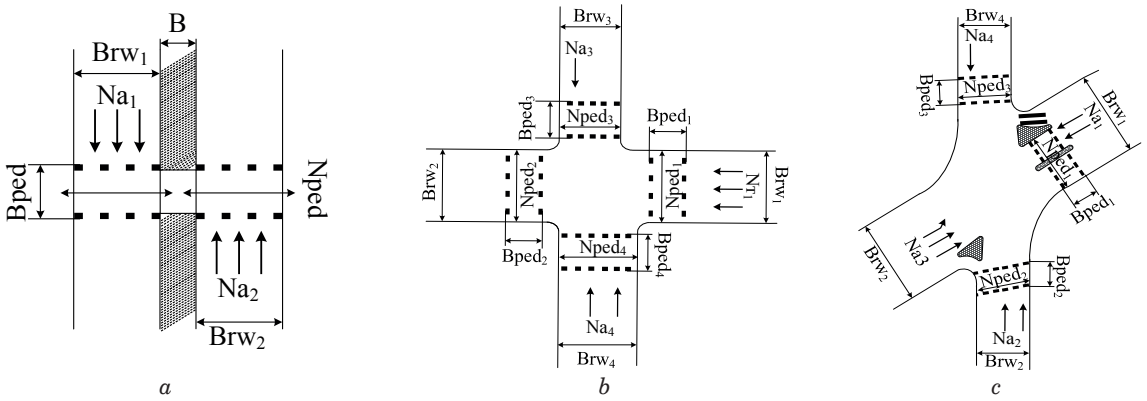

Figure 1 *Situational schemes of formation of the traffic and pedestrian flows, where experimental measurements were carried out: a - signalized crosswalk of type I (signalized pedestrian crosswalk with a dividing traffic lane); b - signalized crosswalks of type II (four-way intersection with four pedestrian crosswalks); c - signalized crosswalks of type III (combined four-way intersection with three pedestrian crosswalks)*

Table 1 *Types of intersections and pedestrian crosswalks in terms of their location in the city*

Type of intersection	Location on the territory of the city	Features of pedestrian flows	Features of traffic flows	Availability of a flow generation center
I	Near transportation hubs	Constantly intense during the peak periods; targeted towards and away from generation centers	High heterogeneity of traffic flow (up to 70% of passenger cars); a significant share of freight traffic and urban public transport, maneuverability in parking lots	Shopping centers, bus and train stations
II	Central zone	Constantly intense throughout the day	Significant homogeneity of the traffic flow (up to 95% of passenger cars)	The distribution of pedestrian flows across the territory is uniform
III	Residential area	Variable, unidirectional in the entire zone	The share of passenger cars is 80 - 85%, urban public transport - up to 10%; freight traffic is practically absent	Stopping points of urban public transport

During the research, the effectiveness and adequacy of the proposed solutions for the traffic control at pedestrian crosswalks was evaluated. This evaluation included checking how well the new control systems can control pedestrian and vehicular traffic, ensuring safety and convenience for all road users.

All these crosswalks can be conditionally divided into three types, depending on their location in the city (Table 1).

The research was conducted during the day in good weather conditions. The study tested several working hypotheses:

1. Different types of intersections and pedestrian traffic conditions require different durations of traffic signals to meet the needs of pedestrians to improve traffic safety.
2. As the traffic volume and length of the crosswalk decrease, pedestrians are more likely to try to cross the roadway when the traffic light is red.
3. The purpose of pedestrian movement can influence pedestrian behavior, changing their decisions about crossing the roadway.

This will provide more accurate information about the impact of different conditions on pedestrian behavior and the effectiveness of traffic management systems.

The sample size for traffic and pedestrian flow, required to ensure the representativeness of the data, was determined following the methodology outlined in [27]:

$$n = \frac{Z^2 \cdot p \cdot (1-p)}{E^2}, \tag{1}$$

where n - necessary sample size for traffic and pedestrian flow; Z - value for the selected significance level (1.96 is taken for 95%); p - the expected proportion (0.5 is assumed if there is no previous measurement data); E - is the permissible error (0.05 is taken).

Based on the calculations, the minimum number of situational interactions between the traffic and pedestrian flows, to be conducted at each type of intersection (crosswalk) to ensure a representative sample, was determined:

$$n = \frac{1.96^2 \cdot 0.5 \cdot (1-0.5)}{0.05^2} = \\ = 384.16 \approx 385 \, interactions. \tag{2}$$

During the study, various parameters were analyzed

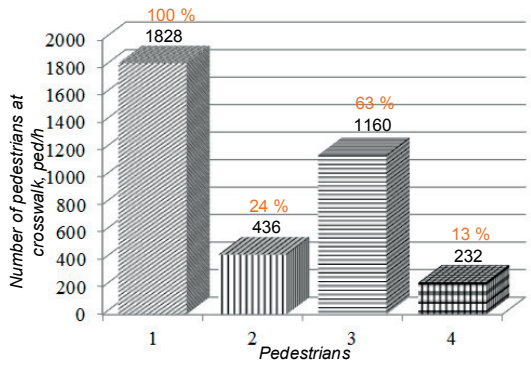

t_p = 25 sec; t_r = 47 sec; B_{rw} = 24 m; N_a = 1695 $auto/h$.

a)

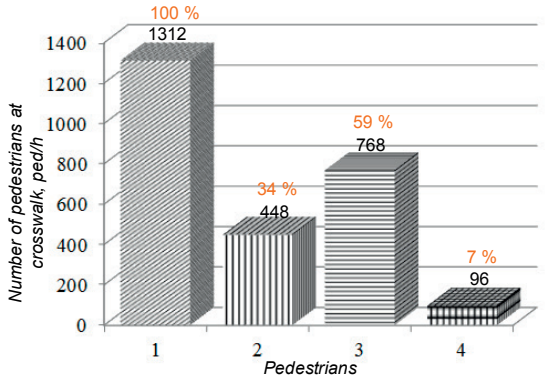

t_p = 32 sec; t_r = 28 sec; B_{rw} = 12.1 m; N_a = 1365 $auto/h$.

b)

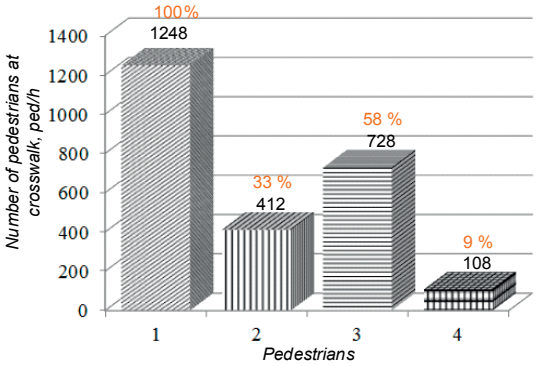

t_p = 32 sec; t_r = 28 sec; B_{rw} = 12.1 m; N_a = 1254 $auto/h$.

c)

Figure 2 *Results of pedestrian flow studies: a - signalized crosswalk of type I; b - signalized crosswalks of type II; c - signalized crosswalks of type III; 1 - the total number of pedestrians who crossed the crosswalk (on the restrictive and permissive traffic signal) and those who were waiting for the permissive traffic signal; 2 - pedestrians who were waiting for a permissive signal; 3 - pedestrians who crossed the crosswalk on a permissive signal; 4 - pedestrians who have crossed the crosswalk on a restrictive signal*

using video recordings made at the study sites, including vehicle and pedestrian characteristics, duration of the traffic signal for vehicles and pedestrians, geometric parameters of the road network, duration of the traffic light cycle, duration of pedestrian crossing, etc.

The graphical results of the study of pedestrian behavior at signalized crosswalks are shown in Figure 2.

Based on the results of the analysis presented in Figure 2, it was possible to confirm the working hypothesis 3. In particular, it was found that the share of people who violate traffic rules at signalized pedestrian crosswalks is 9% in residential areas. In the city's central areas (type II), this indicator is somewhat lower - 7%, while near the transport hubs (type I) it is up to 13%. The working hypotheses 1 and 2 were confirmed as well: to improve traffic safety at different types of intersections, traffic lights appropriate for pedestrian traffic should be used, as pedestrians are more likely to ignore the restrictive signals when the traffic volume and crossing lengths decrease.

Based on the results of these studies and previous ones, it can be concluded that the regulatory approaches to the arrangement of pedestrian crosswalks and the design of traffic control modes should consider the specifics of different types of intersections and pedestrian traffic conditions. These differences are determined primarily by the behavior of pedestrians at junctions, which depends on their psychophysiological characteristics and the purpose of their movement.

Therefore, to ensure the safety and efficiency of pedestrian traffic, it is necessary to develop adaptive and flexible solutions for different types of intersections. This includes planning crosswalks and managing the traffic signal control modes, which must be customized to specific conditions and behavioral patterns.

Thus, a more individualized approach to designing pedestrian crosswalks and controlling pedestrian flows would help to improve overall safety and comfort for all road users.

4 Results of theoretical and experimental studies

For effective planning of signalized pedestrian crosswalks on the road network, it is necessary to study

and simulate traffic flows and pay due attention to pedestrian flows. It is essential to analyze pedestrian behavior depending on the roadway's geometric parameters and the crosswalk's location.

When developing a methodology for adaptive traffic control at pedestrian crosswalks, it is necessary to consider not only the psychophysiological and physical capabilities of people, but to predict the behavior of pedestrians when making complex decisions, as well. One of the main psychophysiological factors is the natural tendency of people to save effort and time by choosing the shortest route between destinations.

Predicting pedestrian behavior allows to adapt infrastructure and controls to minimize risks and ensure safer crossing in different traffic conditions. Figure 3 shows a block diagram of the automated traffic control system at a controlled crosswalk considering pedestrian behavior.

The main point of the above scheme is that intersections are equipped with an automated traffic control system (vehicle detectors), which takes into account fixed-time conditions (planning and geometric parameters of the roadway) and variable conditions (characteristics of traffic flows, road, and climatic conditions, and the number of waiting pedestrians).

As shown in Figure 3, the input variable in the proposed system is a group of pedestrians standing before the traffic light and preparing to cross the road.

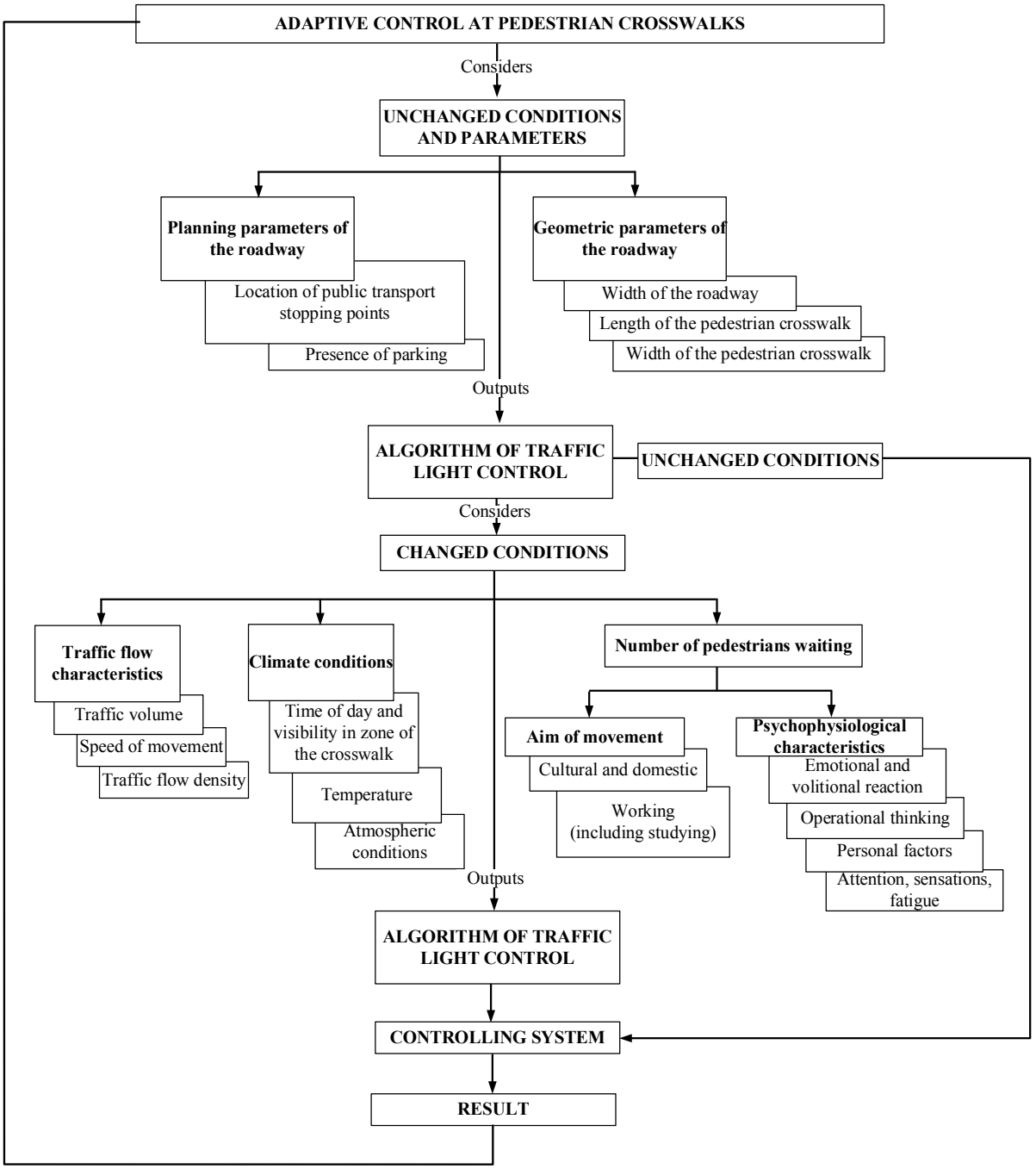

Figure 3 *Block diagram of adaptive traffic control at a controlled crosswalk considering pedestrian behavior*

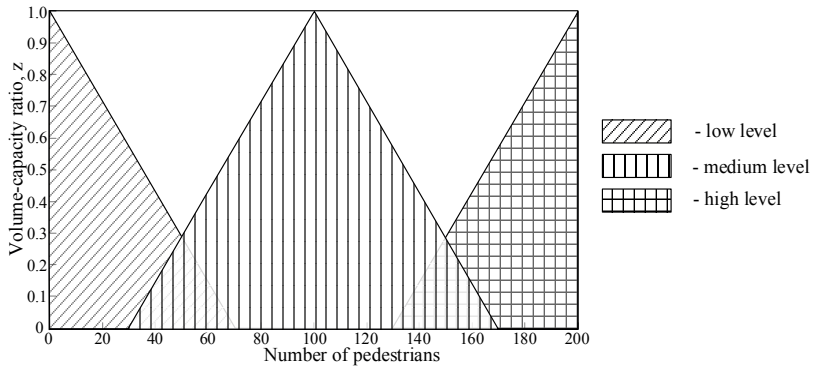

Figure 4 *Triangular membership functions for the number of pedestrians*

Table 2 *Recommendations for selecting the rational traffic signal control modes depending on the traffic delays and pedestrian behavior*

Volume-capacity ratio, z	Recommended duration of traffic light cycle, sec		
	Type of intersection I	Type of intersection II	Type of intersection III
2 phases			
$z < 0.2$	adaptive	adaptive	adaptive
$0.2 \le z \le 0.45$	25 - 40	adaptive	adaptive
$0.45 \le z \le 0.7$	30 - 50	40 - 60	40 - 60
$0.7 \le z \le 1.0$	40 - 60	45 - 70	50 - 70
3 phases			
$z < 0.2$	adaptive	adaptive	adaptive
$0.2 \le z \le 0.45$	40 - 60	50 - 70	50 - 70
$0.45 \le z \le 0.7$	50 - 70	60 - 80	60 - 80
$0.7 \le z \le 1.0$	60 - 90	60 - 90	60 - 90
4 phases			
$z < 0.2$	adaptive	adaptive	adaptive
$0.2 \le z \le 0.45$	60 - 80	60 - 90	60 - 90
$0.45 \le z \le 0.7$	80 - 90	90 - 100	80 - 100
$0.7 \le z \le 1.0$	90 - 100	100 - 110	100 - 120

Various methods can be used to identify and count the size of a group, allowing to detect both static and moving groups of people.

To provide a correct input value for adaptive traffic control at pedestrian crosswalks, this paper uses a methodology based on using pedestrian counting detectors, which allows for an accurate assessment of the number of people in the area before the traffic light.

After describing the proposed scheme of an adaptive traffic control at a controlled crosswalk, it is advisable to focus on the aspects of fuzziness of the inference system that determines the phases of traffic lights. In particular, it is crucial to characterize the membership functions used in this system briefly.

The proposed detector, which includes a fuzzy logic controller, uses three basic membership functions to process the input data and control the output. These functions represent the three levels of volume:

- low level: the membership function corresponds to a small number of pedestrians, which reduces the time of the green phase of the traffic light;
- medium level: the membership function adjusts the time of the green phase of the traffic light accordingly based on the moderate number of pedestrians;
- high level: the membership function provides a longer green phase time for a large number of pedestrians waiting to cross the road.

The controller's input data relating to the number of pedestrians is distributed over these membership functions, with the range of pedestrian counts ranging from 0 to 200.

These membership functions are applied to the traffic light cycles (green, amber, and red) for the traffic light control. The controller output values are directly related to the setting of the duration of each traffic light cycle and of each traffic light phase. This allows adapting the time of green, amber, and red lights to the

actual situation on the road, including the number of pedestrians waiting to cross.

The triangular membership functions for the number of pedestrians are shown in Figure 4, where the road network's volume-capacity ratio (z) is expressed by normalized values in the range from 0 to 1. This allows to clearly define how a specific value of the number of pedestrians affects the control of the traffic light. As for the time of day, unlike the number of pedestrians, obtaining a continuous numerical range is impossible. Instead, the time of day is divided into peak periods (07:00 - 09:00; 13:00 - 14:00; 17:00 - 18:00) and off-peak periods, which have different effects on the level of traffic on the road network.

Thus, recommendations are proposed for choosing the rational traffic signal control modes depending on the traffic delays and pedestrian behavior (Table 2).

The adequacy of these recommendations is checked next. It is taken, for example, a signalized crosswalk of type I (two-phase control). The width of the roadway is 24 m (11.25 m in each direction and a 1.5 m wide dividing lane). The total traffic volume at the crosswalk is 1695 veh/h (volume-capacity ratio - 0.35). Based on the fact that a large share of violators (13%) is observed at the studied facility under existing traffic conditions with a traffic light cycle duration of 78 seconds, it is possible to implement the traffic signal control for intersections of type I with a traffic light cycle duration of 25-40 seconds. For such traffic conditions at intersections of type II and III, it is necessary to implement adaptive traffic control since, in a fixed-time mode, there will be a large share of pedestrians crossing the roadway when the traffic signal is red.

For the two-phase control for intersections of type I with a road-capacity ratio of 0.35, the total cycle time of the traffic signal can be from 25 sec (7 sec green, 13 sec red, and 5 sec amber) to 40 sec (22 sec green, 13 sec red, and 5 sec amber). This cycle of 25 to 40 seconds is the basic cycle for a traffic light and is not an input or output parameter of a fuzzy logic controller.

The output of the fuzzy logic controller detects variations in these parameters, increasing or decreasing the duration of the green and red traffic lights according to the existing volume-capacity ratio on the road network. Pedestrian phases are dynamically updated based on membership functions (Table 3).

For example, for a 25-second cycle, the standard durations for the green, amber, and red traffic lights (at low traffic levels) are 7 s, 5 s, and 13 s, respectively. If the value of the membership function falls in the middle range, the duration of the green traffic signal increases by about 33% with a constant cycle time. In the high range, the increase in the duration of the green traffic signal can reach about 66%.

A similar mechanism for adjusting the duration of green, amber, and red traffic lights is implemented for a 40-second cycle. It allows dynamically adjusting the traffic light phases to optimize the traffic flow and improve pedestrian safety in different conditions.

Since the input data in the mechanism of logical conclusion are fuzzy variables, the fuzzy logic controller must convert these fuzzy outputs into clear values through defuzzification. It allows the actual system to process the result (Table 4).

As shown in Table 4, the output values of the fuzzy logic controller are determined based on six fuzzy rules using the "IF-THEN" construct. For example, if there is a peak period and the number of pedestrians is low, the

Table 3 *Variation of traffic light modes of the fuzzy logic controller*

Membership function	Duration of green signal, sec	Duration of amber signal, sec	Duration of red signal, sec
Traffic light cycle duration - 25 sec			
Low level	7	5	13
Medium level	9 (increase of the phase by 33%)	5	11
High level	12 (increase of the phase by 66%)	5	8
Traffic light cycle duration - 40 sec			
Low level	13	5	22
Medium level	18 (increase of the phase by 33%)	5	17
High level	22 (increase of the phase by 66%)	5	13

Table 4 *Recommendations for selecting the rational traffic signal control modes*

Time of the day	Level of pedestrians	Duration of traffic light phase
Peak period	Low	Medium
Peak period	Medium	Medium
Peak period	High	High
Off-peak period	Low	Low
Off-peak period	Medium	Medium
Off-peak period	High	High

duration of the traffic light phase will be average. Since the results of logical conclusion are fuzzy variables, a fuzzy logic controller converts these fuzzy outputs into clear values using the defuzzification method for the actual system to use them.

For example, in the case of a traffic light cycle (25 or 40 sec), if the result of defuzzification (i.e., a numerical value, not a linguistic value) falls in the middle range, the values for the green, amber, and red light times will be as follows: for a 25-sec cycle: the green phase lasts 9 sec, the amber phase - 5 sec, and the red phase - 11 sec; for a 40-sec cycle: the green phase lasts 18 sec, the amber phase - 5 sec, and the red phase - 17 sec.

These values adjust the duration of the traffic light phase according to the existing traffic conditions.

Thus, defuzzification ensures that the controller's fuzzy results are converted into specific, clear values that can be used to control the traffic signal, ensuring that the duration of the traffic signal phases is optimized to match the existing traffic conditions at the intersection.

5 Discussion

Creating a simulation model to study the rational mode of control at pedestrian crosswalks is critical in determining the optimal conditions for pedestrian and vehicle traffic at such crosswalks. The aim of this process is to ensure the maximum safety and efficiency in managing pedestrian flows.

Based on the results of studies of traffic and pedestrian flows, as well as the parameters of the road network, the optimal control parameters were substantiated. The following main indicators determined the optimal mode of traffic signal control: the level of roadway congestion, the maximum length of the queue of vehicles approaching the stop-line, and the share of time when the restrictive signal is lit for the lane during the traffic signal control cycle. The applicability of these indicators was tested using the PTV VISSIM software. In addition, the pedestrian behavior was taken into account for three types of intersections, depending on the characteristics of traffic on them.

At the initial research stage, PTV VISSIM software was used to model the traffic flows. For this purpose, the initial conditions were set at which the traffic volume varied from 50 to 700 p.c.u./h. The lane capacity on the approach to the intersection was set at 800 p.c.u./h. This value corresponds to ideal traffic conditions, which are characterized by a homogeneous traffic flow (100% passenger cars), good driving conditions and high-quality road surface.

Traffic and pedestrian flows were simulated using various simulation methods, including the static setting of traffic light cycle times. The traffic light system was implemented with one group of signals, and its cycle time was 120 seconds, with alternating red and green signals. The share of the restrictive signal per lane in the traffic light cycle was determined by the ratio $\beta = t_r / T_r$ and varied from 10 to 105 sec. The regulatory limitation on the duration of the traffic light cycle ($25 < T_c < 120$) was also considered, and the value of the main phase duration for transport was not less than t_p = 7 sec. In addition, the installation of surveillance cameras was simulated through the external interface module provided by the PTV VISSIM program to implement the controller based on fuzzy logic. Even in this case, the fuzzy logic approach proposed in this article was applied to 25-120 sec cycles, which could dynamically change depending on the situation.

As for the pedestrian phases, the geometric parameters of the intersection did not change, and the duration of the transition interval was calculated taking into account the average speed of cars approaching the stop-line without braking. It made it possible to optimize the conditions for the safe passage of vehicles through the intersection and ensure the efficient use of traffic signals.

The results of the study, which reflect the change in the maximum queue length, depending on the volume-capacity ratio of the intersection before the stop-line and the share of the duration of the restrictive signal in the traffic lane in the control cycle for three types of intersections, are shown in Figure 5.

The graph in Figure 5 shows that increasing the duration of the pedestrian restrictive signal affects the share of pedestrians who cross the roadway at the restrictive signal, especially for the intersections of type I. It emphasizes the need to adjust the duration of the traffic signal cycle in areas with heavy pedestrian traffic. In addition, shortening the duration of the pedestrian signal reduces vehicle waiting time. If the traffic volume exceeds 500 veh/h per lane, this can lead to queues of vehicles longer than 90 m with a restrictive signal duration of 40 sec.

Table 5 *Dependencies of changes in the maximum queue length depending on the volume-capacity ratio and the share of the restrictive signal in the lane in the control cycle*

Type of intersection	Formulas	Coefficient of determination, R^2
I	$L_r = 156.42 - 265.018 \cdot z - 675.696 \cdot \beta + 117.453 \cdot z^2 + 915.616 \cdot z \cdot \beta + 563.626 \cdot \beta^2$	0.73
II	$L_r = 162.123 + 120.567 \cdot z + 45.432 \cdot \beta - 50.987 \cdot z^2 + 200.346 \cdot z \cdot \beta - 30.211 \cdot \beta^2$	0.72
III	$L_r = 112.852 + 115.568 \cdot z + 47.901 \cdot \beta - 55.436 \cdot z^2 + 198.765 \cdot z \cdot \beta - 28.346 \cdot \beta^2$	0.70

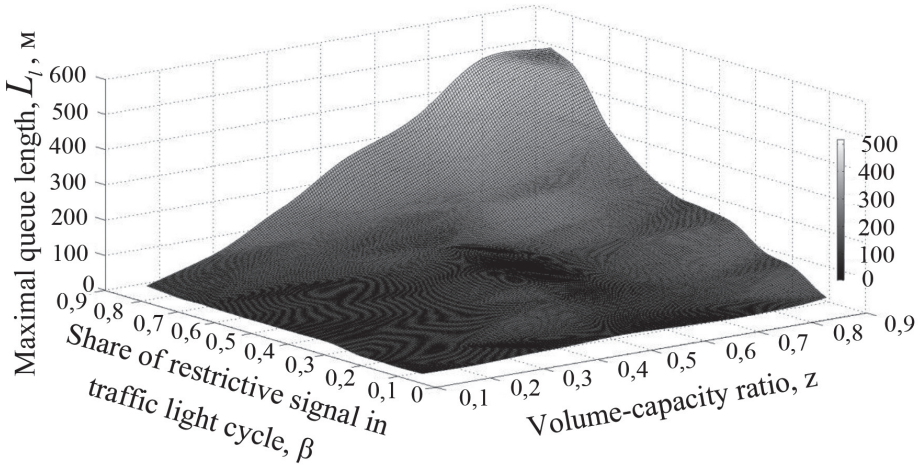

a)

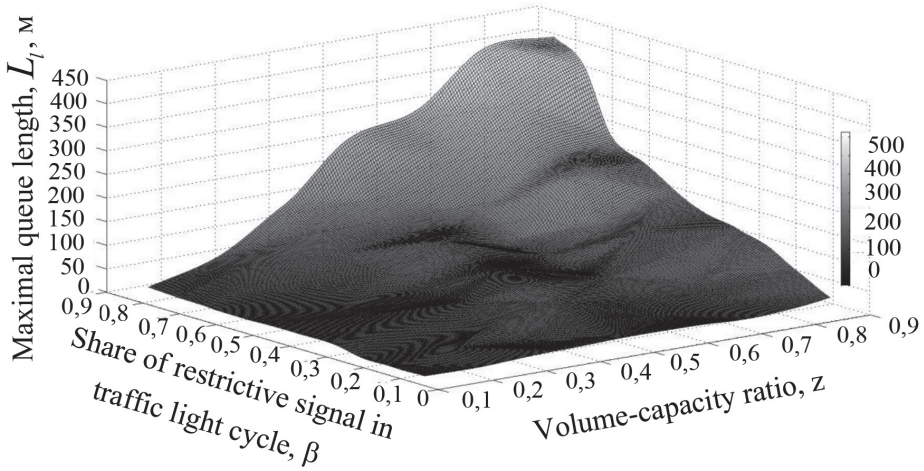

b)

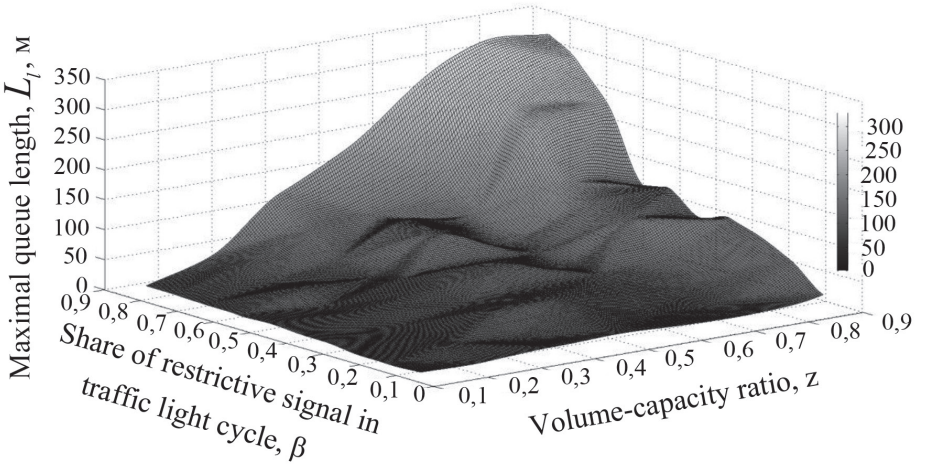

c)

Figure 5 *Change of the maximum queue length depending on the volume-capacity ratio of the roadway and the share of restrictive traffic signals: a - signalized crosswalk of type I; b - signalized crosswalks of type II; c - signalized crosswalks of type III*

After processing the modelling results, an empirical dependence was obtained of the maximum queue length on the volume-capacity ratio and the share of the restrictive signal in the traffic lane in the traffic light cycle (Table 5).

According to the modeling results, the maximum queue length of vehicles before the stop-line is the longest for intersections of type I located near transport hubs and reaches 504.6 m at a volume-capacity ratio of intersection 0.88 and share of a restrictive signal in the traffic lane 0.83. In comparison, for type II (in central areas) and type III (in residential areas) intersections, the queue length is reduced to 403.7 m and 317.9 m, respectively

These results indicate that at intersections of type I, where the traffic load is highest, the traffic signal control modes need to be optimized especially carefully to prevent the excessive vehicle delays. Reduced queue length at intersections of type II and III indicates that less stringent regulatory mechanisms can be applied in less congested areas.

The proposed approach allows reducing vehicle delays effectively and considers pedestrians' needs in traffic signal control systems. It can be especially useful in developing the optimal control strategies at intersections with high traffic volumes and significant pedestrian activity.

6 Conclusions

1. The analysis of patterns and methods for studying the behavior of road users revealed that optimization of traffic signal control modes and parameters depends on a number of factors, such as pedestrian and traffic volumes, waiting time, queue length, and the number of crossing violations. The main research methods used to set up the traffic signal control systems are observation, mathematical modeling, and statistical data analysis. These methods make it possible to adapt traffic light cycles to real traffic conditions to improve the safety and efficiency of traffic flows.
2. An experimental study was conducted at signalized intersections and a midblock signalized pedestrian crosswalk in Lviv. For signalized intersections with different traffic and pedestrian flow conditions, it was found that these conditions depend on the location in the city. Based on this, the intersections are divided into three types according to the traffic characteristics: type I - intersections near transport hubs where there is a high traffic volume and a significant number of pedestrians, especially near train stations, bus stations, and other main urban infrastructure facilities; type II - intersection in the central area of the city, where traffic flows are quite intense, and pedestrian traffic is generated mainly by commercial and business centers; type III - intersections in residential areas where the traffic volume is lower, but still many pedestrians cross roadways near schools, parks, and residential areas. It was found that in residential areas (type III), the share of pedestrian traffic violations is 9%, possibly due to fewer cars and a lower level of control. In the central areas of the city (type II), this indicator is somewhat lower - 7%, as traffic volume increases and people are less likely to ignore traffic signals in a fast-paced environment. Near transport hubs (type I), the share of violators reaches the highest level - 13%, possibly due to the large number of pedestrians and high level of haste.
3. The method of adaptive traffic control at pedestrian crossings has been improved. It considers not only the physical and psychophysiological capabilities of pedestrians but the factors that influence their behavior when deciding to cross the road, as well. The method includes elements of predicting pedestrian behavior based on previous observations and can be adapted to specific conditions of an intersection or crosswalk.
4. Based on the collected data and conducted research, recommendations were developed for choosing the optimal traffic signal control modes at different types of intersections. It takes into account traffic delays, pedestrian volume, and the level of traffic violations. It was found that:
   - ❑ for the two-phase control, the optimal cycle time should be between 25 and 70 sec, depending on the driving conditions;
   - ❑ for the three-phase control - from 40 to 90 sec, taking into account the needs of both vehicles and pedestrians;
   - ❑ for the four-phase control - from 60 to 120 sec, which provides the most comprehensive approach to control different flows.

These recommendations allow for flexible adjustment of traffic signal modes, which helps to reduce delays, increase safety at intersections and pedestrian crosswalks, and improve overall traffic efficiency in urban areas.

Acknowledgement

We would like to express our gratitude to Lviv municipal enterprise "Lvivavtodor" for its valuable assistance and cooperation during the experimental study. Your support and professionalism were an important contribution to the results of our work.

Conflicts of interest

The authors declare that they have no known competing financial interests or personal relationships that could have appeared to influence the work reported in this paper.

References

[1] BOIKIV, M., POSTRANSKYY, T., AFONIN, M. Establishing patterns of change in the efficiency of regulated intersection operation considering the permitted movement directions. *Eastern-European Journal of Enterprise Technologies* [online]. 2022, **118**(3), p. 17-26. ISSN 1729-3774. Available from: https://doi.org/ 10.15587/1729-4061.2022.262250

[2] FORNALCHYK, Y., KODA, E., KERNYTSKYY, I., HRYTSUN, O., ROYKO, Y., BURA, R., OSINSKI, P., BARABASH, R., HUMENUYK, R., POLYANSKY, P. The impact of vehicle traffic volume on pedestrian behavior at unsignalized crosswalks. *Roads and Bridges - Drogi i Mosty* [online]. 2023, **22**(2), p. 201-219. eISSN 2449-769X. Available from: https://doi.org/10.7409/rabdim.023.010

[3] HASSAN, S., HOUNSELL, N., SHRESTHA, B. Investigating the applicability of upstream detection strategy at pedestrian signalised crossings. *Promet - Traffic and Transportation* [online]. 2017, **29**(5), p. 503-510. ISSN 1848-4069. Available from: https://doi.org/10.7307/ptt.v29i5.2225

[4] PAU, G., CAMPISI, T., CANALE, A., SEVERINO, A., COLLOTTA, M., TESORIERE, G. Smart pedestrian crossing management at traffic light junctions through a fuzzy-based approach. *Future Internet* [online]. 2018, **10**(2), 15. ISSN 1999-5903. Available from: https://doi.org/10.3390/fi10020015

[5] HO, T., CHUNG, M. Information-aided smart schemes for vehicle flow detection enhancements of traffic microwave radar detectors. *Applied Sciences* [online]. 2016, **6**(7), 196. eISSN 2076-3417. Available from: https://doi.org/10.3390/app6070196

[6] EL HAMDANI, S., BENAMAR, N., YOUNIS, M. Pedestrian support in intelligent transportation systems: challenges, solutions and open issues. *Transportation Research Part C: Emerging Technologies* [online]. 2020, **121**, 102856. ISSN 0968-090X. Available from: https://doi.org/10.1016/j.trc.2020.10285

[7] SALVO, G., CARUSO, L., SCORDO, A., GUIDO, G., VITALE, A. Traffic data acquirement by unmanned aerial vehicle. *European Journal of Remote Sensing* [online]. 2017, **50**(1), p. 343-351. eISSN 2279-7254. Available from: https://doi.org/10.1080/22797254.2017.1328978

[8] BRANQUINHO, J., SENNA, C., ZUQUETE, A. An efficient and secure alert system for vanets to improve crosswalks' security in smart cities. *Sensors* [online]. 2020, **20**(9), 2473. eISSN 1424-8220. Available from: https://doi.org/10.3390/s20092473

[9] ZHANG, H., ZHANG, C., WEI, Y., CHEN, F. Effects of mobile phone use on pedestrian crossing behavior and safety at unsignalized intersections. *Canadian Journal of Civil Engineering* [online]. 2019, **46**(5), p. 381-38. ISSN 0315-1468, eISSN 1208-6029. Available from: https://doi.org/10.1139/cjce-2017-0649

[10] GIUFFRE, T., CAMPISI, T., TESORIERE, G. Implications of adaptive traffic light operations on pedestrian safety. *IOSR Journal of Mechanical and Civil Engineering* [online]. 2017, **13**, p. 58-63. eISSN 2278-1684. Available from: https://doi.org/10.9790/1684-1306045863

[11] BARBERI, S., ARENA, F., TERMINE, F., CANALE, A., OLAYODE, I. Safety aspects of intelligent transport systems applied to road intersections. *AIP Conference Proceedings* [online]. 2022, **2611**(1), 060012. ISSN 1551-7616. Available from: https://doi.org/10.1063/5.0119774

[12] CHOI, J., AHN, B., KWEON, I. Crosswalk and traffic light detection via integral framework. In: The 19th Korea-Japan Joint Workshop on Frontiers of Computer Vision: proceedings [online]. IEEE. 2013. ISBN 978-1-4673-5620-6, eISBN 978-1-4673-5621-3, p. 309-312. Available from: https://doi.org/10.1109/FCV.2013.6485511

[13] MURALIDHARAN A., COOGAN, S., FLORES, C., VARAIYA, P. Management of intersections with multi-modal high-resolution data. *Transportation Research Part C: Emerging Technologies* [online]. 2016, **68**, p. 101-112. ISSN 0968-090X. Available from: https://doi.org/10.1016/j.trc.2016.02.017

[14] GUANETTI, J., KIM, Y., BORRELLI, F. Control of connected and automated vehicles: state of the art and future challenges. *Annual Reviews in Control* [online]. 2018, **45**, p. 18-40. ISSN 1367-5788. Available from: https://doi.org/10.1016/j.arcontrol.2018.04.011

[15] ROYKO, Y., HRYTSUN, O., BURA, R., YEVCHUK, Y. Provision of a rational control mode at pedestrian crosswalk. *MATEC Web of Conferences* [online]. 2024, **390**, 03011. eISSN 2261-236X. Available from: https://doi.org/10.1051/matecconf/202439003011

[16] ALVER, Y., ONELCIN, P. Gap acceptance of pedestrians at overpass locations. *Transportation Research Part F: Traffic Psychology and Behaviour* [online]. 2018, **56**, p. 436-443. ISSN 1369-8478. Available from: https://doi.org/10.1016/j.trf.2018.05.010

[17] HASSAN, S., HOUNSELL, N., SHRESTHA, B. Verification of puffin modelling using VISSIM. *Journal Technology / Jurnal Teknologi* [online]. 2013, **65**(3), p. 81-84. ISSN 2180-3722. Available from: https://doi.org/10.11113/jt.v65.2150

[18] FAYYAZ, K., SCHULTZ, G., GALVEZ DE LEON, P. Driver compliance at enhanced pedestrian crossings in Utah (No. UT-19.03). Utah: Department of Transportation, 2019.

[19] KHATTAK, Z., MAGALOTTI, J., FONTAINE, M. Estimating safety effects of adaptive signal control technology using the Empirical Bayes method. *Journal of Safety Research* [online]. 2018, **64**, p. 121-128. ISSN 0022-4375. Available from: https://doi.org/ 10.1016/j.jsr.2017.12.016

[20] ASAITHAMBI, G., KUTTAN, M., CHANDRA, S. Pedestrian road crossing behavior under mixed traffic conditions: a comparative study of an intersection before and after implementing control measures. *Transportation in Developing Economies* [online]. 2016, **2**(2), 14. eISSN 2199-9295. Available from: https://doi.org/ 10.1007/s40890-016-0018-5

[21] ASLANI, M., SEIPEL, S., MESGARI, M., WIERING, M. Traffic signal optimization through discrete and continuous reinforcement learning with robustness analysis in downtown Tehran. *Advanced Engineering Informatics* [online]. 2018, **38**, p. 639-655. ISSN 1474-0346. Available from: https://doi.org/10.1016/j.aei.2018.08.002

[22] FRICKER, J., ZHANG, Y. Modeling pedestrian and motorist interaction at semi-controlled crosswalks: The effects of a change from one-way to two-way street operation. *Transportation Research Record* [online]. 2019, **2673**(11), p. 433-446. ISSN 0361-1981. Available from: https://doi.org/10.1177/0361198119850142

[23] HRYTSUN, O. Impact of traffic volume and composition on the change in the speed of traffic flow. *Transport Technologies* [online]. 2023, **2023**(1), p. 12-20. eISSN 2709-5223. Available from: https://doi.org/10.23939/tt2023.01.012

[24] ADAM, I., WAHAB, A., YAAKOP, M., SALAM, A., ZAHARUDIN, Z. Adaptive fuzzy logic traffic light management system. In: 2014 4th International Conference on Engineering Technology and Technopreneuship ICE2T: proceedings [online]. 2014. ISBN 978-1-4799-4621-1, p. 340-343. Available from: https://doi.org/ 10.1109/ICE2T.2014.7006274

[25] BI, Y., SRINIVASAN, D., LU, X., SUN, Z., ZENG, W. Type-2 fuzzy multi-intersection traffic signal control with differential evolution optimization. *Expert Systems with Applications* [online]. 2014, **41**, p. 7338-7349. ISSN 0957-4174. Available from: https://doi.org/10.1016/j.eswa.2014.06.022

[26] STOTSKO, Z., FORNALCHYK, Y., MOHYLA, I. Simulation of signalized intersection functioning with fuzzy control algorithm. *Transport Problems*. 2013, **8**(1), p. 5-16. eISSN 2300-861X.

[27] MONTGOMERY, D., RUNGER, G. *Applied statistics and probability for engineers*. John wiley and sons, 2020. ISBN 978-1119746355.


ŽILINSKÁ UNIVERZITA
V ŽILINE


BiotechUSA
SOM VEDEC
NOC


Strojnícka fakulta
BA BB


E 499062

THE INFLUENCE OF THREE PARENT CROSSBREEDING ON THE DUAL POPULATION GENETIC ALGORTIHM

Esra'a Alkafaween[1,2,*], Obada Alhabashneh[2], Maram M. Al-Mjali[2]

[1]Department of Computer Science, Alzaytoonah University of Jordan, Amman, Jordan
[2]Data Science and Artificial Intelligence Department, Mutah University, Karak, Jordan

*E-mail of corresponding author: esrakafaween86@gmail.com

Esra'a Alkafaween 0000-0001-9525-1459

Resume
A genetic algorithm (GA) is an optimization technique based on natural genetics, using selection, crossover, and mutation. Crossover combines genetic material from two parents to create offspring, maintaining diversity and preventing premature convergence. While the two parents are typically used, multi-parent crossover, involving more than two parents, has shown superior results. in this paper is explored the multi-parent crossover in dual genetic algorithms, which facilitate information exchange between populations through interpolation crossbreeding. Offspring inherit traits from both parent populations, improving adaptability. The Cave-Surface GA (CSGA) with three-parent crossover is tested on 15 Travelling Salesman Problem (TSP) benchmarks. Results show that the CSGA outperforms both traditional GAs and two-parent CSGA. This method demonstrates great potential for complex optimization challenges.

Article info
Received 23 September 2024
Accepted 17 March 2025
Online 16 April 2025

Keywords:
genetic algorithm
TSP
multipopulation
multi-parent order crossover
cave surface GA

Available online: https://doi.org/10.26552/com.C.2025.036

ISSN 1335-4205 (print version)
ISSN 2585-7878 (online version)

1 Introduction

Genetic algorithms (GAs) are efficient heuristic random search strategies that are inspired by evolutionary and natural selection theories [1-2]. In the 1970s, Holland [3] investigated the fundamentals of GA. The GA examines a population of chromosomes, each representing a unique candidate solution to a certain problem. The GA includes various operators, including selection, crossover, and mutation. These operators are employed for candidate solutions to achieve improved population generation [4-6].

Among the well-known operators in genetic algorithms is crossover. The crossover process is essential for creating new chromosomes by combining two or more parent chromosomes in the hopes that the result will be an efficient new chromosome. Crossover happens after the selection of parent chromosome pairs and aids in the exchange of information between parents in order to produce offspring. During the crossover, parent chromosomes are taken in pairs and their genes are transferred in a certain order to produce offspring. These offsprings become the parent chromosomes for the following generation [7-8].

Creating the new crossover operators that fit into one of the many chromosomal representations is an important priority for many researchers. Regretfully, the majority of crossover operators' offspring do not acquire sufficient information from their parents. Currently, a crossover operator's multi-parent extension is employed to raise the quality of solutions for optimisation problems. Typically, crossover occurs between only two parents at a time, resulting in one or two offspring. Naturally, the multi-parent reproduction is not used by any species in the natural world. However, limiting the number of parents for crossover to two is not necessary in computer simulations [9].

Since the population maintains diversity, the GA are more resilient than other local search algorithms. Even now, it is still commonly seen that populations lose diversity too soon and that individuals are stuck in local optima, particularly in complex problems with many peaks in the fitness landscape, this issue is in the literature referred to as premature convergence [10-12]. Various methods have been used in numerous previous works to prevent the risk of premature convergence. These methods include: improving the genetic operators (mutation, crossover, and selection) [12-13], dynamic

parameter control [14], Multipopulation GA (MPGAs) [15], a multi-objective evolutionary algorithm [16] and more.

The multi-population idea divides the population into subpopulations, each of which is more likely to follow a different search path. The migration process exchanges good individuals between subpopulations, while the crossover operator creates new individual. The migration rate is the number of individuals that must be replaced between subpopulations, and it allows for control over the degree of diversity within the subpopulation. Migration interval, which affects the number of times migration occurs, is another element that encourages subpopulation variety [17] and [18].

Dual-population GA (DPGA) is a form of MPGA in which an additional population acts as a reservoir of diversity. The main population is comparable to that of a traditional GA and evolves to find effective solutions. The reserve population evolves to support and diversify the main population. In contrast to MPGAs, which use migration to communicate information between populations, the DPGAs rely on crossbreeding due to their distinct fitness functions [19] and [20].

Crossbreeding is used by dual populations to share information amongst populations. Crossbreeding refers to a recombination of an individual from the main population and an individual from the reserve population. Since the offspring of this crossbreeding contain genetic material from both populations, their fitness values are generally high in either population, and they can serve as a means of information sharing.

The TSP is an NP-hard problem in combinatorial optimization, as well as an old and challenging combinatorial mathematics topic. Enumeration makes it simple to find the shortest path between some cities [21-22]. If n is actually large, there are (n-1)! potential combinations, and the searching space of the routes will show a pattern of explosive growth. Under these conditions, one cannot locate the ideal path using the conventional searching strategy. As a result, several new types of optimization computation methods emerge to get the TSP's optimal solution; among which, the GA receives the most favor of the public and becomes one of the most effective techniques to solve the TSP, because of its wide applicability and the character that does not require to get additional insight into the problems and depends less on the specific fields of the problem [23].

The GA is utilized not just to solve conventional TSPs, but in a variety of other applications, as well, including transportation planning [24], location-based services [25] and urban design [26], etc.

In this paper, the contribution is to the topic of enhancing dual population GA performance employing three parents during population crossbreeding, in an attempt to promote gene variety and introduce significant features, as well as to reduce the premature convergence and so improve the performance of genetic algorithms.

2 Related work

The GAs primarily use two parents for crossover operations, which corresponds to the natural behaviour of evolution, in which individuals adopt only the two parents to generate an offspring. However, studies have shown that multi-parent crossover is more effective and more successful than the two-parent crossover [27-28].

One possible strategy to increase the GA performance is to add new features into the GA, i.e., features that do not fit within the existing GA paradigm, some recent efforts employing the multi-parent recombination operators. An attempt to maintain the basic GA paradigm while improving the GA performance by permitting multi-parent reproduction [29]. Multi-parent crossover can be seen of as a generalisation of conventional two parent crossover in terms of the number of parents. There have been many suggestions for the multi-parent crossover operators. In general, having more parents results in a more thorough survey to identify the genes of the offspring and increases the likelihood of either exploitation, exploration, or both [30].

Several multi-parent crossover methods have been developed for genetic algorithms such as scanning crossover [27], diagonal crossover [27], center of mass crossover, multi-parent feature-wise crossover, and seed crossover [31], simplex crossover [32]. Studies show that the multi-parent crossover is more effective than the two parent crossover. The performance of these multi-parent crossovers is generally studied using numerical optimization problems [33].

To solve combinatorial optimization problems, only a limited number of multi-parent crossovers have been used, including adjacency-based crossover (ABC) [27], multi-parent extension of partially mapped crossover (MPPMX) [33], multi-parent sequential constructive crossover (MPSCX) [9], extended precedence preservative crossover [34] and a multi-parent order crossover (MPOX) [35].

The ABC is suitable for order-based representations, such as TSP, where value positioning is crucial. This crossover uses a marker update approach to pick genes from all parents and produce viable offspring, while this crossover resulted in a viable TSP child.

The MPPMX [33] extends partially mapped crossover to address the multi-parent crossover. The proposed crossover changed the mapping list and legalisation method to include more parents in the partially mapped crossover.

The multi-parent sequential constructive crossover was developed to address the travelling salesman and job shop scheduling problem. Experiments were conducted to assess MPSCX performance with varying parent numbers and mutation probability. Experimental findings on TSPLIB instances demonstrate that MPSCX considerably increases solution quality.

The MPOX [35] extends the Order Crossover (OX) [36; this extension's primary goal is to generate an

acceptable solution from more than two parents that can handle various combinatorial challenges with efficacy. The berth allocation problem (BAP) and TSP have been used to analyse the original OX and MPOX. The outcomes demonstrate that MPOX outperforms the two-parent OX and generates competitive performance for both benchmarks.

3 Experimental settings and result

In the literature, the multiple parent crossovers have successfully demonstrated the power of using more parents. The effectiveness of these operations has been examined experimentally. The performance of MPOX has also been tested on travelling salesman problems, which have been widely studied in the literature. To examine the effectiveness of the multi parent crossover and its effect on the MPGA, and specifically on dual population, the multi-parent order crossover (MPOX) [35] was chosen as a crossbreeding operator between dual population, Specifically in CSGA algorithm.

In this paper, the CSGA algorithm are chosen [37], which uses two populations and is also a type of MPGA. The CSGA method is inspired by the genetic diversity found in Mexican cavefish and is a variation of the Dual Population GA. Through the inter-population crossbreeding, the CSGA enhances variety via the secondary population (cave population) and enables information transmission between populations, effectively preventing the premature convergence.

The CSGA starts with two randomly generated populations: Cave and Surface. Individuals in each population are evaluated with the same fitness functions. The Cave population evolves by a combination of inbreeding within the population and crossbreeding with individuals from the Surface population. Additionally, the surface population evolves predominantly by inbreeding among parents from the same population.

A conventional GA selects two parent chromosomes for a cross-over procedure, yielding two offspring. The CSGA, on the other hand, has two more factors beyond GAs: the crossbreeding interval (CI) and the crossbreeding rate. The crossbreeding interval (CI) is the number of generations between each crossbreeding, whereas the cross-breeding rate (CR) is the number of individuals picked from each group during the cross-breeding. These factors affect both accuracy and computation time. CSGA generates two offsprings through each cross-over operator between the two parents by randomly selecting a number of parents from the two populations for recombination based on the crossbreeding rate. Following that, one of the children is chosen to join the Cave population's next generation through selection for local survival, while the other is transported to the Surface population. In addition to being repeated for each of the two prospective parents, this process is only carried out through particular generations, depending on the CR rate. The pseudocode for CSGA is displayed in Algorithm 1 [37] (see Figure 1).

The MPOX [35] generalizes the Order Crossover (OX) to a multi-parent crossover. To cut each parent into substrings for an n-parent MPOX, n-1 crossing points generated randomly. The second chosen substring, which is between the first and second crossover points, is then duplicated into the newly created offspring at the same absolute position in the following step.

To create a viable offspring from multiple parents, the MPOX begins at the second crossover point of the second parent. It then selects the elements that are not already present in the offspring to fill in the gaps, starting from this crossover point (the third substring).

Algorithm 1: CSGA Algorithm

Begin
step1: initialize input parameters of problems: crossover rate, mutation rate, crossbreeding rate (cr), crossbreeding interval (ci), max generation.
step2: initialize two subpopulations, cave population (cp) and surface population (sp).
step3: For each subpopulation, repeat the following steps until the termination criterion is met.
step4: Calculate fitness value;
step5: inbreeding:
a. Selection
b. Crossover
c. Mutation
step6: crossbreeding (based on ci and cr do):
a. choose individual from cp and choose individual from sp.
b. Crossover
c. Move offspring one to
cp and the second to sp.
step8: output the final best solution.
End.

***Figure 1 The** CSGA Algorithm [37]*

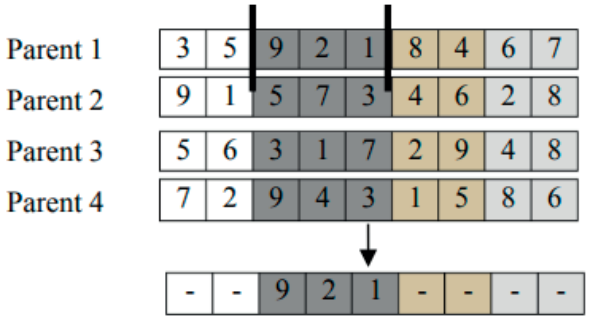

Fig. 4. Substring copy.

Figure 2 *MPOX with four parents [36]*

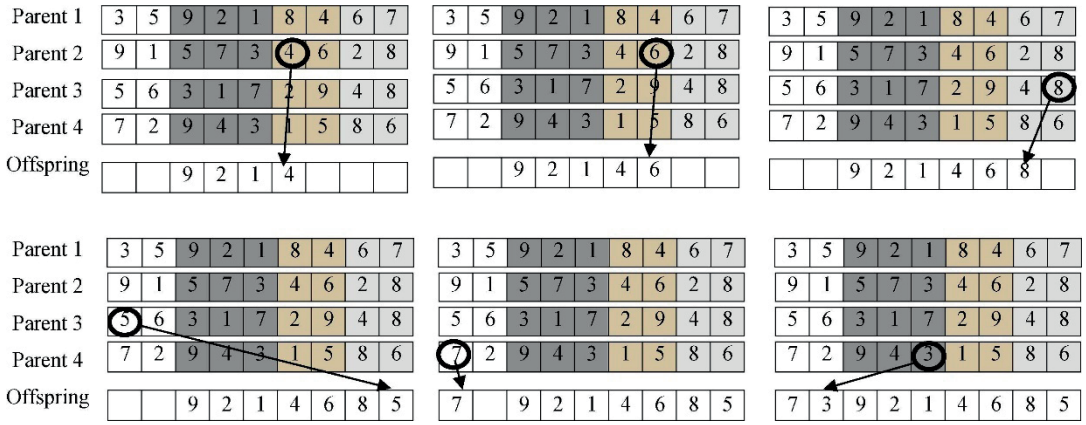

Figure 3 *An example of MPOX-based offspring production [36]*

This process continues until the third substring of the offspring is fully populated.

Next, the MPOX moves to the fourth crossover point of the next parent, again choosing elements not included in the offspring and filling them in from that crossover point. This continues until the next crossover point or the end of the offspring is reached. Once all the parents have been processed, the MPOX starts over with the first parent, selecting any missing elements and copying them into the offspring from the beginning up to the second crossover point. This ensures the offspring is fully completed with all the necessary elements (see Figure 2 and Figure 3).

Going back to step 6 in the CSGA in Algorithm 1, MPOX crossover was used as a crossbreeding operator between the two populations., where the two offspring are selected from the first population and one offspring from the second population. Two of the resulting individuals were sent to the first population, and one was sent to the second population. (see Figure 4). In this way, the population was aimed to be more diverse and thus reduce the premature convergence.

To investigate the effect of utilizing three parents in the crossbreeding of the CSGA algorithm, investigations were conducted in 15 instances from the TSPLIB [38]. The experiment was carried out ten times for each instance.

Table 1 displays the GA parameters that were selected to perform the experiments. Since the primary objective of the study was to validate the effectiveness of the CSGA with 3 parent crossover, the genetic algorithm and CSGA regardless of the parameters used, No complex parameter control procedures were utilized. The GA's simple and standard parameters were used.

The fitness level of each individual was ascertained by a truncated selection process. Truncation selection is the simplest selection technique, and this is a common way to allocate the fitness function to each chromosome in the GA population. This kind of selection involves sorting the population based on fitness and then eliminating the proportion of people who are less fit [39].

Since one-point modified crossover and exchange mutation are two of the most straightforward approaches that have been applied to situations that are classified as permutation problems, they were employed for the reproduction process in our research [22]. One-point modified crossover creates the offspring by using the single point fragmentation of the parents and then combining the parents at the crossover point. One-point crossover chooses two parents for crossover and then chooses any crossover point at random. The parents are then combined at the crossover point to create two offspring. The frequency with which two chromosomes exchange some of their parts during a single generation is known as the crossover rate; crossover rate is in the range of [0,1] [7].

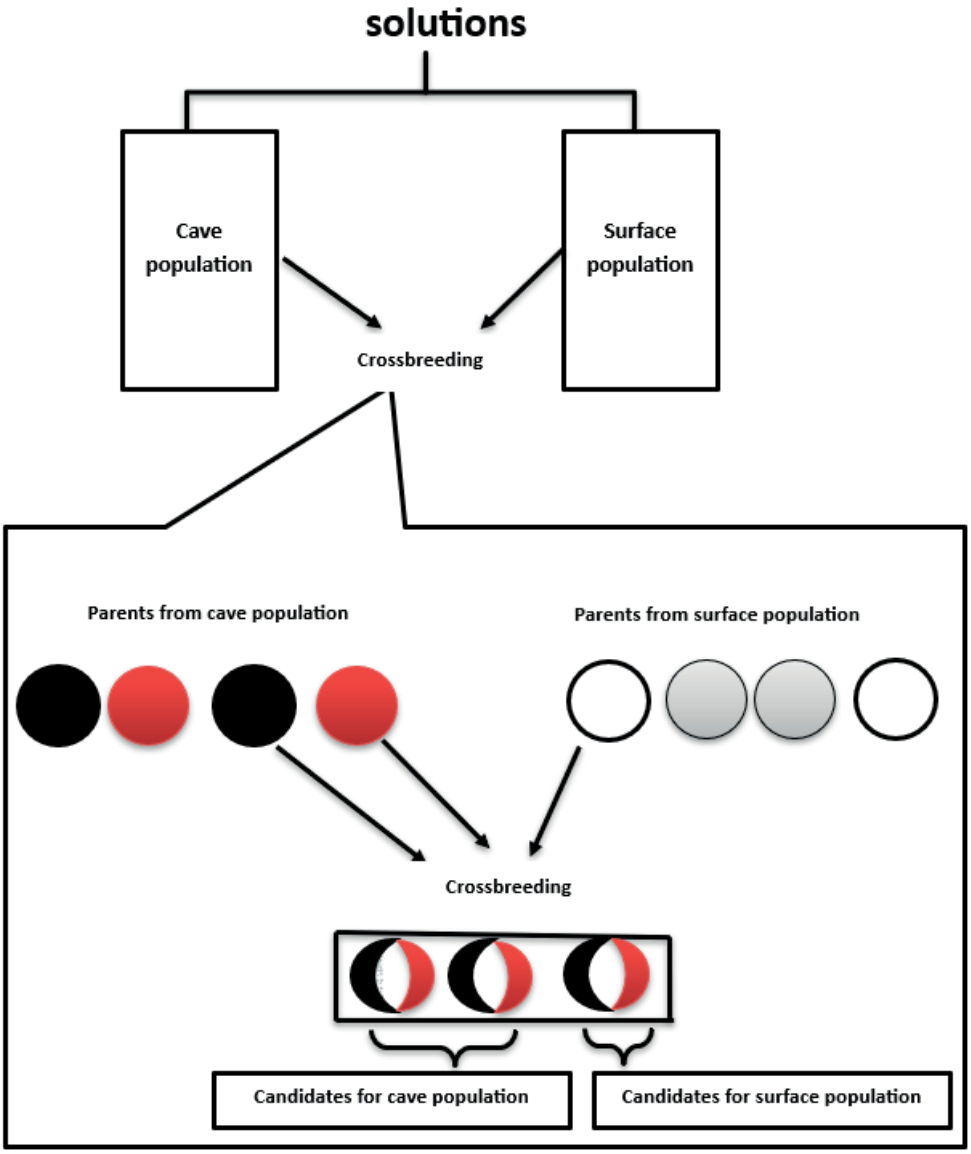

Figure 4 *CSGA method with 3 parents crossbreeding*

Table 1 *GA configuration*

Parameter	Value
Population size	200
Generation limit	3000
Initialization method	Random
Crossover	One-point modified
Crossover rate	0.85
Mutation	Exchange
Mutation rate	0.08
Selection	Truncation Selection
Crossbreeding Rate	5
Crossbreeding Interval	7
Termination criteria	Generation limit
Crossover type used in Crossbreeding	MPOX

The exchange mutation randomly selects two genes and switches their locations. The mutation rate, which ranges from 0 to 1, specifies the number of chromosomes to be modified in a single generation [8].

Our GA employed the reinsertion method, which is an expansion sampling technique, in each experiment [40]. This technique ensures that only the best half of the population - from both the new and old generations - is chosen for the following generation. The old generation competes with the new individuals when a new generation is created.

The genetic algorithm's basic parameters were purposefully and manually selected. Neither parameter tuning, nor intricate control processes, were used. Natural ratios for the crossover and mutation process were the crossover and mutation ratios. In addition, the population size was manual, as well as the number of generations, and this was fixed for all methods for fair comparison. Again, these parameters are standard, and are used in many researches. This strategy is consistent with our paper's primary objective, which is to confirm the efficacy and emphasize the advantages of employing

Table 2 The *TSP instance results obtained through 3000 generations using GA and CSGA algorithms*

Optimal Solution	Instance	GA		CSGA		CSGA with 3 Parent Crossbreeding	
		Min	Average	Min	Average	Min	Average
2579	a280	6952	7587.1	5914‡	6541.2‡	6317	6575.7
10628	att48	35843	41766.4	35704	40468.3	35873	39482‡
7542	berlin52	8253‡	9123.1‡	8497	9572.5	8599	9247
118282	bier127	152453	170944.7	146855‡	161837.4	149325	157590.6‡
6110	ch130	8865	10000.7	8768	9777.2	8442‡	9335.8‡
6528	ch150	10114	10914.667	9965	10906	9455‡	10314.6‡
426	eil51	465	478.3‡	476	502.5	455‡	493
21282	kroA100	27555	32230.6	27175	31655.4	26256‡	28069.9‡
14379	lin105	20153	24129.1	20006	23199.1	17778‡	21983.8‡
108159	pr76	134438	133195.82‡	130101	143111.4	129849‡	144835.2
58537	pr144	112926‡	119005.8‡	117911	134050.4	117026	128547
42029	lin318	125686	139947.1	112936‡	119163.4‡	117471	126146.1
202339	ali535	9484	10249.5	8418‡	8827.6‡	8713	9429.333
8806	rat783	51871	53879.1	46348‡	47547‡	49308	52293.4
29437	kroB200	58704	67404.5	57500	61319.4	51832‡	59243.8‡

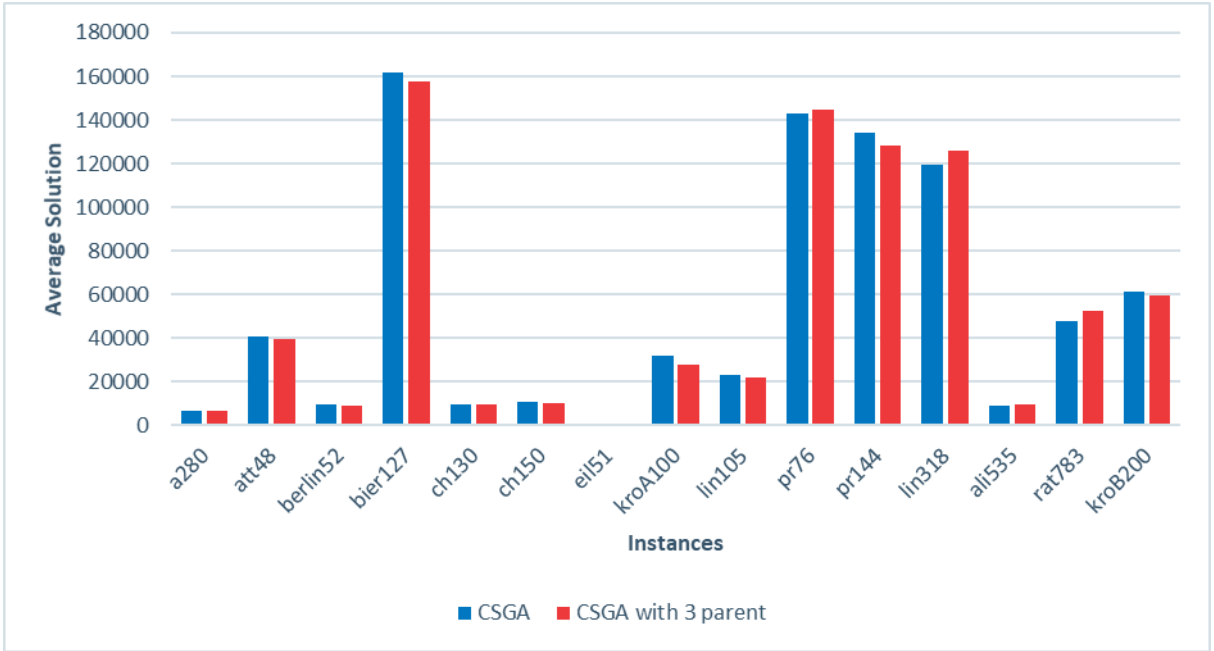

Figure 5 *Average Convergence of each Algorithm in 15 instances*

three parents throughout the crossbreeding process in comparison to the genetic algorithm in terms of diversity.

Table 2 summarizes the results of the three-parent crossover on TSP instances.

As demonstrated in Table 2, in 7 out of 15 cases, the CSGA with 3 parent crossover outperformed the CSGA and GAs. The CSCA with three-parent crossover also had the lowest costs in nine out of the fifteen cities, as can be seen in the table's Min column.

The Average convergence of each algorithm to a minimum value is shown in Figure 5. Once more, the CSGA with three parent crossover performs better in terms of convergence to a minimum value on KroA100 and ch130 than both CSGA and GA. The better convergence becomes possible by the population diversity that the CSGA with three parent crossover provides as shown in Figure 6 and 7.

The contribution of using a crossover with three parent is observed in the attempt to find diversity in the dual population., despite not using any complex parameters, and the stability of the parameters for the two methods, the importance of using the crossover with 3 parent is shown, and what also contributed to the diversity is sending the resulting individuals to the first population, which led to the diversity in the population by allowing the extraction of characteristics from the parents, and thus the resulting offspring possesses good characteristics from the three parents.

As can be seen from Table 3 and Figure 8, GA is the fastest algorithm in all the cases, showing that it requires the least computation. The CSGA takes more time than GA and CSGA with 3 Parent Crossbreeding takes the longest execution time. For small instances, GA might be sufficient. For large instances, CSGA or CSGA with 3 Parent Crossbreeding is preferable.

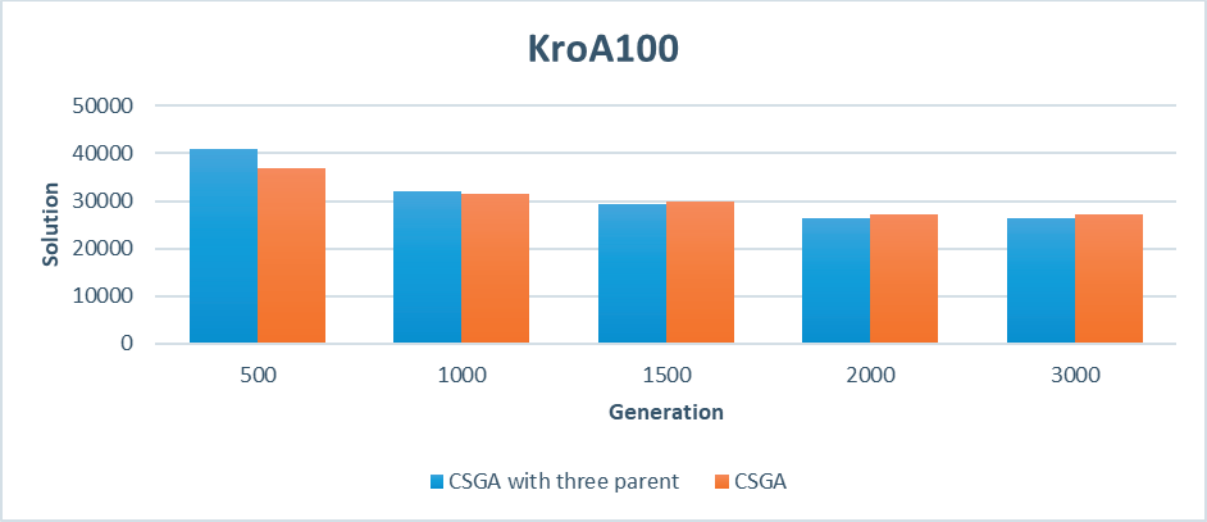

Figure 6 *The KroA100 Convergence of Min value*

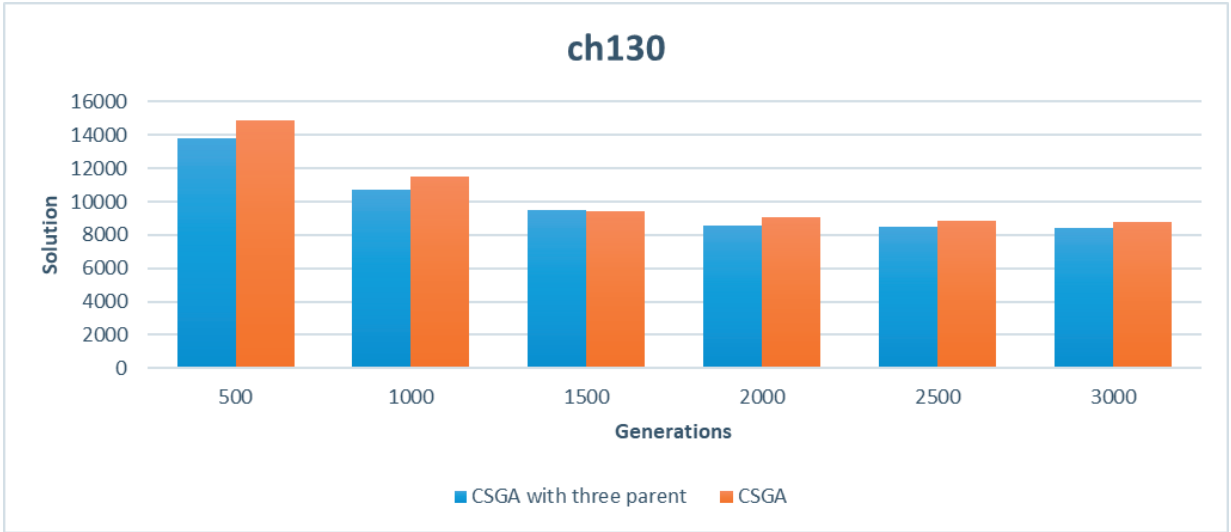

Figure 7 *The ch130 Convergence of min value*

As Table 4 illustrates, the GA is the fastest but least effective in finding optimal solutions. The CSGA improves both the minimum and average solution values, while maintaining a reasonable execution time. The CSGA with 3 Parent Crossbreeding achieves the best solutions, but takes the longest time to execute.

CSGA with 3 Parent Crossbreeding is only suitable if solution quality is more important than speed.

Table 3 *Time consumed by each method after 3000 generations*

Instance	Time, ms		
	GA	CSGA	CSGA with 3 Parent Crossbreeding
a280	48083	65754‡	108230
att48	44117	55874	52664‡
berlin52	39001	58008	54515‡
bier127	46659	73485‡	75473
ch130	44808	87922	70094‡
ch150	72956	69967‡	76813
eil51	52743	37872	37174‡
kroA100	52028	45897‡	57707
lin105	51643	53942‡	58133
pr76	30063	38676‡	40638
pr144	50496	63113‡	65438
lin318	71389	86459‡	106096
ali535	136794	294048	272006‡
rat783	96934	618016	427801‡
kroB200	105338	147291	143102‡

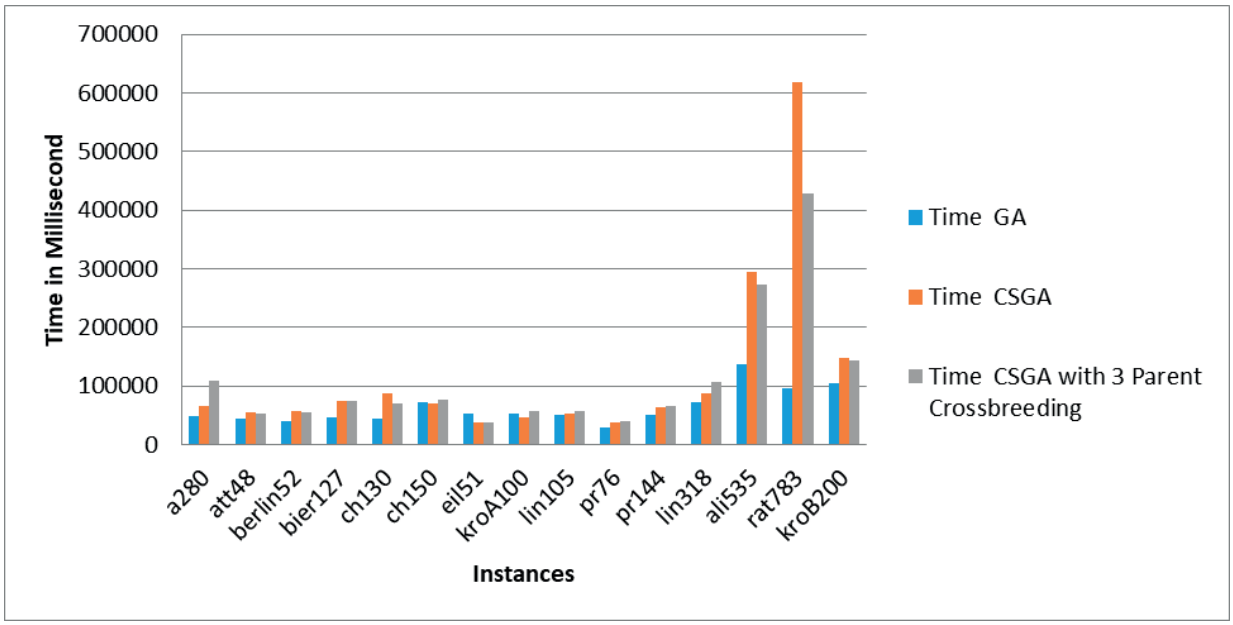

Figure 8 *Time Consumed*

Table 4 *Trade-off between execution time and solution quality*

Algorithm	Solution Quality	Execution Time
GA	Worst	Fastest
CSGA	Good	Moderate
CSGA with 3 Parent Crossbreeding	Best	Slows

4 Conclusion

The multi-parent crossover operator is one of the mechanisms used in evolutionary algorithms to improve the population diversity. Multi-parent crossovers have shown their superiority over the classic two-parent crossovers in several problems as shown in the literature. In this paper, the performance of three parent crossover methods on MPGA was investigated., and more specifically on the crossbreeding process on CSGA. To tackle combinatorial optimisation problems, the MPOX crossover was selected, which is an extension of OX. This extension's primary goal is to generate a workable solution from more than two parents that can be applied to various combinatorial problems effectively. This assessment was conducted on the TSP problem, and a comparison was made between the traditional GA, which uses only two parents in the crossover process, the CSGA algorithm, which uses two parents in the crossbreeding between populations and the CSGA algorithm, which uses three parents in the crossbreeding between populations. According to the results, three parent crossover in crossbreeding typically yields competitive outcomes in terms of solution quality. Finally, the three-parent crossover in crossbreeding with MPGA resolved combinatorial optimisation issues (e.g., CSGA) and yield beneficial results. However, it should be noted that a number of factors influence the genetic algorithm's performance. In future studies, the inbreeding process will be carried out using multi-parents and also the plan is to examine the effect of the number of parents in the multiparent crossover, and how it affects the inbreeding and crossbreeding process. Comprehensive tests and comparisons will be conducted in the next study., with the aim of providing a detailed assessment of the effectiveness of multiparent crossover in the multipopulation approach.

Acknowledgement

The authors received no financial support for the research, authorship and/or publication of this article.

Conflicts of interest

The authors declare that they have no known competing financial interests or personal relationships that could have appeared to influence the work reported in this paper.

References

[1] LIU, X., DENG, Y. A new QoS-aware service discovery technique in the internet of things using whale optimization and genetic algorithms. *Journal of Engineering and Applied Science*. 2024, **71**(1), 4. ISSN 1110-1903, eISSN 2536-9512. Available from: https://doi.org/10.1186/s44147-023-00334-1

[2] ALKAFAWEEN, E., HASSANAT, A. B., TARAWNEH, S. Improving initial population for genetic algorithm using the multi linear regression based technique (MLRBT). *Communications - Scientific Letters of the University of Zilina* [online]. 2021, **23**(1), p. E1-E10. ISSN 1335-4205, eISSN 2585-7878. Available from: https://doi.org/10.26552/com.C.2021.1.E1-E10

[3] HOLLAND, J. H. *Adaptation in natural and artificial systems: an introductory analysis with applications to biology, control, and artificial intelligence* [online]. MIT press, 1992. ISBN 9780262275552. Available from: https://doi.org/10.7551/mitpress/1090.001.0001

[4] BALA, A., SHARMA, A. K. A comparative study of modified crossover operators. In: 2015 3rd International Conference on Image Information Processing ICIIP: proceedings [online]. IEEE. 2015. ISBN 978-1-5090-0148-4. Available from: https://doi.org/10.1109/ICIIP.2015.7414781

[5] ALKAFAWEEN, E. O. Novel methods for enhancing the performance of genetic algorithms [online]. Master's thesis. Jordan: Mutah University, 2015. Available from: https://doi.org/10.48550/arXiv.1801.02827

[6] ALKAFAWEEN, E., HASSANAT, A. B. Improving TSP solutions using GA with a new hybrid mutation based on knowledge and randomness. *Communications - Scientific Letters of the University of Zilina* [online]. 2020, **22**(3), p. 128-139. ISSN 1335-4205, eISSN 2585-7878. Available from: https://doi.org/10.26552/com.C.2020.3.128-139

[7] HASSANAT, A. B., ALKAFAWEEN, E. On enhancing genetic algorithms using new crossovers. *International Journal of Computer Applications in Technology* [online]. 2017, **55**(3), p. 202-212. ISSN 0952-8091, eISSN 1741-5047. Available from: https://doi.org/10.1504/IJCAT.2017.10005868

[8] HASSANAT, A. B., ALKAFAWEEN, E., AL-NAWAISEH, N. A., ABBADI, M. A., ALKASASSBEH, M., ALHASANAT, M. B. Enhancing genetic algorithms using multi mutations: experimental results on the travelling salesman problem. *International Journal of Computer Science and Information Security*. 2016, **14**(7), 785. eISSN 1947-5500.

[9] AHMED, Z. H. Multi-parent extension of sequential constructive crossover for the travelling salesman problem. *International Journal of Operational Research* [online]. 2011, **11**(3), p. 331-342. ISSN 1745-7645, eISSN 1745-7653. Available from: https://doi.org/10.1504/IJOR.2011.041347

[10] LEUNG, Y., GAO Y., XU, Z.-B. Degree of population diversity - a perspective on premature convergence in genetic algorithms and its Markov chain analysis. *IEEE Transactions on Neural Networks* [online]. 1997, **8**(5), p. 1165-1176. ISSN 1045-9227. Available from: https://doi.org/10.1109/72.62321

[11] LIU, L., FEI, T., ZHU, Z., WU, K., ZHANG, Y. A survey of evolutionary algorithms. In: 2023 4th International Conference on Big Data, Artificial Intelligence and Internet of Things Engineering ICBAIE: proceedings [online]. IEEE. 2023. eISBN 979-8-3503-4361-8, p. 22-27. Available from: https://doi.org/10.1109/ICBAIE59714.2023.10281260

[12] HASSANAT, A., ALMOHAMMADI, K., ALKAFAWEEN, E., ABUNAWAS, E., HAMMOURI, A., PRASATH, V. S. Choosing mutation and crossover ratios for genetic algorithms - a review with a new dynamic approach. *Information* [online]. 2019, **10**(12), 390. eISSN 2078-2489. Available from: https://doi.org/10.3390/info10120390

[13] XUE, Y., ZHU, H., LIANG, J., SLOWIK, A. Adaptive crossover operator based multi-objective binary genetic algorithm for feature selection in classification. *Knowledge - Based Systems* [online]. 2021, **227**, 107218. ISSN 0950-7051, eISSN 1872-7409. Available from: https://doi.org/10.1016/j.knosys.2021.107218

[14] JEBARI, K., BOUROUMI, A., ETTOUHAMI, A. Parameters control in GAs for dynamic optimization. *International Journal of Computational Intelligence Systems* [online]. 2013, **6**(1), p. 47-63. eISSN 1875-6883. Available from: https://doi.org/10.1080/18756891.2013.754172

[15] WHITLEY, D., RANA, S., HECKENDORN, R. B. The Island model genetic algorithm: on separability, population size and convergence. *Journal of Computing and Information Technology*. 1999, **7**, p. 33-48. ISSN 1330-1136, eISSN 1846-3908.

[16] DEB, K. Multi-objective evolutionary algorithms. In: *Springer handbook of computational intelligence* [online]. KACPRZYK, J., PEDRYCZ, W. (Eds.). Berlin Heidelberg: Springer-Verlag, 2015. p. 995-1015. ISBN 978-3-662-43504-5, eISBN 978-3-662-43505-2. Available from: https://doi.org/10.1007/978-3-662-43505-2

[17] DENG, D.-S., LONG, W., LI, Y.-Y., SHI, X.-Q. Multipopulation genetic algorithms with different interaction structures to solve flexible job-shop scheduling problems: a network science perspective. *Mathematical Problems in Engineering* [online]. 2020, **2020**(1), 8503454. ISSN 1024-123X, eISSN 1563-5147. Available from: https://doi.org/10.1155/2020/8503454

[18] SHI, X., LONG, W., LI, Y., DENG, D. Multi-population genetic algorithm with ER network for solving flexible job shop scheduling problems. *PloS One* [online]. 2020, **15**(5), e0233759. eISSN 1932-6203. Available from: https://doi.org/10.1371/journal.pone.0233759

[19] PARK, T., RYU, K. R. A dual population genetic algorithm with evolving diversity. In: 2007 IEEE Congress on Evolutionary Computation: proceedings [online]. IEEE. 2007. ISSN 1089-778X, eISSN 1941-0026, ISBN 978-1-4244-1339-3. Available from: https://doi.org/10.1109/CEC.2007.4424928

[20] YANG, S. PDGA: the primal - dual genetic algorithm. In: *Design and application of hybrid intelligent systems* [online]. ABRAHAM, A., KOPPEN, M., FRANKE, K. (Eds.). Amsterdam: IOS Press, 2003. ISBN 978-1586033941, p. 214-223. Available from: https://doi.org/10.13140/RG.2.1.3134.3445

[21] ALKAFAWEEN, E., ELMOUGY, S., ESSA, E., MNASRI, S., TARAWNEH, A. S., HASSANAT, A. IAM-TSP: iterative approximate methods for solving the travelling salesman problem. *International Journal of Advanced Computer Science and Applications* [online]. 2023, **14**(11), p. 420-428. ISSN 2158-107X, eISSN 2156-5570. Available from: https://doi.org/10.14569/IJACSA.2023.0141143

[22] ALKAFAWEEN, E., HASSANAT, A., ESSA, E., ELMOUGY, S. An efficiency boost for genetic algorithms: initializing the GA with the iterative approximate method for optimizing the traveling salesman problem - experimental insights. *Applied Sciences* [online]. 2024, **14**(8), 3151. eISSN 2076-3417. Available from: https://doi.org/10.3390/app14083151

[23] YU, Y., CHEN, Y., LI, T. A new design of genetic algorithm for solving TSP. In: 2011 4th International Joint Conference on Computational Sciences and Optimization: proceedings [online]. IEEE. 2011. ISBN 978-1-4244-9712-6. Available from: https://doi.org/10.1109/CSO.2011.46

[24] KALEYBAR, H. J., DAVOODI, M., BRENNA M, ZANINELLI, D. Applications of genetic algorithm and its variants in rail vehicle systems: a bibliometric analysis and comprehensive review. *IEEE Access* [online]. 2023, **11**, p. 68972-68993. eISSN 2169-3536. Available from: https://doi.org/10.1109/ACCESS.2023.3292790

[25] AMIRI, F. Optimization of facility location-allocation model for base transceiver station antenna establishment based on genetic algorithm considering network effectiveness criteria (case study north of Kermanshah). *Scientia Iranica* [online]. 2023, **30**(5), p. 1841-1854. ISSN 1026-3098, eISSN 2345-3605. Available from: https://doi.org/10.24200/sci.2021.55207.4116

[26] FUENTES-MARILES, O. A., GRACIA-SANCHEZ, J., CHOMPA-ABARCA, J. A., DE, F. Predesign of an urban rainfall drainage network with genetic algorithms. *Journal of Building Technology* [online]. 2024, **6**(2), p. 2717-5103. ISSN 2705-1390, eISSN 2717-5103. Available from: https://doi.org/10.32629/jbt.v6i2.2475

[27] EIBEN, A. E., RAUE, P.-E., RUTTKAY, Z. Genetic algorithms with multi-parent recombination. In: International Conference on Parallel Problem Solving from Nature: proceedings [online]. Springer. 1994, p. 78-87. Available from: https://doi.org/10.1007/3-540-58484-6_252

[28] ROYCHOWDHURY, S., ALLEN, T. T., ALLEN, N. B. A genetic algorithm with an earliest due date encoding for scheduling automotive stamping operations. *Computers and Industrial Engineering* [online]. 2017, **105**, p. 201-209. ISSN 0360-8352, eISSN 1879-0550. Available from: https://doi.org/10.1016/j.cie.2017.01.007

[29] EIBEN, A. E., VAN KEMENADE, C. H. Performance of multi-parent crossover operators on numerical function optimization problems. 1995.

[30] TING, C.-K., CHEN, C.-C. The effects of supermajority on multi-parent crossover. 2007.

[31] TSUTSUI, S., GHOSH, A. A study on the effect of multi-parent recombination in real coded genetic algorithms. In: 1998 IEEE International Conference on Evolutionary Computation and IEEE World Congress on Computational Intelligence (Cat. No. 98TH8360): proceedings [online]. IEEE. 1998. ISBN 0-7803-4869-9. Available from: https://doi.org/10.1109/ICEC.1998.700159

[32] TSUTSUI, S., JAIN, L. C. On the effect of multi-parents recombination in binary coded genetic algorithms. In: 1998 2nd International Conference. Knowledge-Based Intelligent Electronic Systems. Proceedings KES'98 (Cat. No. 98EX111): proceedings [online]. IEEE. 1998. ISBN 0-7803-4316-6. Available from: https://doi.org/ 10.1109/KES.1998.725966

[33] TING, C.-K., SU, C.-H., LEE, C.-N. Multi-parent extension of partially mapped crossover for combinatorial optimization problems. *Expert Systems with Applications* [online]. 2010, **37**(3), p. 1879-1886. ISSN 0957-4174, eISSN 1873-6793. Available from: https://doi.org/10.1016/j.eswa.2009.07.082

[34] SIN, O. C., MOIN, N. H., OMAR, M. Multi parents extended precedence preservative crossover for job shop scheduling problems. *Malaysian Journal of Computer Science* [online]. 2013, **26**(3), p. 170-181. ISSN 0127-9084. Available from: https://ejournal.um.edu.my/index.php/MJCS/article/view/6769

[35] ARRAM, A., AYOB, M. A novel multi-parent order crossover in genetic algorithm for combinatorial optimization problems. *Computers and Industrial Engineering* [online]. 2019, **133**, p. 267-274. ISSN 0360-8352, eISSN 1879-0550. Available from: https://doi.org/10.1016/j.cie.2019.05.012

[36] DAVIS, L. Applying adaptive algorithms to epistatic domains. In: Joint International Conference on Artificial Intelligence IJCAI: proceedings. 1985. p. 162-164.

[37] ALKAFAWEEN, E., HASSANAT, A., ESSA, E., ELMOUGY, S. CSGA: a dual population genetic algorithm based on Mexican cavefish genetic diversity. *Jordanian Journal of Computers and Information Technology* [online]. 2024, **10**(3), p. 1-16. ISSN 2413-9351, eISSN 2415-1076. Available from: https://doi.org/10.5455/jjcit.71-1707664207

[38] REINELT, G. TSBLIB [online] [accessed 2024-09-01]. University of Heidelberg, 1996. Available from: http://comopt.ifi.uni-heidelberg.de/

[39] JEBARI, K., MADIAFI, M. Selection methods for genetic algorithms. *International Journal of Emerging Sciences*. 2013, **3**(4), p. 333-344. ISSN 2222-4254.

[41] DONG, M., WU, Y. Dynamic crossover and mutation genetic algorithm based on expansion sampling. In: *Artificial intelligence and computational intelligence. AICI 2009. Lecture notes in computer science. Vol. 5855* [online]. DENG, H., WANG, L., WANG, F. L., LEI, J. (Eds.). Berlin, Heidelber: Springer, 2009. ISBN 978-3-642-05252-1, eISBN 978-3-642-05253-8. Available from: https://doi.org/10.1007/978-3-642-05253-8_16

UNIVERSITY
OF ŽILINA

In its over 70 years of successful existence, the University of Žilina (UNIZA) has become one of the top universities in Slovakia.

The mission of UNIZA is to develop education on the basis of science, research and art activities within national and democratic traditions, to develop harmonic personality, knowledge, the good and creativity of a man and to contribute to the advancement of education, science, and culture for the welfare of the whole society.

Professional profile of UNIZA is unique and includes transport (road, railway, water, air), transport and postal services, communications, civil engineering construction, electrical engineering, telecommunications, informatics, information and communication technologies, management and marketing, mechanical engineering, materials and technologies, robotics, machinery design, energies, civil engineering, crisis and security management, civil security, fire protection, forensic engineering, applied mathematics, teacher training, library and information sciences, social pedagogy and high mountain biology. Results of science and research activities of the University have an important influence not only on the educational activities but also on the development of international cooperation or interconnection with practice.

UNIVERSITY PARTS
7 faculties
9 research and educational institutes and centres
3 specialized professional and training workplaces
3 information workplaces
1 economic and administrative department
4 dedicated facilities

EDUCATION
7 faculties:
8 000 students
more than 88 000 graduates
172 study programmes

SCIENCE AND RESEARCH
699 creative workers
785 000 hours, annual research capacity
190 domestic scientific projects
45 foreign projects
30 scientific and technical journals
50 scientific and professional events per year

INTERNATIONAL COOPERATION
The University of Žilina in Žilina has almost 50 valid university-wide bilateral agreements, and cooperates with foreign universities in the EU, Asia, America and Africa. It cooperates on foreign non-research projects and has concluded more than 300 agreements in the ERASMUS + programme.

UNIVERSITY OF ŽILINA
Science & Research Department

Univerzitná 8215/1,
010 26 Žilina,
Slovakia

Ing. Janka Macurová
tel.: +421 41 513 5143
e-mail: janka.macurova@uniza.sk

EVACUATION TRANSPORT PROVISION DESIGN USING NETWORK ANALYSIS WITH GIS SUPPORT

Jozef Kubás[1,*], Jozef Ristvej[1], Boris Kollár[1], Katarína Petrlová[2], Alexandra Trličíková[2], Kateřina Blažková[3]

[1]Department of Crisis Management, Faculty of Security Engineering, University of Zilina, Zilina, Slovakia
[2]Mathematical Institute in Opava, Silesian University in Opava, Opava, Czech Republic
[3]Fire Rescue Brigade of Moravian-Silesian Region, Ostrava, Czech Republic

*E-mail of corresponding author: jozef.kubas@uniza.sk

Jozef Kubas 0000-0002-0512-6505,
Boris Kollar 0009-0006-8588-5398,
Jozef Ristvej 0000-0002-2290-1470,
Katarina Petrlova 0009-0003-4490-1097

Resume
The research presented in paper has focused on design of the transportation evacuation during a special flood caused by an accident at a water structure using GIS-enabled network analysis. Freely available population and address point data were used to calculate the number of residents at risk. Three scenarios of time required for each evacuation activity were determined using the PERT method, and the time required for evacuation was determined using a Gantt chart. The approach proposed in the paper is suitable for obtaining relatively quick results that can be taken into account when preparing for crisis events. The results of the case study proved that the evacuation can be carried out in the necessary time, but revealed possible shortcomings of the proposed approach. These shortcomings are discussed along with possible alternative solutions and other factors influencing the evacuation planning process.

Article info
Received 4 March 2025
Accepted 3 June 2025
Online 30 June 2025

Keywords:
evacuation
special flood
network analysis
GIS
crisis management
civil protection

Available online: https://doi.org/10.26552/com.C.2025.044

ISSN 1335-4205 (print version)
ISSN 2585-7878 (online version)

1 Introduction

Nowadays, the increasing occurrence of crisis phenomena and disasters draws attention to the preparedness of individual government bodies, institutions, municipalities and individuals. Preparedness is generally considered to be a key aspect in the successful management of crisis events. Neglecting preparation and preparedness can lead to serious adverse consequences. That is why planning and development of crisis plans is carried out as one of the elements of preparation for crisis phenomena [1]. Crisis planning, as one of the main factors of ensuring preparedness, is also described by other authors [2-5]. Planning as a part of preparedness is also described in the Sendai Framework Terminology on Disaster Risk Reduction. Preparedness generally refers to the knowledge and capacity to respond and recover. Examples include the provision of evacuation of supplies and materials for the population [6].

The importance of preparedness in crisis management has already been addressed by Healy and Malhorta (2009). In their work, they stated that increased investment in preparedness can reduce the damage caused by a crisis event. The authors estimated that one dollar invested in preparedness can be worth $15 in the recovery phase [7]. A more recent study by Chai et al. (2021) reports that one dollar invested in mitigation and preparedness saves $6 in damage repair after a crisis event [8].

Planning for response or recovery after the occurrence of a crisis event is an effective tool to ensure the crisis management preparedness [2]. It is a strategic element for the implementation of civil protection tasks. An emergency or crisis plan should be a structured document that includes a risk analysis of the territory, prepared procedures and defined competences of individual bodies. A crisis plan should be a living document that is clear and ready whenever a crisis response is needed. The development of a crisis plan is a multidisciplinary process. This means that different professions and experts need to be brought together in the development of the crisis plan, while also ensuring that it is regularly updated. The use of information

technology is recommended in the development of crisis plans, as it allows for more efficient coordination of the whole process and reduces the need for hierarchy [3].

Evacuation plans and its comprehensive provision are an important component in crisis planning and preparedness [9]. Evacuation can generally be defined as the removal of endangered populations, animals and belongings from an area [10]. According to the team of authors, evacuation can be defined as a basic means of protecting the population. It is a set of measures ensuring the relocation of people, animals, objects of cultural value, technical equipment, or machinery and material for the purpose of preserving necessary production and hazardous substances from places threatened by a crisis phenomenon to places that provide alternative accommodation and catering for the evacuated population, housing for animals and storage for belongings [11].

For the needs of effective evacuation, it is necessary to take into account in the crisis plans its transport, medical, order, supply and media provision [12-13]. The protection of residents, animals and belongings depends on the individual parts. The information of the population and the transport provision of the evacuation can be considered as a key role in this process.

The transport arrangements for evacuation consist mainly of the designation of transport proto-classes, evacuation assembly points and embarkation stations. Data plays an important role in the evacuation planning process. Data on the number of evacuees, locations of evacuation facilities and their availability for evacuees, capacities of means of transport, vulnerable populations are needed for reliable evacuation arrangements. Finally, data on evacuation routes, their length and load. Therefore, before the actual planning of the evacuation, attention should be paid to data collection and storage. A suitable solution is to implement policies, strategies and technological solutions at all levels of government and local government, as data are crucial in all the phases of crisis management as well as in decision support [12-15]. The data itself can also be applied in risk or vulnerability assessment models, where the results of the assessment can provide useful information just for decision making purposes in the evacuation route planning process [16].

Modern technologies can also be used in the actual creation of evacuation plans and their graphic parts, which are often a mandatory part [11-13, 17]. Examples of the use of modern technologies can be various sensors and weather stations that collect data in real time. These data are then fed into the risk assessment or forecasting models [18]. Geo-graphical Information Systems (GIS) are of great benefit for evacuation planning purposes. The GIS can be used in all the phases of crisis management [19]. The use of GIS in flood risk mapping with respect to the road network in Portugal, has been addressed by Rezvani et al. [17]. The authors used spatial and attribute geographic and geological data to develop a flood risk assessment model for road infrastructure. Using artificial intelligence, machine learning and GIS tools, they identified critical sections of the road network [17]. The use of GIS for decision support has been addressed by several authors. An example is also their use in the development of simulations for decision support in the planning phase [20]. Armenakis et al. have used the analytical tools of GIS programs for planning evacuation zones and evacuation routes. An example is the use of GIS in the planning and designation of evacuation facilities. By spatial analysis, it is possible to map out the location of such a facility so that it is not in the threat area of the crisis or other phenomenon under study [21]. During the September 2024 floods, there were reports of flooded evacuation centers that were not ultimately confirmed [22], or a flooded bus parking lot [23]. It is the bus transport that is often used to evacuate people.

Floods are one of the biggest threats in the world. They are also becoming more frequent due to climate change. Flash floods, caused by extreme rainfall over a short period of time, are also becoming more frequent [24]. A specific case of flash floods is the so-called special floods. An exceptional flood is caused by the failure or breakdown (breakage) of a water works. This accident or its emergency solution causes a crisis situation below the waterworks [25]. Such a flood can cause enormous damage to the property of the state and the population, and its manifestations are more dangerous than in the case of classical floods or flash floods. This is mainly due to the accumulation of large amounts of water in the reservoir, which has a higher elevation than the downstream dwellings. In the event of a breach in the water structure, the force of the flood wave would be magnified by gravity effects [26]. For the event of a special flood, the predicted reach of the flood wave and the time it takes for the wave to reach certain areas are calculated using models to ensure the safety of the population. The calculations also include water level elevations. It is this type of flood that can cause enormous damage [26-28].

There are several cases of water structure breakage and subsequent disaster caused by post-flood waves in the world. An example is the disaster caused by human error and a landslide into the Vajont dam in north-eastern Italy. This disaster caused approximately 1900 casualties and completely razed villages downstream of the Piave River [29]. Another example of the consequences of a dam breach can be found in the Czech Republic. In 1916, the dam began to leak until it broke with an opening 18 meters wide. The tidal wave killed 65 people and deprived another 370 people of all their possessions [30]. Extreme rainfall in September 2024 caused the dam's embankment to break near the Polish town of Stronie Slaskie. The torrential water destroyed the entire town. The water damaged buildings, destroyed infrastructure and utilities, with damage estimated at more than 1 billion PLN [31-32]. The above examples

demonstrate the severity of special floods. Therefore, it is necessary for individual towns and municipalities in their vicinity as well as crisis management authorities to be prepared for this type of event.

The aim of this paper was to propose a procedure for planning the transport provision for evacuation of people during a special flood. To achieve the objective, network analysis method with the support of geographic information system was used. The proposed solution was applied to the conditions of the city of Opava in the Czech Republic, which is threatened by the Slezska Harta and Kruzberk reservoirs. The proposed procedure enables complex planning of the transport provision for evacuation of people with the help of GIS.

2 Materials and methods

The analysis of the flood plans identified the absence of an evacuation plan in the case of a special flood in the city of Opava. Therefore, the paper's focus was on the design of the procedure for planning the transport provision for evacuation with the support of GIS and network analysis. This process consists of identification of evacuation routes, number of inhabitants at risk, available means of transport, as well as analysis of the feasibility of evacuation in terms of time.

The PERT method was used to determine the time requirements for evacuation and individual activities. This approach was chosen since the total duration of the evacuation and the duration of its individual activities cannot be determined deterministically. The PERT method is a probabilistic extension of the CPM method. Therefore, the PERT method assumes that the time of each activity is a random variable that is represented on the interval $\langle a_{ij} | b_{ij} \rangle$, where a_{ij} is the predicted shortest possible time to perform a given activity, and conversely b_{ij} is the predicted longest possible time to perform a given activity. The actual duration of an activity would be somewhere in this interval, and therefore the PERT method further assumes that the most likely duration of m_{ij} for each activity can be determined. When preparing a project for PERT processing, three time characteristics are defined for each activity:

a_{ij} - optimistic estimation
b_{ij} - pessimistic estimation
m_{ij} - modal estimation

Activity duration is a continuous random variable.

Table 1 *Results of experimental measurements for determination of the traffic restriction times - roundabout*

Type of restriction	1. measurement (sec)	2. measurement (sec)	3. measurement (sec)
RA - Krnovska	7	12	15
RA - Benzina (Krnovska)	10	18	10
RA - Nakladni	8	16	21
RA - Globus	15	17	23
RA - Obchvat	14	18	19
Sum of measurements	54	81	88
Total sum			223
Average			14.86666667
Rounding			15

RA- roundabout

Table 2 *Results of experimental measurements for determination of the traffic restriction times - traffic light intersection*

Type of restriction	1. measurement (sec)	2. measurement (sec)	3. measurement (sec)
TL - Praskova	25	50	38
TL - Bilovecka	42	70	50
TL - Tesinska Tesco	30	42	28
TL - Olbrichova	20	15	37
TL - Hradecka	23	16	34
TL - Tyrsova	15	27	26
TL - Vychodni nadrazi	56	29	67
TL - Ratiborska	40	39	54
TL - Rolnicka	59	68	44
Sum of measurements	310	356	378
Total sum			1044
Average			38.66666667
Rounding			39

TL- traffic lights

Table 3 *Activities carried out during evacuation*

No.	Activity
1.	Receipt of information on the need to evacuate
2.	Summoning the flood committee and arriving at the venue
3.	Specification of the evacuation zone
4.	Warning of the population
5.	Closure of premises and territory
6.	Request for buses
7.	Activation of the evacuee assembly point
8.	Activation and operation of evacuation centers
9.	Organization and movement of evacuees to the assembly point
10.	Movement of evacuees to evacuation centers

For all activities, three time points were determined and used to calculate the mean and standard deviation of the duration of the activity. The time data and the individual activities within the evacuation were determined based on expert estimation of firefighters from the Fire Rescue Department of the Moravoslezsky region, who operate in the Integrated Safety Centre in the city of Ostrava [33]. To determining the actual activity durations and actual delays, the following relationships were used:

$$\mu = \frac{a_{ij} + 4m_{ij} + b_{ij}}{6} \tag{1}$$

To calculate the standard deviation, the following relation 2 shall be used:

$$\sigma = \frac{b_{ij} - a_{ij}}{6} \tag{2}$$

The values of individual times for evacuation activities were averaged based on the number of expert estimates. To determine the timing of the last two activities, it was also necessary to use experimental measurements. These were used for the purpose of determining the traffic constraints and to determine the time taken to move from the furthest point adjacent to the evacuee assembly point to the assembly point.

The experimental measurements consisted of driving around the city of Opava several times on different days and at different times. Temporal data from the experimental measurements were supplemented with information obtained on the basis of consultations with the staff of the Integrated Security Centre Ostrava, to determine the temporal data on traffic restrictions in the city in connection with the occurrence of a crisis situation. Experimental runs were conducted with emphasis on routes where the traffic constraints, such as roundabouts, traffic lights and impassable bridges, are encountered. An area constraint represents an area where the traffic situation would be slowed due to evacuation and intersection control or occurring rush hour traffic. The results of the experimental measurements are included in Tables 1 and 2.

The activities carried out as part of the transport support for evacuation are shown in Table 3.

The Microsoft Project (MS Project) project management tool was used to create network graphs and the links between activities. The MS Project also includes a tool that allows creation of the Gantt charts. The Gantt chart allows the creation of a timeline of individual activities. Using this diagram, it is possible to show the duration of the individual activities, their continuity, as well as the total duration of the process/project.

The time required for evacuation is also based on information about the individual evacuation routes. The evacuation route data are particularly necessary for the determination of the last two activities shown in Table 3. To determine the evacuation routes, a network analysis was used, which contains an overview of all the roads in the city of Opava. The Network analysis in a GIS environment is one of the analytical tools. It is used to model movement in networks, such as often times transportation infrastructure. This tool allows to calculate the shortest or longest route, analyzes accessibility and other parameters based on distance and time. Network analysis further uses spatial data and its attributes, such as speed limits, direction of travel or other constraints.

The network analysis for this study included the determination of parameters such as speed, direction and traffic restrictions. The ArcGIS geographic information system was used to create network analysis, to determine the evacuation routes and to determine the number of inhabitants at risk. Traffic constraints were assigned to individual roads using the network analyst tool in ArcGIS. The layer of roads in the city of Opava is shown in Figure 1.

Transport arrangements for evacuation also require information on available means of transport. In a controlled evacuation, mass means of transport are used to move the population at risk. The Ostrava Region Crisis Plan contained information on available buses. This information is included in Table 4.

Municipal transport company Opava and TQM -

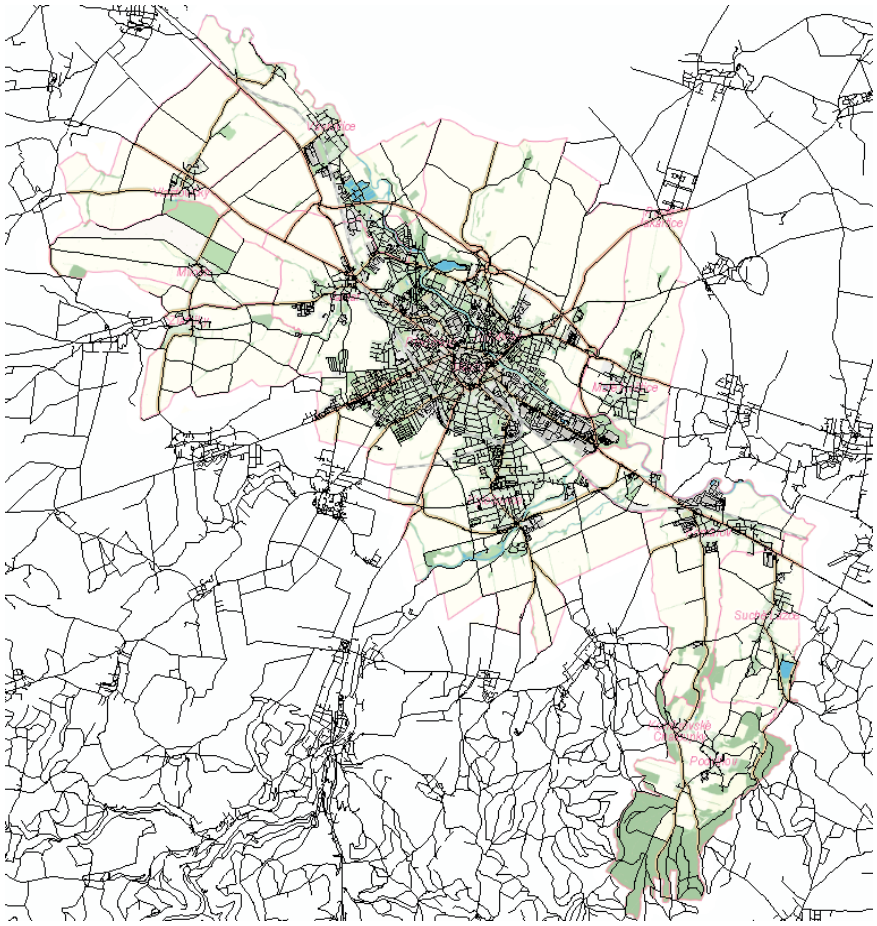

Figure 1 *Network analysis of the city of Opava*

Table 4 *Available means of public transport*

Subject	Number of buses	Max. capacity
Municipal transport company Opava	34	90
TQM - holding s.r.o.	85	90
HZS MSK	7	17

holding s.r.o. have IVECO buses, model bus Urbanway 12 m. HZS MSK would be able to provide the city of Opava with only one of its buses if necessary. However, during evacuation it is necessary to consider that the evacuees have evacuation luggage. Therefore, only 75 % of the total capacity of the buses was considered in the calculations.

For planning and determining the number of inhabitants at risk it was furthermore necessary to use information on the address points of the city of Opava, information on the number of inhabitants of the city of Opava and information on the expected flooded part of the city in case of breach of water structures that threaten the city (more in section 3). The information on the number of inhabitants was obtained from the Czech Statistical Office. Information on the time, depth and extent of inundation due to a special flood was available in the crisis plan. Using the address points layer and the flood zone layer, using the Intersect function in ArcGIS, dwellings in the flood zone were identified.

The number of at-risk residents was in the crisis plan, but this information has not been updated for a long time. Therefore, the following relationship was used to calculate the population at risk:

$$Population\ at\ risk = \left(\frac{total\ number\ of\ inhabitants}{total\ number\ of\ flats}\right) * number\ of\ flats\ at\ risk \tag{3}$$

Using the data on the total population of Opava and the total number of dwellings in Opava, the average number of inhabitants per dwelling unit is calculated. By overlaying the address points with the flood zone layer, the number of dwellings at risk is found. By multiplying these two data the approximate number of inhabitants at risk was obtained.

The number of people at risk, who would need to be evacuated by mass transit, was determined using the census data. The census data on the means of transport used for commuting to work are included,

as well. Further, the average family size needed to be determined. For this purpose, data on the average number of children per woman was used. The resulting number of inhabitants, who would be subject to orderly evacuation in the city of Opava, was used for the percentage, which was then applied to the number of at-risk population subject to orderly evacuation.

The above information and procedures were applied for the purpose of planning the transport provision for evacuation in the event of a special flood in the city of Opava. The main contribution is determination of the evacuation time and its comparison to the time of arrival of the flood wave in the city of Opava.

3 Results

3.1 The city of Opava and a special flood

The town of Opava is situated on the river of the same name in a fertile valley between the Low Jeseniky Mountains and the Poopava Plain. Opava currently covers an area of 90 km^2 and has a population of less than 60 000 inhabitants. The central area of the town is not divided into urban districts and is administered by the municipal authority. It consists of:

- registration part Predmesti
- registration part Katerinky
- registration part Kylesovice
- registration part Jaktar, [34].

The breakdown of the city of Opava is shown in the following Figure 2.

The town of Opava is threatened by a special flood in the event of a breach in the embankment of two water reservoirs. These are the Slezska Harta reservoir and the Kruzberk reservoir. These two reservoirs are interconnected by a cascade system. The regional crisis plan identifies the area of the Statutory City of Opava that would be at risk in the event of a special flood. This area is shown in Figure 3.

Figure 3 shows the flooded part of the town of Opava in the event of a breach of the dams of the Slezska Harta and Kruzberk reservoirs. The breakthrough wave would reach the town in 3 hours and 36 minutes. The water level in the city would reach 10.5 m [35].

3.2 Evacuation routes and traffic restrictions

The determination of evacuation routes and traffic restrictions was based on the network analysis shown in Figure 1. Traffic constraints are represented by roundabouts, traffic lights, intersections and crosswalks, evacuation slowdowns, and high-traffic sections. To determine the time constraints, the experimental measurements, shown in Table 1 and Table 2, were performed. For intersection and crossing type constraints, evacuation slowdowns, and heavy traffic, a slowdown of half was assumed. This means that if the speed limit on the road is 50 km/h, a speed of 25 km/h is assumed. These values were also consulted with experts from the Integrated Safety Centre of the Moravian-Silesian Region in Ostrava. A graphical representation of the traffic restrictions is shown in Figure 4.

Traffic constraints were incorporated into the network analysis using the Network Analyst tool in ArcGIS. Figure 4 shows what each constraint looks like in the ArcGIS software. Point constraints are represented

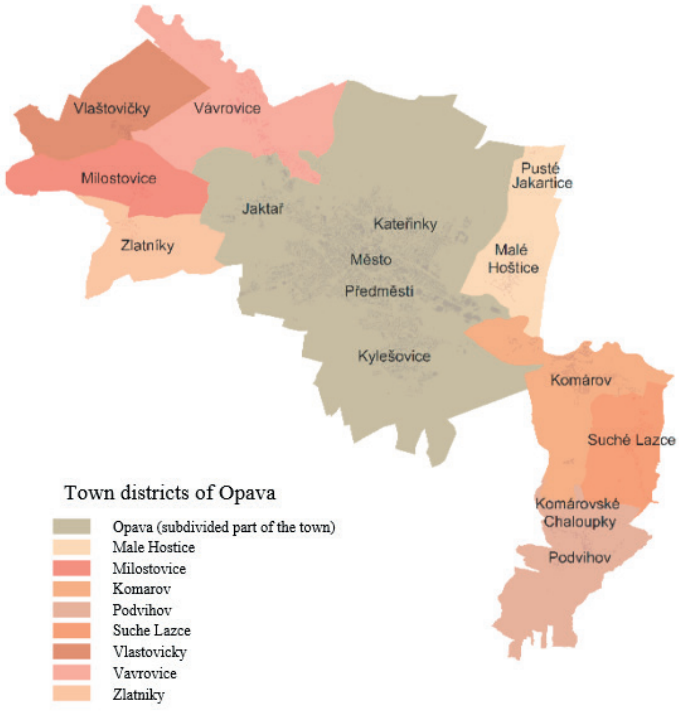

Figure 2 *Breakdown of the central part of Opava and the municipal parts of the city [34]*

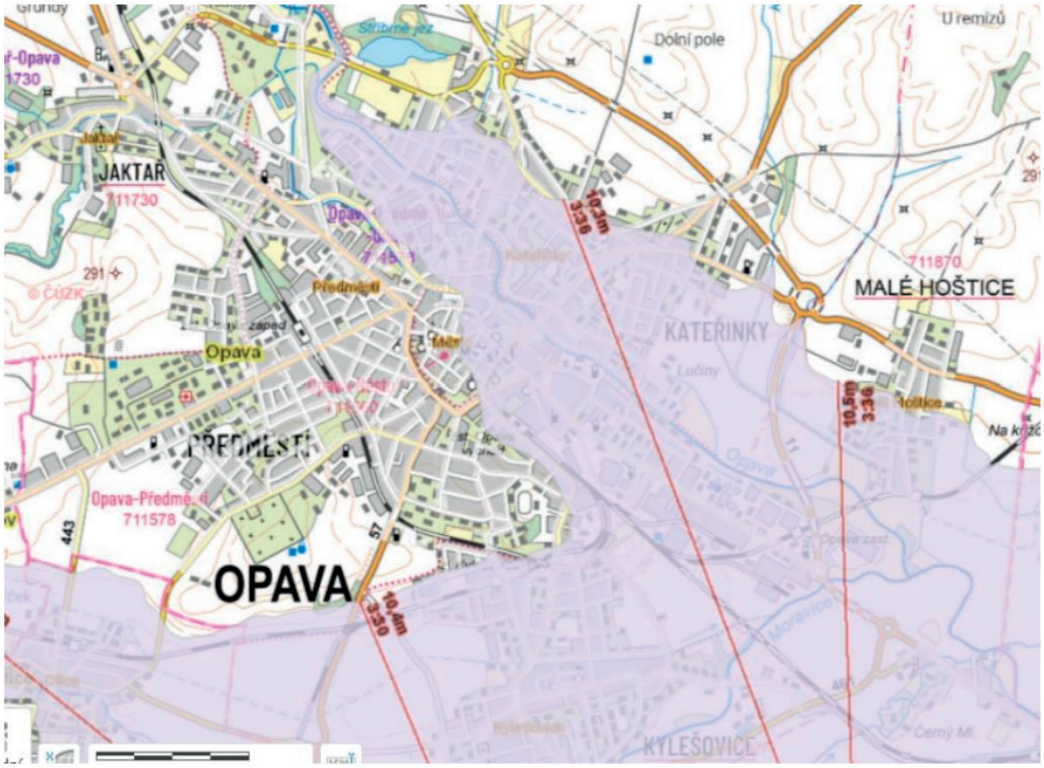

Figure 3 *The area of Opava threatened by a special flood [35]*

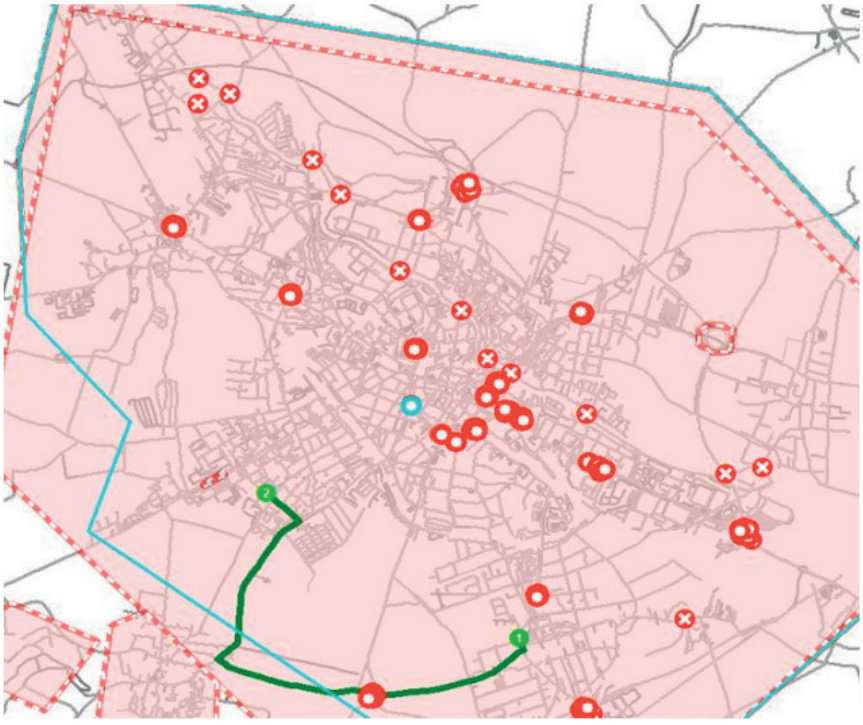

Figure 4 *Traffic restrictions*

by traffic lights, roundabouts and impassable bridges (constraints with a cross in the middle). Polygonal constraints (area-occupying constraints) are constraints associated with the slowing down of traffic due to the circumstances of the traffic situation.

To determine the evacuation routes, it was necessary to determine the beginning of the route. The start of the route is the assembly point (bus stop). The end of the route is the evacuation center (hereafter EC), which is determined in the emergency plan. ArcGIS can calculate the length of the route itself, so it was also possible to determine the time of each route. The evacuation routes were determined by ArcGIS based on the road speed parameters, the constraints that were set, and by specifying the start and end of the route. These routes are shown in Figure 5.

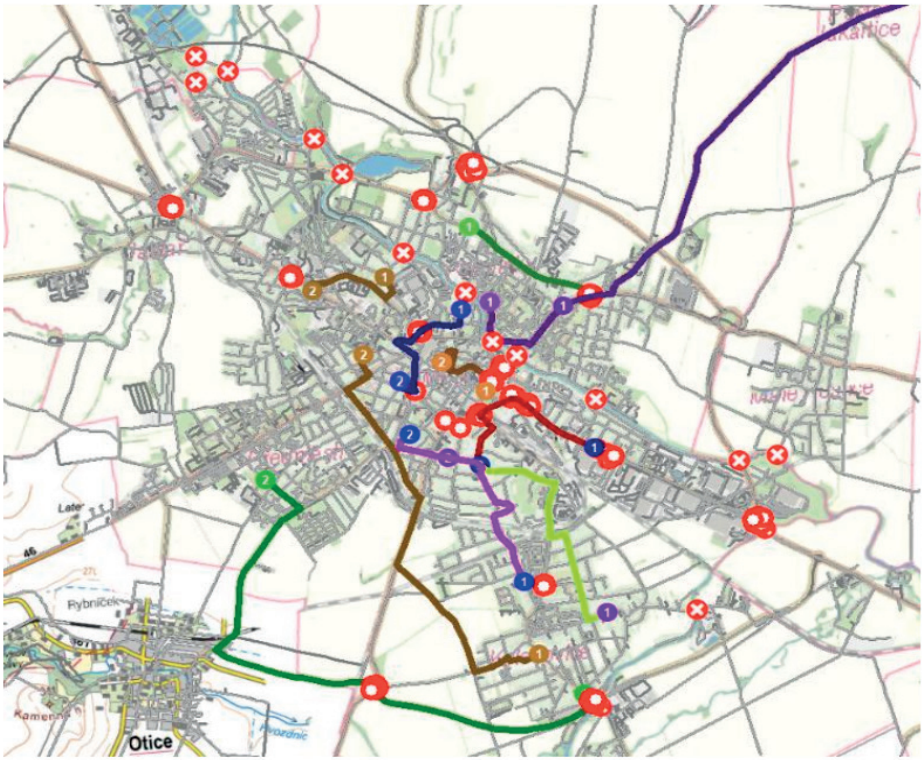

Figure 5 *Evacuation routes*

Table 5 *Description of evacuation routes*

No.	Evacuation routes for part of the town of Kylesovice:	
	Start:	End:
1	SUS stop	Evacuation centre SS zemedelska
2	Kroftova stop	Evacuation centre OA a SS logisticka
3	Bavaria stop	Evacuation centre SS honelnictva a VOS
4	Gudrichova stop	Evacuation centre OA a SS logisticka
	Evacuation routes for part of the town of Katerinky:	
	Start:	End:
5	Rolnicka stop	Evacuation centre Koberice Primary School
6	Partizanska stop	Evacuation centre Bolatice Primary School
7	Ratiborska stop	Evacuation centre Koberice Primary School
	Evacuation routes for the Predmesti:	
	Start:	End:
8	Pekarska stop	Evacuation centre Institute of Mathematics
9	Tesinska stop	Evacuation centre Bozeny Nemcova Primary School
10	Mostni stop	Evacuation centre Opava City Council
	Evacuation route for the Mesto:	
	Start:	End:
11	Praskova stop	Evacuation centre Kolarska

The individual routes have been designed in the program so that the walking distance in time per stop is no more than 30 minutes and that each route covers as large an area as possible. A total of 11 evacuation routes were created. The evacuation routes are included in Table 5.

3.3 Number of inhabitants at risk

The number of inhabitants of the city of Opava threatened by the special flood was determined using statistical data and map layers. In the first step it was necessary to overlay the layers of address points

Table 6 *Number of dwellings at risk in Opava*

Part of the city	Number of flats
Predmesti	3289
Katerinky	10140
Kylesovice	4556
Mesto	947

Table 7 *Number of inhabitants at risk of special flooding*

Part of the city	Number of inhabitants at risk
Predmesti	4638
Katerinky	14298
Kylesovice	6424
Mesto	1336
Total number of inhabitants at risk	26 696

in Opava and the flooded part of the city using the Intersect function in ArcGIS. In this way, dwellings that would be at risk in the event of a special flood were identified. The number of dwellings at risk in each part of the city is shown in Table 6.

Consequently, a procedure based on the census data was chosen. The total population of Opava was 47 985 people [36]. This figure was used to determine the average number of inhabitants per dwelling. The total number of dwellings in the city was determined in ArcGIS and is 33 930.

$$\textit{Average number of inhabitants per apartment} = \\ = \frac{47985}{33930} = 1.41.$$

By multiplying the average number of inhabitants per dwelling in the city of Opava, the number of inhabitants at risk was obtained. The number of inhabitants at risk is shown in Table 7.

3.4 Number of inhabitants at risk subject to orderly evacuation

Today, many people in developed countries have their own means of transport. Therefore, evacuation can be divided into spontaneous evacuation, which is controlled in terms of evacuation routes and orderly provision, and controlled evacuation. Controlled evacuation is managed by the competent authorities and includes the provision of mass transport means and the activation of several evacuation facilities, such as evacuation assembly point, embarkation station, etc. [13].

The census data on population and mode of transport to work are known. From this data it is known that in Opava a total of 6328 people use their own means of transport (car) [37]. Since the cars have a larger capacity than one person, the data on the average number of children per one woman was also used. This value is 1.66 [38]. Therefore, a family of four was considered in calculations.

Number of people evacuated on their own:

$$6328 * 4 = 25312$$

Number of people subject to controlled evacuation:

$$47985 - 25312 = 22673$$

The value of 22 673 people is calculated from the total population of the city. Therefore, we will use this value as a percentage to determine the number of residents who will be subject to orderly evacuation in the at-risk parts of the city.

$$\frac{22673}{47985} = 0.47$$

Total of 47% of the population at risk of special flooding (26 696) is 12 548 people. The number of available means of public transport is available in Table 4. This means that the evacuation would take place in two waves, as the number of people to be evacuated by mass means is 12 548. However, due to evacuation baggage, it will not be possible to use the full capacity of the bus. An optimal use of 75% of the bus capacity was assumed. In that way, the evacuation would still take place in two waves, and it would also be possible to transport passengers with their evacuation luggage. This means that there would be 67 people per bus and 7 973 people could be transported in wave 1 and the remaining 4 575 people in wave 2.

3.5 Evacuation timeline

Determining the timing of evacuation is important to determine whether it can be completed before the flood wave reaches Opava. The exact timing of the evacuation cannot be determined because it is affected by many factors that are not precisely

Table 8 *Evacuation times 1-8*

Activity	a_{ij} (min)	b_{ij} (min)	m_{ij} (min)	2σ (min)	Final time (min)
1	5	15	10	4	14
2	30	120	75	30	102
3	3	10	5	4	10
4	15	45	30	10	40
5	30	75	55	16	74
6	15	25	20	4	24
7	5	10	8	2	10
8	60	90	75	10	89

Table 9 *Times of evacuation actions 9-10 for individual evacuation routes 1-11*

Route	Activity	a_{ij} (min)	b_{ij} (min)	m_{ij} (min)	2σ (min)	Final time (min)
1	9	18	24	19	2	22
	10	11	17	15	2	17
2	9	12	17	15	2	17
	10	15	22	18	2	21
3	9	15	29	23	6	29
	10	9	15	13	2	15
4	9	18	25	20	4	25
	10	8	14	12	2	14
5	9	15	21	18	2	20
	10	19	27	24	2	26
6	9	14	17	15	2	18
	10	25	34	30	4	34
7	9	21	25	22	2	25
	10	16	22	19	2	21
8	9	16	19	17	2	20
	10	6	11	9	2	11
9	9	18	26	22	4	26
	10	5	13	9	4	13
10	9	15	23	18	2	21
	10	3	6	4	2	6
11	9	15	25	16	4	22
	10	3	7	5	2	7

determined. The approximate evacuation time can be determined using the PERT method, which assumes that the individual activities are continuous random variables.

Table 3 lists the different evacuation activities. For the first 8 activities, the individual times according to the PERT method were determined based on expert evaluation. The actual times and standard deviations were calculated according to Equation (1) and (2). The individual times, standard deviations and resulting times plus standard deviation for activities 1-8 are shown in Table 8.

ArcGIS was used to determine the times of the last two evacuation activities along with experimental measurements. These times represent the time required to travel from the farthest part of the evacuation zone to the assembly point (staging area) and the times required to transport evacuees to the evacuation centres. A network analysis of traffic constraints was also used. The time data are calculated for the single-individual evacuation routes, which are shown in Table 5. The times are available in Table 9.

The data thus prepared was then entered into the MS Project, which was used to create a timeline and calculate the total evacuation time. Evacuation times 1-8 and evacuation times 9-10 for evacuation route 6 were entered into the Gantt chart. Route 6 was selected since it takes the longest time to perform activities 9-10 for this route. If the evacuation of people along this route can be completed before the

arrival of the flood wave, the entire evacuation can be completed.

The results from the timeline for Route 6 indicated that the evacuation would take 3 hours and 28 minutes. From the evacuation timeline, calculated from the mean values of Route 6, it is clear that the evacuation can be managed before the flood wave reaches Opava. Since according to the county's crisis plan, the flood wave will be in Opava in 3 hours and 36 minutes from the time of the dam break. This means that even if the evacuation will take place in two waves, it will be possible to complete it in this time. The time margin is 1 hour. As fewer people will be evacuated in Wave 2, buses on the two routes with the longest travel distances (5 and 6) can be afforded to be omitted. In this case, the schedule for Route 6 even with the second wave of evacuations would take 3 hours and 38 minutes, but this exceeds the arrival time of the wave.

If the evacuation is a critical scenario and all the activities preceding the transfer of people to the EC are delayed, it would be difficult to achieve evacuation in the specified manner. In such a case, there would be six routes to which buses could not return and take the rest of the people. This means that only five routes can be used to transport the rest of the evacuees. In this case it would be appropriate to set the capacity of the buses at 80%. This would result in 72 people per bus. In the first wave 8 568 persons would be transported and in the second wave the remaining 3 980 persons would be transported. In the case of the second wave of EC transfers, the capacity of the buses would already be at its maximum; if it were limited, it would not be possible to transport everyone. As a part of the evacuation solution, the Fire and Rescue Service requested that the possibility of only seating on the buses be considered, which would mean that all the buses would have to run 4 times, which, as the previous results show, is not feasible.

4 Discussion

Addressing the issue of evacuation planning in the event of an emergency flood caused by reservoir failure, the current flood plan was found to be inadequate and outdated. It was therefore necessary to propose how to update it and how to align it with the regional crisis plan. There are several possible procedures, methods and tools to address this issue and its sub-steps. The approach chosen by the authors of this paper uses mathematical and statistical tools supported by applications and GIS. These are relatively simplified solutions, but they do not diminish the suitability and meaningful value of the individual outputs. The above approach to the problem addressed is relatively unpretentious in the process of data collection, processing and analysis. Therefore, it is suitable for cases where the required data is not available, or their collection would be time and cost-consuming. As the evacuation of a population is a complex process, influenced by several factors, it is not possible to accurately determine the timing, the number of evacuees and the means of transport required. However, the above results show the following:

If the conditions as set out in this paper are met, the evacuation would be completed before the arrival of the flood wave.

The basic prerequisite for this scenario is to use the capacity of the available means of transport. If only seating capacity were used, the evacuation could not be carried out to the extent required.

The following are some possibilities to achieve results that would be closer to reality. First, the duration of the evacuation routes, here fixed values of the restrictions of the junctions and roundabouts are chosen, from a statistical point of view it would be more appropriate to choose the crossing intervals, but the GIS system does not allow this.

Another limitation of this study is the experimental data. Using these data, traffic constraints were determined. For each traffic constraint, three measurements were taken at different times and days. These data were then summarized and consulted with experts from the Integrated Security Centre Ostrava. The input data was therefore based on expert estimates. The experimental data served as a guide. To increase the accuracy of the reported evacuation planning procedure, it would therefore be advisable to take into account several variables when measuring the time constraints. At the same time, more measurements would be necessary. Important factors that can limit the traffic situation are weather conditions and the times when the monitored road sections are most congested [39-40]. Based on the analysis of the results, several directions for future research can be identified to address the current limitations. First, it would be beneficial to provide a more detailed explanation of how experimental data are collected, with a particular focus on varying conditions under which evacuation may take place - such as peak traffic periods or adverse weather. These factors can significantly influence the capacity of transport infrastructure and the overall evacuation time. Furthermore, greater attention should be paid to the analysis of alternative routes and potential disruptions to evacuation paths, such as traffic accidents, temporary road closures, or failures at key network nodes. Incorporating such scenarios would contribute to a more realistic risk assessment and enhance the practical applicability of the proposed model in the real-world emergency situations.

Another limitation of that approach is that it does not consider the evacuation of health and social facilities. Health and social facilities are considered vulnerable elements as they house people with certain limitations that may prevent them from moving. There are different procedures on how to deal with such facilities in the

event of a flood. These may need to move patients by available ambulances or, in the event of a flood, to move patients to higher floors. Evacuation procedures follow the evacuation plans of specific facilities. The most vulnerable patients should be moved by ambulances to other hospitals or relevant facilities. Those who are mobile are either moved themselves or discharged [41]. There are several approaches that address the issue of evacuation from healthcare facilities [42-44]. The neglect of planning for transport provision and patient transport is described by Yazdani et al. as one of the most ignored components of hospital evacuation planning [43]. However, evacuation planning for healthcare and social service facilities is a topic that lends itself to separate research, which highlights the complexity of the issue at hand.

Along with hospitals, schools and dormitories are another category to consider when planning a city evacuation. Especially if it is a larger city where colleges or universities are located. The projected population may be considerably higher in this case.

In the case of the city of Opava and its threat of a special flood, it is also possible to consider the transfer of evacuees on foot. In this case, only people who are medically fit can be counted on. The expected flood wave resulting from the accident at the Slezska Harta and Kruzberk reservoirs would not flood the entire town and its expected arrival in the town is more than three and a half hours. As the evacuation centres are located within the non-flooded part of the city, it is possible to consider the use of evacuees' transfer on foot. Such a method of evacuation has been addressed, for example, by Parajuli et al. [45]. However, it would be difficult to determine the number of residents who would move to the evacuation centres on foot. It can be assumed that at least the people who are closest to the evacuation centres from their homes would use this method of evacuation. This would reduce the number of people who need to be transported by public transport, which would be used as a priority for the evacuation of school facilities, health facilities, etc.

The determination of the number of people to be spontaneously evacuated and the number of persons subject to orderly evacuation shall be determined based on an estimate. In this case, an alternative solution could be a questionnaire survey. However, the questionnaire would have to be chosen to be accessible to all residents of Opava, which is time-consuming, and its implementation would have to involve all residents of Opava, which is very difficult to implement. Another alternative way is to use available census data. Specifically, this is data on the degree of mobilisation. The degree of mobilisation indicates the number of cars in each area per 1 000 inhabitants. If one focuses on individual parts of the city, the numbers of inhabitants who evacuate themselves and those who are evacuated by the competent authorities are obtained. However, this approach is also heavily influenced by estimation.

Planning the transport arrangements for evacuation is a challenging logistical process. Therefore, the above procedure could be extended in the future by considering the solution of transportation problems by linear programming. In area evacuation, transport problems are used to optimize the transport of people from boarding stations to evacuation centres. In particular, the number of people transported, distances, and possibly unit cost per person are considered in this process [46].

At the same time, it must be considered that the behaviour of residents during an evacuation has a significant impact. Examples of problems related to human behaviour during an evacuation may be inexperience, ignorance, the need to return for belongings, etc. The knowledge and skills of the management staff also play an important role [47]. However, these factors are difficult to consider in the case of area evacuation planning. The solution may be to take these factors into account in the timing of individual activities.

The proposed procedure for planning the transport support for evacuation is a relatively simple approach, however, it provides sufficient information to crisis managers with decision-making authority. This information is particularly useful in preparedness and allows crisis management authorities to react to the current situation and availability of resources. More detailed planning would first require the introduction of a data collection system. More precise information on the number and movement of the population in one-individual parts of the city and hours would allow more accurate data to be established on the number of inhabitants at risk. Given the specific example of the city of Opava, it would also be advisable to consider moving evacuees on foot who have evacuation centres close to their homes.

5 Conclusions

The aim of this research was to propose a traffic evacuation using the network analysis in GIS. The transport provision for evacuation was divided into several activities. First, it was necessary to determine the evacuation routes. For this purpose, it was post-necessary to add traffic-related constraints to the network analysis and to determine the start and end of the route. The start of the route was determined so that the maximum walking distance to the site would be 30 minutes and that as much of the area as possible would be covered. The end of the route (evacuation center) was determined from the County's emergency plan. Using ArcGIS software, 11 evacuation routes were designed. In addition, it was necessary to determine the number of residents located in the area at risk of a special flood. For this purpose, it was necessary to use the address points layer using ArcGIS software and overlay it with the flood wave layer to determine the number of homes at risk.

This data was then multiplied by a factor reflecting the number of inhabitants per house to obtain the number of inhabitants at risk from the special flood.

The number of people at risk from the special flood had to be divided into two groups. The first group was subject to spontaneous evacuation and the second group to controlled evacuation. The number of people subject to controlled evacuation was 12 548. Total of 119 buses with a capacity of 90 seats could be used to transport these people. According to the capacity of the autobuses, considering space for evacuation luggage, there were 2 evacuation waves. In wave 1, 7 973 people could be transported with 75% of the bus capacity and in wave 2, the remaining 4 575 people could be transported.

For verifying the correctness of the proposed solution, the evacuation time course was determined. The times and deviations of individual evacuation activities were determined using the PERT method. A network analysis of the individual activities, their time course and continuity were created using MS Project. The Network analyses were created for all 11 routes in two scenarios. The first scenario was the most likely scenario, and the second scenario was a pessimistic scenario in which all the activities would be delayed. Based on the results of the most likely scenario, the evacuation could be completed in time, even if buses on Routes 5 and 6 were unused. The time margin in this case is 1 hour. In the pessimistic scenario, the evacuation can be managed with 80% occupancy of the buses. The time margin in this case is 2 minutes. However, this would have to delay all activities.

Acknowledgements

Funded by the EU NextGenerationEU through the Recovery and Resilience Plan for Slovakia under the project No. 09I03-03-V05-00002. This work was supported by Grant System of University of Zilina No. 16963/2021 "Research into the readiness of municipalities to deal with emergency events with an emphasis on the safety of the inhabitants" and KEGA 046ZU-4/2025 Educational online platform for preparing inhabitants for self-protection and mutual aid and an interactive university textbook focused on civil protection.

Conflicts of interest

The authors declare that they have no known competing financial interests or personal relationships that could have appeared to influence the work reported in this paper.

References

[1] HEDE, S. Perceptions of crisis preparedness and motivation: a study among municipal leaders. *Safety Science* [online]. 2017, **95**, p. 83-91. ISSN 0925-7535, eISSN 1879-1042. Available from: https://doi.org/10.1016/j.ssci.2017.02.010

[2] DI LUDOVICO, D., CAPANNOLO, CH., D'ALOISIO, G. The toolkit disaster preparedness for pre-disaster planning. *International Journal of Disaster Risk Reduction* [online]. 2023, **96**, 103889. eISSN 2212-4209. Available from: https://doi.org/10.1016/j.ijdrr.2023.103889

[3] FAGA, G., CASAROTTI, CH. A fast assessment methodology for screening of local civil protection plans on a territorial scale basis: a case study of an Italian province. *International Journal of Disaster Risk Reduction* [online]. 2022, **81**, 103284. eISSN 2212-4209. Available from: https://doi.org/10.1016/j.ijdrr.2022.103284

[4] KUBAS, J., POLORECKA, M., HOLLA, K., SOLTES, V., KELISEK, A., STRACHOTA, S., MALY, S. Use of toxic substance release modelling as a tool for prevention planning in border areas. *Atmosphere* [online]. 2022, **13**, 836. eISSN 2073-4433. Available from: https://doi.org/10.3390/atmos13050836

[5] TITKO, M., RISTVEJ, J., ZAMIAR, Z. Population preparedness for disasters and extreme weather events as a predictor of building a resilient society: the Slovak Republic. *International Journal of Environmental Research and Public Health* [online]. 2021, **18**(5), 2311. eISSN 1660-4601. Available from: https://doi.org/10.3390/ijerph18052311

[6] Preparedness - UNDRR [online] [accessed 2024-09-19]. 2007. Available from: https://www.undrr.org/terminology/preparedness

[7] HEALY, A., MALHOTRA, N. Myopic voters and natural disaster policy. *American Political Science Review* [online]. 2009, **103**(3), p. 387-406. ISSN 0003-0554, eISSN 1537-5943. Available from: https://doi.org/10.1017/S0003055409990104

[8] CHAI, L., HAN, Y., HAN, Z., WEI, J., ZHAO, Y. Differences in disaster preparedness between urban and rural communities in China. *International Journal of Disaster Risk Reduction* [online]. 2021, **53**, 102020. eISSN 2212-4209. Available from: https://doi.org/10.1016/j.ijdrr.2020.102020

[9] LU, Q., GEORGE, B., SHEKHAR, S. Evacuation route planning: a case study in semantic computing. *International Journal of Semantic Computing* [online] [accessed 2024-09-20]. 2007, **01**(02), p. 249-303. ISSN 1793-351X, eISSN 1793-7108. Available from: https://doi.org/10.1142/S1793351X07000147

[10] Act of the National Council of the Slovak Republic No. 42/1994 Collection on civil protection of the population.
[11] *Population protection and crisis management*. Scripts. Prague: Ministry of the Interior - General Directorate of the Fire Brigade of the Czech Republic, 2015. ISBN 978-80-86466-62-0.
[12] Decree of the Ministry No. 380/2002 Collection on the preparation and implementation of population protection tasks.
[13] Decree of the Ministry of the Interior of the Slovak Republic No. 328/2012 Collection laying down details on evacuation.
[14] KOLLAROVA, M., GRANAK, T., STRELCOVA, S., RISTVEJ, J. Conceptual model of key aspects of security and privacy protection in a smart city in Slovakia. *Sustainability* [online]. 2023, **15**(8), 6926. eISSN 2071-1050. Available from: https://doi.org/10.3390/su15086926
[15] DARIAGAN, J. D., ATANDO, R. B., ASIS, J. L. B. Disaster preparedness of local governments in Panay Island, Philippines. *Natural Hazards* [online]. 2021, **105**, p. 1923-1944. ISSN 0921-030X, eISSN 1573-0840. Available from: https://doi.org/10.1007/s11069-020-04383-0
[16] KUBAS, J., KOLLAR, B., RISTVEJ, J., PETRLOVA, K., BLAZKOVA, K. Vulnerability assessment of transport infrastructure elements - case study in Rajec. *Communications - Scientific Letters of the University of Zilina* [online]. 2024, **26**(4), p. F23-F35. ISSN 1335-4205, eISSN 2585-7878. Available from: https://doi.org/10.26552/com.C.2024.040
[17] REZVANI, S. M. H. S., SILVA, M. J. F., ALMEIDA, N. M. Mapping geospatial AI flood risk in national road networks. *ISPRS International Journal of Geo-Information* [online]. 2024, **13**(9), 323. eISSN 2220-9964. Available from: https://doi.org/10.3390/ijgi13090323
[18] REHAK, D., SENOVSKY, P., HROMADA, M., LOVECEK, T. Complex approach to assessing resilience of critical infrastructure elements. *International Journal of Critical Infrastructure Protection* [online]. 2019, **25**, p. 125-138. ISSN 1874-5482, eISSN 2212-2087. Available from: https://doi.org/10.1016/j.ijcip.2019.03.003
[19] MILENKOVIC, M., KEKIC, D. Using GIS in emergency management. In: International Scientific Conference Sinteza 2016: proceedings [online]. 2016. ISBN 978-86-7912-628-3, p. 202-207. Available from: https://doi.org/10.15308/Sinteza-2016-202-207
[20] REHAK, D., SENOVSKY, P., SLIVKOVA, S. Resilience of critical infrastructure elements and its main factors. *Systems* [online]. 2018, **6**, 2. eISSN 2079-8954. Available from: https://doi.org/10.3390/systems6020021
[21] ARMENAKIS, C., NIRUPAMA, N. Prioritization of disaster risk in a community using GIS. *Natural Hazards* [online]. 2013, **66**, p. 15-29. ISSN 0921-030X, eISSN 1573-0840. Available from: https://doi.org/10.1007/s11069-012-0167-8
[22] CT24, CTK, Krnov was cut off from the surrounding area by water. It was possible to reach it by car after two days/Krnov voda odrizla od okoli. Autem se tam dalo dostat po dvou dnech (in Czech) [online] [accessed 2024-09-20]. 2024. Available from: https://ct24.ceskatelevize.cz/clanek/regiony/k-odchodu-jsme-vyzyvali-vcas-reagoval-mistostarosta-krnova-na-vytky-sefa-hasicu-353055
[23] Buses and trucks are literally swimming in water - Facebook, www.iMeteo.sk [online] [accessed 2024-09-20]. 2024. Available from: https://www.facebook.com/imeteo/posts/pfbid02mkv4fewjjrmVU1j8so314p5xhFx3UsiLXDb15668ijWpgnYfft5zjdCWjUsHmtAMl
[24] BYARUHANGA, N., KIBIRIGE, D., GOKOOL, S., MKHONTA, G. Evolution of flood prediction and forecasting models for flood early warning systems: a scoping review. *Water* [online]. 2024, **16**(13), 1763. eISSN 2073-4441. Available from: https://doi.org/10.3390/w16131763
[25] Act of the Interior of the Czech Republic No. 254/2001 Collection on Water and on Amendments to Certain Acts (Water Act).
[26] HAILE, T., GOITOM, H., DEGU, A. M., GRUM, B., ABEBE, B. A. Simulation of urban environment flood inundation from potential dam break: case of Midimar Embankment Dam, Tigray, Northern Ethiopia. *Sustainable Water Resources Management* [online]. 2024, **10**(2), 46. ISSN 2363-5037, eISSN 2363-5045. Available from: https://doi.org/10.1007/s40899-023-01008-9
[27] HALTAS, I., ELCI, S., TAYFUR, G. Numerical simulation of flood wave propagation in two-dimensions in densely populated urban areas due to dam break. *Water Resources Management* [online]. 2016, **30**(15), p. 5699-5721. ISSN 0920-4741, eISSN 1573-1650. Available from: https://doi.org/10.1007/s11269-016-1344-4
[28] MUNOZ, D. H., CONSTANTINESCU, G. A. Fully 3-D numerical model to predict flood wave propagation and assess efficiency of flood protection measures. *Advances in Water Resources* [online]. 2018, **122**, p. 148-165. ISSN 0309-1708, eISSN 1872-9657. Available from: https://doi.org/10.1016/j.advwatres.2018.10.014
[29] BOSA, S., PETTI, M. A numerical model of the wave that overtopped the Vajont Dam in 1963. *Water Resources Management* [online]. 2013, **27**(6), p. 1763-1779. ISSN 0920-4741, eISSN 1573-1650. Available from: https://doi.org/10.1007/s11269-012-0162-6
[30] BROZA, V. *Dams of Bohemia, Moravia and Silesia*. Liberec: Knihy 555, 2005. ISBN 80-86660-11-7.

[31] Billion-zloty losses in Stronie Slaskie. This is what the broken dam looks like now - Onet News/Miliardowe straty w Stroniu Slaskim. Tak wygląda teraz przerwana tama - Onet Wiadomosci (in Polish) [online] [accessed 2024-09-23]. 2024. Available from: https://wiadomosci.onet.pl/wroclaw/miliardowe-straty-w-stroniu-slaskim-tak-wyglada-teraz-przerwana-tama-zdjecia/f0cmw28

[32] Polish Press Agency (PAP), Brigadier General Michal Kamieniecki: In Stronie Slaskie and Ladek-Zdroj municipal infrastructure is destroyed/Nadbrygadier Michal Kamieniecki: w Stroniu Slaskim i Ladku-Zdroju instalacje komunalne sa zniszczone - Polska Agencja Prasowa SA (in Polish) [online] [accessed 2024-09-23]. 2024. Available from: https://www.pap.pl/aktualnosci/nadbrygadier-michal-kamieniecki-w-stroniu-slaskim-i-ladku-zdroju-instalacje-komunalne

[33] JABLONSKY, J. *Operational research*. Prague: Professional Publishing, 2007. ISBN 978-80-86946-44-3.

[34] City subdivision - city districts - Opava Tourist Information Centre (in Czech) [online] [accessed 2024-10-02]. Available from: https://www.opava-city.cz/tic/cz/mesto-opava/o-meste/cleneni-mesta-mestske-casti/

[35] Crisis plan of the Moravian-Silesian Region.

[36] Population by sex and urban districts of the selected city - Czech Statistical Office (in Czech) [online] [accessed 2024-03-16]. 2021 Available from: https://vdb.czso.cz/vdbvo2/faces/cs/index.jsf?page=vystupobjekt&pvo=SLD21001-MCOB&z=T&f=TABULKA&skupId=4429&katalog=33515&pvo=SLD21001-MC-OB&pvokc=43&pvoch=505927

[37] Commuters by main means of transport and by urban districts of the selected city - Czech Statistical Office (in Czech) [online] [accessed March 2024-03-16]. 2021. Available from: https://vdb.czso.cz/vdbvo2/faces/cs/index.jsf?page=vystupobjekt&pvo=SLD21095-MCOB&z=T&f=TABULKA&skupId=5357&katalog=34217&pvo=SLD21095-MC-OB&pvokc=43&pvoch=505927

[38] Households by number of household members and by municipalities of the selected SO ORP - Czech Statistical Office (in Czech) [online] [accessed 2024-03-15]. 2021Available from: https://vdb.czso.cz/vdbvo2/faces/cs/index.jsf?page=vystupobjekt&pvo=SLD21079-OBOR&skupId=5054&z=T&f=TABULKA&katalog=34037&pvo=SLD21079-OBOR&pvokc=65&pvoch=8117

[39] DOLEY, D., MAURYA, A. K. An assessment of travel time dependability in urban corridors: Guwahati City case study. In: 2024 16th International Conference on COMmunication Systems and NETworkS COMSNETS: proceedings [online]. IEEE. 2024. eISBN 979-8-3503-8311-9, eISSN 2155-2509, p. 216-221. Available from: https://doi.org/10.1109/COMSNETS59351.2024.10427150

[40] FRENCH, C., O'MAHONY, M. Using automatic vehicle location system data to assess impacts of weather on bus journey times for different bus route types. In: 2021 IEEE International Intelligent Transportation Systems Conference ITSC: proceedings [online]. IEEE. 2021. eISBN 978-1-7281-9142-3, p. 2137-2144. Available from: https://doi.org/10.1109/ITSC48978.2021.9564546

[41] GONIEWICZ, K., MISZTAL-OKONSKA, P., PAWLOWSKI, W., BURKLE, F. M., CZERSKI, R., HERTELENDY, A. J., GONIEWICZ, M. Evacuation from healthcare facilities in Poland: legal preparedness and preparation. *International Journal of Environmental Research and Public Health* [online]. 2020, **17**(5), 1779. eISSN 1660-4601. Available from: https://doi.org/10.3390/ijerph17051779

[42] KIM, K. Y., TOPLU-TUTAY, G., KUTANOGLU, E., HASENBEIN, J. J. A stochastic optimization model for patient evacuation from health care facilities during hurricanes. *International Journal of Disaster Risk Reduction* [online]. 2024, **108**, 104518. eISSN 2212-4209. Available from: https://doi.org/10.1016/j.ijdrr.2024.104518

[43] YAZDANI, M., MOJTAHEDI, M., LOOSEMORE, M., SANDERSON, D. A modelling framework to design an evacuation support system for healthcare infrastructures in response to major flood events. *Progress in Disaster Science* [online]. 2022, **13**, 100218. eISSN 2590-0617. Available from: https://doi.org/10.1016/j.pdisas.2022.100218

[44] TAYFUR, E., TAAFFE, K. A model for allocating resources during hospital evacuations. *Computers and Industrial Engineering* [online]. 2009, **57**(4), p. 1313-1323. ISSN 0360-8352, eISSN 1879-0550. Available from: https://doi.org/10.1016/j.cie.2009.06.013

[45] PARAJULI, G., NEUPANE, S., KUNWAR, S., ADHIKARI, R., ACHARYA, T. D. A GIS-based evacuation route planning in flood-susceptible area of Siraha Municipality, Nepal. *ISPRS International Journal of Geo-Information* [online]. 2023, **12**(7), 286. eISSN 2220-9964. Available from: https://doi.org/10.3390/ijgi12070286

[46] GASPARIKOVA, Z., LEITNER, B. Transportation problems and their application in planning transport provision of area evacuation. In: *TRANSBALTICA XII: Transportation Science and Technology* [online]. PRENTKOVSKIS, O., YATSKIV, I., SKACKAUSKAS, P., JUNEVICIUS, R., MARUSCHAK, P. (Eds.). Cham: Springer International Publishing, 2022. ISBN 978-3-030-94774-3, p. 477-489. Available from: https://doi.org/10.1007/978-3-030-94774-3_47

[47] BAHMANI, H., AO, Y., YANG, D., WANG, D. Students' evacuation behavior during an emergency at schools: a systematic literature review. *International Journal of Disaster Risk Reduction* [online]. 2023, **87**, 103584. eISSN 2212-4209. Available from: https://doi.org/10.1016/j.ijdrr.2023.103584

KOMUNIKÁCIE
COMMUNICATIONS

VEDECKÉ LISTY ŽILINSKEJ UNIVERZITY
SCIENTIFIC LETTERS OF THE UNIVERSITY OF ZILINA
journal for sciences in transport

VOLUME 27 Number 3

July 2025

komunikácie
COMMUNICATIONS

VEDECKÉ LISTY ŽILINSKEJ UNIVERZITY
SCIENTIFIC LETTERS OF THE UNIVERSITY OF ZILINA
journal for sciences in transport

VOLUME 27 Number 3

July 2025

Each paper was reviewed by at least two reviewers.
Individual issues of the journal can be found on: http://komunikacie.uniza.sk
The full author quidelines are available at: https://komunikacie.uniza.sk/artkey/inf-990000-0400_Author-guidelines.php
Published quarterly by University of Žilina in EDIS - Publishing House of the University of Žilina.
Journal for sciences in transport Komunikácie / Communications is currently indexed, abstracted and accepted by CEEOL, CLOCKSS, COPE (Committee on Publication Ethics), Crossref (DOI), digitálne pramene, DOAJ, EBSCO Host, Electronic Journals Library (EZB), ERIH Plus, Google Scholar, Index Copernicus International Journals Master list, iThenticate, JournalGuide, Jouroscope, Norwegian Register for Scientific Journals Series and Publishers, Portico, ROAD, ScienceGate, SCImago Journal & Country Rank, SciRev, SCOPUS, Web of Science database, WorldCat (OCLC).

Journal for sciences in transport Komunikácie - vedecké listy Žilinskej univerzity v Žiline / Communications - Scientific Letters of the University of Žilina has been selected for inclusion in the Web of Science™.

Contact:

Komunikácie - vedecké listy Žilinskej univerzity v Žiline
Communications - Scientific Letters of the University of Žilina
University of Žilina, Univerzitná 8215/1
010 26 Žilina, Slovakia

E-mail: komunikacie@uniza.sk
Web: https://komunikacie.uniza.sk

ISSN (print version): 1335-4205
ISSN (online version): 2585-7878

Registered No. (print version): EV 3672/09
Registered No. (online version): EV 3/22/EPP
Publisher, owner and distribution:
University of Žilina, Univerzitná 8215/1,
010 26 Žilina, Slovakia

Company identification number IČO: 00 397 563
Frequency of publishing: four times a year
Circulation: 30 printed copies per issue
Print edition price: 100 Euro (price without VAT)
Article Processing Charge (APC): 400 Euro (price without VAT)

Publishing has been approved by:
Ministry of Culture, Slovak Republic

UNIVERSITY
OF ŽILINA

In its over 70 years of successful existence, the University of Žilina (UNIZA) has become one of the top universities in Slovakia.

Scientific conferences

organized by University of Žilina

41th DANUBIA – ADRIA Symposium on Advances in Experimental Mechanics 2025
Date and venue: 23. – 26. September 2025, Kragujevac (SRB)
Contact: eva.tillova@fstroj.uniza.sk
Web: http://kmi2.uniza.sk/

Horizons of Railway Transport 2025
Date and venue: 7. – 9. October 2025, Jasná (SK)
Contact: zdenka.bulkova@uniza.sk
Web: https://kzd.uniza.sk/

Globalization and its Socio-Economic Consequences
Date and venue: 8. – 9. October 2025, Rajecké Teplice (SK)
Contact: tomas.kliestik@uniza.sk
Web: https://ke.uniza.sk/

28th International Scientific Conference Crisis situations solution in specific environment
Date and venue: 15. – 16. October 2025, Žilina (SK)
Contact: crisis@uniza.sk
Web: https://www.fbi.uniza.sk/

Existing Bridges 2025
Date and venue: 6. – 7. November 2025, Žilina (SK)
Contact: stav-konf-kskm@uniza.sk
Web: https://existingbridges.uniza.sk/

UNIVERSITY OF ŽILINA
Science & Research Department

Univerzitná 8215/1,
010 26 Žilina,
Slovakia

Ing. Janka Macurová
tel.: +421 41 513 5143
e-mail: janka.macurova@uniza.sk